Design and Stability Analysis of a Switching Contact Task Controller for Hydraulic Actuators

By

Pooya Sekhavat

A thesis
presented to the University of Manitoba
in fulfillment of the
thesis requirement for the degree of
Doctor of Philosophy
in
Mechanical and Manufacturing Engineering
Winnipeg, Manitoba, Canada, 2004

THE UNIVERSITY OF MANITOBA

FACULTY OF GRADUATE STUDIES

*****

COPYRIGHT PERMISSION

Design and Stability Analysis of a Switching Contact Task Controller for Hydraulic Actuators

BY

Pooya Sekhavat

A Thesis/Practicum submitted to the Faculty of Graduate Studies of The University of Manitoba in partial fulfillment of the requirement of the degree

Of

Doctor of Philosophy

Abstract

Electrohydraulic servo actuators are used extensively in industry due to their high payload capability, high durability, rapid response, and high power-to-weight ratio. In this thesis, a switching contact task control scheme is designed for hydraulic actuators. The control scheme essentially consists of three distinct control laws for asymptotic position regulation in free space motion, impact suppression during transition from free to constrained motion, and asymptotic force regulation in the sustained-contact period of motion, all in the presence of actuator's dry friction as well as viscous friction and Stribeck effect.

At the control design stage, the extension of Lyapunov stability theory to nonsmooth systems based on Filippov's solution theory is employed to derive the control laws for various modes of operation of a hydraulic actuator interacting with a non-moving environment. None of the controllers require exact knowledge of the actuator friction, servovalve dynamics, environment stiffness, or hydraulic parameters for the control action as in most practical cases such knowledge is not available. For an actuator with initially centered piston that travels within the mid-point vicinity of the cylinder, the theoretical Lyapunov stability of each phase of motion is studied considering nonlinear hydraulic functions, servovalve dynamics, complete discontinuous model of actuator friction, and realistic impact/contact dynamics (if present) modeled by Hertz contact theory. The performance of each individual controller is then tested through experiments on a fully instrumented hydraulic test rig and their practicality and effectiveness in real operations is verified.

Combination of the three control schemes yields a so-called "switching contact task control scheme". The most important but difficult part of analyzing such a nonsmooth system is the stability analysis. Although Lyapunov stability theory is the basis in deriving the individual control laws at the design stage, switchings between control laws during the complete contact task necessitates an overall stability analysis for the complete task. Removing the dynamic modeling assumptions of the design stage and generalizing the system dynamics by allowing the full stroke piston travel comes with the price of adding extreme difficulty in deriving the Lyapunov functions for the overall non-smooth system. Therefore, in this thesis, a systematic approach is developed for stability analysis of the overall contact task using the concept of

Lyapunov exponents. Since Lyapunov exponents have been initially introduced to analyze smooth dynamical systems, their application to nonsmooth systems involves a number of issues that need special consideration. Solution analysis, linearization at the instants of discontinuity, existence of Lyapunov exponents, and stability of numerical computations are among such important issues that did not exist in the conventional applications of Lyapunov exponents on smooth dynamic systems. These issues are thoroughly addressed using a combination of various existing theorems and algorithms and the resulting methodology has laid a solid framework for stability analysis of switching systems with capability of being extended to other nonsmooth engineering problems.

Acknowledgements

I would like to forward my most sincere appreciation to my advisors, Dr. N. Sepehri and Dr. C. Q. Wu, whose encouragements and supports have made this thesis possible. I feel tremendously fortunate to have such a unique opportunity of working with two advisors whose perfectly blended theoretical and experimental expertise strengthened this project in both directions.

I also wish to sincerely thank Dr. A. B. Gumel from Department of Mathematics, who played a major role in enriching this project by his valuable guidelines and advice on the numerical aspect of this project. Sincere thanks also go to Dr. S. Onyshko for his continued support during the course of this project as my committee member.

On this project, I have had this opportunity to work with Mr. Al. Lohse, the Experimental Robotics and Tele-Operation Laboratory's support engineer, for his practical technical support during my test experiments and Mr. Mark Karpenko, for the time-to-time fruitful discussions regarding the Lab's hydraulic test rig.

I also wish to thank my best friends and lab-mates Mr. Navid Niksefat and Mr. Farshid Najafi who have been my very encouraging and helpful friends during my course of study.

No words describe my heartfelt thanks to my mother (Fateme Baradaran Mahajeri) and father (Jafar Sekhavat) for a lifetime of support and encouragement, which has made me who I am today. I will never forget their exceptional and unlimited support during my long track of studies from kindergarden all the way to Doctor of Philosophy. This thesis is the smallest token of appreciation I can give for their sacrifices throughout my life.

I would also like to thank my sisters, Anoushe and Niyoosha, and my brother-in-law, Arash, whose care and kindness was a great help in continuing my postgraduate studies.

My heartfelt appreciation goes to the Huebert Family (Art, Ruth, Mark, and Brian) who hospitably hosted me in this city at the beginning of my Ph.D. studies and have always been extremely nice and supportive during the past years.

Finally, I wish to acknowledge the support of The Institute of Robotics and Intelligent systems (IRIS) Network Center of Excellence, and the University of Manitoba for their financial support.

To

My Parents

Table of Contents

List of Figures

List of Tables

Chapter 1

Introduction

1.1 Motivation

Due to their high force, high durability, high power-to-weight ratios and rapid responses, electrohydraulic actuators play an important role in the development of manipulators for inspection, maintenance and assembly tasks conducted in marine missions, material testing equipments, oil and gas surveys, telerobotic operations, as well as military applications. An essential issue in such applications is proper interaction between the manipulator and the environment, commonly known as "contact task". The manipulator should be able to follow a free space trajectory and make a stable contact with the environment while the energy of impact is dissipated and the desired contact force is achieved (Payandeh, 1996). A particular example of a robotic contact task is the remote operation of underwater hydraulic manipulators for inspection, maintenance, or assembly. An inspection probe used to track around a weld to detect any cracks, or, the mating of underwater connector and socket arrangements, require both free-space position control and sustained-contact force control with high accuracy (Dunnigan et al., 1996). Accomplishing such tasks generally consists of three operational modes: free-space motion, sustained-contact motion, and the transition between the two called the impact mode.

The intermediate phase of motion is of particular importance as operators normally do not have enough time to control the impacts from driving an otherwise stable controller into instability and preventing serious damages to both the manipulator and the environment (Dunnigan et al., 1996). They are only aware that the end-effector has hit an object when the slave manipulator is no longer spatially correspondent with the master arm. Employing an automatic control scheme that could control the position, possible impacts, and the force applied to the environment would reduce the burden on the operator and increase the likelihood of successfully completing the task with the minimum cost. The general requirement for the design of such a contact task controller is threefold (Fig. 1.1): (*i*) the capability of moving the manipulator to its desired position in case of no contact with an environment (free-space motion), (*ii*) the capability to accomplish a stable contact transition upon contact with an unexpected environment (phase-transition or impact mode), and (*iii*) the capability to follow the desired contact force after sustained contact is established (constrained-motion).

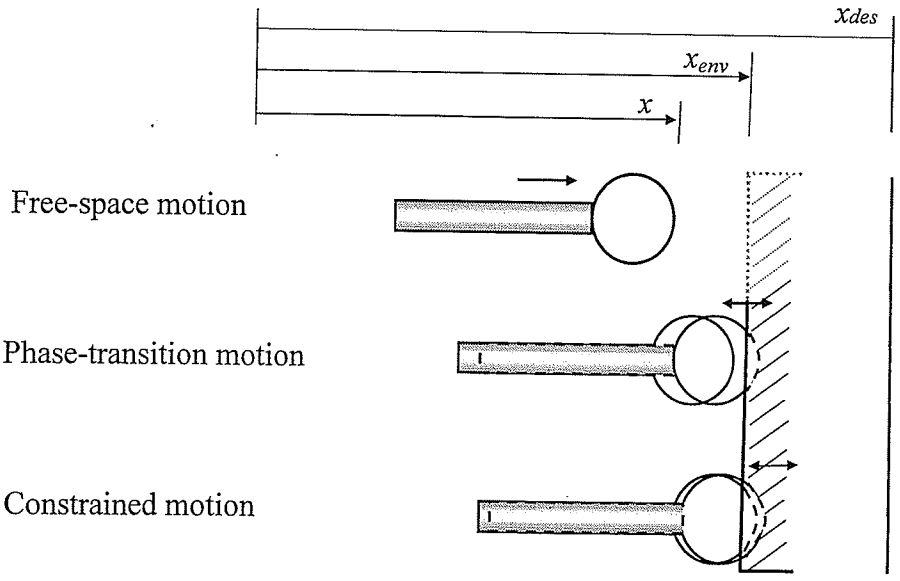

Fig. 1.1 Phases of the implement's motion.

Designing such a switching contact task control strategy for hydraulic actuators interacting with non-moving environments is the main motivation of this research. Including hydraulic actuation and dry friction dynamics in the model of the system and releasing the restrictive modeling assumptions (such as bounce-less contact assumption in Niksefat et al., 2001) rules out the previous attempts on the contact task stability analysis. It is, therefore, imperative to conduct a

rigorous stability analysis despite existence of hydraulic actuation nonlinearities, actuator friction, switching controllers, and characteristics of realistic impact/contact models in the resulting non-smooth system.

1.2 Literature Review

When the manipulator's implement transfers between different modes of operation, the model of the system undergoes substantial changes that make planning and control difficult to achieve. Impedance control (Heinrichs et al., 1997; Bilodeau and Papadopoulos, 1998; Ha et al., 2000; Kazerooni et al., 1990) provides a unified control structure for all various modes of operation with no need for switching between control laws. However, there are a number of drawbacks rendering the algorithm vulnerable in realistic applications (Marth et al., 1994; Vukobratovic, 1997). Firstly, impedance control technique is best applicable for contact tasks where the environment model can be sufficiently described by a linear equation. Secondly, force tracking with impedance control is achieved through tracking of virtual position, and therefore, contact force tracking is only possible if the exact environment model is previously known or identified on-line. Thirdly, the measured interaction force is always present in the control algorithm and the non-zero noisy measured force can corrupt the control performance when the implement is in free-space.

To overcome the above drawbacks, an alternative approach is to divide the overall motion into different operation modes and employ a different control law in each phase of motion (Mills and Lokhorst, 1993a, 1993b; Volpe and Khosla, 1993a, 1993b; Marth et al., 1993, 1994; Tarn et al., 1996; Wu and Payandeh, 1999; Brogliato et al., 1997; Pagilla and Yu, 2001; Niksefat et al., 2001; Hyde and Cutkosky, 1993; Seraji et al., 1996). Switching between the controllers is based on the detection of discrete events (such as detection of the first non-zero force) reported by sensors. The first switching at the beginning of the transition phase is where the implement makes its first contact with the environment. This mode of motion lasts until the implement establishes a stable stationary contact with the environment exerting minimal force on it. Then, the control scheme switches again to follow the desired contact force.

Most of the existing literature on switching contact task control design is directed towards electrically actuated systems. Unlike their electrical counterparts, hydraulically actuated systems

exhibit highly complicated characteristics arising from factors such as pressure-flow relationship in the valve, compressibility of hydraulic fluid, saturation in servovalve, backlash in mounting the cylinder body and rod, deadband in the valve, asymmetric actuation, hysteresis effect resulting from electromagnetic characteristics of the torque motor controlling the spool valve, and friction in the hydraulic cylinder that not only degrades the behavior of hydraulic control systems, but also makes the stability analysis of the resulting nonlinear system a challenging problem. Even if the spool valve dynamics are ignored, the control signal drives the derivative of the actuator torque (not the torque itself) which is not desirable for precise control. Moreover, the operating conditions of hydraulic actuators are subject to change and employing linear control design methods for hydraulically actuated systems cannot provide a satisfactory performance over the overall range of operating conditions.

The recent work of Niksefat et al. (2001) is the only rigorous theoretical and experimental attempt in designing a stable switching contact task controller that allows a hydraulic actuator to follow a desired position in free-space motion and, upon contact with an unknown environment, switches to the contact mode of motion to exert a desired force. The work, however, resorts to several restrictive assumptions in dynamic modeling of the system that are not easy to guarantee in practical applications: (*i*) once the actuator comes in contact with the environment, it will maintain its contact until force regulation is completed, (*ii*) the actuator's dry friction is negligible, (*iii*) the piston is initially centered in the cylinder and is restricted to travel only within the mid-point vicinity of the cylinder during the overall motion. Direct switching from free-space control law to the constrained-motion control law without first damping the possible impacts may lead to severe repeated impacts (Pagilla and Yu, 2001) driving an otherwise stable controller into instability. Also, hydraulic actuators operate under high supply pressures and tight sealing is required to prevent them from internal leakage, leading to considerable dry friction in the system. Such friction effects may cause instability during position or force feedback control (Lischinsky et al., 1999). Therefore, it is imperative to design a more advanced switching contact control scheme that: (*i*) employs an intermediate impact control scheme to regulate the possible transitory impacts as a result of bouncing on initial contact and rests the implement before switching to the constrained-motion control scheme, (*ii*) is capable of counteracting dry friction and accomplishing asymptotic position control, impact regulation and contact-force control, and, (*iii*) leads to a stable control system regardless of the piston's initial location and its travel stroke

during the contact task. In the subsequent sub-sections of this chapter, the previous works on each of these three improving aspects are explained.

1.2.1 Impact (Phase Transition) Control

Even within the general context of contact task control design, only a few recent studies have dealt with the transition mode as a separate mode of motion with special treatment. Brogliato and Orhant (1998) demonstrated the global asymptotic convergence of a one-degree of freedom PD-type controlled system colliding with a spring-like environment. Tornambe (1999) proved the asymptotic stability of continuous control laws (based on only position and velocity feedback) designed for bringing the implement to a steady-state configuration in contact with the environment. Pagilla and Yu (2001) proposed separate control laws for free trajectory tracking, constrained motion and the transition phase between the two and experimentally studied the performances of the system in slow/fast collisions. Xu et al. (2000) incorporated joint acceleration and velocity feedbacks into a classical integral force control to suppress the impact bouncing. Tarn et al. (1996) used an acceleration feedback to control the transient force response and to reduce the peak impulsive force caused by the transient force.

All above studies are directed at electrically driven manipulators. Within the context of hydraulically actuated systems, no control scheme has yet been reported for impact control of an implement colliding with an environment. Consequently, the control schemes developed in the future chapters are the first attempts in introducing effective nonlinear control schemes that could regulate impacts of a hydraulic actuator during the transition phase from free-space to constrained motion.

1.2.2 Friction Compensating Position/Force Control

Hydraulic actuator's friction consumes a large part of actuation force and produces a jerky starting motion due to Stribeck effect (exponential decrease in friction after the stiction force is surmounted). Typical errors caused by actuator friction include steady-state errors (caused by dry friction) and tracking lags (caused by viscous friction) (Canudas de Wit et al., 1991). This necessitates special consideration for reducing or compensating friction during the system's position/force control.

Within the context of friction compensation techniques, Armstrong-Helouvry et al. (1994) conducted an extensive survey and divided the techniques into two major non-model-based and model-based categories. Model-based methods are distinguished from non-model-based methods in that they are based on the knowledge of friction model. Since (*i*) the physical nature of friction is such that it can be rarely determined *a priori* with the accuracy required for cancellation, and, (*ii*) the amount of friction often changes with time and often depends on numerous factors that are challenging to estimate or measure, most model-based methods entail on-line estimation of the friction using observers (Canudas de Wit et al., 1991, 1995, 1997; Armstrong-Helouvry et al., 1994; Friedland and Park, 1992; Amin et al. 1997). Non-modeled compensation techniques such as high gain control laws, dither (injection of an additional high frequency noise), impulsive control, and joint torque control have also their own limitations (see Canudas de Wit et al., 1991, for details). An effective alternative approach for friction compensation has been to employ Lyapunov's direct method to develop a nonlinear discontinuous compensation technique and stabilize a one-DOF system at the desired position (Southward et al., 1991). This thesis follows the latter idea for friction compensation during the position/force control. The following sub-sections provide a complete description of the earlier related works in the literature.

Position Control

Recent experimental comparison of ten different position control schemes shows that the nonlinear schemes achieve a higher accuracy compared to the controllers directly based on linear models (Bonchis et al., 2002). This is due to the highly nonlinear characteristics of hydraulic systems. Most of the recent studies on position control of hydraulically actuated systems are focused on advanced nonlinear control theories such as feedback linearization (Vossoughi and Donath,1995), adaptive control (Yao et al, 2000; Sirouspour and Salcudean, 2001; Tafazoli et al., 1998; Lischinsky et al., 1999), variable structure control (Hwang and Lan, 1994), and direct Lyapunov-based control (Sohl and Bobrow, 1999; Niksefat et al., 2001). However, not all of the above studies considered stick-slip (dry) friction that is a major disturbance in hydraulic cylinders and compensating it could improve the positioning performance (Bonchis et al., 2002).

With respect to the previous relevant work on position regulation of hydraulically actuated systems in the presence of actuator dry friction, Lischinsky et al. (1999) used a nonlinear PI-type controller as the inner torque loop of an outer position control scheme. Neglecting the valve

dynamics, they provided the stability proof of the position control system. Tafazoli et al. (1998) established an adaptive friction compensation technique by combining observer-based friction estimation with an acceleration feedback control. However, no theoretical stability analysis was provided. Yao et al. (2000) included the dynamics of the servovalve and proposed a discontinuous adaptive robust controller supported by a rigorous stability proof for position tracking. In case of position regulation, however, complete stability analysis was not provided; nor did they provide a solution analysis of their resulting nonsmooth system. Sohl and Bobrow (1999) obtained a nonlinear control law using Lyapunov stability analysis. Their control law required knowledge of valve coefficients, fluid bulk modulus, and Coulomb friction, whose values may change during the position control process.

Force Control

Studies that have addressed the issue of actuator's dry friction in force control of hydraulically actuated systems can be grouped into two categories. The first category includes studies that have used force control in combination with another friction compensating position control scheme (Ha et al., 2000; Sohl and Bobrow, 1999; Nguyen et al., 2000; Honegger and Corke, 2001; Lischinsky et al., 1999). Ha et al. (2000) proposed a sliding mode controller for impedance control of excavators. With an observer-based compensation for actuator friction, they employed sliding mode control to implement the target impedance. Sohl and Bobrow (1999) introduced a Lyapunov-like force control scheme for exponential convergence of hydraulic applied force to the desired force. The controller accounts for friction effects only in the inner position tracking loop and requires the estimates of system parameters (valve coefficient and fluid bulk modulus). Similarly, a control scheme was introduced by Nguyen et al. (2000) based on sliding mode control approach, and the load pressure tracking error (and not the actual net force considering friction effects) was guaranteed to converge to zero asymptotically. Honegger and Corke (2001) and Lischinsky et al. (1999), developed cascaded control schemes where a motion controller compensates the friction effects and a cascaded force controller controls the internal states (pressures) of hydraulic actuators without accounting for the friction effects.

The second category of works included dry friction in their theoretical and/or experimental analysis with no attempt to reduce its degrading effects (Alleyne and Hedrick, 1995; Heinrichs et al., 1997; Laval et al., 1996; Zyada et al., 2002). Among them, the works of Heinrichs et al.

(1997), and Laval et al. (1996) were based on the linearized model of hydraulic functions which has serious drawbacks with respect to the robust performance of the control system over a wide range of frequencies (Vossoughi and Donath,1995). Alleyne and Hedrick (1995) developed a sliding control law coupled with an adaptation scheme for force tracking of a quarter car active suspension system. Using Barbalat's Lemma, they proved the asymptotic convergence of the load pressure to its desired value which is not always proportional to the desired force if the actuator friction is not negligible. Zyada et al. (2002) proposed a rule-base fuzzy compensating model to reduce actuator's friction effects in the force control. The method is based on learning rules from measured input/output data and heuristic rules from experience. Force control in all above studies lacks an important issue of friction compensation that has a great role in the controllability, accuracy, and repeatability of motion. Recently, Alleyne and Liu (2000) proposed a Lyapunov-based force control scheme with some practical means for friction cancellation. However, they did not include the friction cancellation in the system's stability analysis as the non-differentiable terms in the dry friction model were not compatible with the assumptions in their Lyapunov stability analysis.

1.2.3 Stability Analysis of Switching Control Systems

The issue of contact stability can be approached from different point of views (Brogliato, 1999):

- study conditions that guarantee no rebound after the first contact;
- relax the bounceless conditions by studying the conditions that ensure Lyapunov stability of the system without guaranteeing that the actuator's tip will never take off the environment's surface.

When the environment stiffness grows unbounded, bounceless conditions are impossible to obtain using finite force control with non-zero contact velocity (Brogliato, 1999). Therefore, in order to conduct a unified realistic stability analysis that applies to both compliant and rigid models, in this research we shall seek the second viewpoint of stability analysis for contact task control analysis.

Some of the main factors affecting the stable contact task control of a manipulator colliding with an environment are interaction forces, approach velocity, and response time of both the manipulator and the force sensors. For switching contact control systems, existence of switchings in the control scheme results in an overall nonsmooth system which no longer has the desirable

uniformity of an impedance control scheme. Solution and stability analysis of such systems using classical techniques are questionable since the fundamental assumptions of conventional solution theories, known as the Lipschitz-continuous requirement, are violated. With respect to classical solution theories, one cannot even define a solution, much less discuss its existence, uniqueness and stability. Furthermore, applicability of the conventional Lyapunov's stability theory, initially developed for smooth systems with a unique solution is questionable.

Due to the existence of the above challenges, many studies on switching contact task control have implicitly addressed the issue of stability via simulations and/or experiments (Volpe and Khosla, 1993a, 1993b; Marth et al., 1993; Pagilla and Yu, 2001; Hyde and Cutkosky, 1993; Seraji et al., 1996). In other studies which include rigorous theoretical stability analyses, the main approach for stability analysis is extending the Lyapunov stability theory to nonsmooth systems (Peleties and DeCarlo, 1993, Tarn et al., 1996; Mills and Lokhorst, 1993a, 1993b; Brogliato et al., 1997; Wu and Sepehri, 2000; Wu and Payandeh, 1999; Niksefat et al., 2001). Among them the work by Brogliato et al. (1997) is the only study that provides Lyapunov-like stability analysis of a three-stage (free-space, impact transition, and sustained contact) control system, and the work reported by Niksefat et al. (2001) is the only work that includes hydraulic actuation in the analysis.

Deriving Lyapunov functions for switching contact task control systems requires heavy mathematical machinery and has obliged many researchers to resort to some restrictive and sometimes unrealistic modeling assumptions that may greatly reduce the generality of the analysis or its practical applications. In Peleties and DeCarlo (1993) and Tarn et al. (1996), it was assumed that the system is comprised of linear subsystems in each region of motion - an assumption which is not realistic for the highly nonlinear hydraulic systems. Mills and Lokhorst (1993a, 1993b) assumed that the exact knowledge of the manipulator and environment kinematic and dynamic parameters are available. Brogliato et al. (1997) assumed impulsive impact with zero deformation in colliding bodies. Finally, the proofs presented in Wu and Sepehri (2000), Wu and Payandeh (1999) and Niksefat et al. (2001) are only valid under the assumption of no rebound as well as no energy dissipation between implement and environment after the initial contact. In other words, they neglected the major impact dynamics effects (bouncings and energy dissipations) in the analysis during the critical transition period from free-space to constrained motion.

1.3 Objectives and Scope of This Thesis

The primary objective of the present research is the design, theoretical stability analysis, and experimental verification of a switching contact task control scheme for hydraulic actuators in the presence of friction. The control scheme will essentially be the combination of three distinct control laws that are individually designed for asymptotic desired position regulation in the free space motion, impact suppression and stable transition from free to constrained motion, and asymptotic desired force regulation during the sustained-contact period of motion, all in the presence of actuator's dry and viscous frictions.

Compared to the earlier studies, the development of Lyapunov-based position and force regulation controllers have the advantage of being asymptotically convergent to the desired set-point despite the existence of actuator friction and without having the complexity of control methods that need friction observers. Moreover, designing an impact control scheme is the first work in its kind to effectively regulate impacts of a hydraulic actuator during the transition phase from free to constrained motion. Rigorous theoretical analysis and extensive experimental verification on a hydraulic test rig will provide the solid foundation for the controllers' practicality and effectiveness in real applications.

Due to the existence of at least two switchings (free-to-impact and impact-to-contact control) in the overall combined switching contact control scheme, the resulting control system is a nonsmooth dynamical system where finding a composite Lyapunov function for it is extremely difficult, if not impossible. Furthermore, the combined overall contact task control system inherits some undesirable modeling assumptions that, although acceptable in the control design stage, reduce the generality of the control scheme's application. Hence, the secondary objective of this thesis is to introduce a systematic approach for a more thorough stability analysis of such a switching control system using the concept of Lyapunov exponents. In that regard, crucial issues such as solution analysis of nonlinear and linearized systems, linearization of nonlinear equations at the instants of discontinuity, existence of Lyapunov exponents for nonsmooth systems, and stability of numerical computations, will be thoroughly investigated using various existing theorems and techniques. The approach will also establish a solid framework for stability analysis of other nonsmooth engineering problems. The theoretical results will be further implemented in practical experiments.

Chapter 2

Theoretical Preliminaries

2.1 Filippov's Solution Theory

One of the earliest and conceptually straightforward approaches which has been often used in the solution analysis of non-smooth systems is the Filippov's solution theory (1960, 1979 and 1988). In his work, a new definition of solution to differential equations with discontinuous terms was given which is referred to here as Filippov's solution, and theorems were proven for existence, uniqueness and continuity dependence on the initial conditions.

2.1.1 Definition of Filippov's Solution

Consider the vector differential equation

$$\dot{x} = \mathbf{f}(x,t) \tag{2.1}$$

where $\mathbf{f} : R^n \times R \to R^n$ is measurable and essentially locally bounded. The solution to equation (2.1) was given by Filippov (1960) as follows:

Definition 1: A vector function $x(t)$, defined on the interval (t_1, t_2), is called a solution of equation (2.1) if it is absolutely continuous and if for almost all $t \in (t_1, t_2)$ and for arbitrary $\delta > 0$ the vector $dx(t)/dt$ belongs to the smallest convex closed set (of n-dimensional space)

containing all the values of the vector function $\mathbf{f}(t, \boldsymbol{x}')$, when $\boldsymbol{x}'$ ranges over almost all of the δ-neighborhood of the point $\boldsymbol{x}(t)$ in the space of $\boldsymbol{x}$ (with t fixed), i.e., the entire neighborhood except for a set of measure zero. In the notation adopted above,

$$\frac{d\boldsymbol{x}(t)}{dt} \in F\{\mathbf{f}(t, \boldsymbol{x}(t))\} \tag{2.2}$$

where

$$F\{\mathbf{f}(t, \boldsymbol{x}(t))\} \equiv \cap_{\delta>0} \cap_{\mu N=0} \overline{co}\, \mathbf{f}(t, \mathbf{B}(\boldsymbol{x}(t), \delta) - N) \tag{2.3}$$

and $\overline{co}$ refers to the convex hull of a set. N are the sets of Lebesgue measure zero.

Remarks

(1) The content of Filippov's solution is that the tangent vector to a solution, where it exists, must lie in the convex closure of the limiting values of the vector field in progressively smaller neighborhoods around the solution point. The above definition allows us to exclude sets of zero measure. This technical detail allows solutions to be defined at points even where the vector field itself is not defined, such as at the interface of two regions in a piecewise defined vector field.

(2) Definition 1 is quite general, that is, it includes more general classes of discontinuous differential equations than those with a piecewise continuous controller. Definition 1 is referred to as a Filippov's solution in this report and the solutions satisfying the classical solution theories are referred to as conventional solutions.

(3) Filippov's solution theory is useful in engineering problems because Filippov's solutions are limits of solutions with the right-hand side averaged over smaller and smaller neighborhoods. Thus, it is expected that the Filippov's trajectories of non-smooth systems will be close to the true trajectories (Paden and Sastry, 1987).

Comparison with conventional solutions

Suppose that for $t_1 < t < t_2$ the graph of the vector function $\boldsymbol{x}(t)$ extends inside the region in which the right-hand side of equation (2.1) is continuous with respect to $(t, \boldsymbol{x})$. In order that $\boldsymbol{x}(t)$ be a solution to equation (2.1) in the sense of definition 1 for these values of t, it is necessary and sufficient that it be a solution to this equation in the usual sense, i.e., that over the entire interval (t_1, t_2) it has a derivative equal to $\mathbf{f}(t, \boldsymbol{x})$.

2.1.2 Theorem on the Existence and Continuation of a Solution

Let the right-hand side of equation (2.1) be measurable† and bounded in a region Ω. Then for an arbitrary initial condition $\boldsymbol{x}(t_0) = \boldsymbol{a}$, where $(t_0, \boldsymbol{a}) \in \Omega$, a solution of equation (2.1) exists satisfying the above initial conditions which is also continuable on the interval (Filippov, 1988).

2.1.3 Theorems on the Uniqueness of the Solutions

The theorems of the uniqueness of the solution were developed separately for the cases where the discontinuity surface‡ is a single surface and the case where the discontinuity surface is the intersection of several discontinuity surfaces.

For the case of single discontinuity surface $S := \{\boldsymbol{x} : s(\boldsymbol{x}) = 0\}$, the region Ω is divided into domains Ω^- and Ω^+ which are defined as $\Omega^- = \{\boldsymbol{x} : s(\boldsymbol{x}) < 0\}$ and $\Omega^+ = \{\boldsymbol{x} : s(\boldsymbol{x}) > 0\}$, respectively. Functions $\mathbf{f}^-$ and $\mathbf{f}^+$ are defined as the right-hand sides of the dynamic equation (2.1) in the regions Ω^- and Ω^+ which are measurable and bounded. Let the functions $\mathbf{f}_i$ be continuous with respect to $x_1,...,x_n$ in Ω^- and Ω^+, and let there exist limiting values of the functions $\mathbf{f}_i$ when system states approach to an arbitrary point on the surface S from domain Ω^- to Ω^+. Vector $\mathbf{h}$ is defined as $\mathbf{h} = \mathbf{f}^+ - \mathbf{f}^-$ at all points of the discontinuity surface S. In addition, h_N is defined as the projection of $\mathbf{h}$ on the normal to the discontinuity surface S. If it is found that $h_N \leq 0$, then in the domain Ω for the system (2.1) we have the uniqueness and continuous dependence of the solution on the initial conditions. Furthermore, if we have $\mathbf{f}_N^+ > 0$ and $\mathbf{f}_N^- > 0$ (or $\mathbf{f}_N^+ < 0$ and $\mathbf{f}_N^- < 0$) at all points of S, the solution goes through S and has only one point in common with S (Filippov, 1960).

For the case where the discontinuity surface is the intersection of several surfaces, the regions Ω_j are projected on the n-dimensional state space regions S_j^n, j=1,2,...,r. The smooth surfaces

† A probability measure for a bounded region assigns nonnegative numbers to any set in the region and is countably additive, i.e., given any countable family of disjoint (nonoverlapping) sets in the region, the measure of the union of these sets is the sum of the measures of the sets.

‡ In this thesis the general discontinuity manifold is referred to as a surface.

bounding the S_j^n will be denoted by S_i^m, where m is the dimension and i is the number of the surfaces. For each $\boldsymbol{x} \in S_i^l$, the intersection of discontinuity surfaces, set $K_i^l(t,\boldsymbol{x})$ is defined as

$$K_i^l(t,\boldsymbol{x}) = F_i^l(t,\boldsymbol{x}) \cap \boldsymbol{P}_i^l(\boldsymbol{x}) \tag{2.4}$$

where $F_i^l(t,\boldsymbol{x}) = F(t,\boldsymbol{x})$ and $\boldsymbol{P}_i^l(\boldsymbol{x})$ is the set of all vectors paralleled to the l-dimensional surface S_i^l at the point on the discontinuity surface including the null vector. $H_i^l(t,\boldsymbol{x})$ is the set of vectors of $K_i^l(t,\boldsymbol{x})$ tangent to S_i^l at the point on the edge (boundary) of S_i^l.

For the case of intersecting discontinuity surface S_i^l, Theorem 1 of Filippov (1979) stated that for $t_1 < t < t_2$ in Ω, 1) each solution of (2.1) goes from one set S_i^l into another only a finite number of times, 2) there is uniqueness of the solution up to the boundary in each S_i^l, and, 3) each S_i^l possesses one of the following two properties: a) for all S_i^p abutting S_i^l the sets $H_i^p(t,\boldsymbol{x})$ are empty for all $\boldsymbol{x} \in S_i^l$, b) only one of these sets is non-empty and $K_i^l(t,\boldsymbol{x})$ is empty. Then, equation (2.1) has the property of unique solution.

2.2 Theory of the Caratheodory Differential Equations

If the n-dimensional vector-valued function $\mathbf{f}(\boldsymbol{x},t)$ is discontinuous in t and continuous in $\boldsymbol{x}$, one can use the concept of Lebesgue integral as the basis of the theory of the Caratheodory differential equations and obtain the definition of a solution to the equation $\dot{\boldsymbol{x}} = \mathbf{f}(\boldsymbol{x},t)$ (Filippov, 1988). The function $\mathbf{f}(\boldsymbol{x},t)$ is assumed to satisfy the following conditions:

Caratheodory Conditions:

In the domain D of the $(\boldsymbol{x},t)$-space, let

1) the function $\mathbf{f}(\boldsymbol{x},t)$ be defined and continuous in $\boldsymbol{x}$ for almost all t;
2) the function $\mathbf{f}(\boldsymbol{x},t)$ be measurable in t for each $\boldsymbol{x}$;
3) $|\mathbf{f}(\boldsymbol{x},t) \le \mathbf{m}(t)|$, the function $\mathbf{m}(t)$ being summable (on each finite interval if t is not bounded in the domain D).

The equation $\dot{x} = \mathbf{f}(x,t)$, where x is a scalar or a vector and the function $\mathbf{f}$ satisfies the above Caratheodory conditions is called the Caratheodory equation. A function $x(t)$ defined on an open or closed interval I is called a solution of the Caratheodory condition if it is absolutely continuous on each closed interval $[\alpha,\beta] \subset I$ and satisfies this equation almost everywhere.

Lemma (Filippov, 1988)**:** Let the function $\mathbf{f}(x,t)$ satisfy the Caratheodory conditions and let the function $x(t)$ $(a \le t \le b)$ be measurable. Then the composite function $\mathbf{f}(x(t),t)$ is measurable.

Theorem (Filippov, 1988): Consider a linear system in the vector notation

$$\dot{x} = \mathbf{A}(t)x + \mathbf{b}(t) \tag{2.5}$$

Let all the elements of the matrix $\mathbf{A}(t)$ and the vector-valued function $\mathbf{b}(t)$ be summable on each segment contained in the interval (α,β). Then for $t_0 \in (\alpha,\beta)$ the solution of system (2.5) with arbitrary initial conditions $x(t_0) = x_0$ exists on the whole interval (α,β) and is unique.

2.3 Nonsmooth Lyapunov Stability Theory

Although Lyapunov's direct method was originally developed for smooth nonlinear systems (Slotine and Li, 1991), its extension to nonsmooth systems based on Filippov's solution theory (Wu et al., 1998a; Shevitz and Paden, 1994) has provided the theoretical foundation for proper stability analysis of nonsmooth systems. The result is a theory applicable to systems with switches, for which Lyapunov functions are only piecewise smooth. There are two options when deriving a Lyapunov function for a nonsmooth system. One is the construction of a nonsmooth Lyapunov function (Shevitz and Paden, 1994; Wu and Sepehri, 2000), and the second option is to derive a smooth Lyapunov function (Wu et al., 1998a). Similar to smooth dynamic systems, the lack of a general constructive method for derivation of the Lyapunov function for any particular system is the main challenge when analyzing the stability of nonsmooth systems. In the case of nonsmooth Lyapunov functions, examination of the sign of the Lyapunov function derivative on a discontinuity surface is an additional burden. This must be done by estimating the sign of each element of a convex set, which is the intersection of a large number of convex sets containing elements related to Clarke's generalized gradient and Filippov's differential inclusion (Shevitz and Paden, 1994). However, this requires heavy mathematical machinery and may become unmanageable for large systems or when the discontinuity surface is the intersection of

several surfaces. On the other hand, the advantage of deriving a smooth Lyapunov function is avoidance of the cumbersome mathematical efforts in the estimation of its derivative. In this section, theorems on nonsmooth Lyapunov stability theory are presented.

Theorem 1 (Shevitz and Paden, 1994): Let $\dot{\boldsymbol{x}} = \mathbf{f}(\boldsymbol{x},t)$ be essentially locally bounded and $0 \in K[\boldsymbol{f}](0,t)$ in a region

$Q \supset \{\boldsymbol{x} \in \mathrm{R}^n \,|\, \|\boldsymbol{x}\| < r\} \times \{t \,|\, t_0 \le t < \infty\}$. Also, let $V: \mathrm{R}^n \times \mathrm{R} \to \mathrm{R}$ be a regular[§] function satisfying $V(0,t)=0$, and $0 < V_1(\|\boldsymbol{x}\|) \le V(\boldsymbol{x},t) \le V_2(\|\boldsymbol{x}\|)$ for $\boldsymbol{x} \ne 0$ in Q for some V_1, $V_2 \in$ class K. Then

1) $\dot{\tilde{V}}(\boldsymbol{x},t) \le 0$ in Q implies $\boldsymbol{x}(t) \equiv 0$ is a uniformly stable solution.

2) If in addition, there exists a class K functions $w(.)$ in Q with the property $\dot{\tilde{V}}(\boldsymbol{x},t) \le -w(\boldsymbol{x}) < 0$ then the solution $\boldsymbol{x}(t) \equiv 0$ is uniformly asymptotically stable.

Theorem 2 (LaSalle) (Shevitz and Paden, 1994): Let Ω be a compact set such that every Filippov solution to the autonomous system $\dot{\boldsymbol{x}} = \mathbf{f}(\boldsymbol{x})$, $\boldsymbol{x}(0) = \boldsymbol{x}(t_0)$ starting in Ω is unique and remains in Ω for all $t \ge t_0$. Let $V: \Omega \to \mathrm{R}$ be a time independent regular function such that $v \le 0$ for all $v \in \dot{\tilde{V}}$ (if $\dot{\tilde{V}}$ is the empty set then this is trivially satisfied). Define $S = \{\boldsymbol{x} \in \Omega \,|\, 0 \in \dot{\tilde{V}}\}$. Then every trajectory in Ω converges to the largest invariant set, **M**, in the closure of S.

Theorem 3 (Wu et al., 1998a): Consider a nonsmooth system described by $\dot{\boldsymbol{x}} = \mathbf{f}(\boldsymbol{x},t)$. Let $V \in \mathrm{R}^+$ be a Lyapunov function of such a system for which $x \in \mathrm{R}^n$ is a unique Filippov solution. Under conditions that V is continuous, positive and definite and $\dot{V}$ (the first-order derivative of V with respect to time) is continuous, negative and at least semi-definite, the Filippov solution to the system is stable in the sense of Lyapunov.

[§] $f(\boldsymbol{x},t): R^m \times R \to R$ is called regular if

1) for all v, the usual one-sided directional derivative $f'(\boldsymbol{x}:v)$ exisits,
2) for all v, $f'(\boldsymbol{x}:v) = \hat{f}(\boldsymbol{x}:v)$ where the generalized derivative $\hat{f}(\boldsymbol{x}:v)$ is defined as

$$\hat{f}(\boldsymbol{x}:v) = \limsup_{y \to x,\, t \downarrow o} \frac{f(y+tv) - f(y)}{t}$$

Note that examples of regular functions include smooth functions and functions that can be written as the pointwise maximum of a set of smooth functions such as $\|x\|$.

2.4 The Concept of Lyapunov Exponents

One important tool in categorizing a system's long-term behavior (or stability) is the concept of Lyapunov exponents. They have been previously employed in the area of robotics to study the stability (Ravishankar and Ghosal, 1999; Wu et al. 2001) and controllability (Grune 1998) of smooth dynamical systems. Lyapunov exponents, λ_i (i=1,...,n), are defined as the average exponential rates of divergence or convergence of nearby orbits in the phase plane and can be considered as the growth rate of the length of each linearized vector over a long period of time (note that *lim* can be replaced by *lim sup* in proving the existence of exponents):

$$\lambda_i = \lim_{t\to\infty} \frac{1}{t} \ln \frac{\|\delta \boldsymbol{x}_i(t)\|}{\|\delta \boldsymbol{x}_i(t_0)\|} \qquad (i = 1,...,n) \tag{2.6}$$

In (2.6), $\|\delta \boldsymbol{x}_i(t)\|$ and $\|\delta \boldsymbol{x}_i(t_0)\|$ denote the length of the i^{th} principal axis of the infinitesimal n-dimensional hyperellipsoid at final and initial times, t and t_0, respectively, and the existence of the $\lim_{t\to\infty}$ can be proved using the Oseledet's multiplicative ergodic theorem (Oseledec, 1968).

If certain non-generic cases with non-hyperbolic attractors are ignored, the signs of the spectrum** of Lyapunov exponents (+, 0, -) can be used to infer the kind of steady-state behavior (equilibrium point, limit cycle, quasi-periodic, or chaotic) the system will ultimately show (Bockman, 1991) and determine the stability of quasi-periodic and chaotic behavior as well as that of equilibrium points and periodic solutions (Parker and Chua, 1989). A stable steady state associated with an attracting fixed point has negative Lyapunov exponents and a stable periodic state associated with an attracting periodic orbit has one zero and other negative Lyapunov exponents. Similarly, a stable quasiperiodic (superposition of periodic) attractor with k frequencies has k zero Lyapunov exponents and the rest are negative (Eckmann and Ruelle, 1985). In a one-dimensional system (Medio and Lines, 2001):

- If the orbit of x_0 converges to a stable periodic orbit, $\lambda(x_0) < 0$.
- If the orbit of x_0 is an unstable periodic orbit, $\lambda(x_0) > 0$.

** Here, the specrum of Lyapunov exponents refers to the complete set of n Lyapunov exponents associated with an n-dimensional phase space.

- If the orbit of x_0 is not periodic or asymptotically periodic (but bounded) and $\lambda(x_0) > 0$, then the orbit is chaotic.
- If the orbit of x_0 converges to a quasiperiodic (aperiodic, nonchaotic) orbit, $\lambda(x_0) = 0$.
- If the orbit of x_0 converges to a periodic orbit that is nonhyperbolic (at bifurcation points) $\lambda(x_0) = 0$.

Conversely, it is possible to deduce from the negativity of the Lyapunov exponents that the ergodic[††] measure[‡‡] describes a steady or a period state (Eckmann and Ruelle, 1985). For a continuous-time dynamical system with all non-zero Lyapunov exponents, if all Lyapunov exponents are negative, the system has an attracting fixed point. For a continuous-time dynamical system with all but one negative Lyapunov exponents, the system either has a fixed point or an attracting periodic orbit (when $\lambda_1 = 0$). In a two-dimensional system:

- $\lambda_1 = 0$, $\lambda_2 < 0$: the system will have fixed points or an attracting period orbit.
- $\lambda_1 > 0$, $\lambda_2 = 0$: the system will have fixed points or a repelling period orbit.
- λ_1 and λ_2 both nonvanishing: the system will have a hyperbolic fixed point. Depending on the sign of λ_1 and λ_2, the fixed point can be attracting or stable ($\lambda_i < 0$, i=1,2), repelling or unstable ($\lambda_i > 0$, i=1,2), or saddle type ($\lambda_1 < 0$ and $\lambda_2 > 0$).

In three or more dimensional systems, an orbit with a positive Lyapunov exponent may be thought of as chaotic or with sensitive dependence on initial conditions provided that the trajectory is bounded and is not converging to an unstable periodic orbit or other limit set (fixed point) on which the dynamics is simple (Stuart and Humphries, 1998; Nusse and Yorke, 1998). Chaotic orbits never converge to a stable fixed point or periodic point, but exhibits sustained instability while remaining forever in a bounded region of the state space. In other words, a discrete or continuous-time dynamical system is chaotic if its typical orbits are aperiodic, bounded, and such that nearby orbits separate fast in time (Medio and Lines, 2001). One or

[††] If an invariant probability measure may not be decomposable into several different pieces, each of which again invariant, the measure is said to be indecomposable of ergodic.

[‡‡] Within the context of Ergodic Theory (which says that the time average equals a space average), the weight with which the space average has to be taken is an invariant measure, ρ', and satisfies the equation $\rho'[f^{-t}(E)] = \rho'(E), t > 0$ where E is the subset of points of $\mathbf{R}^m$ and $f^{-t}(E)$ is the set obtained by evolving each of the points in E backwards during time t (Eckmann and Ruelle, 1985).

another (but not all) of the above properties may be found in nonchaotic systems as well. For example, a linear system characterized by a unique unstable fixed point will have aperiodic orbits separating exponentially fast but they will not be bounded. Also, quasi-periodic systems will have aperiodic, bounded solutions but not separating orbits.

It may be useful to note that the notions of sensitive dependence on initial conditions and divergence of nearby trajectories are meaningful and useful only for those systems that are bounded and have attractors defined as a final state space point, curve, area, and so on that a number of distinct trajectories would eventually approach in state space (Thompson and Stewart, 2002). To illustrate these issues in a counterexample, imagine a ball perched precariously at the unstable equilibrium point at the top of a hill surrounded by an infinite plane surface. This situation displays sensitive dependence on initial conditions since the path that the ball takes depends sensitively on how it is disturbed and pushed away from the top of the hill. If the hill and plane are frictionless, then the ball keeps rolling forever, and there are no bounded trajectories. If friction is present, then the ball eventually stops rolling at some point determined by the direction and size of the initial "push". Each final state is associated with a particular initial condition. There is no attracting region of the state space, which pulls in trajectories from some finite basin of attraction (Hilborn, 2000). In other words, sensitive dependence on initial conditions doesnot imply positive Lyapunov exponents (Demir and Kocak, 2001).

Expliting the fact that Lyapunov exponents measure the rate of contraction or expansion, they can be used as a simple criterion to distinguish between conservative and dissipative systems (Kapitaniak, 2000). For $\sum_{i=1}^{n}\lambda_i = 0$ the volume of a solution in phase space is conserved and in this case we have a conservative system. In dissipative systems, the phase is contracted with $\sum_{i=1}^{n}\lambda_i < 0$, i.e., at least one Lyapunov exponent is negative, the sum of all exponents is negative, and will have an attractor (Wolf et al, 1985). For $\sum_{i=1}^{n}\lambda_i > 0$, the system is expanding and may never reach any attractor.

Although the above discussion is mainly based on the previous works on smooth dynamic systems, recent results of Kuntz (2000) have provided a positive answer to the question of

whether Lyapunov exponents can correctly reflect the dynamical behavior of a non-smooth system such as the pendulum with dry friction. The work serves as a hint that for predictions of the dynamics, one can "rely" on Lyapunov exponents also in nonsmooth dynamical systems (Kuntz, 2000).

2.4.1 Oseledet's Noncommutative Ergodic Theorem

For smooth dynamical systems, a powerful tool to prove the existence of $\lambda_i = \lim_{t\to\infty} \frac{1}{t} \ln \frac{\|\delta \boldsymbol{x}_i(t)\|}{\|\delta \boldsymbol{x}_i(t_0)\|}$ $(i = 1,...,n)$ in (2.6) is given by Oseledet's multiplicative ergotic theorem (Oseledec, 1968):
Let X be a measure space with normalized measure μ on which a classical dynamical system in defined. For example X could be a Euclidean space, with the dynamical system defined by the equation

$$\frac{d\boldsymbol{x}(t)}{dt} = \mathbf{f}(\boldsymbol{x}) \tag{2.7}$$

where $\mathbf{f}(\boldsymbol{x})$ is a smooth vector function. Let T_x^t denote the state at time t of the dynamical system which at time 0 was at $\boldsymbol{x}$. This yields the flow $\{T^t\}$. The tangent space at $\boldsymbol{x}$ is mapped onto the tangent space at $T^t\boldsymbol{x}$ by the differential $(dT^t)_x$, the linear part at $\boldsymbol{x}$ of the nonlinear map T^t, where $\mathrm{R}(t,\boldsymbol{x})$ is the matrix corresponding to $(dT^t)_x$. A function $\mathrm{R}(t,\boldsymbol{x})$ satisfying the following relation is called a multiplicative cocycle with respect to the dynamical system $\{T^t\}$:

$$\mathrm{R}(t+s, \boldsymbol{x}) = \mathrm{R}(t, T^t\boldsymbol{x})\ \mathrm{R}(s, \boldsymbol{x}) \tag{2.8}$$

For example, the fundamental matrix $\mathrm{R}(t,\boldsymbol{x})$ of the system of linear differential equations is a multiplicative cocycle.

We shall consider only cocycles R for which

$$\sup_{-1\le\theta\le 1} \ln^+ \left\|\mathsf{R}^{\pm 1}(\theta,\boldsymbol{x})\right\| \in L^1(X,\mu) \tag{2.9}$$

Multiplicative Ergodic Theorem

If condition (2.9) is satisfied, then for μ-almost all $\boldsymbol{x}$ Lyapunov characteristic numbers (or Lyapunov characteristic exponents) of all orders, $\vartheta_\pm(\boldsymbol{x}, e^k; \mathsf{R})$, defined as

$$\vartheta_{\pm}(\boldsymbol{x},\boldsymbol{e}^k;\mathsf{R}) = \lim_{t\to\pm\infty}\frac{1}{|t|}\ln\lambda(\boldsymbol{e}^k,\mathsf{R}(t,\boldsymbol{x})) \tag{2.10}$$

exist, where $\boldsymbol{e}^k$ is a subspace generated by an orthogonal set $\boldsymbol{e}_1,\boldsymbol{e}_2,\ldots,\boldsymbol{e}_k$ in R^m and $\lambda(\boldsymbol{e}^k,\mathsf{R}(t,\boldsymbol{x}))$ is the coefficient of expansion in the k-dimensional direction $\boldsymbol{e}^k$ (Oseledec, 1968).

Particularly, for a system of linear differential equations

$$\frac{d\boldsymbol{y}}{dt} = \mathbf{a}(T^t\boldsymbol{x})\boldsymbol{y} \tag{2.11}$$

where the measurable matrix function $\mathbf{a}(\boldsymbol{x})$ satisfies

$$\|\mathbf{a}(\boldsymbol{x})\| \in L^1(X,\mu) \tag{2.12}$$

one can prove the regularity and existence of characteristic numbers using Tonelli's theorem (Oseledec, 1968). In this proof, $\mathsf{R}(t,\boldsymbol{x})$ is, for almost all $\boldsymbol{x}$, a continuous function of t and is differentiable for almost all t. However, it is valid even if $\mathsf{R}(t,\boldsymbol{x})$ is piecewise continuous function of t. Further details are available in (Oseledec, 1968).

2.4.2 Calculation of Lyapunov Exponents for Smooth Dynamic Systems

Since, in general, it is almost impossible to determine the Lyapunov exponents of complicated systems analytically, they often have to be calculated numerically (Kunze, 2000). To calculate the exponents using discrete QR algorithm, the fiducial trajectory is created by integrating the nonlinear equations of motion for some post-transient initial conditions. Simultaneously, the linearized equations of motion are integrated for n different initial conditions defining an arbitrarily oriented frame of n orthonormal vectors anchored to the fiducial trajectory (Wolf et al., 1985). This leads to the following set of combined nonlinear and linearized equations (Parker and Chua, 1989):

$$\begin{Bmatrix}\dot{\boldsymbol{x}}\\ \dot{\psi}_t\end{Bmatrix} = \begin{Bmatrix}\boldsymbol{f}(\boldsymbol{x})\\ \boldsymbol{F}(t)\psi_t\end{Bmatrix} \tag{2.13}$$

where ψ_t is called the state transition matrix of the linearized system $\delta\boldsymbol{x}(t) = \psi_t\,\delta\boldsymbol{x}_0$ and the variational equation $\dot{\psi}_t = \boldsymbol{F}(t)\psi_t$ is a matrix-valued time-varying linear differential equation

derived by linearization of the nonlinear vector field along the trajectory $x(t)$. The Jacobian $F(t)$ is defined as

$$F(t) = \left.\frac{\partial f}{\partial x^T}\right|_{x=x(t)} \tag{2.14}$$

and the initial conditions for numerical integrations are $\begin{Bmatrix} x(t_0) \\ \psi_t(t_0) \end{Bmatrix} = \begin{Bmatrix} x_0 \\ I \end{Bmatrix}$ where I is the identity matrix.

Lyapunov exponents are calculated by following the evolution of the area of the hyperellipsoid spanned by $\{\delta x_1, \cdots, \delta x_n\}$ via separately following the evolutions of $\delta x_1, \delta x_2, \ldots, \delta x_n$ using an integration method. Note that $\delta x(t)$ may be interpreted in two ways (Parker and Chua, 1989): as an infinitesimal perturbation of the original nonlinear system or as a vector-valued solution of the linearized system.

The problem that may occur, however, is that $\delta x_1(t), \delta x_2(t)$, ..., or $\delta x_n(t)$ may tend to align as $t \to \infty$. This alignment makes the calculations unreliable (Parker and Chua, 1989). To resolve the problem, $\delta x_1, \delta x_2, \ldots, \delta x_n$ are reorthonormalized at each integration step. This is done by including the Gram-Schmidt Reorthonormalization (GSR) scheme in the calculation procedure. Gram-Schmidt reorthonormalization generates an orthonormal set $\{u_1, \cdots, u_n\}$ of n vectors with the property that $\{u_1, \cdots, u_i\}$ spans the same subspace as $\{\delta x_1, \cdots, \delta x_i\}$ for i=1,...,n.

Figure 2.1 shows the geometrical interpretation of the orthonormalization for $\delta x_1^{(k)}$ and $\delta x_2^{(k)}$ (k=1,...,K and K is the number of integration steps), i.e, their orthogonalization into $v_1^{(k)}$ and $v_2^{(k)}$ normalization into $u_1^{(k)}$ and $u_2^{(k)}$. The vector $v_1^{(k)}$ is equal to $\delta x_1^{(k)}$, and the vector $u_1^{(k)}$ is a normalized version of $v_1^{(k)}$. The factor $\left\langle \delta x_2^{(k)}, u_1^{(k)} \right\rangle$ is the length of the orthogonal projection of $\delta x_2^{(k)}$ onto $u_1^{(k)}$. Normalization of $v_2^{(k)}$ yields the orthonormal vector $u_2^{(k)}$ and the area of the hyperellipsoid spanned by $\left\{\delta x_1^{(k)}, \delta x_2^{(k)}\right\}$ is

$$\text{Volume } \left\{\delta x_1^{(k)}, \delta x_2^{(k)}\right\} = \left\|v_1^{(k)}\right\| \cdot \left\|v_2^{(k)}\right\| \tag{2.15}$$

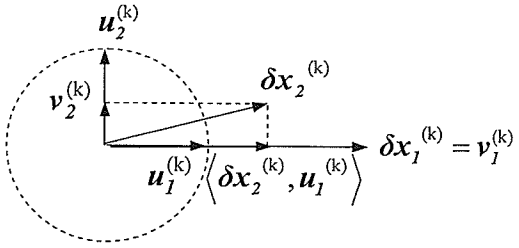

Fig. 2.1 Orthonormalization of two vectors $\delta x_1^{(k)}$ and $\delta x_2^{(k)}$.

The above approach for calculating Lyapunov exponents for ODEs is not directly applicable to experimental data as the linear system is not available (Wolf et al. 1985). Experimental data typically consist of discrete measurements of a single observable. The well-known technique of phase space reconstruction with delay coordinated makes it possible to obtain an atttractor from such a time series whose Lyapunov spectrum is identical to that of the original attractor (Wolf et al. 1985). Wolf et al. (1985) developed a method for estimation of Lyapunov exponents for such a reconstructed attractor. The approach involves working in a reconstructed attractor, examining orbital divergence on length scales that are always as small as possible, and using an approximate GSR procedure in the reconstructed phase space as necessary. For more details, interested readers are reffered to (Wolf et al., 1985).

2.4.3 Demonstrative Example

The above procedure of calculating Lyapunov exponents in smooth systems is demonstrated on the simple three-dimensional Lorenz system with the following dynamic equations (Parker and Chua, 1989):

$$\begin{cases} \dot{x}_1 = a\,(x_1 + x_2) \\ \dot{x}_2 = x_1(c - x_3) - x_2 \\ \dot{x}_3 = x_1 x_2 - b x_3 \end{cases} \tag{2.16}$$

where a, b, and c are constants.

From (2.14), the linearized equations of motion are:

$$\begin{bmatrix} \dot{\psi}_{11} & \dot{\psi}_{12} & \dot{\psi}_{13} \\ \dot{\psi}_{21} & \dot{\psi}_{22} & \dot{\psi}_{23} \\ \dot{\psi}_{31} & \dot{\psi}_{32} & \dot{\psi}_{33} \end{bmatrix} = \begin{bmatrix} a & a & 0 \\ c - x_3 & -1 & -x_1 \\ x_2 & x_1 & -b \end{bmatrix} \begin{bmatrix} \psi_{11} & \psi_{12} & \psi_{13} \\ \psi_{21} & \psi_{22} & \psi_{23} \\ \psi_{31} & \psi_{32} & \psi_{33} \end{bmatrix} \tag{2.17}$$

To start the calculations, let δx_1, δx_2, and δx_3 be three linearly independent vectors anchored to the fiducial trajectory of the above three dimensional system at x. The initial perturbation vector is $\delta x_0 = (\delta x_1, \delta x_2, \delta x_3)$ and the arbitrary initial states $x_0 = (x_{1_0}, x_{2_0}, x_{3_0})$ belong to the basin of attraction of the attractor under study.

Define $\delta x_1^{(0)} := \delta x_1$ and $u_1^{(0)} := \delta x_1 / \|\delta x_1\|$. Likewise, define $\delta x_2^{(0)}$ and $u_2^{(0)}$ with respect to δx_2, and, $\delta x_3^{(0)}$ and $u_3^{(0)}$ with respect to δx_3. Also, define $x^{(0)} := x_0$ and $x^{(k)} := \chi(x^{(k-1)})$ for k=1,...,K where χ is the solution of original nonlinear equation $\dot{x} = f(x)$. Calculation of the Lyapunov exponents λ_i $(i = 1 \cdots 3)$ evolves by step-by-step integrating the variational equation (2.17) from $u_i^{(0)}$ $(i = 1 \cdots 3)$ with the time-step of h seconds.

At the first step:

$$\begin{cases} \delta x_1^{(1)} := \delta x(h; u_1^{(0)}, x^{(0)}) := \psi(x^{(0)}) u_1^{(0)} \\ \delta x_2^{(1)} := \delta x(h; u_2^{(0)}, x^{(0)}) := \psi(x^{(0)}) u_2^{(0)} \\ \delta x_3^{(1)} := \delta x(h; u_3^{(0)}, x^{(0)}) := \psi(x^{(0)}) u_3^{(0)} \end{cases} \tag{2.18}$$

To find all three Lyapunov exponents, the set of three linearly independent perturbation vectors δx_i is repeatedly integrated and orthonormalized.

At the k^{th} step, the perturbation equations are

$$\begin{cases} \delta x_1^{(k)} := \delta x(h; u_1^{(k-1)}, x^{(k-1)}) := \psi(x^{(k-1)}) u_1^{(k-1)} \\ \delta x_2^{(k)} := \delta x(h; u_2^{(k-1)}, x^{(k-1)}) := \psi(x^{(k-1)}) u_2^{(k-1)} \\ \delta x_3^{(k)} := \delta x(h; u_3^{(k-1)}, x^{(k-1)}) := \psi(x^{(k-1)}) u_3^{(k-1)} \end{cases} \tag{2.19}$$

and the orthonormalization equations are

$$\begin{cases} v_1^{(k)} = \delta x_1^{(k)} \\ u_1^{(k)} := v_1^{(k)} / \|v_1^{(k)}\| \\ v_2^{(k)} = \delta x_2^{(k)} - \langle \delta x_2^{(k)}, u_1^{(k)} \rangle u_1^{(k)} \\ u_2^{(k)} := v_2^{(k)} / \|v_2^{(k)}\| \\ v_3^{(k)} = \delta x_3^{(k)} - \langle \delta x_3^{(k)}, u_1^{(k)} \rangle u_1^{(k)} - \langle \delta x_3^{(k)}, u_2^{(k)} \rangle u_2^{(k)} \\ u_3^{(k)} := v_3^{(k)} / \|v_3^{(k)}\| \end{cases} \tag{2.20}$$

At the K^{th} stage, the orthonormalization produces three vectors $\{v_1, v_2, v_3\}$ and for the K chosen large enough, the exponents are:

$$\begin{cases} \lambda_1 \approx \dfrac{1}{Kh}\sum_{k=1}^{K} \ln\left\|v_1^{(k)}\right\| \\ \lambda_2 \approx \dfrac{1}{Kh}\sum_{k=1}^{K} \ln\left\|v_2^{(k)}\right\| \\ \lambda_3 \approx \dfrac{1}{Kh}\sum_{k=1}^{K} \ln\left\|v_3^{(k)}\right\| \end{cases} \tag{2.21}$$

2.4.4 Calculation of Lyapunov Exponents for Systems with Discontinuities

One of the major requirements in calculation of the variational equation is linearizability of the original state-space equations. This introduces a major problem in calculation of Lyapunov exponents for systems with discontinuity. The problem is addressed by Muller (1995) and Kunze (2000) who have generalized the calculation procedure to systems with discontinuity. The extension is based on normal linearization of dynamic equations in smooth regions of motion supplemented by transition conditions at the instant of discontinuities:

Let the vector $\boldsymbol{x}=(x_1,...,x_n)$ denote the states of the original nonlinear system. The nonlinear system behaves smoothly before (region 1) and after (region 2) the first discontinuity instant, t_1. The equations of motion in each region of motion are as follows:

Region1 : $$\dot{\boldsymbol{x}} = \boldsymbol{f}_1(\boldsymbol{x}) \ , \ \boldsymbol{x}(t_0) = \boldsymbol{x}_0 \quad ; \quad t_0 < t < t_1 \tag{2.22}$$

Region2 : $$\dot{\boldsymbol{x}} = \boldsymbol{f}_2(\boldsymbol{x}) \ , \ \boldsymbol{x}(t_1) = \boldsymbol{x}(t_{1+}) \quad ; \quad t_1 < t < t_2 \tag{2.23}$$

The variation equation in each smooth region of motion is obtained by linearizing (2.22) and (2.23) before and after t_1:

Region1 : $$\delta\dot{\boldsymbol{x}} = \boldsymbol{F}_1(t)\,\delta\boldsymbol{x} \ , \ \delta\boldsymbol{x}(t_0) = \delta\boldsymbol{x}_0 \quad ; \quad t_0 < t < t_1 \tag{2.24}$$

Region2 : $$\delta\dot{\boldsymbol{x}} = \boldsymbol{F}_2(t)\,\delta\boldsymbol{x} \ , \ \delta\boldsymbol{x}(t_1) = \delta\boldsymbol{x}_1 \quad ; \quad t_1 < t < t_2 \tag{2.25}$$

where $\boldsymbol{F}_1(t)$ and $\boldsymbol{F}_2(t)$ are Jacobians defined as:

$$\boldsymbol{F}_1(t) = \left.\frac{\partial \boldsymbol{f}_1}{\partial \boldsymbol{x}^T}\right|_{x=x(t)} \quad ; \quad \boldsymbol{F}_2(t) = \left.\frac{\partial \boldsymbol{f}_2}{\partial \boldsymbol{x}^T}\right|_{x=x(t)} \tag{2.26}$$

Muller (1995) and Kunze (2000) proved that, instead of linearizing the nonlinear equations at discontinuity instant, the variational equations can be evaluated using the indicator function, $h(\boldsymbol{x})$, and the transition function, $\boldsymbol{g}(\boldsymbol{x})$, both defined based on the physical behavior of the system. The indicator function is at least one time continuously differentiable function and determines the instant of the discontinuity. The transition function describes the transition conditions of system states at each instant of discontinuity. It relates the values of the system states just after and just before the discontinuity instant and can be defined using the physical characterists of each system. The general form of the variational equations of motion at the instant of discontinuity, t_1, is (Muller, 1995; Kunze, 2000):

$$\delta \boldsymbol{x}_+ = \boldsymbol{G}_1(\boldsymbol{x}_-)\delta \boldsymbol{x}_- + [\boldsymbol{G}_1(\boldsymbol{x}_-)\boldsymbol{f}_1(\boldsymbol{x}_-) - \boldsymbol{f}_2(\boldsymbol{x}_+)]\frac{\boldsymbol{H}_1(\boldsymbol{x}_-)\delta \boldsymbol{x}_-}{\boldsymbol{H}_1(\boldsymbol{x}_-)\boldsymbol{f}_1(\boldsymbol{x}_-)} \tag{2.27}$$

where $\boldsymbol{H}_1(\boldsymbol{x}_-) = \left.\frac{\partial h_1(\boldsymbol{x})}{\partial \boldsymbol{x}^T}\right|_{x=x(t_{1\_})}$ and $\boldsymbol{G}_1(\boldsymbol{x}_-) = \left.\frac{\partial \boldsymbol{g}_1(\boldsymbol{x})}{\partial \boldsymbol{x}^T}\right|_{x=x(t_{1\_})}$ are the Jacobians of the indicator function $h_1(\boldsymbol{x})$ and the transition condition $\boldsymbol{g}_1(\boldsymbol{x})$, and plus and minus signs denote the values just after (t_{1_+}) and before ($t_{1\_}$) the discontinuity instant, respectively.

If the system trajectory returns to the original region at the discontinuity instant $t=t_2$, the transition condition of the linearized equations is:

$$\delta \boldsymbol{x}_+ = \boldsymbol{G}_2(\boldsymbol{x}_-)\delta \boldsymbol{x}_- + [\boldsymbol{G}_2(\boldsymbol{x}_-)\boldsymbol{f}_2(\boldsymbol{x}_-) - \boldsymbol{f}_1(\boldsymbol{x}_+)]\frac{\boldsymbol{H}_2(\boldsymbol{x}_-)\delta \boldsymbol{x}_-}{\boldsymbol{H}_2(\boldsymbol{x}_-)\boldsymbol{f}_2(\boldsymbol{x}_-)} \tag{2.28}$$

with the Jacobian matrices $\boldsymbol{H}_2$ and $\boldsymbol{G}_2$ similarly derived as $\boldsymbol{H}_1$ and $\boldsymbol{G}_1$.

Equations (2.22-2.28) represent the generalized method of calculating the variational equation and can be used to calculate the Lyapunov exponents of the systems with discontinuity (Muller, 1995).

2.4.5 Calculation of the Basin of Attraction

The basin of attraction of the system can be numerically determined by adopting the algorithm developed by Nusse and Yorke (1998). First, the region of interest is divided into a number of grid boxes where the grid box at the origin of the state-space (also called 'center box') contains the stable equilibrium point. Next, the size of neighboring grid boxes are chosen and each neighboring box is tested for the following conditions: (*i*) the trajectory, starting from the

neighboring grid box, must enter the center box within a specific time period T_0; (*ii*) the trajectory, once having entered the center box, remains there ever after. If the above two conditions hold, the neighboring grid box belongs to the same basin of attraction.

2.5 Mickens' Nonstandard Discretization Technique

In order to reduce numerical instabilities while calculating numerical solutions of dynamic systems, Mickens (2002) introduced a framework for nonstandard finite difference discretization (NSFΔ) of nonlinear differential equations which is essentially discrete representation of the system constructed according to the following rules:

Rule 1. The orders of the discretized derivatives should be equal to the orders of the corresponding derivatives of the differential equations. If the orders of the discretized derivatives are larger than those of the differential equation, spurious solutions (convergence to false steady-state) and scheme-dependent (contrived) numerical instabilities would occur.

Rule 2. Discrete representations for derivatives must, in general, have nontrivial denominator functions. For example, the discrete first derivative of the continuous equation $\frac{dx}{dt} = f(x)$ in nonstandard scheme takes the form:

$$\frac{dx}{dt} \rightarrow \frac{x^{(k+1)} - x^{(k)}}{\phi(h, R^*)} \tag{2.29}$$

where

$$\phi(h, R^*) = \frac{1 - e^{-R^* h}}{R^*} \tag{2.30}$$

The value of R^* is determined as the maximum value of R_i:

$$R^* \equiv \max\{| R_i |; i = 1,2,..I\} \tag{2.31}$$

where R_i is defined as

$$R_i \equiv \left.\frac{df}{dx}\right|_{x=\bar{x}^{(i)}} \tag{2.32}$$

and $\{\bar{x}^{(i)}; i = 1,2,..I\}$ is the set of the system's fixed points.

Thus, $0 < \phi(h, R^*) < \frac{1}{R^*}$ and the function ϕ can be interpreted as a "renormalized" or "rescaled" time step-size such that its value is never larger than the smallest time scale of the system $T^* = \frac{1}{R^*}$.

Rule 3. Nonlinear terms should, in general, be replaced by nonlocal discrete representations. For example, the term x^2 can be represented by $x^{(k+1)}x^{(k)}$ or even $2(x^{(k)})^2 - x^{(k+1)}x^{(k)}$.

Rule 4. Special conditions that hold for the solutions of the differential equations should also hold for the solution of the finite difference scheme. For example, for many dynamical systems a condition of positivity holds for the dependent variable. If the numerical scheme leads to solutions that can violate this condition, then numerical instabilities will eliminate any possibility of obtaining meaningful results.

2.6 Convergence of the Computed Solutions of Discontinuous Differential Equations to the Exact Solution

Filippov (2001) has shown that in order to perform approximate computations of differential equations with discontinuous right-hand sides, one can use the well-known approximate Runge-Kutta (of any order) without entering the arrangements of the lines and surfaces of discontinuity into the computer program.

Suppose the following conditions are fulfilled:

1) The differential equation and the initial condition

$$\frac{dx}{dt} = \mathbf{f}(t, x), \quad x(t_0) = x_0, \quad (t_0, x_0) \in G \tag{2.33}$$

are defined in the bounded domain G of the space t, x ($t \in \mathrm{R}^1, x \in \mathrm{R}^n, n \geq 1$). The vector-function $\mathbf{f}$ is bounded. The domain G consists of a finite number of domains G_i, i=1,2,…,q in each of which the function $\mathbf{f}$ is continuous, and the sets $\mathbf{M}$ of measure zero are the closures of the sets of discontinuity points.

2) Each of the domains G_i satisfies the condition γ from (Filippov, 1988; Sec. 6), i.e., for almost all t the section of the boundary of the domain G_i by the plane t=*const.* coincides with the boundary of the section of the domain G_i by this plane.

3) At each point $(t,\boldsymbol{x}) \in \mathbf{M}$ the vector-function $\mathbf{f}$ must assume a value equal to the limit, as $k \to \infty$, of the values $\mathbf{f}(t^{(k)}, \boldsymbol{x}^{(k)})$ with respect to any sequence $(t^{(k)}, \boldsymbol{x}^{(k)}) \to (t, \boldsymbol{x})$ consisting of points of discontinuity of the function $\mathbf{f}$ (or for $(t,\boldsymbol{x}) \in \mathbf{M}$ the value $\mathbf{f}(t,\boldsymbol{x})$ must belong to the least convex set which contains these limits).

4) In order to compute an approximate solution of (2.33) on the interval $[t_0, t_0 + t_f]$, we take a lattice $t^{(i)} = t_0 + ih, i = 1,2,...,N$ $(Nh = t_f)$, and consequently calculate the values $\boldsymbol{x}^{(i)}$ of the approximate solution a the points t_i with the use of some method so that

$$\boldsymbol{x}^{(i)} = \boldsymbol{x}^{(i-1)} + h\sum_{j=1}^{k} \alpha_j \mathbf{f}(t + \beta_j h, \boldsymbol{x}^{(i-1,j)}), \quad t^{(i)} = t^{(i-1)} + h \tag{2.34}$$

where all $\alpha_j, \beta_j \in [0,1]$, $\alpha_1 + ... + \alpha_k = 1$, $|\boldsymbol{x}^{(i-1,j)} - \boldsymbol{x}^{(i-1)}| \le cmh$. The numbers α_j, β_j, c, k and the technique of finding the points $\boldsymbol{x}^{(i-1,j)}$ are determined by the chosen method, $m = \sup|\mathbf{f}|$ in G.

Euler's method and the methods of Runge-Kutta of any order satisfy these conditions (Filippov, 2001).

Theorem (Filippov, 2001): If the solution $\boldsymbol{x}(t)$ of problem (2.33) in the sense of definition 1 in Section 2.1.1 for $t_0 \le t \le t_0 + t_f$ exists and is unique (and is also unique on any smaller interval $[t_0, t_0 + t'], t' < t_f$), then the approximate solution obtained by method (2.34) exists, for a sufficiently small h, on the same interval and, as $h \to 0$, converges uniformly to $\boldsymbol{x}(t)$ on this interval, including the cases where the solution $\boldsymbol{x}(t)$ has sections of sliding mode, which pass along the line or surface of discontinuity of the function $\mathbf{f}$.

According to the above theory, an approximate solution is proven to converge to the exact one as the mesh width of the lattice decreases.

Chapter 3

Description of the System Under Study

3.1 Experimental Test Station

The experimental test rig is shown in Fig. 3.1. The hydraulic circuit consists of an actuator controlled by a Moog D765 high-performance, closed-center nozzle-flapper servovalve, mounted on a reinforced steel table. The power supply is capable of supplying filtered fluid at a maximum pressure of 3000 *psi*. The actuator has an annulus area of 0.98 in^2 and a 24 *in* stroke. The servovalve can flow 8.98 *Gallons/min* at 3000 *psi* and has a rise time of 2 *ms*. It uses a mechanical feedback spring with a linear variable differential transformer (LVDT) that measures the position of the spool. The LVDT output (and hence the position of the valve spool) can also be monitored and recorded. Two Ashcroft transducers with a 0-3000 *psi* range and a full-scale accuracy of ±0.5% relay fluid pressure information at the supply and return ports of the servovalve. Two Sensotech-FPG transducers with a range of 0-3000 *psi* and a full-scale accuracy of ±0.1% measure the fluid pressure at the actuator chambers. A rotary encoder with a resolution of 1024 *counts/revolution* (linear resolution of 0.0015 *in*) establishes the relative position of the actuator.

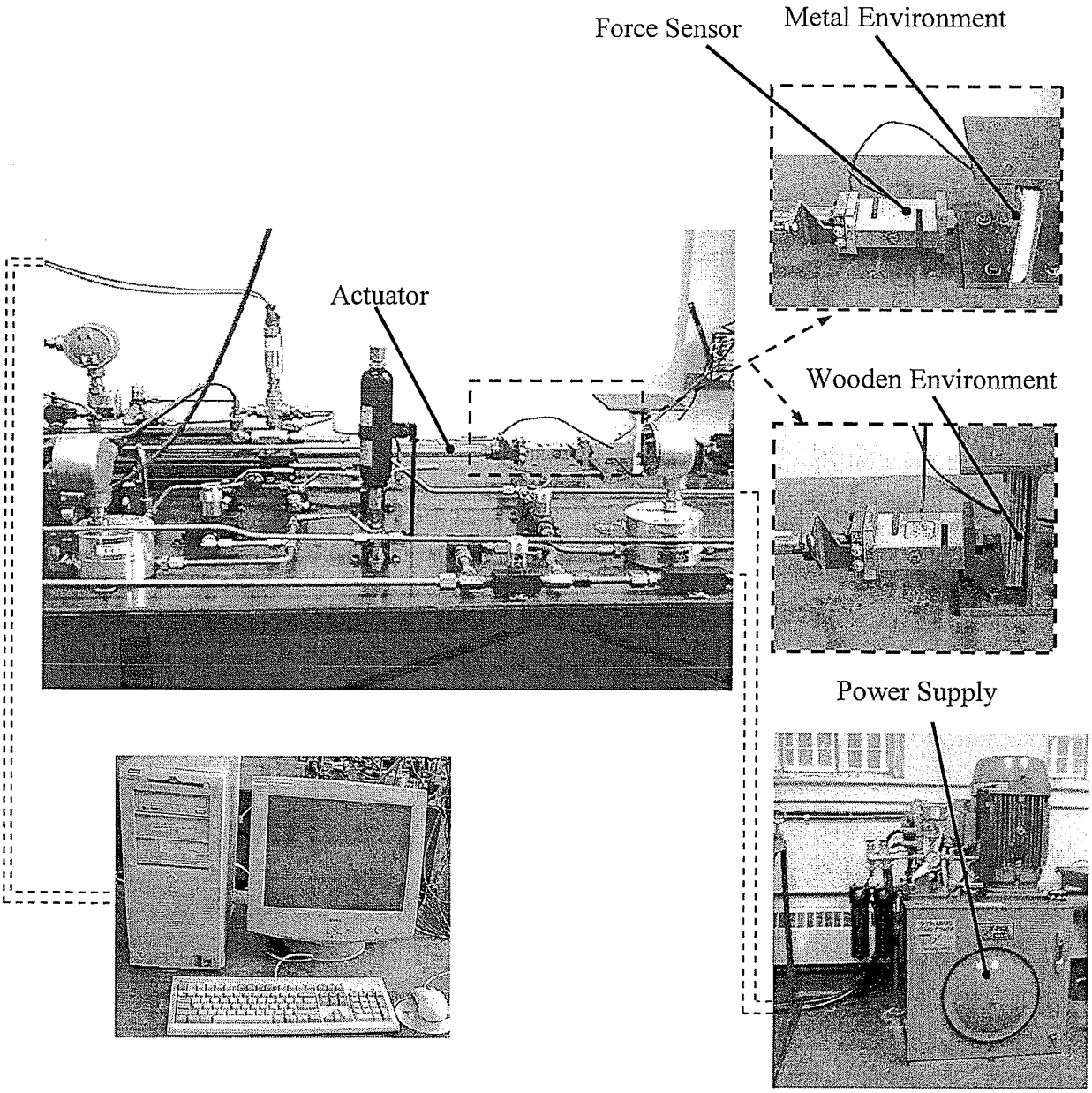

Fig. 3.1 Schematic of the experimental test rig.

Aluminum sheet and wooden plate, bolted to an I-beam mounted to the test station base, are used to represent the environment with different stiffnesses. An S-beam type load cell detects and measures the contact force between the actuator and the environment. To further enhance the point contact between the actuator end-point and the environment, a spherical surface is attached to the end-point of the actuator. This makes the actual configuration of contact similar to the Hertz contact model (Timoshenko and Goodier, 1970), which assumes a point contact between the manipulator tip and the environment surface.

The data acquisition system is comprised of a personal computer responsible to control the servovalve. A DAS-16F input/output board is installed in the PC and is capable of monitoring 16 single-ended analog to digital input channels and supporting 2 channels of digital to analog outputs. All sensor outputs are directed to the appropriate I/O board with the exception of the position encoder, which is supported by an independent Metrabyte M5312 quadrature incremental encoder card.

3.2 Mathematical Models

Complete mathematical modeling of the hydraulic actuator interacting with the non-moving environment is described below.

3.2.1 Hydraulic Actuator Dynamic Equations

The system is composed of a double-ended horizontal hydraulic actuator heading towards the desired position, x_{des}, but coming in contact with a non-moving unexpected environment (Fig. 3.2). The equation of motion of the system is described by the following equation:

$$m\ddot{x} = A(P_i - P_o) - F_f - F_{env} \tag{3.1}$$

where x is the piston position, F_f is the friction force, F_{env} is the environment reaction force,

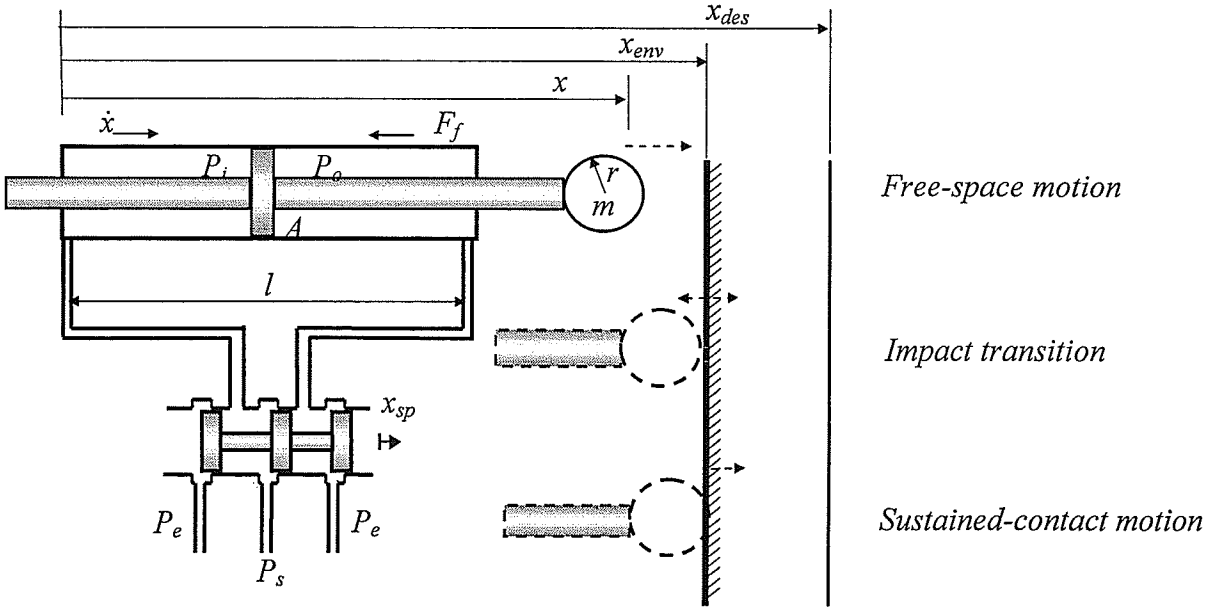

Fig. 3.2 Actuator-environment configuration.

and P_i and P_o are the forward (input) and return (output) chamber pressures. Parameters m and A are the mass of actuator's moving parts and piston area, respectively.

Assuming that the pressure in each chamber is everywhere the same and does not saturate or cavitate, fluid velocities in the chambers are small so that minor losses are negligible, internal (cross-port) and external (line to case drain) leakages are negligible, line phenomena are absent, and temperature and density are constant, the continuity equations of oil flow through the cylinder yields (Merritt , 1967):

$$Q_i = \frac{dV_i(x)}{dt} + \frac{V_i(x)}{\beta}\frac{dP_i}{dt} \tag{3.2a}$$

$$-Q_o = \frac{dV_o(x)}{dt} + \frac{V_o(x)}{\beta}\frac{dP_o}{dt} \tag{3.2b}$$

where Q_i and Q_o are forward and return flows, respectively. For valves with square-edged matched and symmetric orifice areas, pressure changes with time can be rearranged as (Merritt , 1967):

$$\dot{P}_i = \frac{\beta}{V_i(x)}\left(-A\dot{x} + \sqrt{\frac{2}{\rho}}c_d w x_{sp}\sqrt{\frac{P_S - P_e}{2} + sign(x_{xp})\left(\frac{P_S + P_e}{2} - P_i\right)}\right) \tag{3.3a}$$

$$\dot{P}_o = \frac{\beta}{V_o(x)}\left(A\dot{x} - \sqrt{\frac{2}{\rho}}c_d w x_{sp}\sqrt{\frac{P_S - P_e}{2} + sign(x_{xp})\left(P_o - \frac{P_S + P_e}{2}\right)}\right) \tag{3.3b}$$

where the function $sign(x_{sp})$ is defined as:

$$sign(x_{sp}) = \begin{cases} x_{sp}/|x_{sp}| & ; \quad x_{sp} \neq 0 \\ 0 & ; \quad x_{sp} = 0 \end{cases} \tag{3.4}$$

In equations (3.2) and (3.3), x_{sp} is the spool displacement, P_s and P_e are the supply and return pressures across the valve, β is the effective bulk modulus of the hydraulic fluid, w is the orifice area gradient, ρ is the hydraulic fluid density, and c_d is the orifice coefficient of discharge that accounts for the fact that the jet formed from the flow through the orifice is smaller than the actual orifice due to turbulent flow (Dunnigan et al., 1996). $V_i(x)$ and $V_o(x)$ are the volumes of the fluid trapped at the sides of the actuator which could be expressed as:

$$V_i(x) = \overline{V}_i + A\delta x \tag{3.5}$$

$$V_o(x) = \overline{V}_o - A\delta x \tag{3.6}$$

where $\overline{V}_i$ and $\overline{V}_o$ are the initial fluid volumes trapped in each side of the piston and $\delta x = x - x_0$ is the piston displacement from its initial position x_0.

Although the dynamics between the spool displacement, x_{sp}, and the input voltage, u, is best modeled as a third-order system (Merritt, 1967), experimental and simulation studies have revealed that the real pole of the two-stage servovalve model dominates the servovalve response and the higher frequency dynamics of the valve can be ignored for applications operating below 200 Hz and (Alleyne, 1996). Thus, the reduced-order model is a first order system with the same real pole as follows:

$$\dot{x}_{sp} = -\frac{1}{\tau}x_{sp} + \frac{k_{sp}}{\tau}u \tag{3.7}$$

where k_{sp} and τ are valve gain and time constant, respectively.

Combining equations (3.1) to (3.7) yields the following state-space model for the hydraulic system under study:

$$\begin{cases} \dot{x} = v \\ \dot{v} = \dfrac{A(P_i - P_o)}{m} - \dfrac{F_f}{m} - \dfrac{F_{env}}{m} \\ \dot{P}_i = \dfrac{\beta}{\overline{V}_i + A\delta x}\left(-Av + \sqrt{\dfrac{2}{\rho}}c_d w x_{sp}\sqrt{\dfrac{P_S - P_e}{2} + sign(x_{sp})\left(\dfrac{P_S + P_e}{2} - P_i\right)}\right) \\ \dot{P}_o = \dfrac{\beta}{\overline{V}_o - A\delta x}\left(Av - \sqrt{\dfrac{2}{\rho}}c_d w x_{sp}\sqrt{\dfrac{P_S - P_e}{2} + sign(x_{sp})\left(P_o - \dfrac{P_S + P_e}{2}\right)}\right) \\ \dot{x}_{sp} = -\dfrac{1}{\tau}x_{sp} + \dfrac{k_{sp}}{\tau}u \end{cases} \tag{3.8}$$

In many position (Yao et al., 2001; Hwang and Lan, 1994) and force control (Alleyne and Hedrick, 1995; Liu and Alleyne, 2000) applications, a simplified model is employed that is based on assumptions without which the analysis becomes much involved and the results are quite difficult to interpret. The simplified model is derived as follows (Merritt , 1967):

Assume that the piston is centered ($x_0 = l/2$) such that the volumes of the fluid trapped at the sides of the actuator are equal, i.e.

$$\overline{V}_i = \overline{V}_o = V_0 \tag{3.9}$$

Experience has shown that stability problems are more acute when the piston is centered so that the assumption of equal chamber volumes should be conservative (Merritt , 1967). Obviously, the sum of the two volumes is constant and independent of piston position. Therefore,

$$V_t = V_i(x) + V_o(x) = \overline{V}_i + \overline{V}_o = 2V_0 \tag{3.10}$$

where V_t is the total volume of fluid under compression in both chambers.

Because there is no direct connection between the chambers, a continuous flow through the cylinder is achieved only if the volume of one chamber steadily increases while the other chamber volume decreases with piston displacement. This is physically possible because when the cylinder fills with fluid, the trapped fluid is transported to the other chamber where it empties. Hence, the time derivatives of (3.5) and (3.6) are given by

$$\frac{dV_i(x)}{dt} = A\frac{dx}{dt} = -\frac{dV_o(x)}{dt} \tag{3.11}$$

and represent the steady-state flow to and from the cylinder, respectively.

Defining $Q_L = \dfrac{Q_i + Q_o}{2}$ and substituting (3.5), (3.6), and (3.11) into (3.2) yields:

$$Q_L = \frac{Q_i + Q_o}{2} = \frac{1}{2}\left(\frac{dV_i(x)}{dt} + \frac{V_i(x)}{\beta}\frac{dP_i}{dt} - \frac{dV_o(x)}{dt} - \frac{V_o(x)}{\beta}\frac{dP_o}{dt}\right)$$

$$= \frac{1}{2}\left(2A\frac{dx}{dt} + \frac{V_0 + A\delta x}{\beta}\frac{dP_i}{dt} - \frac{V_0 - A\delta x}{\beta}\frac{dP_o}{dt}\right) = A\dot{x} + \frac{V_0}{2\beta}\frac{d(P_i - P_o)}{dt} + \frac{A\delta x}{2\beta}\frac{d(P_i + P_o)}{dt} \tag{3.12}$$

i.e,

$$Q_L = A\dot{x} + \frac{V_0}{2\beta}\dot{P}_L + \frac{A\delta x}{2\beta}\frac{d(P_i + P_o)}{dt} \tag{3.13}$$

where $P_L = P_i - P_o$ is the load pressure. Let us now examine the last term on the right in (3.13). This term may be neglected by assuming that $|A\delta x| << V_0$ or by differentiating equations $P_i = \dfrac{P_s + P_L}{2}$ and $P_o = \dfrac{P_s - P_L}{2}$, which are assumed to be applicable, to show that $\dfrac{dP_i}{dt} + \dfrac{dP_o}{dt} = 0$ (Merritt , 1967). Therefore, (3.13) can now be simplified as

$$Q_L = A\dot{x} + \frac{V_0}{2\beta}\dot{P}_L \tag{3.14}$$

Finally, for ideal critical center valves with matched and symmetrical orifices and rectangular ports where $Q_L = \frac{c_d w}{\sqrt{\rho}} x_{sp} \sqrt{P_s - sign(x_{sp}) P_L}$, the simplified form pressure-time changes is:

$$\dot{P}_L = \frac{1}{C}\left(- A\dot{x} + \frac{c_d w}{\sqrt{\rho}} x_{sp} \sqrt{P_s - sign(x_{sp}) P_L} \right) \tag{3.15}$$

where the constant $C = V_t / 4\beta$ is the hydraulic compliance.

Equation (3.15) is the simplified form of equations (3.3) and will be used as the system's dynamic model at the control design stage to make the Lyapunov stability analysis manageable. Thus, the model of the hydraulic system during control design stage is:

$$\begin{cases} \dot{x} = v \\ \dot{v} = \dfrac{A P_L}{m} - \dfrac{F_f}{m} - \dfrac{F_{env}}{m} \\ \dot{P}_L = \dfrac{1}{C}\left(- A\dot{x} + \dfrac{c_d w}{\sqrt{\rho}} x_{sp} \sqrt{P_s - sign(x_{sp}) P_L} \right) \\ \dot{x}_{sp} = -\dfrac{1}{\tau} x_{sp} + \dfrac{k_{sp}}{\tau} u \end{cases} \tag{3.16}$$

Note that models (3.8) and (3.16) do not incorporate the dead-zone nonlinearities caused by possible spool valve overlap. Leakage flow across the actuator's piston is also neglected since it inherently has stabilizing effect by providing damping for hydraulic resonant mode (Vossoughi and Donath, 1995). For the double-rod cylinder under investigation, directional nonlinearity is not an issue and the servovalve saturation nonlinearity can be prevented if the valve is never allowed to saturate.

Due to its fewer number of system states, the simplified model (3.16) is appealing for control design using Lyapunov direct method. Numerical stability analysis of the overall contact task control system using the concept of Lyapunov exponents, however, will be conducted using the complete state space equations (3.8) which is valid for the system's full-stroke motion.

3.2.2 Friction Model

Tustin's Friction Model

It is well known that the major components of friction are Coulomb force, viscous force,

Stribeck effects and position dependent forces (Song et al., 1998). However, experiments carried out in industrial manipulators have shown that position dependence is relatively weak and can be neglected for most purposes (Canudas de Wit et al., 1991). Low velocity experiments have also confirmed Tustin's discontinuous friction model which includes Coulomb/static force, viscous force, and Stribeck effects. The model is widely used in many general (Canudas de Wit et al., 1991) as well as hydraulic (Laval et al., 1996) control systems:

$$F_f = \left[F_C + (F_S - F_C)e^{-(\dot{x}/v_s)^2}\right]\mathrm{sgn}(\dot{x}) + d\,\dot{x} \tag{3.17}$$

In (3.17), $\dot{x}$ is the actuator velocity, F_C is the Coulomb friction, F_S is the stiction force (the force needed to start the motion), and d is the viscous friction coefficient. Stribeck effect is characterized by $e^{-(\dot{x}/v_s)^2}$ where v_s is a threshold velocity where the downward bend in friction appears after the stiction (breakaway) force is surmounted. When the system is at rest, the static friction ($F_S\,\mathrm{sgn}(0)$) is opposite to the applied force and can acquire any value in the range of $[-F_S, F_S]$. This opposing static friction increases with the increase in the net external force until it reaches the breakaway force, F_S, where the piston starts to slide and the friction drops due to Stribeck effect. The function $\mathrm{sgn}(\dot{x})$ is thus defined as

$$\begin{cases} \mathrm{sgn}(\dot{x}) = \{\dot{x}/|\dot{x}|\} & : \quad \dot{x} \neq 0 \\ \mathrm{sgn}(\dot{x}) \in [-1,1] & : \quad \dot{x} = 0 \end{cases} \tag{3.18}$$

Note that sgn(0):=0 is not a right choice since it only implies zero friction during the sticking phase of motion. A typical plot of friction force (3.17) with velocity is depicted in Fig. 3.3.

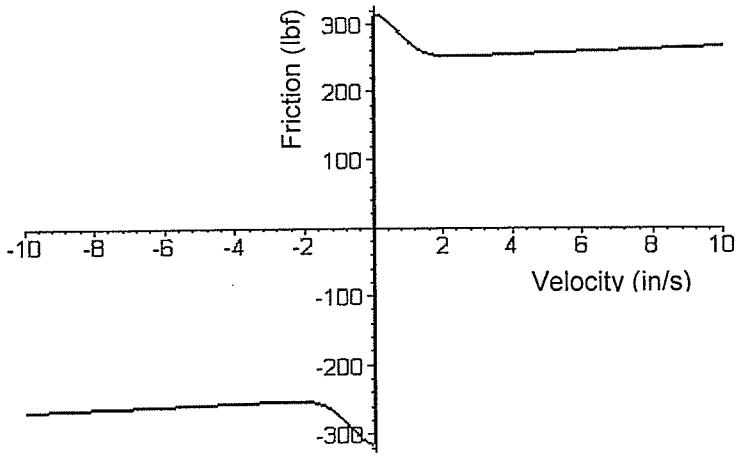

Fig. 3.3 Typical friction force-velocity relation in Tustin's friction model.

LuGre's Friction Model

The continuous LuGre friction model (Canudas de Wit et al. 1995) is a recently developed model and is able to capture stick-slip friction effects at microscopic level, presliding displacements due to spring-like behavior of surface asperities, frictional lag due to hysteresis, and the varying break-away force depending on the rate of the external force (Canudas de Wit et al. 1995). The model is being used in both general (Vedagarbha et al. 1999) and hydraulic (Lischinsky et al. 1999; Owen et al., 2003) applications. By visualizing the friction between two surfaces as two bodies that make contact though elastic bristles (Fig. 3.4), the resisting friction force upon applying the external force is modeled as the deflections of thousands of bristles whose average is denoted by $z(t)$. Movement will continue to be resisted by bristles until the bond between the asperities breaks or asperities are sheared.

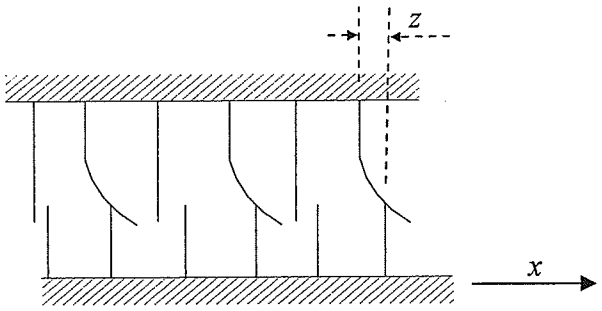

Fig. 3.4 Friction thought as contact between bristles.

The force required to break the bonds are defined as the static friction, F_S. The mathematical model of the above approach to friction can be described by the following equations:

$$F_f = \sigma_0 z + \sigma_1 \dot{z} + d\dot{x} \tag{3.19}$$

$$\dot{z} = \dot{x} - \frac{\sigma_0 |\dot{x}|}{F_C + (F_S - F_C) e^{-(\dot{x}/v_s)^2}} z \tag{3.20}$$

where σ_0 and σ_1 are the bristle-spring and bristle-damping constants. Parameters F_S, F_C, d, and v_s characterize the static, Coulomb, viscous, and Stribeck friction effects, respectively. The other two parameters σ_0 and σ_1 can be considered as the stiffness and damping coefficients of the microscopic deformations of z and can be used to interpret stiction.

The internal state, z, introduced by the LuGre's model is not measurable and the two parameters σ_0 and σ_1 are hard to estimate. Therefore, friction compensating control design procedures

using the above friction model utilize friction observers. When the control scheme is available, however, the continuity of the model is a great advantage in conducting numerical analyses and, in particular, calculating the system's Lyapunov exponents for stability analysis of the control system.

Throughout this thesis, the above two friction models, widely used in the literature, are employed to model actuator friction. The trends of the results of the two models are previously reported to be similar. LuGre model is continuous and captures a variety of behaviors, such as pre-sliding displacement, hysteresis effect, stick-slip motion, and varying break-away force. The price paid for such a versatile model is that it is a six-parameter model. Tustin's model is simpler than LuGre model as it uses four parameters only. The model, however, is discontinuous and is more suitable for Lyapunov-based control design as it has less number of states and state dependent terms. For stability analysis using numerical calculation of Lyapunov exponents, continuity of the LuGre friction model is a great advantage and the additional state introduced to the dynamic model by this friction model is also accommodable by this numerical procedure.

3.2.3 Implement -Environment Interaction Model

Interaction between an implement and an environment, commonly referred to as impact or contact, is a dynamic phenomenon and is very difficult to model realistically. As a result of implement-environment interactions, a portion of the original kinetic energy is converted into strain energy within the interacting parts in the form of deformation. Some fraction of the strain energy is reconverted back into the kinetic energy of the detaching parts, whereas the remainder of the energy is trapped within the system in the form of exciting various modes of vibration and/or is dissipated as energy of plastic deformation. Impact is a complex physical phenomenon which occurs when two or more bodies collide with each other in a very brief duration and involves development of high force levels, rapid dissipation of energy, and large accelerations and decelerations (Gilardi and Sharf, 2002). Contact is a more ambiguous term that is frequently used interchangeably with impact. Here, we use the latter term to describe situations where the implement is in touch with a nonmoving environment. Consequently, the sustained-contact phase of contact task is assumed to be the period when the implement never loses its touch with the environment until the desired contact force is achieved.

In general, two different modeling categories can be distinguished for implement-environment interactions (impact/contact): rigid modelling (Pagilla and Yu, 2001; Brogliato et al., 1997, Brogliato and Orhant, 1998; Brogliato, 1999; Tarn et al., 1996; Zheng and Hemami, 1985), and compliant modelling (Payandeh, 1996; Wu and Payandeh, 1999; Niksefat et al., 2001; Mills, 1990; Vukobratovic et al., 2001; Kazerooni et al., 1990; Eppinger and Seering, 1987; Gilardi and Sharf, 2002; Fujita and Hattori, 1980; Hunt and Crossley, 1975). Rigid body models are mostly used to model the impacts and compliant models are used for both impact and sustained-contact modeling. Selection of the implement-environment model is particularly crucial for the choice of the control algorithm. For example, Yousef-Toumi and Gutz (1994) showed that an integral force feedback helps in stabilizing impacts when the environment is sufficiently rigid, whereas Volpe and Khosla (1993b) showed that the same control scheme is not suitable for flexible environments. Aside from clearly rigid environments made of hard materials (stone, iron) and clearly flexible ones, some other environments might be considered to belong to one class or the other one depending on the task, masses of the bodies that collide, accuracy of the measurements, actuators limits, etc. (Brogliato, 1999). The main features of each modeling category are discussed next.

Rigid body collision is defined as a phenomenon that occurs when the colliding bodies show "sufficiently small" deformation so that they are geometrically rigid at a global observation scale (Brogliato, 1999). In this case, collision is modeled as an instantaneous phenomena and the arising contact force depends on the configuration of the bodies at the instant of impact, their velocities before impact, and the coefficient of restitution (Lin et al., 1995). Therefore, effects such as elastic or inelastic deformation of the implement or environment would not be modeled in the dynamic equations. Rigid modeling allows simplification of the dynamical contact/impact problem, but at the same time involves some deep mathematical issues related to existence, uniqueness and stability analysis of problems with unilateral constraints, or nonsmooth dynamics (Brogliato, 1999). Furthermore, uncertainties of the rigid body collision coefficients, difficulty in modeling the transition period to and from sustained contact, unrealistic negligence of surface compliance, and the practical need to consider actual contact forces rather than impulsive approximations, are among other problems associated with the rigid body modeling approach (Marhefka and Orin, 1996). Such modeling is also not easily extendible to impacts involving multiple bodies and multiple contact points (Gilardi and Sharf, 2002).

Compliant models recognize the compliance of the implement and/or environment. Two of the main compliant approaches are the spring-damper model and the Hertz model. Spring-damper models have been used in various forms such as single spring, combination of spring-damper or a complete second-order mass-spring-damper system. The presence of compliance increases the effectiveness of the controller to maintain contact with the environment at various approach velocities (Payandeh, 1995) and allows the controller to accomplish fast force regulation at post-impact stage (Payandeh, 1996). On the other hand, spring-damper models exhibit the following drawbacks (Gilardi and Sharf, 2002):

- Because of the parallel spring-damper configuration, the contact force at the beginning of impact is discontinuous;
- As the objects are separating, i.e., the indentation tends to zero, their relative velocity tends to be negative leading to a negative force holding the objects together;
- It does not accommodate the impact velocity in the model.

Although the spring-damper model is not physically realistic, its simplicity has made it a popular choice. It provides a reasonable method of capturing the energy dissipation associated with the normal forces without explicitly considering plastic deformation issues (Gilardi and Sharf, 2002). The model has been further improved (Mills and Nguyen, 1992) to provide a continuous contact force at the moments of contact and separation by adding a compliant "skin" to the original mass-spring-damper model.

The second approach in compliant modeling of implement-environment interactions is the nonlinear Hertz contact model. According to this model, the implement and the non-moving environment are not connected even during the contact period and the contact force develops due to the local deformations of the implement and the environment surfaces during a finite measurable time. Consequently, the Hertz contact model is capable of incorporating realistic bouncings and local elastic deformations in the analysis. The original Hertz model has been introduced by assuming: (*i*) frictionless and point contact, (*ii*) elastic deformations are concentrated in the vicinity of the contact area, (*iii*) elastic wave motion is neglected, and (*iv*) the total mass of each body moves with the velocity of its mass centre. However, the model can be augmented to account for plastic deformation (by introducing hysteresis in the contact force law) or friction (Gilardi and Sharf, 2002). Energy dissipation has also been included in the extensions

of the model and recent theoretical and experimental studies have confirmed that such extension is a good representative of the real behavior of the system during both impact and sustained-contact phases of motion and can offer the highest modeling fidelity for complicated contact bodies and arbitrary constrained motions (Van Vliet et al., 2002; Marhefka and Orin, 1999; Gilardi and Sharf, 2002). In this thesis, the Hertz contact model is employed to model impact and sustained-contact motion between the implement and the environment.

Original Hertz Model

With reference to Fig. 3.5, the original Hertz contact model is expressed as follows (Timoshenko and Goodier, 1970; Gilardi and Sharf, 2002):

$$F_{env} = \begin{cases} H(x - x_{env})^n & ; \quad (x - x_{env} > 0) \\ 0 & ; \quad otherwise \end{cases} \tag{3.21}$$

where x_{env} is the position of the environment and n and H are constants that depend on material and geometric properties of the colliding bodies and are determined using elastoplastic theory. The index n is often close to one and depends on the surface geometry of the contact. For sphere on sphere contact under elastic conditions, n is equal to 3/2. For contact between perfectly flat surfaces, at least ideally, the area of the zone of contact doesnot chage during the time of contact and n=1 (linear) would apply. For parallel cylinders in longitudinal contact along a narrow zone on either side of a line, an index n between 1 and 1.5 is expected to to match the conditions fairly well (Hunt and Crossley, 1975).

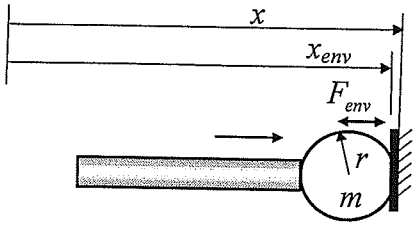

Fig. 3.5 Implement-environment configuration

For a spherical end-effector pressed into a plane surface (Timoshenko and Goodier, 1970):

$$H = \frac{4E_1E_2}{3\left(E_2\left(1-\upsilon_1^2\right)+E_1\left(1-\upsilon_2^2\right)\right)}\sqrt{r} \tag{3.22}$$

where $E_1, E_2, \upsilon_1, \upsilon_2$ are the Young's modulus and Poisson's ratio of the two colliding bodies, and r is the radius of implement's contact surface.

Since the above model does not account for the energy dissipation, it is most suitable for force regulation during the low velocity post-impact period of motion (Gilardi and Sharf, 2002).

Hertz-Type Contact Model

To account for energy dissipations during higher velocity impacts and retain the advantages of the Hertz model, the extension of the Hertz model has been introduced which is also continuous and, therefore, complies with the inherently continuous behavior of implements during collisions (Gilardi and Sharf, 2002; Fujita and Hattori, 1980; Hunt and Crossley, 1975). According to this model, the condition of contact/non-contact is defined by both relative displacement and relative velocity and the contact force is derived from production of the original Hertzian restoring force and a damping term. For the case of collision between the implement with spherical tip and a flat environment, the Hertz-type impact force is (Fujita and Hattori, 1980):

$$F_{env} = \begin{cases} (1+p\dot{x})H(x-x_{env})^n & ; \quad (x-x_{env}>0)\ \&\ (1+p\dot{x}>0) \\ 0 & ; \quad otherwise \end{cases} \tag{3.23}$$

where $\dot{x}$ is the implement's velocity. The term '$1+p\dot{x}$' accounts for the energy dissipation caused by collision where the nonnegative damping parameter p (s/m) denotes the energy loss that comes from the motion difference in the acceleration and deceleration during collision (Shoji et al., 1991). The value of p is selected so that the following experimentally obtained equation applies between the approach velocity at the instant of touching the environment, $\dot{x}_0$, and the coefficient of restitution, e, (Fujita and Hattori, 1980):

$$e = \frac{1}{p\dot{x}_0} - \left(1+\frac{1}{p\dot{x}_0}\right)\exp\{-(1+e)p\dot{x}_0\} \tag{3.24}$$

Experimental results of the relation between coefficient of restitution and approach velocity of a typical steel ball collision is depicted in Fig. 3.6 (Fujita and Hattori, 1980).

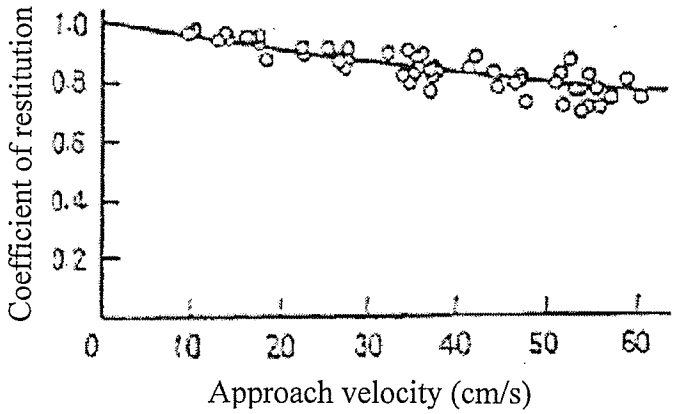

Fig.3.6 Typical experimental results of steel balls collision (Takafumi and Hattori, 1980).

According to this figure, the coefficient of restitution for the contacts starting with zero approach velocity is one which is in agreement with (3.24) regardless of the value of p. Therefore, for low velocity interactions, the original Hertz model (3.21) is adequate to model the implement-environment interactions (p=0) and the more general model (3.23) can be simplified to (3.21).

3.2.4 System Parameters

The parameters of the mathematical model comprised of equations (3.8), (3.17), (3.19) and (3.23) are required for numerical simulations as well as calculation of Lyapunov exponents. Some of the required parameters can be extracted from the manufacturer's catalogues and the rest can be measured through parameter identification experiments. The parameter values of the system shown in Fig. 3.1 are tabulated in Table 3.1 and will be used in Chapter 8 for the overall system's stability analysis.

Table 3.1 Test station parameters.

Parameters related to the hydraulic actuator dynamics			
$m\ (lb)$	26.46	$\beta\ (psi)$	99930
$A\ (in^2)$	0.9812	$w\ (in)$	0.8169
$\rho\ (lb/in^3)$	0.0306	$k_{sp}\ (in/V)$	0.001598
c_d	0.6	$\tau\ (1/s)$	0.002
$V_{line}\ (in^3)$	1.305908	$l\ (in)$	23.89
Friction related parameters			
$F_C\ (lb)$	247.3	$F_S\ (lb)$	314.7
$\sigma_0\ (lb/in)$	57.1	$v_s\ (in/s)$	23.62
$\sigma_1\ (lb\,s/in)$	0.571	$d, \sigma_2\ (lb/in)$	1.998
Environment related parameters			
e	0.6	n	1.5
$H_{metal}\ (lb/in^{1.5})$	273004	$H_{wood}\ (lb/in^{1.5})$	81901

Chapter 4

Position Control Design for Free-Space Motion

4.1 Introduction

As detailed in Chapter one, previous studies on position control of hydraulic actuators are either with no rigorous theoretical analysis (Tafazoli et al., 1998) or with an analysis that neglects the servovalve dynamics (Lischinsky et al., 1999), neglects the actuator dry friction (Niksefat et al., 2001), is not extendible to position regulation (Yao et al., 2000), or, requires knowledge of system parameters for control action (Sohl and Bobrow, 1999). In this chapter, the above shortcomings are addressed by designing a position regulation control scheme that does not require the exact knowledge of system parameters. Furthermore, the effects of actuator dry friction, nonlinear hydraulic functions, and servovalve dynamics are included in the theoretical analyses by combining equations (3.16), (3.17), and (3.23) as follows (Note that F_{env}=0 at all times during free-space motion):

$$\begin{cases} \dot{x} = v \\ \dot{v} = \dfrac{A P_L}{m} - \dfrac{\left[F_C + (F_S - F_C)e^{-(\dot{x}/v_s)^2}\right]\mathrm{sgn}(\dot{x}) + d\,\dot{x}}{m} \\ \dot{P}_L = \dfrac{1}{C}\left(- A\dot{x} + \dfrac{c_d w}{\sqrt{\rho}} x_{sp}\sqrt{P_s - sign(x_{sp})P_L} \right) \\ \dot{x}_{sp} = -\dfrac{1}{\tau}x_{sp} + \dfrac{k_{sp}}{\tau}u \end{cases} \tag{4.1}$$

where the function *sign* and sgn are as defined in (3.4) and (3.18):

$$sign(x_{sp}) = \begin{cases} x_{sp}/|x_{sp}| & ; \quad x_{sp} \neq 0 \\ 0 & ; \quad x_{sp} = 0 \end{cases}$$

$$\begin{cases} \mathrm{sgn}(\dot{x}) = \{\dot{x}/|\dot{x}|\} & : \quad \dot{x} \neq 0 \\ \mathrm{sgn}(\dot{x}) \in [-1,1] & : \quad \dot{x} = 0 \end{cases}$$

In the following sections, the analysis starts with first including dry friction effects in the control system introduced by Niksefat et al. (2001) and rigorously proving the global asymptotic convergence of the entire system's states towards the system's equilibria. Inclusion of dry friction in the analysis, however, results in steady-state error in the actuator position. To eliminate the steady-state position errors, in the next step, a Lyapunov-based nonlinear friction compensation technique is designed for the asymptotic position regulation of the hydraulic actuator in the presence of actuator's dry friction. Using similar state feedbacks and same number of control gains, the new control system is proven to converge to system equilibria with no steady-state position error. Due to the discontinuity of the controller, the control system is nonsmooth. Therefore, existence, continuation and uniqueness of Filippov's solution of the system are, first, investigated. The extension of Lyapunov stability theory to nonsmooth systems is then employed to guarantee the global asymptotic convergence of the entire system's states towards the equilibria. The major challenge in using Lyapunov's second method is that there is no constructive rule on constructing a Lyapunov function for any particular nonlinear control system. Particularly, finding the Lyapunov function for the hydraulic system shown in (4.1) requires thorough mathematical manipulations and several trial adjustments in both the system's control law and Lyapunov function. Inspired by the results reported in Niksefat et al. (2001), the scalar functions introduced in Chapters 4,5, and 6 of this thesis are derived as a result of

extensive mathematical efforts in the form of recursive manipulation of the control law and the Lyapunov function candidates.

4.2 Position Control without Friction Compensation

The position control algorithm introduced by Niksefat et al. (2001) is as follows:

$$u = -\left(K_p P_L + K_x\left(x - x_{des}\right)\right)\sqrt{P_s - sign(x_{sp})\,P_L} \tag{4.2}$$

where K_p and K_x are positive constant gains. In the presence of only viscous friction (i.e., $F_f = d\dot{x}$), the stability analysis of the system's unique equilibrium point, $\mathbf{e}_{eq} := (x^{ss} - x_{des}, \dot{x}^{ss}, P_L^{ss}, x_{sp}^{ss})^T = (0,0,0,0)^T$ was conducted by Niksefat et al. (2001) [Note $(.)^{ss}$ denotes the steady-state value of (.)]. Here, dry friction is also included in the model of the system and the stability of the position control system is revisited.

Defining $e_1 = x - x_{des}$, $e_2 = \dot{x}$, $e_3 = P_L$, and $e_4 = x_{sp}$, equations (4.1) and (4.2) are combined and the error-state equations of motion are derived as follows:

$$\begin{cases} \dot{e}_1 = e_2 \\ \dot{e}_2 = \dfrac{A}{m}e_3 - \dfrac{\left[F_C + (F_S - F_C)e^{-(e_2/\dot{x}_s)^2}\right]\mathrm{sgn}(e_2) + d\,e_2}{m} \\ \dot{e}_3 = \dfrac{1}{C}\left(-Ae_2 + \dfrac{c_d w}{\sqrt{\rho}}e_4\sqrt{P_S - sign(e_4)\,e_3}\right) \\ \dot{e}_4 = -\dfrac{1}{\tau}e_4 - \dfrac{k_{sp}}{\tau}\left(K_p e_3 + K_x e_1\right)\sqrt{P_S - sign(e_4)\,e_3} \end{cases} \tag{4.3}$$

The equilibrium of the system, $\mathbf{e}_{eq} = (e_1^{ss}, e_2^{ss}, e_3^{ss}, e_4^{ss})^T$ is obtained by equating the right-hand side of (4.3) to zero:

$$\begin{cases} e_1^{ss} = -\dfrac{K_p}{K_x}\dfrac{F_S\,\mathrm{sgn}(0)}{A} \in \left[-\dfrac{K_p}{K_x}\dfrac{F_S}{A}, \dfrac{K_p}{K_x}\dfrac{F_S}{A}\right] \\ e_2^{ss} = 0 \\ e_3^{ss} = \dfrac{F_S\,\mathrm{sgn}(0)}{A} \in \left[-\dfrac{F_S}{A}, \dfrac{F_S}{A}\right] \\ e_4^{ss} = 0 \end{cases} \tag{4.4}$$

It follows from (4.4) that decreasing K_p/K_x decreases the band on the steady-state position error, e_1^{ss}. However, as will be detailed in the stability analysis (Section 4.2.2), K_p/K_x can not

be chosen arbitrarily small. Before continuing with stability analysis, note that the discontinuous friction model and the discontinuous nature of the control law have resulted in a nonsmooth control system. Filippov's solution concept is used to first investigate the solution of the system.

4.2.1 Solution Analysis

With reference to (4.3), the discontinuity surface of the control system is one of the following three surfaces:

Surface 1 $S_1^3 := \{\mathbf{e} : e_2 = 0 \;\&\; e_4 \neq 0\}$

Surface 2 $S_2^3 := \{\mathbf{e} : e_2 \neq 0 \;\&\; e_4 = 0\}$

Surface 3 $S_3^2 := \{\mathbf{e} : e_2 = 0 \;\&\; e_4 = 0\}$ (4.5)

The subscript and superscript denote the number of the discontinuity surfaces and their dimension, respectively. Surface S_3^2 is the intersection of surfaces S_1^3 and S_2^3. The conditions for existence and continuity of the Filippov's solution, such as right-hand sides of (4.3) are measurable and bounded, are all satisfied. Thus, the existence and continuity of the solutions are guaranteed. To study the uniqueness of Filippov's solution on the discontinuity surface S_1^3, the solution region is divided into two parts: $\Omega^+ := \{\mathbf{e} : e_2 > 0\}$ and $\Omega^- := \{\mathbf{e} : e_2 < 0\}$. The normal to this surface, $\mathbf{N}_1$, is:

$$\mathbf{N}_1 = (0 \quad 1 \quad 0 \quad 0)^T \tag{4.6}$$

Following the procedure outlined in Section 2.3.1, we have

$$h_{N_1} = \mathbf{N}_1 . \mathbf{h}_1 = -2\frac{F_S}{m} < 0 \tag{4.7}$$

where $\mathbf{h_1}$ is defined as $\mathbf{h}_1 = \mathbf{f}_1^+ - \mathbf{f}_1^-$ at all points of the discontinuity surface S_1^3 and $\mathbf{f}_1^-$ and $\mathbf{f}_1^+$ are defined as the right-hand sides of the dynamic equations (4.3) in the regions Ω^- and Ω^+. Since $h_{N_1} < 0$, according to Lemma 7 in Filippov (1979), the uniqueness of the Filippov's solution for equations (4.3) is guaranteed. The solution analysis on S_2^3 can be analyzed in the same manner and is not repeated here. Similar to the analysis presented in Section 4.3.2, the solution analysis on S_3^2 requires extensive mathematical manipulations and is not presented.

4.2.2 Stability Analysis

With respect to equation (4.3), the smooth positive definite regular function V is derived as

$$V = \frac{K_x C}{2(K_p A - K_x C)}\left(\frac{A e_1}{C} + e_3\right)^2 + \frac{m}{2C}e_2^2 + \frac{1}{2}e_3^2 + \frac{\tau c_d w A}{2k_{sp}\sqrt{\rho}\, C(K_p A - K_x C)}e_4^2 \qquad (4.8)$$

which is positive as long as $(K_p A - K_x C) > 0$. This condition implies

$$\frac{K_p}{K_x} > \frac{C}{A} \qquad (4.9)$$

Note that K_p/K_x can not be equal to C/A as it makes the function V indefinite. The derivative of V in the continuous regions is

$$\dot{V} = \frac{K_x c_d w}{(K_p A - K_x C)\sqrt{\rho}}\left(\frac{A e_1}{C} + e_3\right)e_4\sqrt{P_s - sign(e_4)e_3}$$

$$+\frac{1}{C}e_2\left(Ae_3 - \left(\left[F_C + (F_S - F_C)e^{-(e_2/\dot{x}_s)^2}\right]\mathrm{sgn}(e_2) + d\,e_2\right)\right) + \frac{e_3}{C}\left(-Ae_2 + \frac{c_d w}{\sqrt{\rho}}e_4\sqrt{P_s - sign(e_4)e_3}\right)$$

$$+\frac{\tau c_d w A}{k_{sp}\sqrt{\rho}\, C(K_p A - K_x C)}e_4\left(-\frac{1}{\tau}e_4 - \frac{k_{sp}}{\tau}\left(K_p e_3 + K_x e_1\right)\sqrt{P_s - sign(e_4)e_3}\right)$$

$$= -\frac{\left(F_C + (F_S - F_C)e^{-(e_2/\dot{x}_s)^2}\right)}{C}|e_2| - \frac{d}{C}e_2^2 - \frac{c_d w A}{k_{sp}C\sqrt{\rho}\,(K_p A - K_x C)}e_4^2 \qquad (4.10)$$

which is continuous and negative semi-definite. On the discontinuity surface, S_1^3, we have

$$\dot{V}(\mathbf{e} \in S_1^3) \in co[\dot{V}^{S_1^{3+}}, \dot{V}^{S_1^{3-}}] \qquad (4.11)$$

where $\dot{V}^{S_1^{3+}}$ and $\dot{V}^{S_1^{3-}}$ are the limit values of $\dot{V}$ as the solution trajectory approaches S_1^3 from both sides:

$$\dot{V}^{S_1^{3+}} = \lim_{e_2 \to 0^+}\dot{V} = -\frac{c_d w A}{k_{sp}C\sqrt{\rho}\,(K_p A - K_x C)}e_4^2 \qquad (4.12)$$

$$\dot{V}^{S_1^{3-}} = \lim_{e_2 \to 0^-}\dot{V} = -\frac{c_d w A}{k_{sp}C\sqrt{\rho}\,(K_p A - K_x C)}e_4^2 \qquad (4.13)$$

Thus, the convex set described in (4.11) contains only one element which is negative and we write:

$$\dot{V}(\mathbf{e} \in S_1^3) = -\frac{c_d w A}{k_{sp} C \sqrt{\rho}\,(K_p A - K_x C)} e_4^2 \tag{4.14}$$

Equations (4.10) and (4.14) show that $\dot{V}$ is negative and continuous on discontinuity surface S_1^3. Similarly the derivatives of the Lyapunov function on S_2^3 and S_3^2 can be proven to include only negative or zero elements. Thus, we conclude that $\dot{V}$ is negative semi-definite throughout the solution region including the discontinuity surfaces. Therefore, according to the extended LaSalle's invariance principle to non-smooth systems (Theorem 2 in Section 2.3), every solution trajectory in Ω globally converges to the largest invariant set, **M**, in the closure of **R**, which is the set of all points where $\dot{V}(\mathbf{e}) = 0$. Next, we prove that the largest invariant set, **M**, contains only points that belong to the set $\mathbf{e}_{eq} = \left(e_1^{ss}, 0, e_3^{ss}, 0\right)^T$ with e_1^{ss} and e_3^{ss} defined in (4.4). This can be proven by contradiction. Assuming that **M** contains a point other than $\mathbf{e}_{eq}$, equation (4.3) implies $\dot{e}_2 \neq 0$ and/or $\dot{e}_4 \neq 0$, which will result in $e_2 \neq 0$ and/or $e_4 \neq 0$. This contradicts the fact that **M** is the largest invariant set in **R**. Thus, e_1 and e_3 can only have values shown in (4.4) and it is proven that every solution trajectory in Ω will converge to the largest invariant set **M** containing only the equilibria. Furthermore, combination of (4.4) and (4.9) yields the following band for the system's steady-state position error:

$$e_1^{ss} \in \left[-\left(\frac{C}{A} + \varepsilon\right)\frac{F_S}{A}, \left(\frac{C}{A} + \varepsilon\right)\frac{F_S}{A} \right] \tag{4.15}$$

where ε is an infinitesimally small positive number.

In summary, for the hydraulic actuator with dry friction, the controller (4.2) brings the system trajectories to the equilibria described by (4.4). The system, however, will experience steady-state position error which would at least be within the range shown in (4.15).

4.2.3 Experimental Verification

Experiments were conducted on the test rig explained in Chapter 3 to demonstrate the theoretical conclusions drawn in the previous section. The first experiment was to bring the actuator to the desired position $x_{des} = 8$ *in.* The control gains, K_x and K_p, were chosen such that

$\frac{K_p}{K_x} \approx \frac{C}{A} = \frac{V_t}{4\beta A}$, which leads to the smallest steady-state position error band [see (4.15)]. Considering the system parameters shown in Table 3.1, the control gains were chosen as K_x=0.1 $V/psi^{1/2}in$ and K_p=8×10^{-6} $V/psi^{3/2}$ to prevent the input signal saturation at the extreme measurable limits of motion with the supply pressure of P_s=2000 *psi*. The above values of control gains and system parameters (Table 3.1) were further inserted into equation (4.4) which determined the bands of steady-state position and load pressure errors as $e_1^{ss} \in [-0.026, 0.026]$ *in* and $e_3^{ss} \in [-321, 321]$ *psi*. Note that the choice of control gains does not affect the bounds of steady-state load pressure error.

Figure 4.1 shows the experimental response of the system. Both steady-state position and load pressure error bounds are shown as dash- double dotted lines. The plots clearly demonstrate the convergence of the system trajectory to the equilibria given by (4.4), i.e., both position and load pressure responses remain within the bounds, while control signal as well as valve spool displacement both converge to zero.

The second experiment was conducted to observe the performance of the control scheme when the control gain ratio, K_p/K_x, was set to be two times greater than before. Increasing the gain ratio can be done by either increasing K_p or decreasing K_x. Dotted lines in Fig. 4.2 illustrate the system response when K_x=0.05 $V/psi^{1/2}in$ and dashed lines denote the response of the system with K_p=16×10^{-6} $V/psi^{3/2}$. As expected, in both cases the system trajectories converge to the equilibria denoted in (4.4) which is consistant with the theoretical analysis proving that in the presence of dry friction, the control scheme (4.2) is capable of bringing the actuator to the vicinity of the desired position with a predictable steady-state error band. Note that the steady-state position error band increases with the increase of the ratio K_p/K_x.

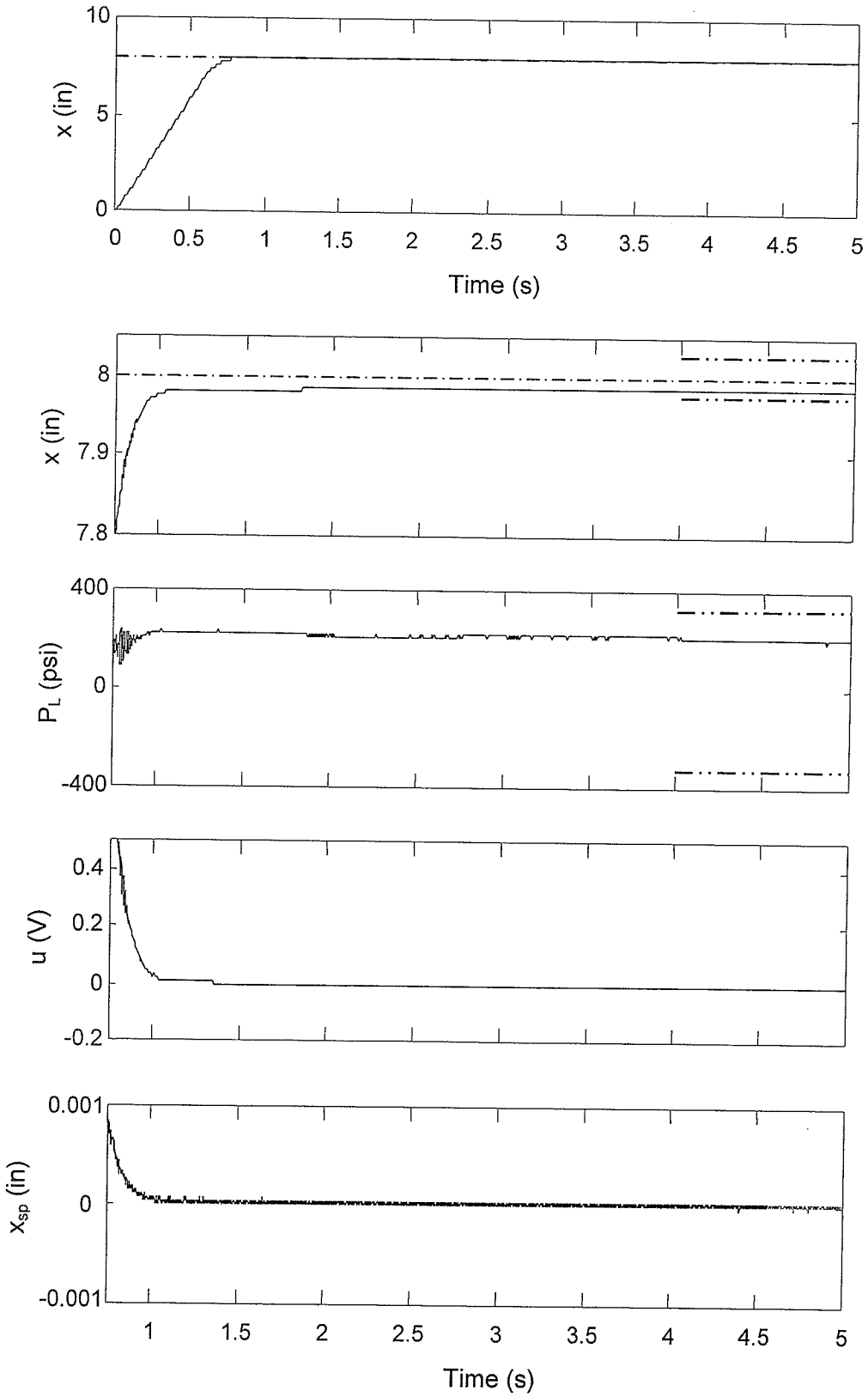

Fig. 4.1 Response of the position control system without friction compensation, K_x=0.1 $V/psi^{1/2}in$, K_p=8x10^{-6} $V/psi^{3/2}$.

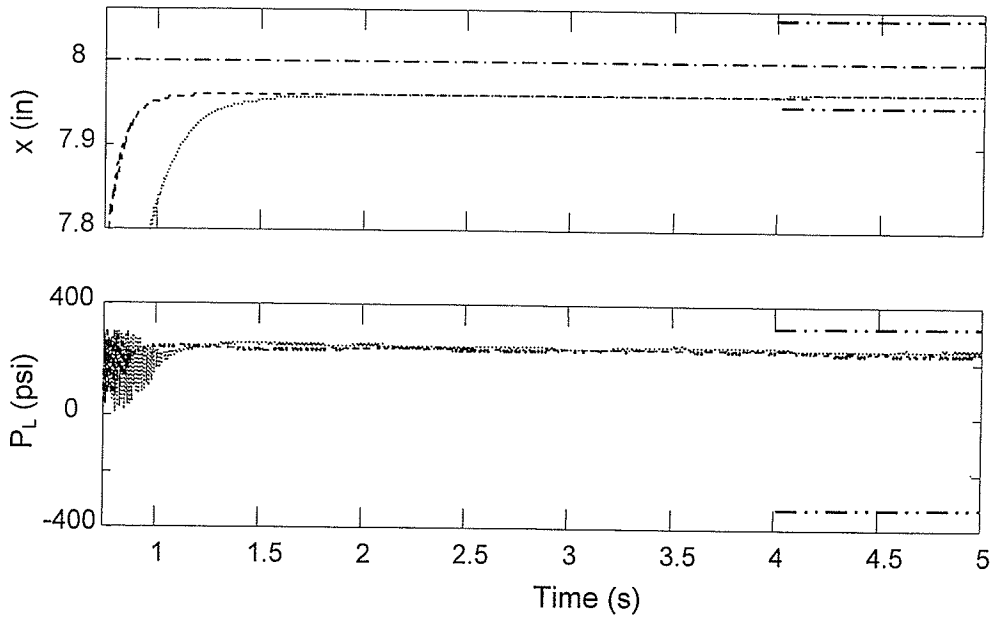

Fig. 4.2 Position control system responses:
..... K_x=0.05 $V/psi^{1/2}in$; K_p=8×10^{-6} $V/psi^{3/2}$
---- K_x=0.1 $V/psi^{1/2}in$; K_p=16×10^{-6} $V/psi^{3/2}$

4.3 Friction Compensating Position Control

4.3.1 Control Design

Although the control scheme proposed by Niksefat et al. (2001) is still effective for position control in the presence of dry friction, it is not capable of position regulation with no steady-state error. Inspired by the study conducted by Southward et al. (1991), in this section, a nonlinear friction compensation technique is designed that is capable of the asymptotic position regulation despite actuator's dry friction. Following the Lyapunov stability theory (detailed in Section 4.3.3) the position control law is proposed as follows:

$$u = -\left(K_p |P_L| sign(x_{sp}) + K_x (x - x_{des})\right)\sqrt{P_s - sign(x_{sp}) P_L} \tag{4.16}$$

where K_p and K_x are positive constant gains.

Compared to the controller (4.2), the above control scheme will be proven to be able to eliminate steady-state position error without requiring additional state feedback or control parameter or introduction of additional discontinuity surface to the dynamic system. Substituting (4.16) into

(4.1) and defining the error states as $e_1 = x - x_{des}$, $e_2 = \dot{x}$, $e_3 = P_L$, and $e_4 = x_{sp}$, yields the following error-space model for the system:

$$\begin{cases} \dot{e}_1 = e_2 \\ \dot{e}_2 = \dfrac{A}{m} e_3 - \dfrac{\left[F_C + (F_S - F_C)e^{-(e_2/\dot{x}_s)^2}\right]\mathrm{sgn}(e_2) + d\,e_2}{m} \\ \dot{e}_3 = \dfrac{1}{C}\left(- Ae_2 + \dfrac{c_d w}{\sqrt{\rho}} e_4 \sqrt{P_s - sign(e_4)\,e_3} \right) \\ \dot{e}_4 = -\dfrac{1}{\tau} e_4 - \dfrac{k_{sp}}{\tau}\left(K_p |e_3| sign(e_4) + K_x e_1\right)\sqrt{P_s - sign(e_4)\,e_3} \end{cases} \tag{4.17}$$

The equilibrium point for the above system is obtained by equating the right-hand side of (4.17) to zero: s

$$\begin{cases} e_1^{ss} = 0 \\ e_2^{ss} = 0 \\ e_3^{ss} = \dfrac{F_S\,\mathrm{sgn}(0)}{A} \\ e_4^{ss} = 0 \end{cases} \tag{4.18}$$

where $F_S\,\mathrm{sgn}(0) \in [-F_S, F_S]$ represents the static friction at the equilibrium point. Depending on the magnitude and direction of the net force applied to the actuator, the equilibrium point of the system can be $\mathbf{e}_{eq} = (0,0,e_3^{ss},0)^T$ where

$$e_3^{ss} = \frac{F_S\,\mathrm{sgn}(0)}{A} \in \left[-\frac{F_S}{A}, \frac{F_S}{A} \right] \tag{4.19}$$

Hence, despite friction effects, the equilibria of the system are always where the actuator follows the desired position asymptotically, i.e., $e_1^{ss} = x^{ss} - x_{des} = 0$.

4.3.2 Solution Analysis

With reference to (4.17), the discontinuity surface of the system is one of the following three surfaces:

Surface 1 $\quad S_1^3 := \{\mathbf{e} : e_2 = 0 \;\&\; e_4 \neq 0\}$

Surface 2 $\quad S_2^3 := \{\mathbf{e} : e_2 \neq 0 \;\&\; e_4 = 0\}$

Surface 3 $\quad S_3^2 := \{\mathbf{e} : e_2 = 0 \;\&\; e_4 = 0\}$ (4.20)

Existence and continuation of Filippov's solution

Let the region $\Omega = R^4 \times R$ and let D be an arbitrary compact set in Ω. The right-hand sides of equations (4.17) are defined everywhere in Ω, and are bounded by $B(t)$. Let $B(t)=L$, which is obviously integrable on D. Furthermore, each term of the right-hand sides of (4.17) is measurable. Thus, the right-hand sides of equations (4.17) satisfy condition B of the Filippov's solution theory (Filippov, 1960) and we have the local existence of a solution which is continuable on $[t_0, t_f]$.

Uniqueness of Filippov's solution

The vector-valued function of the right-hand sides of equations (4.17) is continuous up to the discontinuity surfaces and the discontinuity surfaces are smooth and independent of time *t*. Therefore, conditions A, B and C of Filippov's solution theory (Filippov, 1979) are satisfied. Next, the analysis of the uniqueness of Filippov's solution must be carried out for each discontinuity surface. The uniqueness analysis for the surface S_1^3 is similar to the analysis conducted in Section 4.2.1 and is not repeated.

To prove the uniqueness of Filippov's solution on the discontinuity surface S_2^3, Ω^+ and Ω^- are defined as $\Omega^+ := \{\mathbf{e} : e_4 > 0\}$ and $\Omega^- := \{\mathbf{e} : e_4 < 0\}$ and the normal to this surface, $\mathbf{N}_2$, is:

$$\mathbf{N}_2 = \left(\frac{\partial S_2^3}{\partial e_1} \quad \frac{\partial S_2^3}{\partial e_2} \quad \frac{\partial S_2^3}{\partial e_3} \quad \frac{\partial S_2^3}{\partial e_4} \right)^T = (0 \quad 0 \quad 0 \quad 1)^T \tag{4.21}$$

Defining the vector functions $\mathbf{f}_2^+$ and $\mathbf{f}_2^-$ as the right-hand sides of the dynamic equations (4.17) in the regions Ω^+ and Ω^-, projection of $\mathbf{h}_2 = \mathbf{f}_2^+ - \mathbf{f}_2^-$ on the normal to the discontinuity surface, $\mathbf{N}_2$, is

$$h_{N_2} = \mathbf{N}_2 . \mathbf{h}_2 = -\frac{k_{sp} K_p |e_3|}{\tau} \left(\sqrt{P_s - e_3} + \sqrt{P_s + e_3} \right) - \frac{k_{sp} K_x e_1}{\tau} \left(\sqrt{P_s - e_3} - \sqrt{P_s + e_3} \right) \tag{4.22}$$

According to (4.22), when $K_p |e_3| > |K_x e_1|$, $h_{N_2} < 0$ and according to Lemma 7 in Filippov (1979), the uniqueness of the Filippov's solution for equations (4.17) is guaranteed. For uniqueness analysis when $K_p |e_3| \le |K_x e_1|$, the projections of $\mathbf{f}_2^+$ and $\mathbf{f}_2^-$ along $\mathbf{N}_2$ are derived as

$$\mathbf{f}_{\mathbf{N}_2}^+ = -\frac{k_{sp}}{\tau} \left(K_p |e_3| + K_x e_1 \right) \sqrt{P_s - e_3}$$

$$\mathbf{f}_{N_2}^{-} = -\frac{k_{sp}}{\tau}\left(-K_p|e_3| + K_x e_1\right)\sqrt{P_s + e_3} \tag{4.23}$$

Since $K_p|e_3| \le |K_x e_1|$, (4.23) implies that $\mathbf{f}_{N_2}^{+} > 0$ **&** $\mathbf{f}_{N_2}^{-} > 0$ when $e_1 < 0$ and $\mathbf{f}_{N_2}^{+} < 0$ **&** $\mathbf{f}_{N_2}^{-} < 0$ when $e_1 > 0$. Therefore, according to Lemma 9 of Filippov (1960), the solution goes through the discontinuity surface S_2^3 with an isolated point.

The uniqueness of the Filippov's solution to the nonsmooth dynamic system shown in (4.17) when the discontinuity surface is the intersection surface $S_1^2 := \{\mathbf{e} : e_2 = 0 \;\&\; e_4 = 0\}$ is presented next.

The solution region Ω is divided into four regions described as follows:

$$S_1^4 := \{\mathbf{e} : e_2 > 0 \;\&\; e_4 > 0\} \quad , \quad S_2^4 := \{\mathbf{e} : e_2 > 0 \;\&\; e_4 < 0\}$$
$$S_3^4 := \{\mathbf{e} : e_2 < 0 \;\&\; e_4 > 0\} \quad , \quad S_4^4 := \{\mathbf{e} : e_2 < 0 \;\&\; e_4 < 0\} \tag{4.24}$$

The above regions are bounded by smooth surfaces denoted by S_i^p as follows:

$$S_1^3 := \{\mathbf{e} : e_2 = 0 \;\&\; e_4 > 0\} \quad , \quad S_2^3 := \{\mathbf{e} : e_2 = 0 \;\&\; e_4 < 0\} \quad , \quad S_3^3 := \{\mathbf{e} : e_2 > 0 \;\&\; e_4 = 0\}$$
$$S_4^3 := \{\mathbf{e} : e_2 < 0 \;\&\; e_4 = 0\} \quad , \quad S_1^2 := \{\mathbf{e} : e_2 = 0 \;\&\; e_4 = 0\} \tag{4.25}$$

where superscript p is the dimension of the surface and the subscript i is the number of the surface. With respect to Filippov (1979), we first find the vectors parallel to the p-dimensional tangent to S_i^p at point $\mathbf{e} \in S_i^2$:

$$\mathbf{P}_1^3 = \frac{1}{C_1}\begin{pmatrix} \tilde{e}_1 - e_1 \\ 0 \\ \tilde{e}_3 - e_3 \\ \tilde{e}_4 \end{pmatrix}_{\tilde{e}_4 > 0} , \quad \mathbf{P}_2^3 = \frac{1}{C_2}\begin{pmatrix} \tilde{e}_1 - e_1 \\ 0 \\ \tilde{e}_3 - e_3 \\ \tilde{e}_4 \end{pmatrix}_{\tilde{e}_4 < 0} , \quad \mathbf{P}_3^3 = \frac{1}{C_3}\begin{pmatrix} \tilde{e}_1 - e_1 \\ \tilde{e}_2 \\ \tilde{e}_3 - e_3 \\ 0 \end{pmatrix}_{\tilde{e}_2 > 0} , \quad \mathbf{P}_4^3 = \frac{1}{C_4}\begin{pmatrix} \tilde{e}_1 - e_1 \\ \tilde{e}_2 \\ \tilde{e}_3 - e_3 \\ 0 \end{pmatrix}_{\tilde{e}_2 < 0}$$

$$\mathbf{P}_1^4 = \frac{1}{C_5}\begin{pmatrix} \tilde{e}_1 - e_1 \\ \tilde{e}_2 \\ \tilde{e}_3 - e_3 \\ \tilde{e}_4 \end{pmatrix}_{\substack{\tilde{e}_2 > 0 \\ \tilde{e}_4 > 0}} , \quad \mathbf{P}_2^4 = \frac{1}{C_6}\begin{pmatrix} \tilde{e}_1 - e_1 \\ \tilde{e}_2 \\ \tilde{e}_3 - e_3 \\ \tilde{e}_4 \end{pmatrix}_{\substack{\tilde{e}_2 > 0 \\ \tilde{e}_4 < 0}} , \quad \mathbf{P}_3^4 = \frac{1}{C_7}\begin{pmatrix} \tilde{e}_1 - e_1 \\ \tilde{e}_2 \\ \tilde{e}_3 - e_3 \\ \tilde{e}_4 \end{pmatrix}_{\substack{\tilde{e}_2 < 0 \\ \tilde{e}_4 > 0}} , \quad \mathbf{P}_4^4 = \frac{1}{C_8}\begin{pmatrix} \tilde{e}_1 - e_1 \\ \tilde{e}_2 \\ \tilde{e}_3 - e_3 \\ \tilde{e}_4 \end{pmatrix}_{\substack{\tilde{e}_2 < 0 \\ \tilde{e}_4 < 0}}$$

$$\mathbf{P}_1^2 = \frac{1}{C_9}\begin{pmatrix} \tilde{e}_1 - e_1 \\ 0 \\ \tilde{e}_3 - e_3 \\ 0 \end{pmatrix} \tag{4.26}$$

where $\tilde{\mathbf{e}}$ is on the p-dimensional surface tangential to S_i^p and C_i (i=1,..,9) are positive denominator constants. Now, we calculate Filippov's differential inclusion $F_i^m(t,\mathbf{e})$:

$$F_1^3 = \overline{co}\left\{\begin{pmatrix} 0 \\ \frac{A}{m}e_3 \mp \frac{F_S}{m} \\ 0 \\ -\frac{k_{sp}}{\tau}\left(K_x e_1 + K_p|e_3|\right)\sqrt{P_S - e_3} \end{pmatrix}\right\}, \quad F_2^3 = \overline{co}\left\{\begin{pmatrix} 0 \\ \frac{A}{m}e_3 \mp \frac{F_S}{m} \\ 0 \\ -\frac{k_{sp}}{\tau}\left(K_x e_1 - K_p|e_3|\right)\sqrt{P_S + e_3} \end{pmatrix}\right\}$$

$$F_3^3 = \overline{co}\left\{\begin{pmatrix} 0 \\ \frac{A}{m}e_3 - \frac{F_S}{m} \\ 0 \\ -\frac{k_{sp}}{\tau}\left(K_x e_1 \mp K_p|e_3|\right)\sqrt{P_S \pm e_3} \end{pmatrix}\right\}, \quad F_4^3 = \overline{co}\left\{\begin{pmatrix} 0 \\ \frac{A}{m}e_3 + \frac{F_S}{m} \\ 0 \\ -\frac{k_{sp}}{\tau}\left(K_x e_1 \mp K_p|e_3|\right)\sqrt{P_S \pm e_3} \end{pmatrix}\right\}$$

$$F_1^4 = \overline{co}\left\{\begin{pmatrix} 0 \\ \frac{A}{m}e_3 - \frac{F_S}{m} \\ 0 \\ -\frac{k_{sp}}{\tau}\left(K_x e_1 + K_p|e_3|\right)\sqrt{P_S - e_3} \end{pmatrix}\right\}, \quad F_2^4 = \overline{co}\left\{\begin{pmatrix} 0 \\ \frac{A}{m}e_3 - \frac{F_S}{m} \\ 0 \\ -\frac{k_{sp}}{\tau}\left(K_x e_1 - K_p|e_3|\right)\sqrt{P_S + e_3} \end{pmatrix}\right\}$$

$$F_3^4 = \overline{co}\left\{\begin{pmatrix} 0 \\ \frac{A}{m}e_3 + \frac{F_S}{m} \\ 0 \\ -\frac{k_{sp}}{\tau}\left(K_x e_1 + K_p|e_3|\right)\sqrt{P_S - e_3} \end{pmatrix}\right\}, \quad F_4^4 = \overline{co}\left\{\begin{pmatrix} 0 \\ \frac{A}{m}e_3 + \frac{F_S}{m} \\ 0 \\ -\frac{k_{sp}}{\tau}\left(K_x e_1 - K_p|e_3|\right)\sqrt{P_S + e_3} \end{pmatrix}\right\}$$

$$F_1^2 = \overline{co}\left\{\begin{pmatrix} 0 \\ \frac{A}{m}e_3 \mp \frac{F_S}{m} \\ 0 \\ -\frac{k_{sp}}{\tau}\left(K_x e_1 \mp K_p|e_3|\right)\sqrt{P_S \pm e_3} \end{pmatrix}\right\} \tag{4.27}$$

where $\overline{co}$ denotes the closure of the convex hull.

To prove the uniqueness of the solution on S_1^2, we need to prove that there is right-sided uniqueness up to the boundary of S_1^2 and one and only one of sets $K_i^m = F_i^m \cap \mathbf{P_i^m}$ is non-empty [Theorem 1 in Filippov (1979)]. The right-sided uniqueness of the solution on the intersection surface S_1^2 can be directly proven based on the definition given in Filippov (1979). For the initial value $\mathbf{e} = (e_1^{ini}, 0, e_3^{ini}, 0)^T$, the error-state equation becomes (Note: $\mathbf{e}(t)$ is on the surface S_1^2):

$$\begin{cases} \dot{e}_1 = 0 \\ \dot{e}_2 = \dfrac{A}{m} e_3^{ini} - \dfrac{F_S \operatorname{sgn}(0)}{m} \\ \dot{e}_3 = 0 \\ \dot{e}_4 = -\dfrac{k_{sp} K_x}{\tau} e_1^{ini} \sqrt{P_s} \end{cases} \tag{4.28}$$

In general, the right-hand sides of (4.28) are non-zero, and therefore, at the subsequent time instant, e_2 and/or e_4 are not zero, i.e., the solution trajectory moves away from S_1^2. This means only one point of the solution trajectory is on S_1^2 and the solution is unique on this discontinuity surface. If the right-hand sides of (4.28) remain zero, we have $e_2 = e_4 = 0$ at all time. The solution in this case would be $\mathbf{e}(t) = \left(0, 0, \dfrac{F_S}{A}\operatorname{sgn}(0), 0\right)^T$. Therefore, in both cases the Filippov solution is unique on S_1^2.

We next prove that one and only one of the sets $K_i^m = F_i^m \cap \mathbf{P_i^m}$ is non-empty. The proof is based on the property of a convex set in normal linear spaces, i.e., if two points belong to a convex set, every point on the segment connecting these two points also belongs to the same convex set. Note that since all of the first and third elements of the points belonging to K_i^m are zero, the analysis is limited to the two-dimensional investigation of the second element (**x**) and the forth elements (**y**) of each set. For the system studied in this thesis, the emptiness of sets K_i^4, K_i^3 (i=1,..,4) and K_1^2 are proven according the following rules:

1) If the signs of the state variable in the vector of sets F_i^4 are the same as those of $\mathbf{P_i^4}$, then K_i^4 is non-empty. Otherwise, K_i^4 is empty.

2) Two vectors in sets F_i^3 represent two points in **oxy** plane with **x** and **y** as axes and **o** as the origin. In order to prove that K_1^3, for example, is non-empty, we need to prove that the segment connecting two points has an intersection with **y** and such an intersection is on the positive **x** axis [Note: $\mathbf{P}_1^3$ has the form of $(\tilde{e}_1 - e_1, 0, \tilde{e}_3 - e_3, \tilde{e}_4)^T$ where $\tilde{e}_4 > 0$)].
3) Four vectors in set F_1^2 form a simplex in **oxy** plane. Since $\mathbf{P}_1^2$ is a null set, to prove that K_1^2 is non-empty, we should first determine the intersections of the segments connecting any two points with **x** and **y** axes and then find at least two intersections on either **x** or **y** axes which are on two sides of the origin **o** or on the origin. Otherwise K_1^2 is empty.

The rest of the proof is developed based on the relationship between $\frac{A}{m}e_3$, $\frac{F_S}{m}$, $K_x e_1$, and $K_p|e_3|$. Physically, the stick friction, F_S, is never greater than the net applied force, $|Ae_3|$. Thus, we do not consider cases where $|Ae_3| < F_S$. The remaining possible cases are:

Case 1: $|Ae_3| > F_S$ & $|K_x e_1| > K_p|e_3|$

In this case, $\frac{A}{m}e_3 \pm \frac{F_S}{m}$ are of the same sign and so are $K_x e_1 \mp K_p|e_3|$. The segments connecting any two points in sets F_i^3 and F_1^2 cannot intersect with either **x** or **y** axes. One and only one of K_i^4 (i=1,..,4) is non-empty and all other sets are empty.

Case 2: $|Ae_3| > F_S$ & $|K_x e_1| \le K_p|e_3|$

Again $\frac{A}{m}e_3 \pm \frac{F_S}{m}$ are of the same sign. Here, one and only one of the sets K_3^3 or K_4^3 is non-empty and the rest of the sets are empty.

Case 3: $|Ae_3| = F_S$ & $|K_x e_1| > K_p|e_3|$

In this case, one and only one of K_1^3 or K_2^3 is a non-empty set and the rest of the sets are empty.

Case 4: $|Ae_3| = F_S$ & $|K_x e_1| \le K_p|e_3|$

By observing F_i^m and $\mathbf{P_i^m}$, it is seen that all sets K_i^3 and K_i^4 (i=1,..,4) are empty and the only nonempty set is K_1^2.

In the above analysis, the properties of sets K_i^m were discussed and it was found that one and only one of the sets K_i^m is empty in each possible case. Empty K_i^m means empty H_i^m where H_i^m is the set of the vectors of K_i^m at the point on the edge (boundary) of S_i^p (see Filippov, 1979). Thus, according to Theorem 1 in Filippov (1979), the uniqueness of the solution to (4.17) is verified when the discontinuity is the intersection of two surfaces S_1^3 and S_2^3.

4.3.3 Stability Analysis

Let V be the following smooth positive definite regular function:

$$V = \frac{1}{2}\left(\frac{A e_1}{C} + e_3\right)^2 + \frac{\varepsilon\, m}{2C} e_2^2 + \frac{\varepsilon}{2} e_3^2 + \frac{\tau c_d w A}{2 k_{sp} K_x \sqrt{\rho}\, C^2} e_4^2 \tag{4.29}$$

where ε is an arbitrary small positive constant. The derivative of the above function is

$$\begin{aligned}
\dot{V} = {} & \left(\frac{A e_1}{C} + e_3\right)\frac{c_d w}{C\sqrt{\rho}} e_4 \sqrt{P_s - sign(e_4) e_3} + \frac{\varepsilon}{C} e_2 \left(A e_3 - \left(\left[F_C + (F_S - F_C) e^{-(e_2/\dot{x}_s)^2}\right] \mathrm{sgn}(e_2) + d\, e_2\right)\right) \\
& + \frac{\varepsilon\, e_3}{C}\left(-A e_2 + \frac{c_d w}{\sqrt{\rho}} e_4 \sqrt{P_s - sign(e_4) e_3}\right) + \\
& \frac{\tau c_d w A}{k_{sp} K_x \sqrt{\rho}\, C^2} e_4 \left(-\frac{1}{\tau} e_4 - \frac{k_{sp}}{\tau}\left(K_p |e_3| sign(e_4) + K_x e_1\right)\sqrt{P_s - sign(e_4) e_3}\right) \\
= {} & -\frac{c_d w A}{k_{sp} K_x \sqrt{\rho}\, C^2} e_4^2 - \frac{\varepsilon \left(F_C + (F_S - F_C) e^{-(e_2/\dot{x}_s)^2}\right)}{C} |e_2| - \frac{\varepsilon\, d}{C} e_2^2 \\
& - \frac{c_d w}{C\sqrt{\rho}}\left(\frac{A K_p}{C K_x} |e_3 e_4| - (\varepsilon + 1) e_3 e_4\right)\sqrt{P_s - sign(e_4)\, e_3}
\end{aligned} \tag{4.30}$$

According to (4.30), in order to have negative semi-definite $\dot{V}$, the following condition must be imposed on the control gain ratio:

$$\frac{K_p}{K_x} > \frac{(\varepsilon + 1) C}{A} \tag{4.31}$$

Note that since $0 < \varepsilon << 1$, equation (4.31) implies that the lower limit on the control gain ratio, K_p / K_x, is C/A. However, it cannot be equal to C/A as it would not provide a negative semi-difinite $\dot{V}$.

Equation (4.30) denotes that $\dot{V}$ is continuous and negative semi-definite throughout the solution region except for the discontinuity surfaces S_1^3, S_2^3 and S_1^2; On the discontinuity surface, S_1^3:

$$\dot{V}(\mathbf{e} \in S_1^3) \in co[\dot{V}^{S_1^{3+}}, \dot{V}^{S_1^{3-}}] \tag{4.32}$$

where $\dot{V}^{S_1^{3+}}$ and $\dot{V}^{S_1^{3-}}$ are the limit values of $\dot{V}$ as a solution trajectory approaches S_1^3 from both sides:

$$\dot{V}^{S_1^{3+}} = \lim_{e_4 \to 0^+} \dot{V} = -\frac{\varepsilon\left(F_C + (F_S - F_C)e^{-(e_2/\dot{x}_s)^2}\right)}{C}|e_2| - \frac{\varepsilon\, d}{C}e_2^2$$

$$\dot{V}^{S_1^{3-}} = \lim_{e_4 \to 0^-} \dot{V} = -\frac{\varepsilon\left(F_C + (F_S - F_C)e^{-(e_2/\dot{x}_s)^2}\right)}{C}|e_2| - \frac{\varepsilon\, d}{C}e_2^2 \tag{4.33}$$

Equations (4.33) imply that the convex set described in (4.32) only contains one negative element. Thus,

$$\dot{V}(\mathbf{e} \in S_1^3) = -\frac{\varepsilon\left(F_C + (F_S - F_C)e^{-(e_2/\dot{x}_s)^2}\right)}{C}|e_2| - \frac{\varepsilon\, d}{C}e_2^2 \tag{4.34}$$

Similar proof can be given for the derivatives of the Lyapunov function on S_2^3 and S_1^2. Therefore, $\dot{V}$ is negative semi-definite throughout the solution region including the discontinuity surfaces. Consequently, according to the extended LaSalle's invariance principle to nonsmooth systems, every solution trajectory in Ω globally converges to the largest invariant set, **M**, as $t \to \infty$ [see theorem 2 in Section 2.3]. Following the similar contradiction-based analysis explained in Section 4.2.2, it can be proved that this largest invariant set, **M**, contains only the points that belong to the system's equilibria $\mathbf{e}_{eq} = (0,0,e_3^{ss},0)^T$ with e_3^{ss} defined in (4.18). In other words, the control system (4.17) is guaranteed to be capable of completely counteracting friction effects and achieving asymptotic position regulation with no steady-state error in spite of actuator dry friction.

It is important to show that although the system equilibria (4.18) was derived from the simplified state space model (4.1), it is also the equilibria of the more complete model (3.8). Defining the error states as $e_1 = x - x_{des}$, $e_2 = \dot{x}$, $e_3 = P_i$, $e_4 = P_o$ and, $e_5 = x_{sp}$, the control law (4.16) and the friction model (3.17) are combined with (3.8) resulting in the following error state model ($F_{env} = 0$):

$$\begin{cases} \dot{e}_1 = e_2 \\ \dot{e}_2 = \dfrac{A(e_3 - e_4)}{m} - \dfrac{\left[F_C + (F_S - F_C)e^{-(e_2/\dot{x}_s)^2}\right]\mathrm{sgn}(e_2) + d\,e_2}{m} \\ \dot{e}_3 = \dfrac{\beta}{\overline{V}_i + A(e_1 + x_{des} - x_0)}\left(-Ae_2 + \sqrt{\dfrac{2}{\rho}}c_d w e_5 \sqrt{\dfrac{P_S - P_e}{2} + sign(e_5)\left(\dfrac{P_S + P_e}{2} - e_3\right)}\right) \\ \dot{e}_4 = \dfrac{\beta}{\overline{V}_o - A(e_1 + x_{des} - x_0)}\left(Ae_2 - \sqrt{\dfrac{2}{\rho}}c_d w e_5 \sqrt{\dfrac{P_S - P_e}{2} + sign(e_5)\left(e_4 - \dfrac{P_S + P_e}{2}\right)}\right) \\ \dot{e}_5 = -\dfrac{1}{\tau}e_5 - \dfrac{k_{sp}}{\tau}\left(K_p|e_3 - e_4|sign(e_5) + K_x e_1\right)\sqrt{P_s - sign(e_5)(e_3 - e_4)} \end{cases} \tag{4.35}$$

The system's equilibria are derived by equating the right-hand sides of the system to zero:

$$\begin{cases} e_1^{ss} = 0 \\ e_2^{ss} = 0 \\ e_3^{ss} - e_4^{ss} = \dfrac{F_S\,\mathrm{sgn}(0)}{A} \in \left[-\dfrac{F_S}{A}, \dfrac{F_S}{A}\right] \\ e_5^{ss} = 0 \end{cases} \tag{4.36}$$

Thus, the equilibria of the more complete dynamic model is the same as the one for the simplified model proven to be convergent.

4.3.4 Experimental Verification

Experiments were conducted on the electrohydraulic actuator explained in Chapter 3 to show that the proposed control scheme can effectively counteract frictional effects and achieve the desire position asymptotically. In all experiments, the actuator accelerated from rest to the desired position $x_{des} = 8$ *in* under controller (4.16). The first experiment was performed using the ratio of the control gains $\dfrac{K_p}{K_x} \approx \dfrac{C}{A} + \varepsilon$ which is slightly greater than $\dfrac{C}{A}$ and, thus, in the stability region [see (4.31)]. The control gains for the new sets of tests are chosen the same as the ones used in the controller (4.2): K_x=0.1 $V/psi^{1/2}in$ and K_p=8x10^{-6} $V/psi^{3/2}$. These values do not saturate the actuator at the extreme measurable limits of motion when the supply pressure is P_s=2000 *psi*. Figure 4.3 shows the response of the system. The position response of the system demonstrates asymptotic convergence of the system trajectory to the desired position and verifies the friction compensation capability of the proposed controller in a hydraulic actuator. The small position error in this figure is observed to be 0.0014 *in* which is within the resolution of encoder

measurements (0.0015 *in*) and cannot be detected by the controller. Figure 4.3 also confirms that the steady-state load pressure is within the range denoted in (4.18), i.e., $[-321,321\ ]\ psi$.

In order to observe the performance of the control scheme with control gains that place the ratio K_p/K_x greater than the one used, the second set of experiments with the same position regulation task was setup with K_p/K_x twice as big as before. Increasing the gain ratio can be done by either decreasing K_x or increasing K_p. Figure 4.4 illustrates the system response when K_x was halved and Fig. 4.5 shows the response when K_p was doubled. It is seen that in both cases, the proposed control system convergences to the desired position, asymptotically. Figures 4.4 and 4.5 also illustrate that decreasing K_x results in a slower response with larger rise time and increasing K_p dampens the system response, yet the response is asymptotically converging to the desired position. Both steady-state pressure errors are in agreement with the expected steady-state load pressure error from theory, i.e., $e_3^{ss} \in [-321,321\ ]\ psi$ (see 4.18).

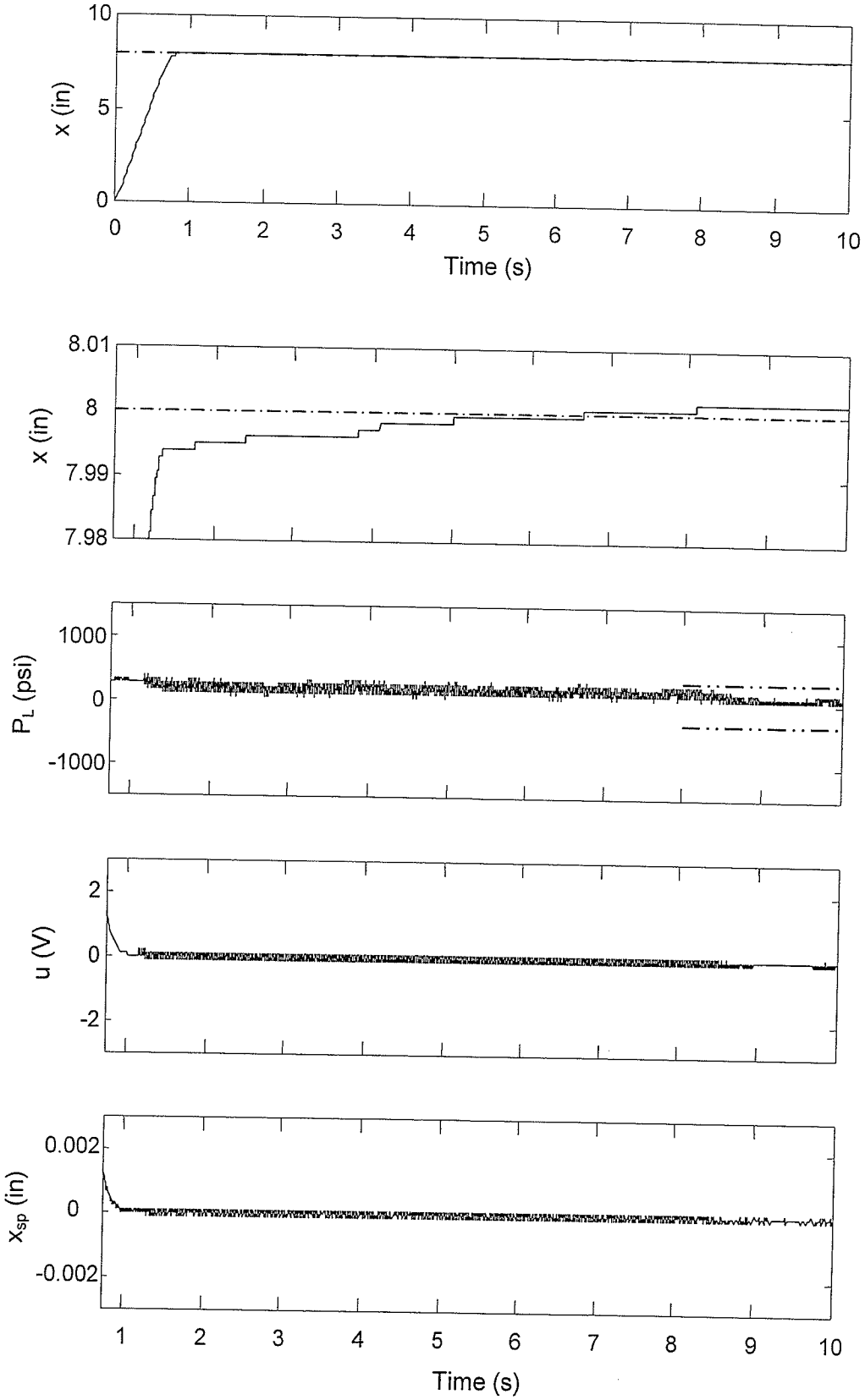

Fig. 4.3 Response of the position control system with friction compensation, K_x=0.1 $V/psi^{1/2}in$, K_p=8x10^{-6} $V/psi^{3/2}$.

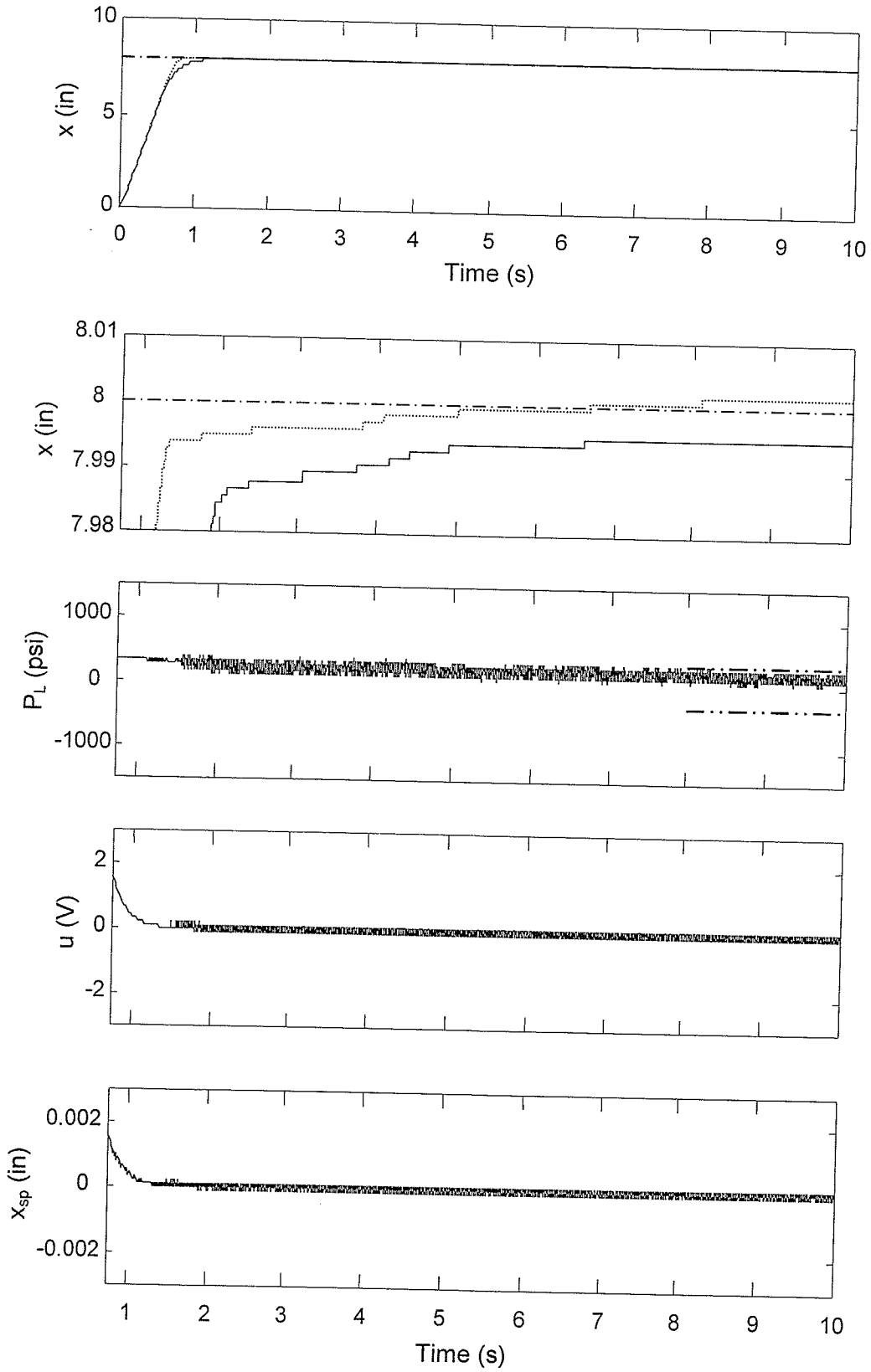

Fig. 4.4 Friction compensating system response: K_x=0.05 $V/psi^{1/2}in$, K_p=8x10^{-6} $V/psi^{3/2}$. Displacement response of Fig. 4.3 is shown as dotted line for reference.

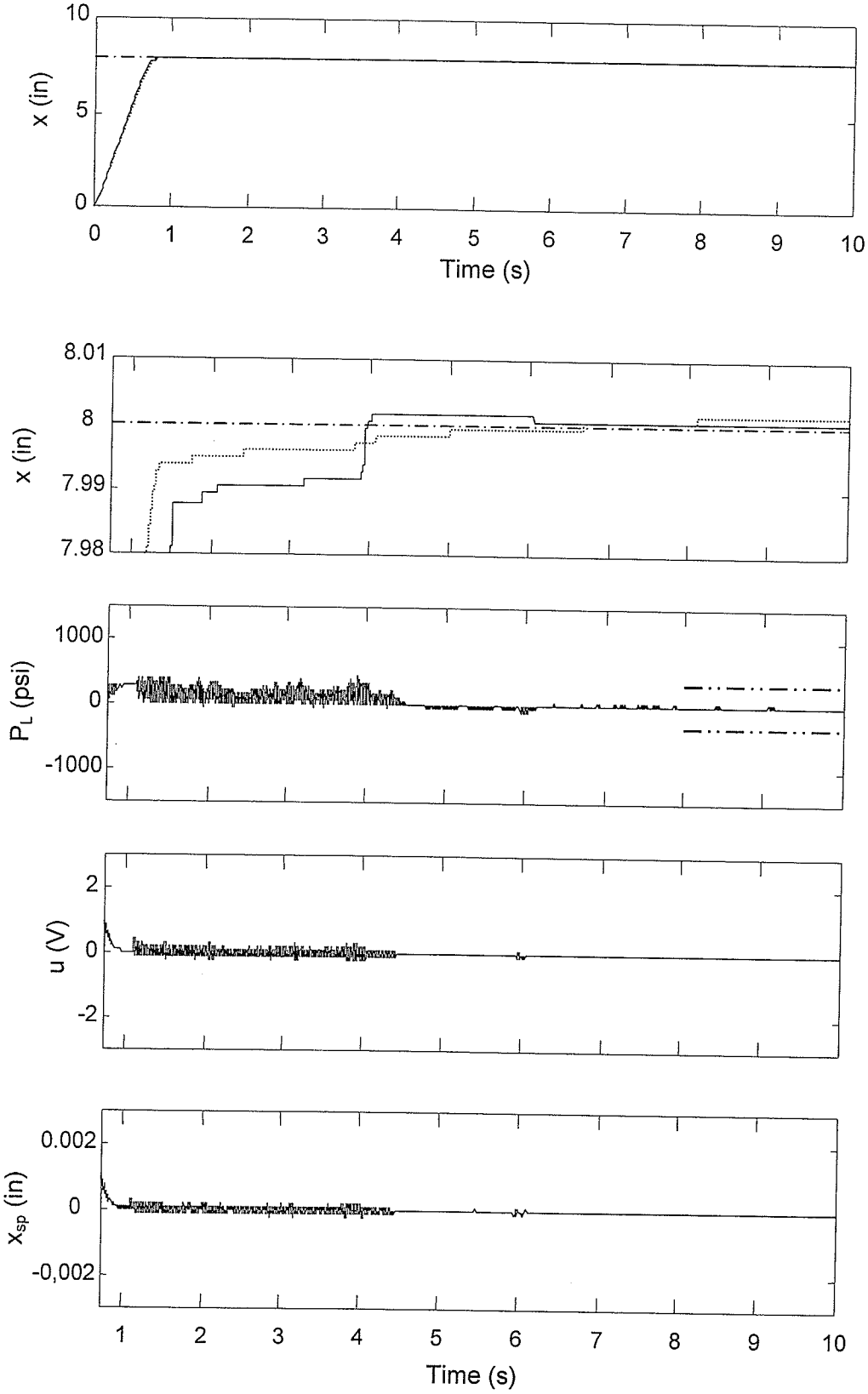

Fig. 4.5 Friction compensating system response: K_x=0.1 $V/psi^{1/2}in$, K_p=16x10^{-6} $V/psi^{3/2}$. Displacement response of Fig. 4.3 is shown as dotted line for reference.

Chapter 5

Impact Control Design for Contact Transition

5.1 Introduction

Stabilization of manipulators during the transition from free-space motion to constraint motion is essential in contact task control design and has not been previously addressed for hydraulically actuated implements colliding with the environment. Nonlinear hydraulic functions, the nonlinear impact model, and the variable operating conditions in the hydraulically actuated systems rules out the linear control design methods and necessitates development of high-performance nonlinear control schemes. Friction is another inevitable problem in hydraulic actuators degrading the system's performance and making precise control difficult to achieve. This chapter presents the design, theoretical analysis and experimental evaluation of Lyapunov-based control schemes to regulate the possible impacts of a hydraulic actuator that comes in contact with a nonmoving environment. The model of the hydraulic system used for control design is the one shown in (3.16) and is combined with the Tustin's friction model (3.17) and Hertz-type impact dynamics (3.23) to represent the complete dynamics of the system in the presence of friction effects and reaction forces arising from a non-moving environment:

$$\begin{cases} \dot{x} = v \\ \dot{v} = \dfrac{A P_L}{m} - \dfrac{F_f}{m} - \dfrac{F_{env}}{m} \\ \dot{P}_L = \dfrac{1}{C}\left(- A\dot{x} + \dfrac{c_d w}{\sqrt{\rho}} x_{sp} \sqrt{P_s - sign(x_{sp}) P_L} \right) \\ \dot{x}_{sp} = -\dfrac{1}{\tau} x_{sp} + \dfrac{k_{sp}}{\tau} u \end{cases} \tag{5.1a}$$

$$F_f = \left[F_C + (F_S - F_C) e^{-(\dot{x}/v_s)^2} \right] \mathrm{sgn}(\dot{x}) + d\,\dot{x} \tag{5.1b}$$

$$F_{env} = \begin{cases} (1 + p\dot{x}) H(x - x_{env})^n & ; \quad (x - x_{env} > 0) \;\&\; (1 + p\dot{x} > 0) \\ 0 & ; \quad otherwise \end{cases} \tag{5.1c}$$

where

$$sign(x_{sp}) = \begin{cases} x_{sp} / |x_{sp}| & ; \quad x_{sp} \neq 0 \\ 0 & ; \quad x_{sp} = 0 \end{cases}$$

$$\begin{cases} \mathrm{sgn}(\dot{x}) = \{ \dot{x} / |\dot{x}| \} & : \quad \dot{x} \neq 0 \\ \mathrm{sgn}(\dot{x}) \in [-1, 1] & : \quad \dot{x} = 0 \end{cases}$$

The impact control schemes are designed to, upon sensing a nonzero force, position the actuator at the location where the force was sensed; exerting minimal force on a non-moving environment. First, a nonlinear control scheme is designed for an ideal hydraulic actuator that exhibits negligible dry friction. Working with both hard and soft environments and with various approach velocities, theoretical and experimental results confirm that the proposed controller could effectively stabilize the actuator during the transition phase. Next, actuator dry friction is included in the dynamic model of the system and a second Lyapunov-based nonlinear control scheme is designed for impact suppression. Despite being successful in stabilizing the implement in the presence of actuator friction, the control scheme is shown to be ineffective in counteracting dry friction effects and produces steady-state position error. Finally, the position controller designed in Chapter 4 is examined for the purpose of impact control during the transition phase. Therefore, the solution and stability analyses are reproduced towards the new goal of guaranteed asymptotic impact control (with no steady-state error) of hydraulic actuators coming in contact with unexpected environments.

All three control schemes require similar state feedbacks and the same number of control gains. No knowledge of the impact dynamics, friction effects, servovalve dynamics, or hydraulic parameters is required for control action. Continuous measurement of contact force or implement's velocity is also not required during the short period of impact, making the control schemes desirable for practical purposes. Furthermore, due to the discontinuity of all three control schemes, the control systems are nonsmooth. Therefore, solution and stability analyses of the system are studied using Filippov's solution theories (Filippov, 1960, 1979) and the extension of Lyapunov stability theory to nonsmooth systems (Wu et al., 1998a; Shevitz and Paden, 1994). The control schemes are then experimentally evaluated to verify their practicality and effectiveness in collisions with hard and soft environments and with various approach velocities.

5.2 Impact Control Design for Hydraulic Actuators without Dry Friction

5.2.1 Control Design

Inspired by the previous studies of Brogliato and Orhant (1998) and Tornambe (1999), the control design starts with employing the following PD-type controller to regulate the contact transition phase in the presence of possible impacts:

$$f = -K_x(x - x_{des}) - K_v\dot{x} \tag{5.2}$$

where f is the control signal and x_{des} is the desired position of the implement. K_x and K_v are positive control gains. Since the control goal is to rest the implement on the surface of the environment, x_{des} is taken as the location of the environment, x_{env}, which, in case of an unknown environment, is the recorded position of the implement when the first non-zero force is sensed. Within the context of hydraulic applications, the control signal is provided by the actuator force, AP_L. Therefore

$$AP_L = -K_x(x - x_{env}) - K_v\dot{x} \tag{5.3}$$

Since the system is assumed to have negligible dry friction, the only existing friction force is the viscous friction ($F_f = d\dot{x}$). Thus, differentiating (5.3) and combining the result with (5.1a) gives the following relation for spool displacement:

$$x_{sp} = \left(\frac{C\sqrt{\rho}}{mAc_d w}\right)\frac{-AK_v P_L + K_v F_{env} + \left(-mK_x + K_v d + m\frac{A^2}{C}\right)\dot{x}}{\sqrt{P_s - sign(x_{sp})P_L}} \tag{5.4}$$

Due to the fact that the dynamics of the servovalve are much faster than the dynamics of other system components, it is reasonable to, at least for control design purposes, assume that the spool displacement, x_{sp}, is proportional to the valve input voltage, u (Bilodeau and Papadopoulos, 1998) [For stability analysis, however, the full dynamics of the servovalve will be included in the analysis]:

$$u = \frac{1}{k_{sp}}\left(\frac{C\sqrt{\rho}}{mAc_d w}\right)\frac{-AK_v P_L + K_v F_{env} + \left(-mK_x + K_v d + m\frac{A^2}{C}\right)\dot{x}}{\sqrt{P_s - sign(x_{sp})P_L}} \tag{5.5}$$

Furthermore, it is not realistic to assume that the interaction force F_{env} is measurable and can be compensated for during the short transition phase (Brogliato and Orhant, 1998). The force sensor frequency may even show considerable vibrations that deviate the force measurements (Chiu and Lee, 1996). Therefore, considering the fact that every environment has a certain amount of stiffness, K_s, the interaction force is approximated by its relation to position in the controller design procedure, i.e, $F_{env} = K_s(x - x_{env})$. This will modify the control law to:

$$u = \frac{1}{k_{sp}}\left(\frac{C\sqrt{\rho}}{mAc_d w}\right)\frac{-AK_v P_L + K_v K_s(x - x_{env}) + \left(-mK_x + K_v d + m\frac{A^2}{C}\right)\dot{x}}{\sqrt{P_s - sign(x_{sp})P_L}} \tag{5.6}$$

Furthermore, since the actuator velocity changes very quickly during collision, velocity feedback in the control law of high stiffness collisions yields to practical drawbacks. To circumvent this drawback, an important improvement would be to only use measured position in the control algorithm (Tornambe, 1996). Therefore, Equation (5.3) is substituted in (5.6) to eliminate the velocity feedback:

$$u = \frac{1}{k_{sp}}\left(\frac{C\sqrt{\rho}}{mAc_d w}\right)\frac{-AK_v P_L + K_v K_s(x - x_{env}) + \left(-mK_x + K_v d + m\frac{A^2}{C}\right)\left(-\frac{AP_L}{K_v} - \frac{K_x}{K_v}(x - x_{env})\right)}{\sqrt{P_s - sign(x_{sp})P_L}} \tag{5.7}$$

The above equation can be rearranged as:

$$u = \frac{-K_P P_L - K_X (x - x_{env})}{\sqrt{P_s - sign(x_{sp}) P_L}} \tag{5.8}$$

where K_X and K_P are the final controller gains:

$$K_P = \frac{1}{k_{sp}} \left(\frac{C\sqrt{\rho}}{mAc_d w} \right) \left(AK_v + \left(-mK_x + K_v d + m\frac{A^2}{C} \right) \frac{A}{K_v} \right)$$

$$K_X = \frac{1}{k_{sp}} \left(\frac{C\sqrt{\rho}}{mAc_d w} \right) \left(\left(-mK_x + K_v d + m\frac{A^2}{C} \right) \frac{K_x}{K_v} - K_v K_s \right) \tag{5.9}$$

Following the Lyapunov stability theory discussed in the next section, we need to restrict the sign of the second term of (5.8) to guarantee the convergence of the control system to its equilibrium point. The final expression for the control law is, therefore:

$$u = \frac{-K_P P_L - K_X |x - x_{env}| sign(x_{sp})}{\sqrt{P_s - sign(x_{sp}) P_L}} \tag{5.10}$$

Note that, in practice, $(P_s - sign(x_{sp}) P_L)$ is seldom zero since $|P_L|$ is seldom close to P_s. In the rare cases that it becomes zero (e.g. due to noise), it will be set to a small positive number to avoid the problem of dividing by zero [a similar approach as in (Liu and Alleyne, 2000)]. The existence of pressure feedback in the control law is, in fact, useful for damping out the resonance of the hydraulic cylinder and achieving a higher bandwidth (Tafazoli et al., 1998).

Substituting (5.10) into (5.1) and defining the error states as $\mathbf{e} = (e_1, e_2, e_3, e_4)^T = (x - x_{env}, \dot{x}, P_L, x_{sp})^T$ yields the following error space equations of motion:

$$\begin{cases} \dot{e}_1 = e_2 \\ \dot{e}_2 = \dfrac{A}{m} e_3 - \dfrac{d}{m} e_2 - \dfrac{F_{env}}{m} \\ \dot{e}_3 = \dfrac{1}{C} \left(-Ae_2 + \dfrac{c_d w}{\sqrt{\rho}} e_4 \sqrt{P_s - sign(e_4) e_3} \right) \\ \dot{e}_4 = -\dfrac{1}{\tau} e_4 + \dfrac{k_{sp}}{\tau} \dfrac{-K_P e_3 - K_X |e_1| sign(e_4)}{\sqrt{P_s - sign(e_4) e_3}} \end{cases} \tag{5.11}$$

where F_{env} in error space is defined as:

$$F_{env} = \begin{cases} (1 + pe_2) H e_1^{\,n} & ; \quad (e_1 > 0) \,\&\, (1 + p e_2 > 0) \\ 0 & ; \quad otherwise \end{cases} \tag{5.12}$$

The equilibrium point of the above system is obtained by equating the right-hand side of (5.11) to zero: $\mathbf{e}_{eq} = (0,0,0,0)^T$.

Before studying the stability of the above nonsmooth system, the first step is the solution analysis.

5.2.2 Solution Analysis

The discontinuity surface of the system described in (5.11) is

$$S = \{\mathbf{e} : e_4 = 0\} \tag{5.13}$$

The equilibrium point, $\mathbf{e}_{eq} = (0,0,0,0)^T$, is the point where the actuator position is on the surface of the environment and the spool displacement, x_{sp}, is on the discontinuity surface. The discontinuity surface, S, divides the solution domain, Ω, into two regions: $\Omega^- := \{\mathbf{e} : e_4 < 0\}$ and $\Omega^+ := \{\mathbf{e} : e_4 > 0\}$. The right-hand sides of the equations in (5.11) are defined everywhere in Ω, and are measurable and bounded. Therefore, equations (5.11) satisfy condition B of Filippov's solution theory. Thus, by Theorems 4 and 5 of Filippov (1960), the local existence and continuity of a solution is established.

Next, we prove the uniqueness of the solution. Since the right-hand sides of equations (5.11) are continuous before and after the discontinuity surface, and the discontinuity surface, S, is smooth and independent of time, conditions A, B and C of Filippov's solution theory are satisfied (Filippov, 1979). Following the procedure introduced in Filippov (1960), the vector functions $\mathbf{f}^+$ and $\mathbf{f}^-$ are defined as:

$$\mathbf{f}^+ = \begin{cases} e_2 \\ \dfrac{A}{m}e_3 - \dfrac{d}{m}e_2 - \dfrac{F_{env}}{m} \\ \dfrac{1}{C}\left(-Ae_2 + \dfrac{c_d w}{\sqrt{\rho}}e_4\sqrt{P_s - e_3}\right) \\ \dfrac{k_{sp}}{\tau}\cdot\dfrac{-K_P e_3 - K_X|e_1|}{\sqrt{P_s - e_3}} \end{cases} \qquad \mathbf{f}^- = \begin{cases} e_2 \\ \dfrac{A}{m}e_3 - \dfrac{d}{m}e_2 - \dfrac{F_{env}}{m} \\ \dfrac{1}{C}\left(-Ae_2 + \dfrac{c_d w}{\sqrt{\rho}}e_4\sqrt{P_s + e_3}\right) \\ \dfrac{k_{sp}}{\tau}\cdot\dfrac{-K_P e_3 + K_X|e_1|}{\sqrt{P_s + e_3}} \end{cases} \tag{5.14}$$

For all points on the discontinuity surface, S, the vector $\mathbf{h}$ is defined as

$$\mathbf{h}=\mathbf{f}^{+}-\mathbf{f}^{-}=\left\{\begin{array}{c}0\\0\\0\\\dfrac{k_{sp}}{\tau}\cdot\left(\dfrac{-K_P e_3-K_X|e_1|}{\sqrt{P_s-e_3}}-\dfrac{-K_P e_3+K_X|e_1|}{\sqrt{P_s+e_3}}\right)\end{array}\right\} \tag{5.15}$$

which is along with the normal to the discontinuity surface, $\mathbf{N}=(0,0,0,1)^T$. Therefore, for $|K_P e_3|<|K_X e_1|$, the scalar, h_N, calculated as

$$h_N=\mathbf{N}\cdot\mathbf{h}=\frac{k_{sp}}{\tau}\cdot\left(\frac{-K_P e_3\left(\sqrt{P_s+e_3}-\sqrt{P_s-e_3}\right)-K_X|e_1|\left(\sqrt{P_s+e_3}+\sqrt{P_s-e_3}\right)}{\sqrt{P_s^2-e_3^2}}\right) \tag{5.16}$$

is negative and the uniqueness of the Filippov solution is guaranteed (Lemma 7 in (Filippov, 1979)). For $|K_P e_3|\geq|K_X e_1|$, the projections of $\mathbf{f}^{+}$ and $\mathbf{f}^{-}$ along $\mathbf{N}$ are

$$\begin{aligned}\mathbf{f}_{\mathrm{N}}^{+}&=\frac{k_{sp}}{\tau}\cdot\frac{-K_P e_3-K_X|e_1|}{\sqrt{P_s-e_3}}\\ \mathbf{f}_{\mathrm{N}}^{-}&=\frac{k_{sp}}{\tau}\cdot\frac{-K_P e_3+K_X|e_1|}{\sqrt{P_s+e_3}}\end{aligned} \tag{5.17}$$

The above equation implies that the signs of both $\mathbf{f}_{\mathrm{N}}^{+}$ and $\mathbf{f}_{\mathrm{N}}^{-}$ only depend on the sign of $-K_P e_3$ and are always the same. Thus, it follows from Lemma 9 of Filippov (1960) that the system has a unique solution.

5.2.3 Stability Analysis

To study the stability of the system shown in (5.11), in this section, we invoke to the extended LaSalle's invariance principle to nonsmooth systems (Theorem 2 in Section 2.3) and guarantee the convergence of the solutions trajectories to the system's equilibrium point.

Let V be the following piecewise-defined regular function (Note that regular functions include smooth functions and functions which can be written as the pointwise maximum of a set of smooth functions):

$$V=\begin{cases}e_2^{\,2}+\dfrac{C}{m}e_3^{\,2}+\dfrac{\tau c_d w P_s}{\sqrt{\rho}\,k_{sp}K_P m}e_4^{\,2} & ;\ (\mathbf{e}\in\Omega_1)\\ \dfrac{4H}{5m}e_1^{\,n+1}+e_2^{\,2}+\dfrac{C}{m}e_3^{\,2}+\dfrac{\tau c_d w P_s}{\sqrt{\rho}\,k_{sp}K_P m}e_4^{\,2} & ;\ (\mathbf{e}\in\Omega_2)\end{cases} \tag{5.18}$$

where $\Omega_1 = \{\mathbf{e} : e_1 \le 0\}$ and $\Omega_2 = \{\mathbf{e} : e_1 > 0\}$ are the subsets of Ω representing noncontact and contact regions of motion, respectively. Although (5.12) shows that transition between noncontact and contact regions of motion depends on the two conditions on e_1 and $(1 + p e_2)$, the condition on $(1 + p e_2)$ does not really contribute to the judgment of non-contact to contact state change and the state changes are judged by only the sign of displacement state error (Shoji et al., 1991). This is due to the fact that the coefficient of restitution is always positive and according to (3.24), for any positive approach velocity, p is normally a positive small value. Thus, when F_{env} changes from a zero to a nonzero value due to an impact occurrence, the condition $(1 + p e_2 > 0)$ is always satisfied. Conversely, the only case where the condition $(1 + p e_2 > 0)$ can be lost while $(e_1 > 0)$ is when the control force is larger relative to the impact force and is applied to the direction of the environment reaction force. This case is also not likely to happen in rigid collisions with fast approach velocity and is excluded from the Lyapunov stability analysis (It can, however, be included in the overall system's stability analysis using the concept of Lyapunov exponents). Therefore, Ω_1 and Ω_2 represent the noncontact and contact regions of motion and the function V in (5.18) is a continuous function.

Differentiating (5.18) with respect to time and substituting (5.11) into it, yields:

$$\dot{V} = \begin{cases} -\dfrac{2d}{m} e_2^{\,2} + \dfrac{2c_d w}{m\sqrt{\rho}} e_3 e_4 \sqrt{P_s - sign(e_4) e_3} - \dfrac{2c_d w}{m\sqrt{\rho}} e_3 e_4 \dfrac{P_s}{\sqrt{P_s - sign(e_4) e_3}} - \dfrac{2c_d w P_s}{m\sqrt{\rho}\, k_{sp} K_P} e_4^{\,2} \\ \quad - \dfrac{2c_d w K_X P_s}{m\sqrt{\rho}\, k_{sp} K_P} \cdot \dfrac{|e_1| e_4 sign(e_4)}{\sqrt{P_s - sign(e_4) e_3}} \\ \qquad\qquad\qquad\qquad\qquad\qquad\qquad\qquad ; \quad (\mathbf{e} \in \Omega_1) \\ -\dfrac{2pH}{m} e_1^{\,n+1} e_2^{\,2} - \dfrac{2d}{m} e_2^{\,2} + \dfrac{2c_d w}{m\sqrt{\rho}} e_3 e_4 \sqrt{P_s - sign(e_4) e_3} - \dfrac{2c_d w}{m\sqrt{\rho}} e_3 e_4 \dfrac{P_s}{\sqrt{P_s - sign(e_4) e_3}} \\ \quad - \dfrac{2c_d w P_s}{m\sqrt{\rho}\, k_{sp} K_P} e_4^{\,2} - \dfrac{2c_d w K_X P_s}{m\sqrt{\rho}\, k_{sp} K_P} \cdot \dfrac{|e_1| e_4 sign(e_4)}{\sqrt{P_s - sign(e_4) e_3}} \\ \qquad\qquad\qquad\qquad\qquad\qquad\qquad\qquad ; \quad (\mathbf{e} \in \Omega_2) \end{cases} \tag{5.19}$$

Knowing that the load pressure is never greater than the supply pressure ($|e_3| < P_s$) and $e_1 > 0$ in the contact region (Ω_2), $\dot{V}$ is continuous and negative semi-definite throughout the solution

region except for the discontinuity surface, S. On the discontinuity surface, S, we have:

$$\dot{V}(\mathbf{e} \in S) \in co[\dot{V}^{S^+}, \dot{V}^{S^-}] \tag{5.20}$$

where $\dot{V}^{S^+}$ and $\dot{V}^{S^-}$ are the limit values of $\dot{V}$ as a solution trajectory approaches S from both sides:

$$\dot{V}^{S^+} = \lim_{e_4 \to 0^+} \dot{V} = \begin{cases} -\dfrac{2d}{m} e_2^{\,2} & ; \quad (\mathbf{e} \in \Omega_1) \\ -\dfrac{2pH}{m} e_1^{\,n} e_2^{\,2} - \dfrac{2d}{m} e_2^{\,2} & ; \quad (\mathbf{e} \in \Omega_2) \end{cases} \tag{5.21a}$$

$$\dot{V}^{S^-} = \lim_{e_4 \to 0^-} \dot{V} = \begin{cases} -\dfrac{2d}{m} e_2^{\,2} & ; \quad (\mathbf{e} \in \Omega_1) \\ -\dfrac{2pH}{m} e_1^{\,n} e_2^{\,2} - \dfrac{2d}{m} e_2^{\,2} & ; \quad (\mathbf{e} \in \Omega_2) \end{cases} \tag{5.21b}$$

Equations (5.21) imply that the convex set described in (5.20) only contains one negative element. Thus, on the discontinuity surface, we have

$$\dot{V}(\mathbf{e} \in S) = \begin{cases} -\dfrac{2d}{m} e_2^{\,2} & ; \quad (\mathbf{e} \in \Omega_1) \\ -\dfrac{2pH}{m} e_1^{\,n} e_2^{\,2} - \dfrac{2d}{m} e_2^{\,2} & ; \quad (\mathbf{e} \in \Omega_2) \end{cases} \tag{5.22}$$

Based on the above analysis, we can conclude that $\dot{V}$ is negative semi-definite in the entire contact and noncontact regions of motion as well as on the discontinuity surface, S. Therefore, according to the extended LaSalle's invariance principle to nonsmooth systems (Theorem 2 in Section 2.3), every solution trajectory in Ω converges to the largest invariant set, **M,** as $t \to \infty$. This largest invariant set, **M**, is further proven to contain only the equilibrium point, $\boldsymbol{e}_{eq} = (0,0,0,0)^T$. This can be proven by contradiction: Let **R** be the set of all points within the solution region Ω where $\dot{V} = 0$. According to (5.19), $\dot{V} = 0$ requires that for all the points in **R**, $e_2 = 0$ and $e_4 = 0$. Thus, both $\dot{e}_2$ and $\dot{e}_4$ are zero. Let **M** be the largest invariant set in **R** and contain a point where at least one of the error states, e_1 or e_3 is not zero. The second and forth equations of (5.11) imply that if any of e_1 or e_3 is not zero, then either $\dot{e}_2 \neq 0$ and/or $\dot{e}_4 \neq 0$. This necessitates the solution trajectory to immediately move out of the set **R** and certainly out of set **M,** which contradicts the initial assumption that **M** is the largest invariant set in **R**. Thus, we can conclude that both $e_1 = 0$ and $e_3 = 0$ and the largest invariant set **M** can only contains the

equilibrium point $e_{eq} = (0,0,0,0)^T$, i.e., every solution trajectory in Ω will only converge to the equilibrium point $e_{eq} = (0,0,0,0)^T$.

5.3 Impact Control Design for Actuator with Dry Friction

Despite being successful in stabilizing the impacts and resting the implement on the surface of the environment, the theoretical analysis provided in the previous section remains questionable in the presence of actuator dry friction. In this section, a Lyapunov-based controller is developed for impact control in the presence of actuator's dry friction.

5.3.1 Control Design

The feedback control scheme is designed based on the Lyapunov direct method (detailed in Section 5.3.3):

$$u = -\frac{K_p P_S P_L + K_x (x - x_{env})(P_s - sign(x_{sp})\, P_L)}{\sqrt{P_s - sign(x_{sp})\, P_L}} \tag{5.23}$$

where K_p and K_x are positive constant gains and $sign(x_{sp})$ is as defined in (3.4). Note that in practice, $(P_s - sign(x_{sp})P_L)$ is seldom zero and in the rare cases that it becomes zero (e.g., due to any noise), it will be set to a small positive number to avoid the problem of large control output (Liu and Alleyne, 2000).

With respect to (5.23), the new control law has the following characteristics:

i) It does not require the interaction force or actuator velocity as feedback;

ii) Measurements of the actuator position, hydraulic line pressures, supply pressure and the knowledge about the direction of the valve spool displacement are the only required parameters for the control scheme;

iii) No knowledge of the environmental characteristics or actuator friction is required for the control action.

Defining the error states $\mathbf{e} = (e_1, e_2, e_3, e_4)^T = (x - x_{env}, \dot{x}, P_L, x_{sp})^T$ and combining (5.23) with (5.1) constitutes the error state equations of motion:

$$\begin{cases} \dot{e}_1 = e_2 \\ \dot{e}_2 = \dfrac{A}{m} e_3 - \dfrac{\left(F_C + (F_S - F_C) e^{-(e_2/v_s)^2}\right) \mathrm{sgn}(e_2) + d\, e_2}{m} - \dfrac{F_{env}}{m} \\ \dot{e}_3 = -\dfrac{A}{C} e_2 + \dfrac{c_d w}{C\sqrt{\rho}} e_4 \sqrt{P_s - sign(e_4)\, e_3} \\ \dot{e}_4 = -\dfrac{e_4}{\tau} - \dfrac{k_{sp}\left(K_p P_s e_3 + K_x e_1 (P_s - sign(e_4)\, e_3)\right)}{\tau \sqrt{P_s - sign(e_4)\, e_3}} \end{cases} \tag{5.24}$$

where F_{env} is defined as:

$$F_{env} = \begin{cases} (1 + p e_2) H e_1^{\,n} & ; \quad (e_1 > 0) \,\&\, (1 + p e_2 > 0) \\ 0 & ; \quad otherwise \end{cases} \tag{5.25}$$

The equilibrium point of the above system is obtained by equating its right-hand side to zero:

$$\begin{cases} e_2^{ss} = 0 \\ A\, e_3^{ss} - F_S\, \mathrm{sgn}(0) - \widetilde{F}_{env} = 0 \\ e_4^{ss} = 0 \\ K_p e_3^{ss} + K_x e_1^{ss} = 0 \end{cases} \Rightarrow \begin{cases} e_1^{ss} = -\dfrac{K_p}{K_x} \dfrac{F_S\, \mathrm{sgn}(0) + \widetilde{F}_{env}}{A} \\ e_2^{ss} = 0 \\ e_3^{ss} = \dfrac{F_S\, \mathrm{sgn}(0) + \widetilde{F}_{env}}{A} \\ e_4^{ss} = 0 \end{cases} \tag{5.26}$$

where

$$\widetilde{F}_{env} = \begin{cases} H (e_1^{ss})^n & ; \quad e_1^{ss} > 0 \\ 0 & ; \quad e_1^{ss} \le 0 \end{cases} \tag{5.27}$$

The term $F_S\, \mathrm{sgn}\,(0) \in [-F_S, F_S]$ represents the static friction at the equilibrium point. Therefore, depending upon the magnitude and direction of the net external force, the equilibrium point of the system could be every point $\mathbf{e}_{eq} = (e_1^{ss}, 0, e_3^{ss}, 0)^T$ with

$$\begin{cases} e_1^{ss} = -\dfrac{K_p}{K_x} \dfrac{F_S\, \mathrm{sgn}(0) + \widetilde{F}_{env}}{A} \in \left[-\dfrac{K_p}{K_x} \dfrac{F_S + \widetilde{F}_{env}}{A}, -\dfrac{K_p}{K_x} \dfrac{-F_S + \widetilde{F}_{env}}{A} \right] \\ e_3^{ss} = \dfrac{F_S\, \mathrm{sgn}(0) + \widetilde{F}_{env}}{A} \in \left[\dfrac{-F_S + \widetilde{F}_{env}}{A}, \dfrac{F_S + \widetilde{F}_{env}}{A} \right] \end{cases} \tag{5.28}$$

From (5.26), if the actuator stops with no contact with the environment, $e_1^{ss} < 0$ and $\widetilde{F}_{env} = 0$. Thus, $e_1^{ss} \in \left[-\dfrac{K_p}{K_x} \dfrac{F_S}{A}, 0 \right]$ and $e_3^{ss} \in \left[0, \dfrac{F_S}{A} \right]$. Consequently, decreasing K_p / K_x would result in

a decrease in the bounds on e_1^{ss} values. On the other hand, if the actuator remains at rest while in contact with the environment, $e_1^{ss} > 0$ and $\widetilde{F}_{env} = H(e_1^{ss})^n$. Substituting these equations in (5.26) yields:

$$-\frac{K_x}{K_p}e_1^{ss} - \frac{H(e_1^{ss})^n}{A} = \frac{F_S \operatorname{sgn}(0)}{A} \tag{5.29}$$

Inspecting (5.29), it can be shown that the bound on e_1^{ss} values is related to K_p/K_x. For example, for n=1 or n=2, the ranges of e_1^{ss} in the contact region are:

$$\underline{n=1:} \qquad e_1^{ss} \in \left[0, \frac{F_S}{H + AK_x/K_p}\right]$$

$$\underline{n=2:} \qquad e_1^{ss} \in \left[0, \frac{1}{2H}\left(\sqrt{(AK_x/K_p)^2 + 4HF_S} - AK_x/K_p\right)\right] \tag{5.30}$$

It is observed that decreasing K_p/K_x would reduce the bound on e_1^{ss} values when the actuator is in contact with environment.

The above discussion concludes that choosing a small K_p/K_x can effectively counteract frictional effects (by reducing the band of steady-state position error) and locate the actuator end-effector in a close vicinity of the surface of the environment. However, as will be seen next, restrictions imposed by Lyapunov stability analysis prevents choosing the ratio arbitrarily small. It may also be useful to note that in the absence of actuator dry friction, the equilibrium point of the system would bė the unique point $\boldsymbol{e}_{eq} = (0,0,0,0)^T$, i.e., the equilibrium point would be exactly on the surface of the environment.

Due to the discontinuity of the friction model, i.e., the 'sgn' function in (5.1b) and the control law, i.e., '*sign*' function in (5.23), the resulting system described by (5.24) is nonsmooth. In the next section, we outline the proof of the existence, uniqueness and continuation of Filippov's solution for such a nonsmooth system.

5.3.2 Solution Analysis

With respect to (5.24), the control system under study has the following discontinuity surfaces:

Surface 1 $\qquad S_1^3 := \{\mathbf{e} : e_2 = 0 \;\&\; e_4 \neq 0\}$

Surface 2 $S_2^3 := \{\mathbf{e} : e_2 \neq 0 \;\&\; e_4 = 0\}$

Surface 3 $S_3^2 := \{\mathbf{e} : e_2 = 0 \;\&\; e_4 = 0\}$ (5.31)

where the superscripts and subscripts denote the dimension and the number of the discontinuity surfaces, respectively. The surface S_3^2 is the intersection of surfaces S_1^3 and S_2^3.

Existence and continuation of Filippov's solution

Let region $\Omega = R^4 \times R$ and let D be an arbitrary compact set in Ω. The right-hand sides of equations (5.24) are defined everywhere in Ω, and are bounded by $B(t)$. Let $B(t)=L$, which is obviously integrable on D. Furthermore, each term of the right-hand sides of (5.24) is measurable. Thus, the right-hand sides of equations (5.24) satisfy condition B of Filippov's solution theory (Filippov, 1960) and we have the local existence of a solution which is continuous on $[t_0, t_f]$.

Uniqueness of Filippov's solution

The vector-valued function of the right-hand sides of equations (5.24) is continuous up to the discontinuity surfaces and the discontinuity surfaces are smooth and independent of time *t*. Therefore, conditions A, B and C of Filippov's solution theory (Filippov, 1979) are satisfied. The discontinuity surface S_1^3 divides the solution region into two parts: $\Omega^+ := \{\mathbf{e} : e_2 > 0\}$ and $\Omega^- := \{\mathbf{e} : e_2 < 0\}$. The normal to this surface, $\mathbf{N}_1$, is:

$$\mathbf{N}_1 = \left\{ \frac{\partial S_1^3}{\partial e_1} \quad \frac{\partial S_1^3}{\partial e_2} \quad \frac{\partial S_1^3}{\partial e_3} \quad \frac{\partial S_1^3}{\partial e_4} \right\} = \{0 \quad 1 \quad 0 \quad 0\}^T \tag{5.32}$$

Similar to the analysis in Section 4.2.1, is can be shown that

$$h_{N_1} = \mathbf{N}_1 . \mathbf{h}_1 = -2\frac{F_S}{m} < 0 \tag{5.33}$$

where $\mathbf{h}_1 = \mathbf{f}_1^+ - \mathbf{f}_1^-$ at all points of the discontinuity surface S_1^3 and $\mathbf{f}_1^-$ and $\mathbf{f}_1^+$ are defined as the right-hand sides of the dynamic equations (5.24) in the regions Ω^- and Ω^+. Thus, the uniqueness of the Filippov's solution for S_1^3 is guaranteed (Lemma 7 in (Filippov, 1979)). The uniqueness analysis for S_2^3 can be done in a similar way. The uniqueness analayis for the

intersection surface S_3^2 can be conducted following a similar procedure as in Section 4.3.2 and is not detailed.

5.3.3 Stability Analysis

To study the system stability, two smooth positive regular functions are constructed for contact and noncontact phases of motion. Each function guarantees the convergence of the system trajectories to the system's largest invariant set, proven to contain only the points belonging to its equilibria. Combination of both functions results in a continuous composite regular function for the overall system.

Noncontact Region: In the noncontact region of motion, the following regular function V_n is defined:

$$V_n = \frac{K_p C^2}{2m(K_p A - K_x C)}\left(\frac{A e_1}{C} + e_3\right)^2 + \frac{1}{2}e_2^2 + \frac{C}{2m}e_3^2 + \frac{\tau c_d w A}{2mk_{sp}\sqrt{\rho}\,(K_p A - K_x C)}e_4^2 \tag{5.34}$$

which is positive definite under the following condition:

$$\frac{K_p}{K_x} > \frac{C}{A} \tag{5.35}$$

The derivative of V_n is

$$\dot{V}_n = -\frac{c_d w A}{k_{sp}\sqrt{\rho}\, m(K_p A - K_x C)}\left(e_4^2 + \frac{k_{sp}K_p e_3^2 |e_4|}{\sqrt{P_s - sign(e_4)\, e_3}}\right) - \frac{\left(F_C + (F_S - F_C)e^{-(e_2/v_s)^2}\right)}{C}|e_2| - \frac{d}{C}e_2^2 \tag{5.36}$$

which is continuous and negative semi-definite throughout the noncontact region.

Contact Region: In the contact region where $(e_1 > 0)$ and $(1 + pe_2 > 0)$, the following positive definite regular function is introduced [Note that $\frac{K_p}{K_x} > \frac{C}{A}$]:

$$V_c = \frac{K_p C^2}{2m(K_p A - K_x C)}\left(\frac{A e_1}{C} + e_3\right)^2 + \frac{1}{2}e_2^2 + \frac{C}{2m}e_3^2 + \frac{\tau c_d w A}{2mk_{sp}\sqrt{\rho}\,(K_p A - K_x C)}e_4^2 + \frac{H}{(n+1)m}e_1^{n+1} \tag{5.37}$$

Differentiating the above function yields:

$$\dot{V}_c = -\frac{c_d w A}{k_{sp}\sqrt{\rho}\, m(K_p A - K_x C)}\left(e_4^2 + \frac{k_{sp}K_p e_3^2|e_4|}{\sqrt{P_s - sign(e_4)\, e_3}}\right) - \frac{pH}{m}e_2^2 e_1^n - \frac{\left(F_C + (F_S - F_C)e^{-(e_2/v_s)^2}\right)}{C}|e_2| - \frac{d}{C}e_2^2 \tag{5.38}$$

which is continuous and negative semi-definite in the contact region.

Combination of (5.34) and (5.37) constructs the overall composite regular function, V:

$$V = \begin{cases} V_n & ; \quad noncontact \\ V_c & ; \quad contact \end{cases} \tag{5.39}$$

Following similar discussion outlined in Section 5.2.3 (and under similar assumption of $e_1 = 0$ at all contacts and separations), the above composite function V is continuous throughout the solution region. The derivative of V is determined from $\dot{V}_n$ and $\dot{V}_c$ that were shown to be continuous and negative semi-definite throughout the solution region except for the discontinuity surfaces [see (5.36) and (5.38)]. On the discontinuity surface, S_1^3:

$$\dot{V}(\mathbf{e} \in S_1^3) \in co[\dot{V}^{S_1^{3+}}, \dot{V}^{S_1^{3-}}] \tag{5.40}$$

where $\dot{V}^{S_1^{3+}}$ and $\dot{V}^{S_1^{3-}}$ are the limit values of $\dot{V}$ as a solution trajectory approaches S_1^3 from both sides:

$$\dot{V}^{S_1^{3+}} = \lim_{e_4 \to 0^+}\dot{V} = \begin{cases} -\dfrac{\left(F_C + (F_S - F_C)e^{-(e_2/v_s)^2}\right)}{C}|e_2| - \dfrac{d}{C}e_2^2 & ; \quad noncontact \\ -\dfrac{pH}{m}e_2^2 e_1^n - \dfrac{\left(F_C + (F_S - F_C)e^{-(e_2/v_s)^2}\right)}{C}|e_2| - \dfrac{d}{C}e_2^2 & ; \quad contact \end{cases} \tag{5.41}$$

$$\dot{V}^{S_1^{3-}} = l\lim_{e_4 \to 0^-}\dot{V} = \begin{cases} -\dfrac{\left(F_C + (F_S - F_C)e^{-(e_2/v_s)^2}\right)}{C}|e_2| - \dfrac{d}{C}e_2^2 & ; \quad noncontact \\ -\dfrac{pH}{m}e_2^2 e_1^n - \dfrac{\left(F_C + (F_S - F_C)e^{-(e_2/v_s)^2}\right)}{C}|e_2| - \dfrac{d}{C}e_2^2 & ; \quad contact \end{cases} \tag{5.42}$$

Equations (5.41) and (5.42) imply that the convex set described by (5.40) only contains negative elements and we have

$$\dot{V}(\mathbf{e} \in S_1^3) = \overline{co}\left[-\frac{pH}{m}e_2^2 e_1^n - \frac{\left(F_C + (F_S - F_C)e^{-(e_2/v_s)^2}\right)}{C}|e_2| - \frac{d}{C}e_2^2, -\frac{\left(F_C + (F_S - F_C)e^{-(e_2/v_s)^2}\right)}{C}|e_2| - \frac{d}{C}e_2^2\right] \tag{5.43}$$

Similar approach can be used to derive the derivative of $\dot{V}$ on S_2^3 and S_3^2 and we can now conclude that $\dot{V}$ is negative semi-definite in the entire contact and noncontact regions of motion as well as on the discontinuity surfaces. Thus, it follows from the extended LaSalle's invariance principle for nonsmooth systems [Theorem 2 in Section 2.3] that every solution trajectory in Ω converges to the largest invariant set, **M**, as $t \to \infty$. Using similar contradiction method as in Section 4.2.2, it can further be proven that this largest invariant set, **M**, contains only the equilibria. This concludes proving that, subject to the condition $K_p/K_x > C/A$, the control system (5.24) is guaranteed to converge to the system's equilibria.

Remarks

i) According to (5.28) and (5.30), in order to decrease the steady-state position error, K_p/K_x must be kept as small as possible. Therefore, the smallest possible range of the system's steady-state position error in the presence of dry friction is imposed by (5.35) and would be when $K_p/K_x = C/A$. By knowing an estimate of the hydraulic compliance, C, and the piston area, A, (and not the exact values) one could decide on control gains that would produce smallest position error bounds without jeopardizing the stability.

ii) When the actuator has negligible dry friction, the only discontinuity surface $S = \{\mathbf{e} : e_4 = 0\}$ is due to the controller discontinuity and the system has the unique equilibrium point $\mathbf{e}_{eq} = (0,0,0,0)^T$. In this case, (5.39) would be the system's positive-definite Lyapunov function with the derivative:

$$\dot{V} = \begin{cases} -\dfrac{c_d w A}{k_{sp}\sqrt{\rho m(K_p A - K_x C)}}\left(e_4^2 + \dfrac{k_{sp}K_p e_3^2|e_4|}{\sqrt{P_s - sign(e_4)\,e_3}}\right) & ; \quad noncontact \\ -\dfrac{c_d w A}{k_{sp}\sqrt{\rho m(K_p A - K_x C)}}\left(e_4^2 + \dfrac{k_{sp}K_p e_3^2|e_4|}{\sqrt{P_s - sign(e_4)\,e_3}}\right) - \dfrac{pH}{m}e_2^2 e_1^n & ; \quad contact \end{cases} \tag{5.44}$$

which is negative and semi-definite. A similar analysis to what explained above proves that $\dot{V}$ is also negative on discontinuity surface S. Therefore, based on the theorem 3 in Section 2.3, the equilibrium point of the system is asymptotically stable subject to the condition (5.35).

5.3.4 Experimental Verification

Experiments were conducted on the electrohydraulic test rig explained in Section 3.1 to demonstrate the theoretical results in practice. In all experiments, the actuator accelerated from free space given a step input control signal and struck the environment. When the force transducer senses a nonzero force, its corresponding position measured by the encoder is taken as the position of the environment surface. Control is then switched to the control law (5.23) with the goal of stabilizing the actuator on the surface of the environment.

The first set of experiments was performed to study the behavior of the controller in collisions with hard or soft non-moving environments, resembled by metal sheet and wooden plate, respectively. The second set of experiments was to observe the performance of the controller at low or high approach velocities.

Supply pressure of P_s=2000 *psi* was used in each experiment and the sampling time of the system was ≈2*ms*. Knowing the parameters of the system from Table 3.1, the control gains were chosen as K_x=1.3 $V/in\sqrt{psi}$ and K_p=1.4×10^{-5} $V/\sqrt{psi^3}$ which satisfied (5.35). Given the approximate theoretical values of H=3.32×10^6 $lbf/\sqrt[3]{in^2}$ for aluminum sheet and H=0.84×10^6 $lbf/\sqrt[3]{in^2}$ for the wooden plate, the steady-state position and load pressure errors were theoretically calculated to be within the range of $e_1^{ss} \in \left[-3.5\text{x}10^{-3}, 1.45\text{x}10^{-3}\right]$ *in* and $e_3^{ss} \in [-135, 325]$ *psi* for the metal sheet, and $e_1^{ss} \in \left[-3.5\text{x}10^{-3}, 2.4\text{x}10^{-3}\right]$ *in* and $e_3^{ss} \in [-223, 325]$ *psi* for the wooded plate (see (5.28)-(5.30) for calculation of the bounds).

Figures 5.1 and 5.3 show the responses when the actuator hits the two types of environments with low (3.0 *in/s*) and high (8.5 *in/s*) approach velocities. These results clearly demonstrate that the proposed controller is capable of stabilizing the actuator in the vicinity close to the surface of the environment regardless of the stiffness of the environment and the magnitude of the approach velocity. The close-up responses of the states during the steady-state period are shown in Figs. 5.2 and 5.4 and illustrate the small steady-state errors in actuator position with respect to the exact wooden (W) and metallic (M) environment locations. When the actuator settles in free space ($e_1^{ss} < 0$), the corresponding steady-state load pressure error is positive ($e_3^{ss} > 0$), and vice versa. These observations are in-line with, and validate the theoretical derivations and show that

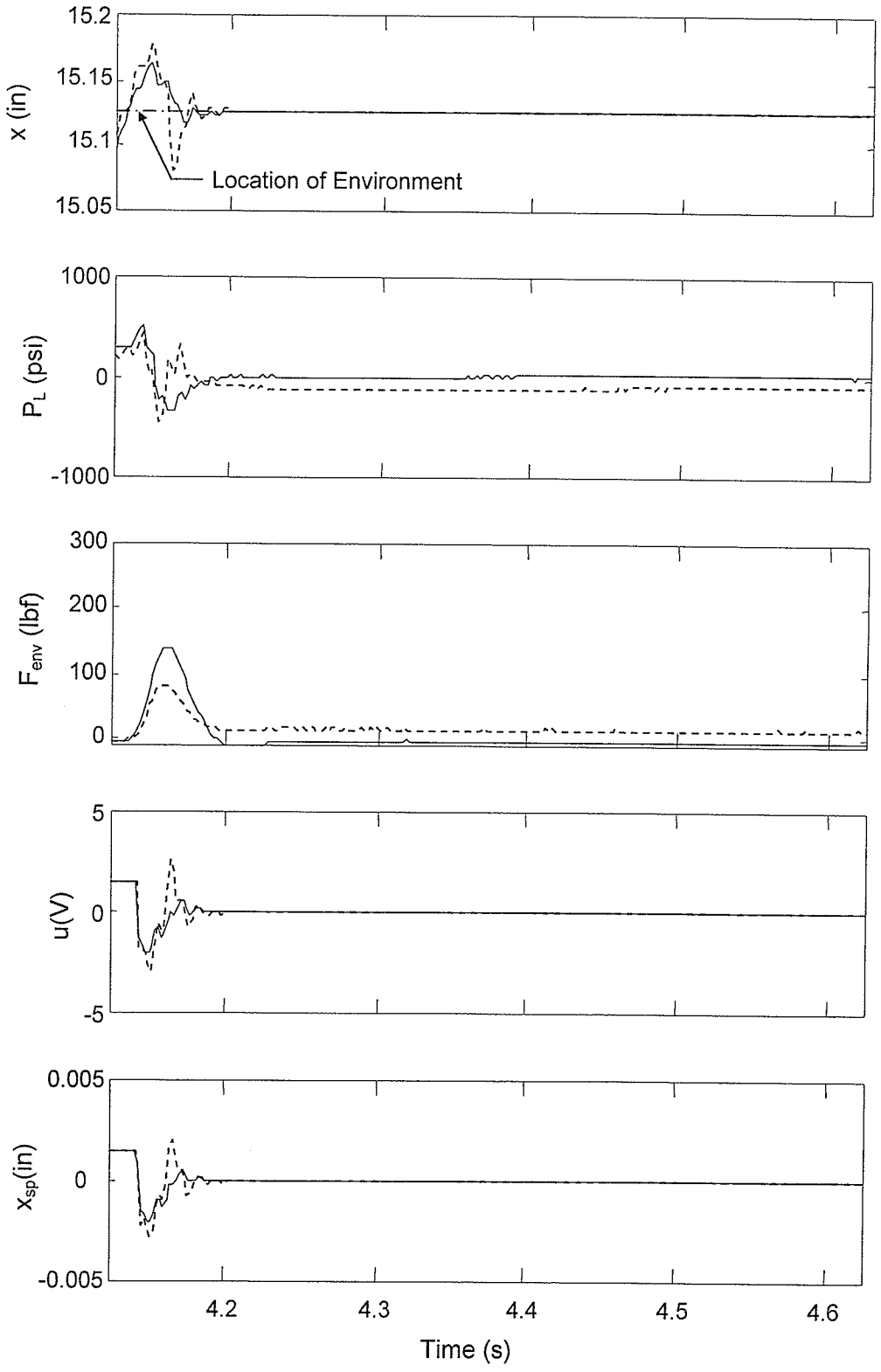

Fig. 5.1 Low velocity impact response (3.0 *in/s*); —— metal, ---- wood.

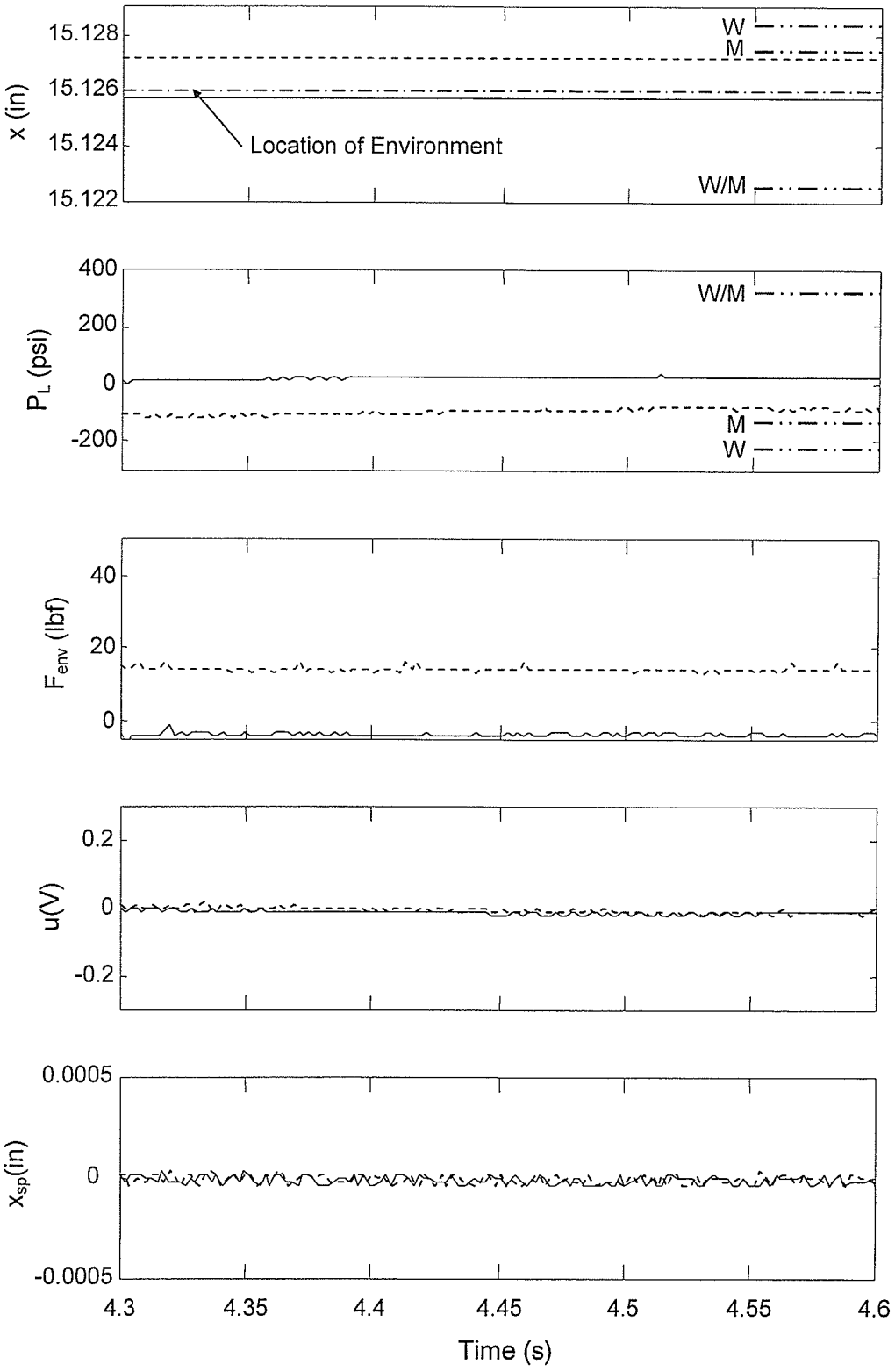

Fig. 5.2 Close-up of responses in Fig. 5.1.

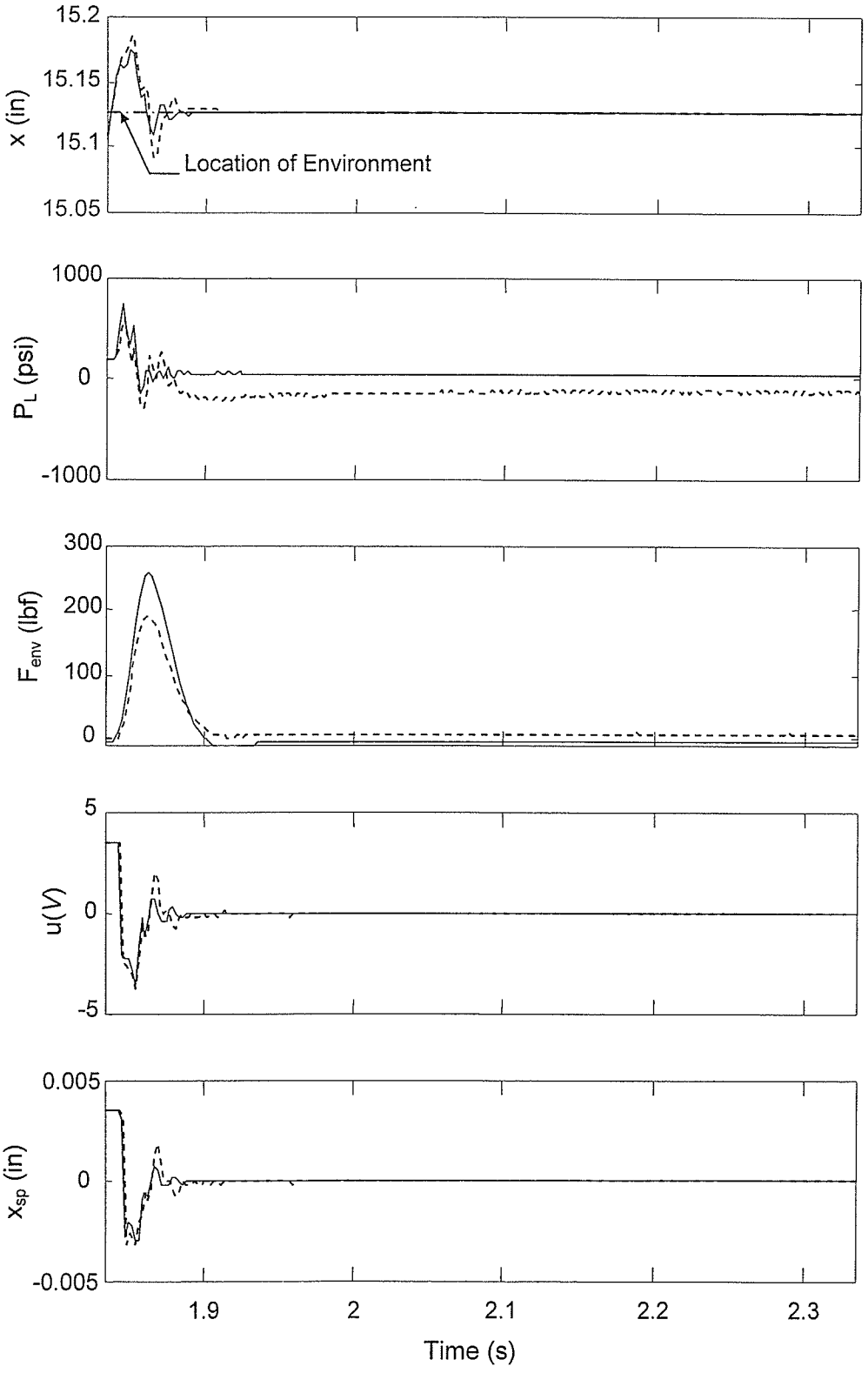

Fig. 5.3 High velocity impact response (8.5 *in/s*); —— metal, ---- wood.

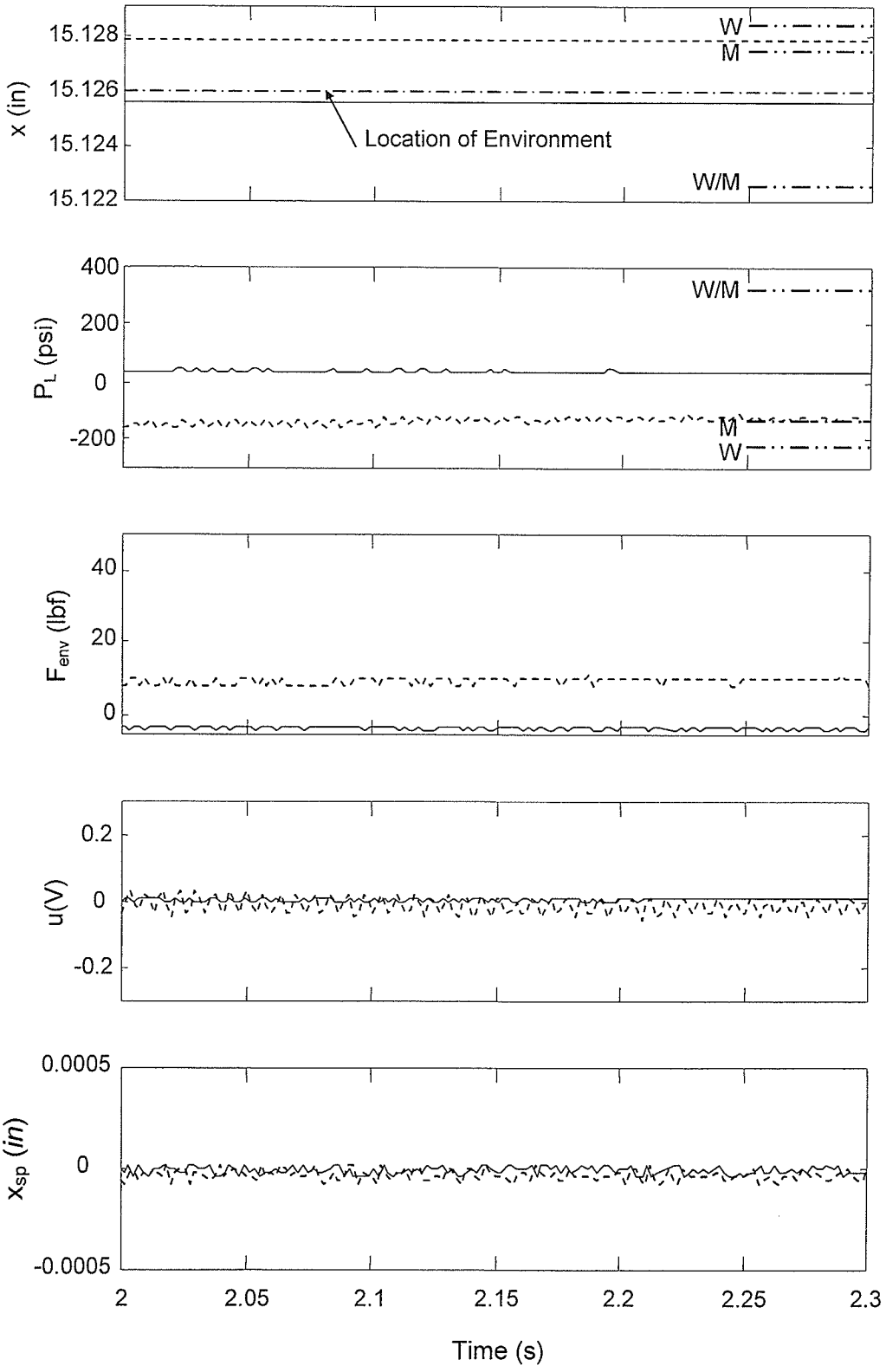

Fig. 5.4 Close-up of responses in Fig. 5.3.

the bounds on the steady-state errors are limited to those derived above analytically. Fig. 5.5 shows the frequency profile of the spool displacement for the high velocity impact with the wooden plate calculated from the experimental data. It validates the previous modeling assumption in Chapter 3 that the dominant frequencies are well below the 200 Hz threshold needed for the first-order approximation of servovalve dynamics (Alleyne, 1996).

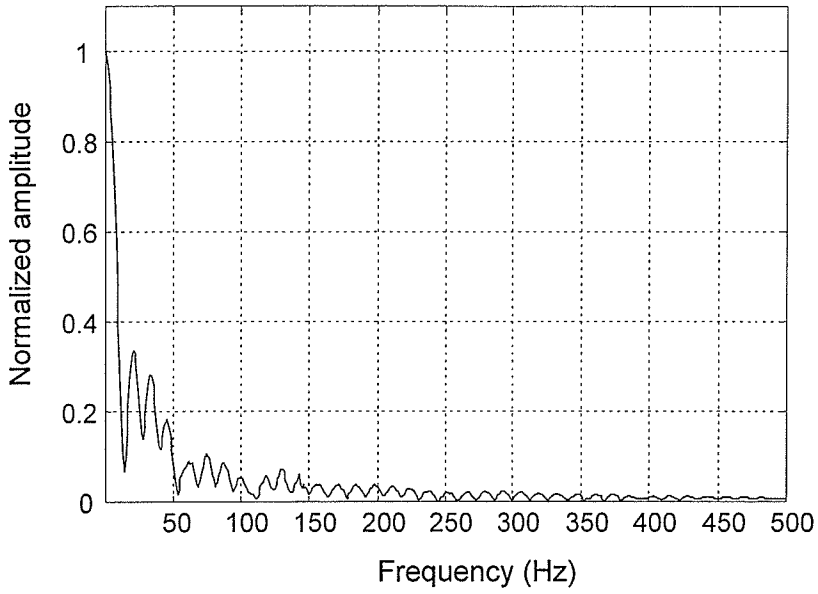

Fig. 5.5 Frequency profile of control signal.

5.4 Friction Compensating Impact Control

5.4.1 Description of the Control System

Despite being successful in stabilizing the implement in the presence of actuator friction, the control scheme developed in Section 5.3 did not counteract actuator's dry friction and ended up with steady-state position error. As a remedy, in the present section, the solution and stability analyses of the friction compensating position control scheme introduced in Section 4.3 is examined towards the new goal of guaranteed asymptotic impact control with no position steady-state error. Substituting the desired position, x_{des}, with the environment location, x_{env} (recorded on the onset of the first impact), the controller (4.16) is re-stated as follows:

$$u = -\left(K_p |P_L| sign(x_{sp}) + K_x (x - x_{env})\right)\sqrt{P_s - sign(x_{sp})\, P_L} \tag{5.45}$$

where K_p and K_x are positive constant gains. Although this controller was initially designed for position control, it enjoys all the positive features that are appropriate for impact control and explained in Section 5.3.1.

Defining the error states $\mathbf{e} = (e_1, e_2, e_3, e_4)^T = (x - x_{env}, \dot{x}, P_L, x_{sp})^T$ and substituting (5.45) into (5.1) constitutes the error space equations of motion:

$$\begin{cases} \dot{e}_1 = e_2 \\ \dot{e}_2 = \dfrac{A}{m} e_3 - \dfrac{\left(F_C + (F_S - F_C) e^{-(e_2/v_s)^2}\right)\mathrm{sgn}(e_2) + d\, e_2}{m} - \dfrac{F_{env}}{m} \\ \dot{e}_3 = -\dfrac{A}{C} e_2 + \dfrac{c_d w}{C\sqrt{\rho}} e_4 \sqrt{P_s - sign(e_4)\, e_3} \\ \dot{e}_4 = -\dfrac{e_4}{\tau} - \dfrac{k_{sp}}{\tau}\left(K_p |e_3| sign(e_4) + K_x e_1\right)\sqrt{P_s - sign(e_4)\, e_3} \end{cases} \tag{5.46}$$

where

$$F_{env} = \begin{cases} (1 + p e_2)\, H\, e_1^{\,n} & ; \quad (e_1 > 0)\ \&\ (1 + p\, e_2 > 0) \\ 0 & ; \quad otherwise \end{cases} \tag{5.47}$$

The equilibrium of the above system, $\mathbf{e}_{eq} = (e_1^{ss}, e_2^{ss}, e_3^{ss}, e_4^{ss})^T$, is obtained by equating the right-hand side of (5.47) to zero:

$$\begin{cases} e_1^{ss} = 0 \\ e_2^{ss} = 0 \\ e_3^{ss} = \dfrac{F_S \operatorname{sgn}(0)}{A} \\ e_4^{ss} = 0 \end{cases} \tag{5.48}$$

Equation (5.48) implies that, subject to proving the system's stability (which would be the subject of next sections), the equilibria of the system with dry friction is where the implement is exactly on the surface of the environment (with no steady-state error). In the absence of actuator dry friction, the system equilibria would change into the unique equilibrium point $\mathbf{e}_{eq} = (0,0,0,0)^T$.

Due to the discontinuities caused by the control law and the employed model of friction, the existence, uniqueness and continuation of Filippov's solution for the nonsmooth system described by (5.46) should first be investigated.

5.4.2 Solution Analysis

The discontinuity surfaces of the system (5.46) are the following three surfaces:

Surface 1 $\quad S_1^3 := \{\mathbf{e} : e_2 = 0 \;\&\; e_4 \neq 0\}$

Surface 2 $\quad S_2^3 := \{\mathbf{e} : e_2 \neq 0 \;\&\; e_4 = 0\}$

Surface 3 $\quad S_3^2 := \{\mathbf{e} : e_2 = 0 \;\&\; e_4 = 0\}$ (5.49)

The conditions for existence and continuity of the Filippov's solution, such as right-hand sides of (5.46) be measurable and bounded, are all satisfied. Those equations also satisfy condition B of the Filippov's solution theory (Filippov, 1960) and we have the local existence of a solution which is continuable on $[t_0, t_f]$.

To study the uniqueness of Filippov's solution for the first discontinuity surface, S_1^3, the solution region is divided into $\Omega^+ := \{\mathbf{e} : e_2 > 0\}$ and $\Omega^- := \{\mathbf{e} : e_2 < 0\}$. The normal to this surface, $\mathbf{N}_1$, is:

$$\mathbf{N}_1 = \left(\frac{\partial S_1^3}{\partial e_1} \quad \frac{\partial S_1^3}{\partial e_2} \quad \frac{\partial S_1^3}{\partial e_3} \quad \frac{\partial S_1^3}{\partial e_4} \right)^T = (0 \quad 1 \quad 0 \quad 0)^T \tag{5.50}$$

Defining the vector functions $\mathbf{f}_1^+$ and $\mathbf{f}_1^-$ as the limiting values of the right-hand sides of (5.46) in Ω^+ and Ω^- as the solution trajectory approaches S_1^3, the projection of $\mathbf{h}_1 = \mathbf{f}_1^+ - \mathbf{f}_1^- = \begin{Bmatrix} 0 \\ -2\dfrac{F_S}{m} \\ 0 \\ 0 \end{Bmatrix}$ on $\mathbf{N}_1$ for all points on the discontinuity surface S_1^3 ($e_2 = 0$) is:

$$h_{N_1} = \mathbf{N}_1 \cdot \mathbf{h}_1 = -2\frac{F_S}{m} < 0 \tag{5.51}$$

Therefore, according to Lemma 7 of Filippov (1960), the uniqueness of the Filippov's solution for S_1^3 is guaranteed.

To prove the uniqueness of Filippov's solution on the discontinuity surface S_2^3, Ω^+ and Ω^- are defined as $\Omega^+ := \{\mathbf{e} : e_4 > 0\}$ and $\Omega^- := \{\mathbf{e} : e_4 < 0\}$. Defining $\mathbf{f}_2^+$ and $\mathbf{f}_2^-$ as the right-hand sides of the dynamic equations (5.46) in the regions Ω^+ and Ω^-, the projections of $\mathbf{f}_2^+$ and $\mathbf{f}_2^-$ along $\mathbf{N}_2$ are:

$$\mathbf{f}_{N_2}^+ = -\frac{k_{sp}}{\tau}\left(K_p|e_3| + K_x e_1\right)\sqrt{P_s - e_3}$$

$$\mathbf{f}_{N_2}^- = -\frac{k_{sp}}{\tau}\left(-K_p|e_3| + K_x e_1\right)\sqrt{P_s + e_3} \tag{5.52}$$

Also, for all the points on the discontinuity surface S_2^3 ($e_4 = 0$), the projection of $\mathbf{h}_2 = \mathbf{f}_2^+ - \mathbf{f}_2^-$ on $\mathbf{N}_2 = \begin{pmatrix} \dfrac{\partial S_2^3}{\partial e_1} & \dfrac{\partial S_2^3}{\partial e_2} & \dfrac{\partial S_2^3}{\partial e_3} & \dfrac{\partial S_2^3}{\partial e_4} \end{pmatrix}^T = (0,0,0,1)^T$, is obtained as

$$h_{N_2} = \mathbf{N}_2 \cdot \mathbf{h}_2 = -\frac{k_{sp}K_p|e_3|}{\tau}\left(\sqrt{P_s - e_3} + \sqrt{P_s + e_3}\right) - \frac{k_{sp}K_x e_1}{\tau}\left(\sqrt{P_s - e_3} - \sqrt{P_s + e_3}\right) \tag{5.53}$$

According to (5.53), when $K_p|e_3| > |K_x e_1|$, $h_{N_2} < 0$ and Lemma 7 in Filippov (1979), guarantees the uniqueness of the Filippov's solution for S_2^3. When $K_p|e_3| \le |K_x e_1|$, (5.52) can be used to show that $\mathbf{f}_{N_2}^+ > 0$ **&** $\mathbf{f}_{N_2}^- > 0$ when $e_1 < 0$ and $\mathbf{f}_{N_2}^+ < 0$ **&** $\mathbf{f}_{N_2}^- < 0$ when $e_1 > 0$. Therefore, in this case Lemma 9 of Filippov (1960) guaranteed that the solution goes through the discontinuity surface S_2^3 with an isolated point.

The solution analysis on the S_1^2 (i.e., the intersection of the surfaces S_1^3 and S_2^3) requires a similar mathematical machinery as in Section 4.3.2 and is ommited from the analysis.

5.4.3 Stability Analysis

For position regulation task in free-space motion, stability of the hydraulic system under control scheme (5.45) was discussed in Section 4 without including any environmental reaction force in the analyses. In impact control application, however, the system interacts with an environment and system stability should be revisited considering the effects of environment impacts. In this section, two positive smooth regular functions are constructed for contact and noncontact phases of motion, each guaranteeing the convergence of the system trajectories to the system's largest invariant set that only contains the points belonging to system's equilibria.

Noncontact Region: In the noncontact region, $F_{env} = 0$ and the following positive definite smooth regular function V_n is defined (ε is an arbitrary small positive constant $0 < \varepsilon << 1$):

$$V_n = \frac{1}{2}\left(\frac{Ae_1}{C} + e_3\right)^2 + \frac{\varepsilon\, m}{2C}e_2^2 + \frac{\varepsilon}{2}e_3^2 + \frac{\tau c_d w A}{2k_{sp}K_x\sqrt{\rho C^2}}e_4^2 \tag{5.54}$$

The derivative of V_n with respect to time is

$$\dot{V}_n = -\frac{c_d w A}{k_{sp}K_x\sqrt{\rho C^2}}e_4^2 - \frac{\varepsilon\,(F_C + (F_S - F_C)e^{-(e_2/v_s)^2})}{C}|e_2| - \frac{\varepsilon\, d}{C}e_2^2 - \frac{c_d w}{C\sqrt{\rho}}\left(\frac{AK_p}{CK_x}|e_3 e_4| - (\varepsilon+1)e_3 e_4\right)\sqrt{P_s - sign(e_4)\,e_3} \tag{5.55}$$

With respect to (5.55), $\dot{V}$ is continuous and negative semi-definite throughout the noncontact region of motion subject to the following condition imposed on the selected control gain ratio:

$$\frac{K_p}{K_x} > \frac{(\varepsilon+1)C}{A} \tag{5.56}$$

i.e., the lower limit on the control gain ratio, K_p/K_x, is C/A.

Contact Region: In the contact region where $F_{env} \neq 0$ and $e_1 > 0$, positive definite smooth regular function is introduced as

$$V_c = \frac{1}{2}\left(\frac{Ae_1}{C} + e_3\right)^2 + \frac{\varepsilon\, m}{2C}e_2^2 + \frac{\varepsilon}{2}e_3^2 + \frac{\tau c_d w A}{2k_{sp}K_x\sqrt{\rho C^2}}e_4^2 + \frac{\varepsilon H}{(n+1)C}e_1^{n+1} \tag{5.57}$$

Differentiating the above function yields:

$$\dot{V}_c = \frac{c_d w A}{k_{sp} K_x \sqrt{\rho} C^2} e_4^2 - \frac{\varepsilon \left(F_C + (F_S - F_C) e^{-(e_2/v_s)^2}\right)}{C} |e_2| - \frac{\varepsilon d}{C} e_2^2 - \frac{c_d w}{C\sqrt{\rho}} \left(\frac{AK_p}{CK_x} |e_3 e_4| - (\varepsilon + 1) e_3 e_4 \right) \sqrt{P_s - sign(e_4) e_3} - \frac{\varepsilon pH}{C} e_2^2 e_1^n \tag{5.58}$$

which is continuous and negative semi-definite in the contact region as long as condition (5.56) is in effect.

Combination of (5.54) and (5.57) constitutes the overall composite regular function, V, for the system interacting with the environment:

$$V = \begin{cases} V_n & ; \quad noncontact \\ V_c & ; \quad contact \end{cases} \tag{5.59}$$

As explained in Section 5.2.3, the only case where the condition $(1 + p e_2 > 0)$ can be lost while $(e_1 > 0)$ is when the control force is larger relatively to the impact force and is applied to the direction of the environment reaction force. Excluding this rare case from the analysis results in a continuous composite function, V. The derivative of V can be obtained by combining (5.55) and (5.58) and is continuous and negative semi-definite throughout the solution region except for the discontinuity surfaces. On the discontinuity surface, S_1^3:

$$\dot{V}(\mathbf{e} \in S_1^3) \in co[\dot{V}^{S_1^{3+}}, \dot{V}^{S_1^{3-}}] \tag{5.60}$$

where $\dot{V}^{S_1^{3+}}$ and $\dot{V}^{S_1^{3-}}$ are the limit values of $\dot{V}$ as a solution trajectory approaches S_1^3 from both sides:

$$\dot{V}^{S_1^{3+}} = \lim_{e_2 \to 0^+} \dot{V} = \begin{cases} -\frac{c_d w A}{k_{sp} K_x \sqrt{\rho} C^2} e_4^2 - \frac{c_d w}{C\sqrt{\rho}} \left(\frac{AK_p}{CK_x} |e_3 e_4| - (\varepsilon + 1) e_3 e_4 \right) \sqrt{P_s - sign(e_4) e_3} & ; \quad noncontact \\ -\frac{c_d w A}{k_{sp} K_x \sqrt{\rho} C^2} e_4^2 - \frac{c_d w}{C\sqrt{\rho}} \left(\frac{AK_p}{CK_x} |e_3 e_4| - (\varepsilon + 1) e_3 e_4 \right) \sqrt{P_s - sign(e_4) e_3} & ; \quad contact \end{cases} \tag{5.61}$$

$$\dot{V}^{S_1^{3-}} = \lim_{e_2 \to 0^-} \dot{V} = \begin{cases} -\frac{c_d w A}{k_{sp} K_x \sqrt{\rho} C^2} e_4^2 - \frac{c_d w}{C\sqrt{\rho}} \left(\frac{AK_p}{CK_x} |e_3 e_4| - (\varepsilon + 1) e_3 e_4 \right) \sqrt{P_s - sign\,(e_4) e_3} & ; \quad noncontact \\ -\frac{c_d w A}{k_{sp} K_x \sqrt{\rho} C^2} e_4^2 - \frac{c_d w}{C\sqrt{\rho}} \left(\frac{AK_p}{CK_x} |e_3 e_4| - (\varepsilon + 1) e_3 e_4 \right) \sqrt{P_s - sign\,(e_4) e_3} & ; \quad contact \end{cases} \tag{5.62}$$

Equations (5.61) and (5.62) imply that the convex set described in (5.60) only contains one element which, considering (5.56), is negative. Thus, on the discontinuity surface S_1^3:

$$\dot{V}(\mathbf{e}\in S_1^3)=-\frac{c_d wA}{k_{sp}K_x\sqrt{\rho C^2}}e_4^2-\frac{c_d w}{C\sqrt{\rho}}\left(\frac{AK_p}{CK_x}|e_3e_4|-(\varepsilon+1)e_3e_4\right)\sqrt{P_s-sign(e_4)\,e_3}<0 \tag{5.63}$$

Similarly, it can be proven that, on the discontinuity surfaces S_2^3 and S_3^2, the convex set of $\dot{V}$ only contains negative and/or zero elements, respectively:

$$\dot{V}(\mathbf{e}\in S_2^3)=\overline{co}\left[-\frac{\varepsilon\left(F_C+(F_S-F_C)e^{-(e_2/v_s)^2}\right)}{C}|e_2|-\frac{\varepsilon\, d}{C}e_2^2-\frac{\varepsilon\, pH}{C}e_2^2e_1^n,-\frac{\varepsilon\left(F_C+(F_S-F_C)e^{-(e_2/v_s)^2}\right)}{C}|e_2|-\frac{\varepsilon\, d}{C}e_2^2\right] \tag{5.64}$$

$$\dot{V}(\mathbf{e}\in S_3^2)=0 \tag{5.65}$$

Therefore, $\dot{V}$ is negative semi-definite in the entire contact and noncontact regions of motion as well as on the discontinuity surface, S_1^3, S_2^3 and S_3^2. We can now conclude that according to the extended LaSalle's invariance principle to nonsmooth systems (Theorem 2 in Section 2.3), every solution trajectory in Ω converges to the largest invariant set, **M**, as $t\to\infty$. A contradiction analysis similar to what is conducted in Sections 5.2.3, would further prove that the system's largest invariant set, **M**, contains only the points that belong to equilibria, $\mathbf{e}_{eq}=\left(0,0,e_3^{ss},0\right)^T$, where $e_3^{ss}=\frac{F_S\,\mathrm{sgn}(0)}{A}$. This completes the proof that, in the event of unexpected collisions, the control scheme given in (5.45) places the hydraulic actuator on the surface of the non-moving environment with no steady-state error in the presence of actuator dry friction.

Before proceeding to the experimental verification, it is useful to note that the equilibria of the system (5.46) that was proved to be convergent would still be the system equilibria if the more complete model (3.8) was used for dynamic modeling. This is shown by first defining the error states $e_1=x-x_{env}$, $e_2=\dot{x}$, $e_3=P_i$, $e_4=P_o$ and, $e_5=x_{sp}$ and substituting the control law (5.45) and the friction model (3.17) into (3.8):

$$\begin{cases} \dot{e}_1 = e_2 \\ \dot{e}_2 = \dfrac{A(e_3 - e_4)}{m} - \dfrac{\left[F_C + (F_S - F_C)e^{-(e_2/\dot{x}_s)^2}\right]\mathrm{sgn}(e_2) + d\,e_2}{m} - \dfrac{F_{env}}{m} \\ \dot{e}_3 = \dfrac{\beta}{\overline{V}_i + A(e_1 + x_{env} - x_0)}\left(-Ae_2 + \sqrt{\dfrac{2}{\rho}}c_d w e_5 \sqrt{\dfrac{P_S - P_e}{2} + sign(e_5)\left(\dfrac{P_S + P_e}{2} - e_3\right)}\right) \\ \dot{e}_4 = \dfrac{\beta}{\overline{V}_o - A(e_1 + x_{env} - x_0)}\left(Ae_2 - \sqrt{\dfrac{2}{\rho}}c_d w e_5 \sqrt{\dfrac{P_S - P_e}{2} + sign(e_5)\left(e_4 - \dfrac{P_S + P_e}{2}\right)}\right) \\ \dot{e}_5 = -\dfrac{1}{\tau}e_5 - \dfrac{k_{sp}}{\tau}\left(K_p|e_3 - e_4|sign(e_5) + K_x e_1\right)\sqrt{P_s - sign(e_5)(e_3 - e_4)} \end{cases} \tag{5.66}$$

where

$$F_{env} = \begin{cases} (1 + pe_2)\,H\,e_1^{\,n} & ; \quad (e_1 > 0)\ \&\ (1 + p\,e_2 > 0) \\ 0 & ; \quad otherwise \end{cases} \tag{5.67}$$

To obtain the system's equilibria, the right-hand sides of (5.66) are equated to zero:

$$\begin{cases} e_1^{ss} = 0 \\ e_2^{ss} = 0 \\ e_3^{ss} - e_4^{ss} = \dfrac{F_S\,\mathrm{sgn}(0)}{A} \in \left[-\dfrac{F_S}{A}, \dfrac{F_S}{A}\right] \\ e_5^{ss} = 0 \end{cases} \tag{5.68}$$

Equations (5.48) and (5.68) indicate that the equilibria of the more complete dynamic model is the same as the one for the simplified model proven to be convergent.

5.4.4 Experimental Verification

The theoretical results obtained in the previous sections are further verified through similar experimental test as in Section 5.3.4 where the actuator accelerated from free space given a step input control signal and struck the environment. Upon sensing a nonzero force for the first time, this position was taken as the position of the environment surface and the proposed control law (5.45) was activated to stabilize the actuator on the surface of the environment. Contrary to the control scheme (5.23) which showed a steady-state error in the resting position of the end-effector, the experimental results using the control law (5.45) are shown to be free of steady-state position error despite the existence of dry friction in the hydraulic actuator.

Two fast (8.5 *in/s*) and slow (3.0 *in/s*) approach velocities were examined and the hard and soft impacts were simulated by metal and wooden environments. The control gains were chosen as

K_x=0.8 $V/psi^{1/2}in$ and K_p=10^{-5} $V/psi^{3/2}$, which do not saturate the input signal at the extreme measurable limits of motion with the supply pressure of P_s=2000 *psi*. For the system with the parameters listed in Table 3.1, the steady-state load pressure error, equation (5.48), is estimated to be within $e_3^{ss} = [-321,321]$ *psi*.

Figures 5.6 and 5.8 show the experimental responses of the system when the actuator hits the two types of environments with low (3.0 *in/s*) and high (8.5 *in/s*) approach velocities. They demonstrate that the controller is capable of impact suppression and stabilizing the actuator regardless of the environment stiffness and the approach velocity. The close-up responses 5.7 and 5.9 illustrate the convergence of the system trajectory to the equilibria given in (5.48). They particularly show that the end-effector is being rested on the surface of the environment (dash-dotted line) with no steady-state position errors despite the existence of dry friction in the hydraulic actuator. The load pressures, however, exhibit a steady-state error that is within the theoretically derived bounds (dash-double dotted lines) of $e_3^{ss} = [-321,321]$ *psi*.

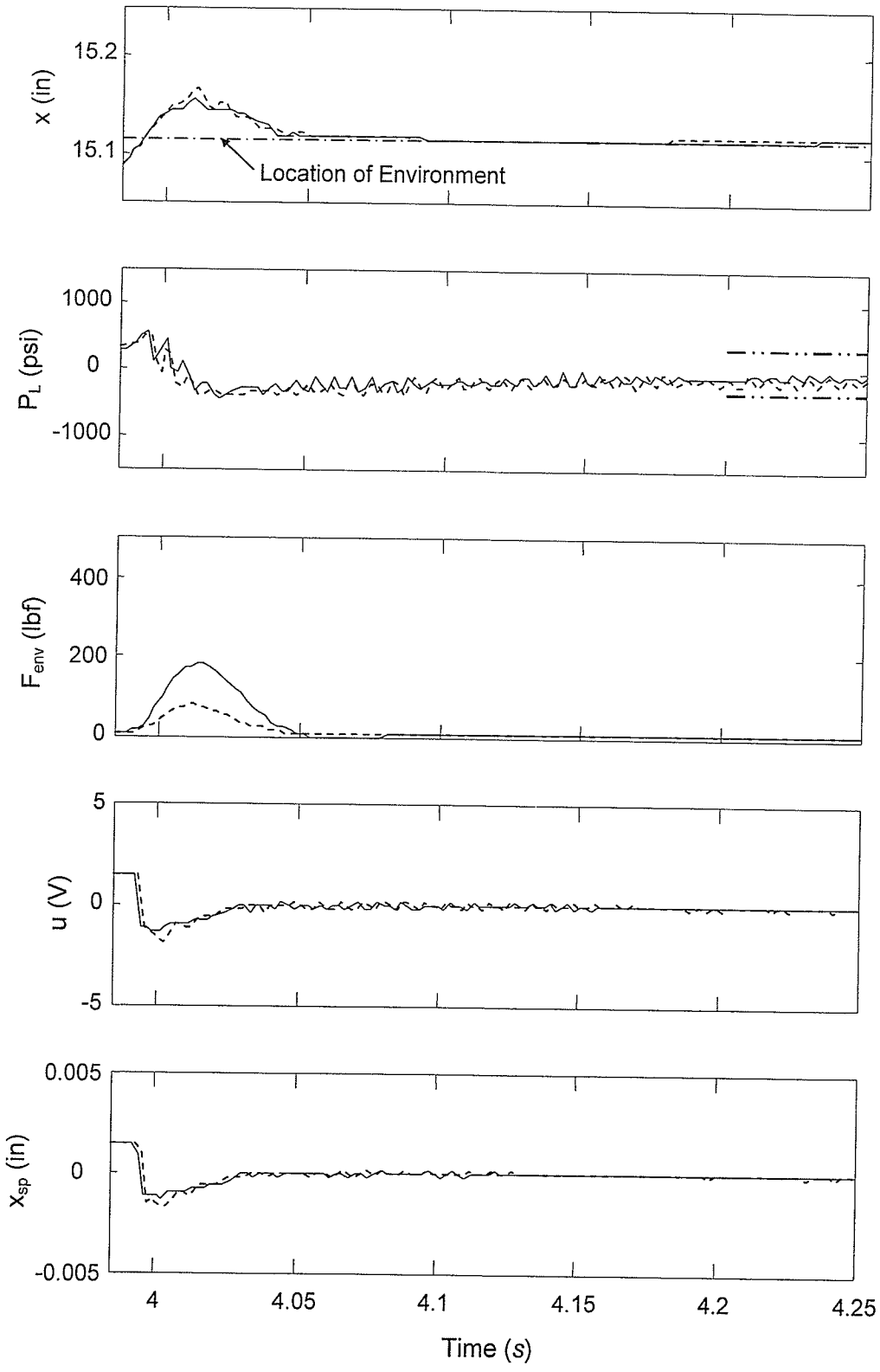

Fig. 5.6 Low velocity impact response (3.0 *in/s*); —— Metal, ---- Wood.

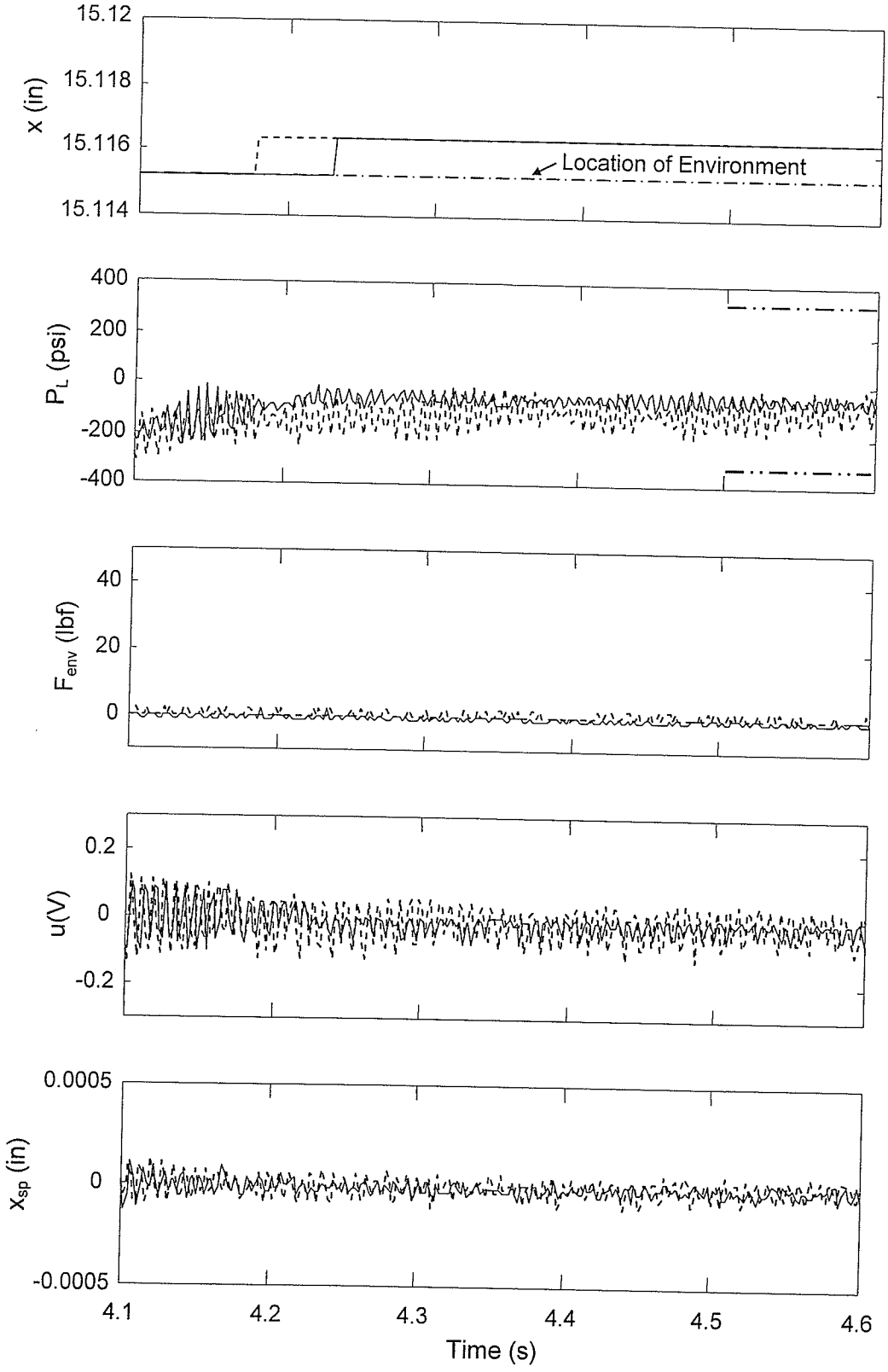

Fig. 5.7 Close-up of responses in Fig. 5.6.

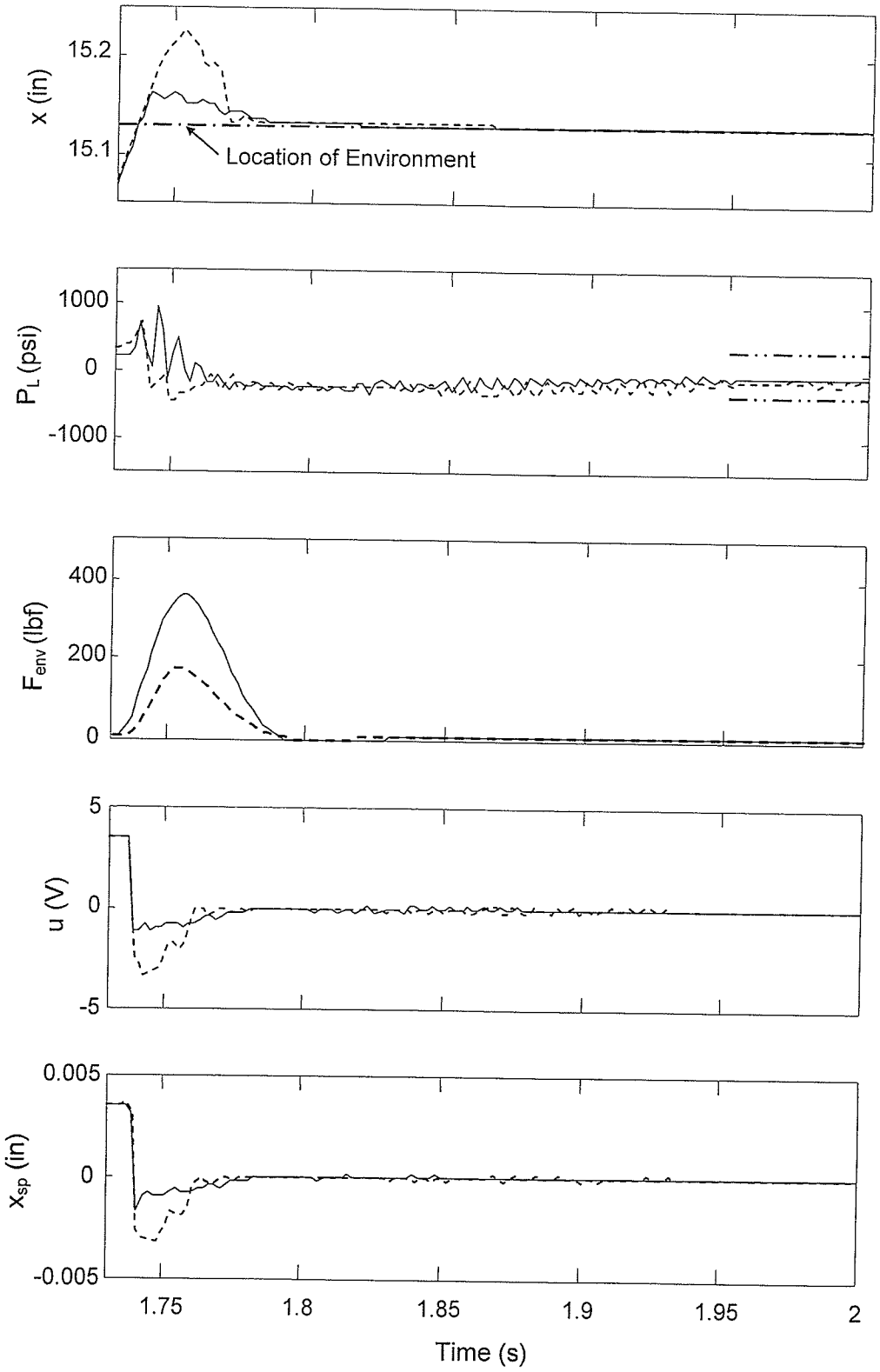

Fig. 5.8 High velocity impact response (8.5 *in/s*); —— Metal, ---- Wood.

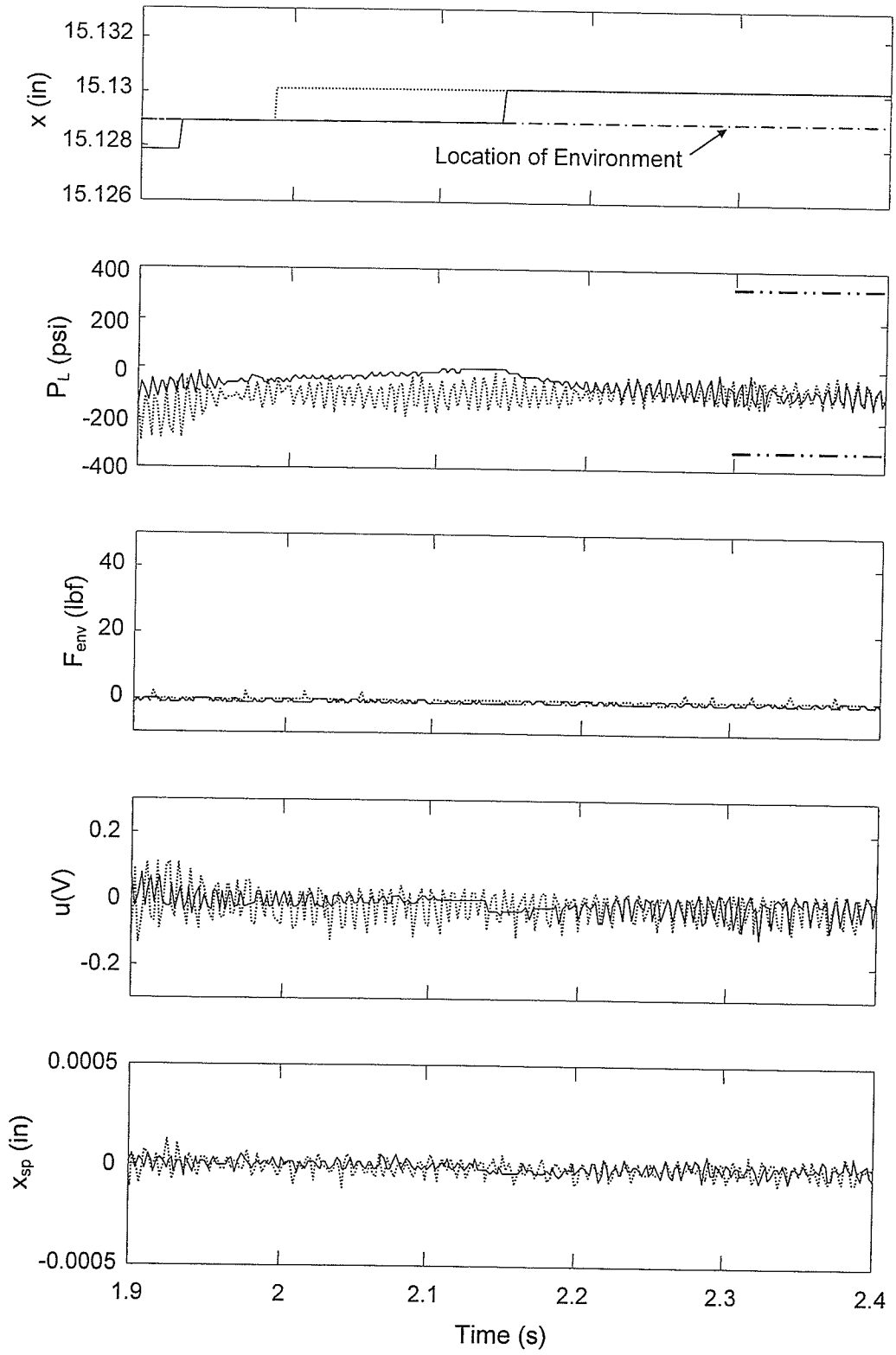

Fig. 5.9 Close-up of responses in Fig. 5.8.

Chapter 6

Force Control Design for Sustained-Contact Motion

6.1 Introduction

Published work on force control/tracking of hydraulic control systems with rigorous stability analysis in the presence of actuator friction either did not include friction in the control design and stability analysis or, only included viscous friction and neglected actuator's dry friction. In this chapter, a Lyapunov-based force control scheme is designed for asymptotic force regulation of a hydraulic actuator in spite of actuator's dry friction. The actuator dynamics is modeled using equation (3.16) which includes the effects of actuator friction, environment reaction force, nonlinear hydraulic functions, and servovalve dynamics in the analysis:

$$\begin{cases} \dot{x} = v \\ \dot{v} = \dfrac{A P_L}{m} - \dfrac{F_f}{m} - \dfrac{F_{env}}{m} \\ \dot{P}_L = \dfrac{1}{C}\left(- A\dot{x} + \dfrac{c_d w}{\sqrt{\rho}} x_{sp} \sqrt{P_s - sign(x_{sp}) P_L} \right) \\ \dot{x}_{sp} = -\dfrac{1}{\tau} x_{sp} + \dfrac{k_{sp}}{\tau} u \end{cases} \tag{6.1}$$

In (6.1), F_f is the friction force modeled by the Tustin's friction model (3.17) and F_{env} is the contact force modeled in (3.23):

$$F_f = \left[F_C + (F_S - F_C)e^{-(\dot{x}/v_s)^2}\right]\mathrm{sgn}(\dot{x}) + d\,\dot{x} \tag{6.2}$$

$$F_{env} = \begin{cases} (1+p\dot{x})H(x-x_{env})^n & ; \quad (x-x_{env}>0)\ \&\ (1+p\dot{x}>0) \\ 0 & ; \quad otherwise \end{cases} \tag{6.3}$$

where

$$sign(x_{sp}) = \begin{cases} x_{sp}/|x_{sp}| & ; \quad x_{sp} \neq 0 \\ 0 & ; \quad x_{sp} = 0 \end{cases}$$

$$\begin{cases} \mathrm{sgn}(\dot{x}) = \{\dot{x}/|\dot{x}|\} & : \quad \dot{x} \neq 0 \\ \mathrm{sgn}(\dot{x}) \in [-1,1] & : \quad \dot{x} = 0 \end{cases}$$

Since the sustained-contact motion is the last part of the overall contact task which starts when the impacts are dissipated and the implement is rested on the surface of environment, the original Hertz contact model (3.21) can be used for environment reaction modeling:

$$F_{env} = \begin{cases} H(x-x_{env})^n & ; \quad (x-x_{env}>0) \\ 0 & ; \quad otherwise \end{cases} \tag{6.4}$$

Combination of (6.1) to (6.4) constitutes the following state-state model of the system:

$$\begin{cases} \dot{x} = v \\ \dot{v} = \dfrac{A\,P_L}{m} - \dfrac{\left[F_C + (F_S - F_C)e^{-(\dot{x}/v_s)^2}\right]\mathrm{sgn}(\dot{x}) + d\,\dot{x}}{m} - \dfrac{F_{env}}{m} \\ \dot{P}_L = \dfrac{1}{C}\left(-A\dot{x} + \dfrac{c_d w}{\sqrt{\rho}} x_{sp}\sqrt{P_s - sign(x_{sp})P_L}\right) \\ \dot{x}_{sp} = -\dfrac{1}{\tau}x_{sp} + \dfrac{k_{sp}}{\tau}u \end{cases} \tag{6.5}$$

6.2 Control Design

The goal of the force control scheme is to exert the desired force, F_{des}, on the environment. Using the Lyapunov stability method (detailed in Section 6.4), the control law is introduced as follows:

$$u = -\left(K_p \left| P_L - \frac{F_{des}}{A} \right| sign(x_{sp}) + K_f (F_{env} - F_{des}) \right) \sqrt{P_s - sign(x_{sp})\, P_L} \tag{6.6}$$

where K_p and K_f are positive constant gains

With respect to equation (6.6), the measurements of the contact force (sensed by the force sensor), hydraulic line pressures, supply pressure and the knowledge about the direction of the valve spool displacement are the only requirements of the proposed control scheme. No exact knowledge about the environmental characteristics, friction nature, or hydraulic parameters is required for the control action.

Before finding the system's equilibria, the error state vector, $\mathbf{e} = (e_1, e_2, e_3, e_4)^T$ is defined as $e_1 = x - (x_{env} + \delta)$, $e_2 = \dot{x}$, $e_3 = P_L - \frac{F_{des}}{A}$, $e_4 = x_{sp}$ where δ is the local elastic deformation of actuator end-point and/or environment when the actuator exerts the desired contact force on the environment (see Fig. 6.1):

$$\delta^{n} = \frac{F_{des}}{H} \tag{6.7}$$

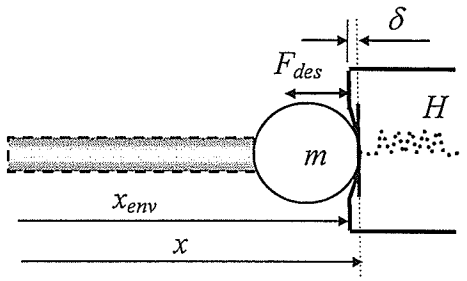

Fig. 6.1 Steady-state implement configuration in contact mode.

Combining (6.5) and (6.6) with the above definition of error states constitutes the following error-state model of the system:

$$\begin{cases} \dot{e}_1 = e_2 \\ \dot{e}_2 = \dfrac{A}{m}\left(e_3 + \dfrac{F_{des}}{A} \right) - \dfrac{\left(F_C + (F_S - F_C) e^{-(e_2/v_s)^2} \right) \mathrm{sgn}(e_2) + d\, e_2}{m} - \dfrac{F_{env}}{m} \\ \dot{e}_3 = -\dfrac{A}{C} e_2 + \dfrac{c_d w}{C\sqrt{\rho}} e_4 \sqrt{P_s - sign\,(e_4)\left(e_3 + \dfrac{F_{des}}{A} \right)} \\ \dot{e}_4 = -\dfrac{1}{\tau} e_4 - \dfrac{k_{sp}}{\tau} \left(K_p |e_3|\, sign\,(e_4) + K_f (F_{env} - F_{des}) \right) \sqrt{P_s - sign\,(e_4)\left(e_3 + \dfrac{F_{des}}{A} \right)} \end{cases} \tag{6.8}$$

where F_{env} is the simplified contact force (6.4) expressed in the error space:

$$F_{env} = \begin{cases} H(e_1 + \delta)^n & ; \ (e_1 + \delta > 0) \\ 0 & ; \ otherwise \end{cases} \tag{6.9}$$

The equilibria of the system shown in (6.8), $\mathbf{e}_{eq} = (e_1^{ss}, e_2^{ss}, e_3^{ss}, e_4^{ss})^T$, is obtained by equating the right hand sides of (6.8) to zero:

$$\begin{cases} e_1^{ss} = 0 \\ e_2^{ss} = 0 \\ e_3^{ss} = \dfrac{F_S \ \mathrm{sgn}(0)}{A} \\ e_4^{ss} = 0 \end{cases} \tag{6.10}$$

Note that $e_1^{ss} = 0$ indicates that $F_{env} = F_{des}$.

The equilibria of the system is, thus, every point $\mathbf{e}_{eq} = (0,0,e_3^{ss},0)^T$ with

$$e_3^{ss} = \frac{F_S \ \mathrm{sgn}(0)}{A} \in \left[\frac{-F_S}{A}, \frac{F_S}{A} \right] \tag{6.11}$$

Equations (6.10) imply that, if proven to be stable (the subject of Section 6.3), the proposed control system could effectively counteract frictional effects and follow the desired force asymptotically ($e_1^{ss} = 0$ or $F_{env} = F_{des}$). In the absence of the actuator dry friction, the system has a unique equilibrium point $\mathbf{e}_{eq} = (0,0,0,0)^T$.

Before studying the stability of the system, Filippov's solution concept is used to investigate the solution of the nonsmooth system shown in (6.8).

6.3 Solution Analysis

According to (6.8), the discontinuity surface of the system is one of the following three surfaces:

$$\begin{aligned} &\textit{Surface 1} && S_1^3 := \{\mathbf{e} : e_2 = 0 \ \& \ e_4 \neq 0\} \\ &\textit{Surface 2} && S_2^3 := \{\mathbf{e} : e_2 \neq 0 \ \& \ e_4 = 0\} \\ &\textit{Surface 3} && S_3^2 := \{\mathbf{e} : e_2 = 0 \ \& \ e_4 = 0\} \end{aligned} \tag{6.12}$$

where the superscripts and subscripts denote the dimension and the number of the discontinuity surfaces, respectively. Note that the surface S_3^2 is the intersection of surfaces S_1^3 and S_2^3.

Existence and continuation of Filippov's solution

Let region $\Omega = R^4 \times R$ and let D be an arbitrary compact set in Ω. The right-hand sides of equations (6.8) are defined everywhere in Ω, and are bounded by $B(t)$. Let $B(t)=L$, which is obviously integrable on D. Furthermore, each term of the right-hand sides of (6.8) is measurable. Thus, the right-hand sides of equations (6.8) satisfy condition B of Filippov's solution theory (Filippov, 1960) and we have the local existence of a solution which is continuous on $[t_0, t_f]$.

Uniqueness of Filippov's solution

The vector-valued function of the right-hand sides of equations (6.8) is continuous up to the discontinuity surfaces and the discontinuity surfaces are smooth and independent of time t. Therefore, conditions A, B and C of Filippov's solution theory (Filippov, 1979) are satisfied. Next, the analysis of the uniqueness of Filippov's solution is carried out for each discontinuity surface.

We start with studying the uniqueness of Filippov's solution for the discontinuity surface S_1^3. This discontinuity surface divides the solution region into two regions: $\Omega^+ := \{\mathbf{e} : e_2 > 0\}$ and $\Omega^- := \{\mathbf{e} : e_2 < 0\}$. Following the procedure introduced in (Filippov, 1960), the vector functions $\mathbf{f}_1^+$ and $\mathbf{f}_1^-$ are defined as the limiting values of the right-hand sides of error space equations (6.8) in Ω^+ and Ω^-. For all points on S_1^3 ($e_2 = 0$), the vector $\mathbf{h}_1 = \mathbf{f}_1^+ - \mathbf{f}_1^-$ is constructed as

$$\mathbf{h}_1 = \begin{Bmatrix} 0 \\ -2\dfrac{F_S}{m} \\ 0 \\ 0 \end{Bmatrix} \tag{6.13}$$

which is along with the normal to the discontinuity surface, $\mathbf{N}_1 = (0,1,0,0)^T$. The scalar, h_{N_1}, defined as the projection of $\mathbf{h}_1$ on $\mathbf{N}_1$, is calculated as

$$h_{N_1} = \mathbf{N}_1 \cdot \mathbf{h}_1 = -2\frac{F_S}{m} < 0 \tag{6.14}$$

Thus, according to Lemma 7 of Filippov (1960), the uniqueness of the Filippov's solution for equations (6.8) is guaranteed.

To prove the uniqueness of Filippov's solution on the discontinuity surface S_2^3, Ω^+ and Ω^- are defined as $\Omega^+ := \{\mathbf{e} : e_4 > 0\}$ and $\Omega^- := \{\mathbf{e} : e_4 < 0\}$. Defining $\mathbf{f}_2^+$ and $\mathbf{f}_2^-$ as the right-hand sides of the dynamic equations (6.8) in the regions Ω^+ and Ω^-, the projections of $\mathbf{f}_2^+$ and $\mathbf{f}_2^-$ along $\mathbf{N}_2$ are:

$$\mathbf{f}_{\mathbf{N}_2}^+ = -\frac{k_{sp}}{\tau}\left(K_p|e_3| + K_f(F_{env} - F_{des})\right)\sqrt{P_s - \left(e_3 + \frac{F_{des}}{A}\right)}$$

$$\mathbf{f}_{\mathbf{N}_2}^- = -\frac{k_{sp}}{\tau}\left(-K_p|e_3| + K_f(F_{env} - F_{des})\right)\sqrt{P_s + \left(e_3 + \frac{F_{des}}{A}\right)} \qquad (6.15)$$

Also, for all the points on the discontinuity surface S_2^3 ($e_4 = 0$), the projection of $\mathbf{h}_2 = \mathbf{f}_2^+ - \mathbf{f}_2^-$ on $\mathbf{N}_2 = \left(\frac{\partial S_2^3}{\partial e_1} \quad \frac{\partial S_2^3}{\partial e_2} \quad \frac{\partial S_2^3}{\partial e_3} \quad \frac{\partial S_2^3}{\partial e_4}\right)^T = (0,0,0,1)^T$, is obtained as

$$h_{N_2} = \mathbf{N}_2 \cdot \mathbf{h}_2 = -\frac{k_{sp}K_p|e_3|}{\tau}\left(\sqrt{P_s - (e_3 + F_{des}/A)} + \sqrt{P_s + (e_3 + F_{des}/A)}\right) - \frac{k_{sp}K_f(F_{env} - F_{des})}{\tau}\Delta \qquad (6.16)$$

where $\Delta = \sqrt{P_s - (e_3 + F_{des}/A)} - \sqrt{P_s + (e_3 + F_{des}/A)}$.

According to (6.16), when $K_p|e_3| > |K_f(F_{env} - F_{des})|$, $h_{N_2} < 0$ and according to Lemma 7 of Filippov (1960), the system has a unique solution. When $K_p|e_3| \le |K_f(F_{env} - F_{des})|$, (6.15) implies that $\mathbf{f}_{\mathbf{N}_2}^+ > 0$ **&** $\mathbf{f}_{\mathbf{N}_2}^- > 0$ when $K_f(F_{env} - F_{des}) < 0$ and $\mathbf{f}_{\mathbf{N}_2}^+ < 0$ **&** $\mathbf{f}_{\mathbf{N}_2}^- < 0$ when $K_f(F_{env} - F_{des}) > 0$. Therefore, Lemma 9 of Filippov (1960) guarantees the uniqueness of the solution.

The solution analysis on the S_3^2 (the intersection of the surfaces S_1^3 and S_2^3) requires heavier mathematical machinery and is omitted from the analysis.

6.4 Stability Analysis

Analytical stability of the proposed control system using Lyapunov stability theory is now investigated. In particular, the extension of LaSalle's invariance principle to nonsmooth systems is employed to prove that all the solution trajectories converge to the equilibria. In the absence of

actuator dry friction, the control system is shown to be asymptotically stable. In order to make the Lyapunov stability analysis manageable (being able to prove that $\dot{V}$ is negative semi-definite), the value of n in contact force model (6.4) is assumed to be one. For the overall stability analysis using the concept of Lyapunov exponents (Section 8), however, n can have any value depending on the geometry of the colliding bodies.

Let V be the positive definite smooth regular function introduced for the nonsmooth system given in (6.8):

$$V = \frac{H}{2}\left(\frac{Ae_1}{C} + e_3\right)^2 + \frac{\varepsilon m}{2C}e_2^2 + \frac{\varepsilon}{2}e_3^2 + \frac{\tau c_d w A}{2k_{sp}K_f\sqrt{\rho}C^2}e_4^2 + \frac{\varepsilon H}{2C}e_1^2 \tag{6.17}$$

where ε is an infinitesimally small positive number. Differentiating (6.17) with respect to time and substituting (6.4) into it, yields (n=1):

$$\begin{aligned}\dot{V} = &-\frac{\varepsilon d}{C}e_2^2 - \frac{c_d w}{C\sqrt{\rho}}\left(\frac{AK_p}{CK_f}|e_3e_4| - (\varepsilon + H)e_3e_4\right)\sqrt{P_s - sign(e_4)\left(e_3 + \frac{F_{des}}{A}\right)} \\ &- \frac{\varepsilon\left(F_C + (F_S - F_C)e^{-(e_2/v_s)^2}\right)}{C}|e_2| - \frac{c_d w A}{k_{sp}K_f\sqrt{\rho}C^2}e_4^2\end{aligned} \tag{6.18}$$

which would be negative semi-definite if the following condition is imposed on the control gain ratio when choosing the control gains:

$$\frac{K_p}{K_f} > \frac{(\varepsilon + H)C}{A} \tag{6.19}$$

Thus, the lower limit on the control gain ratio, $\frac{K_p}{K_f}$, is $\frac{HC}{A}$. Equation (6.18) with the condition (6.19) denotes that $\dot{V}$ is continuous and negative semi-definite throughout the solution region except for the discontinuity surfaces S_1^3, S_2^3 and S_3^2. On the discontinuity surface, S_1^3, we have:

$$\dot{V}(\mathbf{e} \in S_1^3) \in co[\dot{V}^{S_1^{3+}}, \dot{V}^{S_1^{3-}}] \tag{6.20}$$

where $\dot{V}^{S_1^{3+}}$ and $\dot{V}^{S_1^{3-}}$ are the limit values of $\dot{V}$ as a solution trajectory approaches S_1^3 from both sides:

$$\dot{V}^{S_1^{3+}} = \lim_{e_2 \to 0^+} \dot{V} = -\frac{c_d w A}{k_{sp} K_f \sqrt{\rho} C^2} e_4^2 - \frac{c_d w}{C\sqrt{\rho}} \left(\frac{A K_p}{C K_f} |e_3 e_4| - (\varepsilon + H) e_3 e_4 \right) \sqrt{P_s - sign(e_4) \left(e_3 + \frac{F_{des}}{A} \right)}$$

$$\dot{V}^{S_1^{3-}} = \lim_{e_2 \to 0^-} \dot{V} = -\frac{c_d w A}{k_{sp} K_f \sqrt{\rho} C^2} e_4^2 - \frac{c_d w}{C\sqrt{\rho}} \left(\frac{A K_p}{C K_f} |e_3 e_4| - (\varepsilon + H) e_3 e_4 \right) \sqrt{P_s - sign(e_4) \left(e_3 + \frac{F_{des}}{A} \right)} \tag{6.21}$$

Thus, by implementing the condition (6.19) on the control gains, the convex set described in (6.20) only contains one negative element:

$$\dot{V}(\mathbf{e} \in S_1^3) = -\frac{c_d w A}{k_{sp} K_f \sqrt{\rho} C^2} e_4^2 - \frac{c_d w}{C\sqrt{\rho}} \left(\frac{A K_p}{C K_f} |e_3 e_4| - (\varepsilon + H) e_3 e_4 \right) \sqrt{P_s - sign(e_4) \left(e_3 + \frac{F_{des}}{A} \right)} \tag{6.22}$$

Similarly, on the discontinuity surfaces S_2^3 and S_3^2 the convex set of $\dot{V}$ only contains one element, which is negative and zero, respectively:

$$\dot{V}(\mathbf{e} \in S_2^3) = -\frac{\varepsilon \left(F_C + (F_S - F_C) e^{-(e_2/v_s)^2} \right)}{C} |e_2| - \frac{\varepsilon\, d}{C} e_2^2 \tag{6.23}$$

$$\dot{V}(\mathbf{e} \in S_3^2) = 0 \tag{6.24}$$

Equations (6.18) and (6.23) to (6.24) imply that $\dot{V}$ is negative semi-definite in the entire regions of motion as well as on the discontinuity surfaces. According to the extended LaSalle's invariance principle to nonsmooth systems (Theorem 2 in Section 2.3), every solution trajectory in Ω converges to the largest invariant set, **M**, as $t \to \infty$. We next prove that this largest invariant set, **M**, contains only the equilibria $\mathbf{e}_{eq} = (0, 0, e_3^{ss}, 0)^T$ where e_3^{ss} is defined in (6.11). This is proven by contradiction:

Let **R** be the set of all points within the solution region Ω where $\dot{V} = 0$. With respect to (6.18), $\dot{V} = 0$ requires that for all the points in **R**, $e_2 = 0$ and $e_4 = 0$. Thus, both $\dot{e}_2$ and $\dot{e}_4$ are zero. Let **M** be the largest invariant set in **R** and contain a point where either $e_1 \neq 0$ and/or e_3 is not equal to e_3^{ss} described by (6.11). According to equations (6.8), this will result in either $\dot{e}_2 \neq 0$ and/or $\dot{e}_4 \neq 0$ which necessitates the solution trajectory to immediately move out of the set **R** and certainly set **M**. This contradicts with the initial assumption that **M** is the largest invariant set in **R**. Therefore, e_1 can only be equal to zero and e_3 can only be equal to e_3^{ss} described in (6.11),

i.e., every solution trajectory in Ω will converge to the largest invariant set **M** that only contains the system's equilibria.

According to the above analysis, when the condition $\frac{K_p}{K_f} > \frac{HC}{A}$ is satisfied, the control scheme proposed in (6.6) is guaranteed to perform asymptotic force regulation with no steady-state error despite the actuator's dry friction. When the actuator has negligible dry friction, the only discontinuity surface (due to the controller discontinuity) is $S := \{\mathbf{e} : e_4 = 0\}$ and the system (6.8) has the unique equilibrium point $\mathbf{e}_{eq} = (0,0,0,0)^T$. In that case, the function V described by (6.17) would be the system's positive-definite Lyapunov function with the following derivative

$$\dot{V} = -\frac{c_d w A}{k_{sp} K_f \sqrt{\rho C^2}} e_4^2 - \frac{c_d w}{C\sqrt{\rho}} \left(\frac{A K_p}{C K_f} |e_3 e_4| - (\varepsilon + H) e_3 e_4 \right) \sqrt{P_s - sign(e_4)\left(e_3 + \frac{F_{des}}{A} \right)} \qquad (6.25)$$

which is negative and semi-definite subject to satisfying inequality (6.19). Similar to the analysis of the system with dry friction, it can be proven that $\dot{V}$ is also negative on the discontinuity surface, S. Therefore, based on the theorem3 in Section 2.3, the equilibrium point of the system is asymptotically stable.

Remarks

i) It should be noted that the exact values of H, C and A are not required for control action. However, knowing their rough estimates is required to draw the line where the control gains should be chosen. The value of the piston area, A, can be taken from manufacturer's specifications. The environment stiffness, H, can be over-estimated from the knowledge of possible stiffnesses of colliding bodies. The hydraulic compliance, C, can be determined using any parameter identification scheme (Sepehri et al., 1994).

ii) It is also useful to note that the equilibria of the system (6.8) that was proved to be convergent would still be the system equilibria if the more complete model (3.8) was used for dynamic modeling. This is shown by first defining the error states $e_1 = x - (x_{env} + \delta)$, $e_2 = \dot{x}$, $e_3 = P_i$, $e_4 = P_o$ and, $e_5 = x_{sp}$ and substituting the control law (6.6) and the friction model (3.17) into (3.8):

$$\begin{cases} \dot{e}_1 = e_2 \\ \dot{e}_2 = \dfrac{A(e_3 - e_4)}{m} - \dfrac{\left[F_C + (F_S - F_C)e^{-(e_2/\dot{x}_s)^2}\right]\mathrm{sgn}(e_2) + d\,e_2}{m} - \dfrac{F_{env}}{m} \\ \dot{e}_3 = \dfrac{\beta}{\overline{V}_i + A(e_1 + x_{env} + \delta - x_0)}\left(-Ae_2 + \sqrt{\dfrac{2}{\rho}}c_d w e_5 \sqrt{\dfrac{P_S - P_e}{2} + sign(e_5)\left(\dfrac{P_S + P_e}{2} - e_3\right)}\right) \\ \dot{e}_4 = \dfrac{\beta}{\overline{V}_o - A(e_1 + x_{env} + \delta - x_0)}\left(Ae_2 - \sqrt{\dfrac{2}{\rho}}c_d w e_5 \sqrt{\dfrac{P_S - P_e}{2} + sign(e_5)\left(e_4 - \dfrac{P_S + P_e}{2}\right)}\right) \\ \dot{e}_5 = -\dfrac{1}{\tau}e_5 - \dfrac{k_{sp}}{\tau}\left(K_p\left|e_3 - e_4 - \dfrac{F_{des}}{A}\right|sign(e_5) + K_f(F_{env} - F_{des})\right)\sqrt{P_s - sign(e_5)(e_3 - e_4)} \end{cases} \tag{6.26}$$

where

$$F_{env} = \begin{cases} H(e_1 + \delta)^n & ;\ (e_1 + \delta > 0) \\ 0 & ;\ otherwise \end{cases}$$

To obtain the system's equilibria, the right-hand sides of (6.26) are equated to zero:

$$\begin{cases} e_1^{ss} = 0 \\ e_2^{ss} = 0 \\ e_3^{ss} - e_4^{ss} - \dfrac{F_{des}}{A} = \dfrac{F_S\,\mathrm{sgn}(0)}{A} \in \left[-\dfrac{F_S}{A}, \dfrac{F_S}{A}\right] \\ e_5^{ss} = 0 \end{cases} \tag{6.27}$$

Equations (6.10) and (6.27) indicate that the equilibria of the more complete dynamic model are the same as the one for the simplified model proven to be convergent.

6.5 Experimental Verification

To observe the performance of the proposed force control scheme through interactions with different environments and determine its capability in regulating various desired forces, several sets of experiments were performed. Metal sheet and wooden plate were used to represent different environmental stiffnesses. For each environment, two tests were conducted for desired forces of 250 *lbf* and 500 *lbf*. In all experiments, the actuator motion started from where it was in touch with the environment surface. In order to choose proper control gains that fulfill condition (6.19) needed to guarantee the convergence of the system trajectories to the system's equilibria, an estimate of A, C, and H is required. With respect to the system parameters given in Table 3.1,

A =0.9812 in^2 and $C = \frac{V_t}{4\beta}$ is calculated to be 7.14x10^{-5} in^3/psi. Since exerting 500 lbf on the test rig's environment results in both manipulator-environment local deformations as well as slight bending in the environment's I-beam support, the value of environment stiffness are experimentally measured to be $H_M = 6000$ lbf/in and $H_W = 3000$ lbf/in, respectively. The control gains were, therefore, selected according to (6.19) as K_f=4×10^{-5} $V/lbf\sqrt{psi}$ and K_p=1.8×10^{-5} $V/\sqrt{psi^3}$. The supply pressure in each experiment was P_s=2000 psi and the sampling time of the system was ≈2ms. The steady-state load pressure does not depend on the environment stiffness or the choice of control gains [See (6.11)] and for the system with parameters tabulated in Table 3.1 is expected to be within the following range:

$$e_3^{ss} \in \left[\frac{F_{des}-315}{0.98}, \frac{F_{des}+315}{0.98}\right] \tag{6.28}$$

Figures 6.2 and 6.3 show the system response when the actuator is in contact with various environments following the desired force of F_{des}=250 lbf. The force response of the system demonstrates the asymptotic convergence of the system trajectory to the desired force and verifies the friction compensation capability of the force control scheme proposed for hydraulic actuators. Note that the steady-state force error is observed to be within ± 10 lbf of the desired force which is acceptable considering the resolution of measurements. Figure 6.3 also confirms that the steady-state load pressure is within the range denoted in (6.28) ,i.e., $e_3^{ss} = [-67, 577]$ psi.

Figures 6.4 and 6.5 show the response when the actuator follows the desired force of F_{des}=500 lbf. These results also demonstrate that the proposed control scheme is stable and capable of regulating the desired force without steady-state error (the slight steady-state error is believed to be due to measurement resolutions and small deadband in the spool valve). Moreover, the steady-state load pressure error is within the bounds derived in (6.28) analytically, i.e., $e_3^{ss} = [189, 832]$ psi. All experimental observations are in-line with, and verify the theoretical derivations outlined earlier.

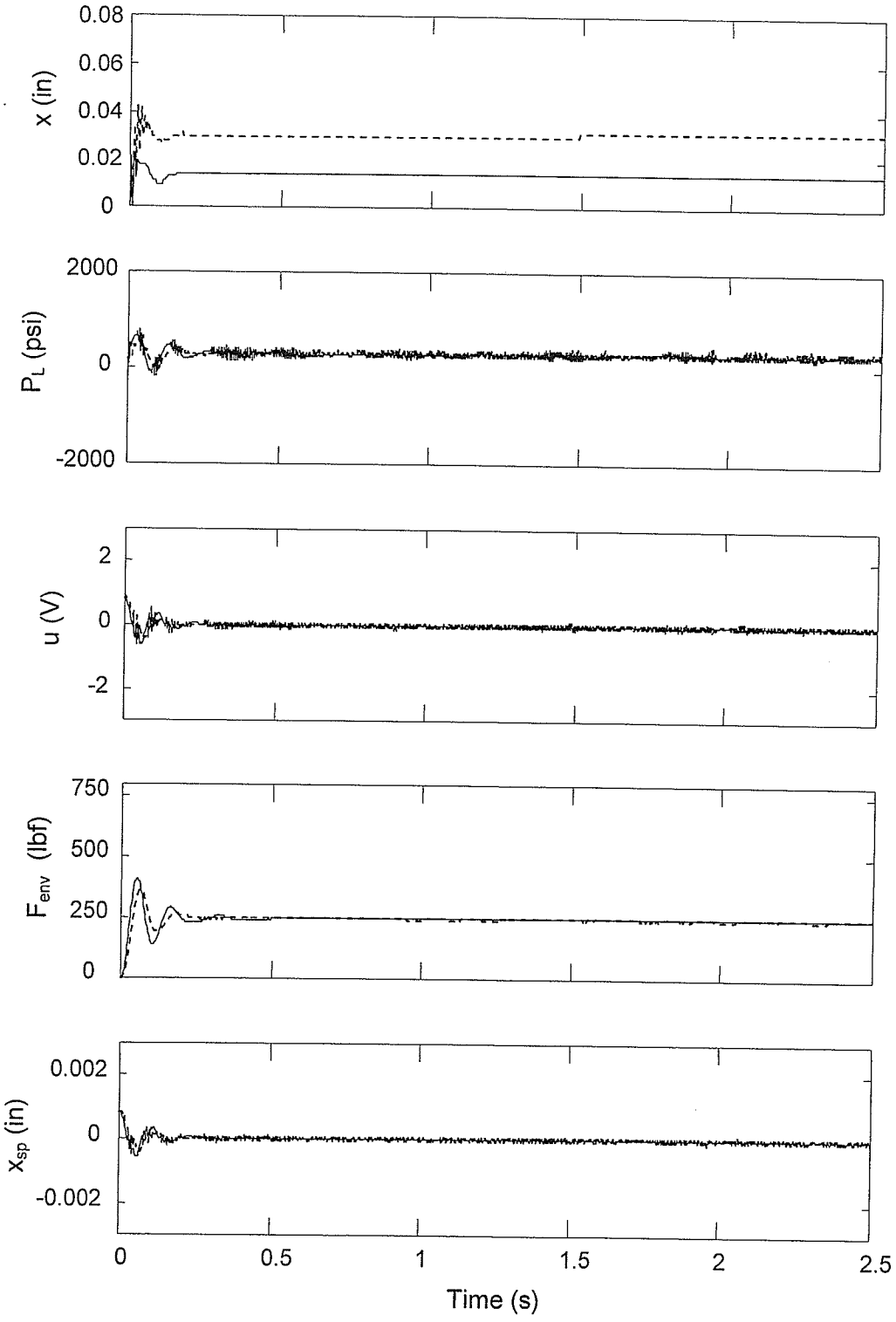

Fig. 6.2 Force control response for F_{des}=250 *lbf*, —— Metal, ---- Wood.

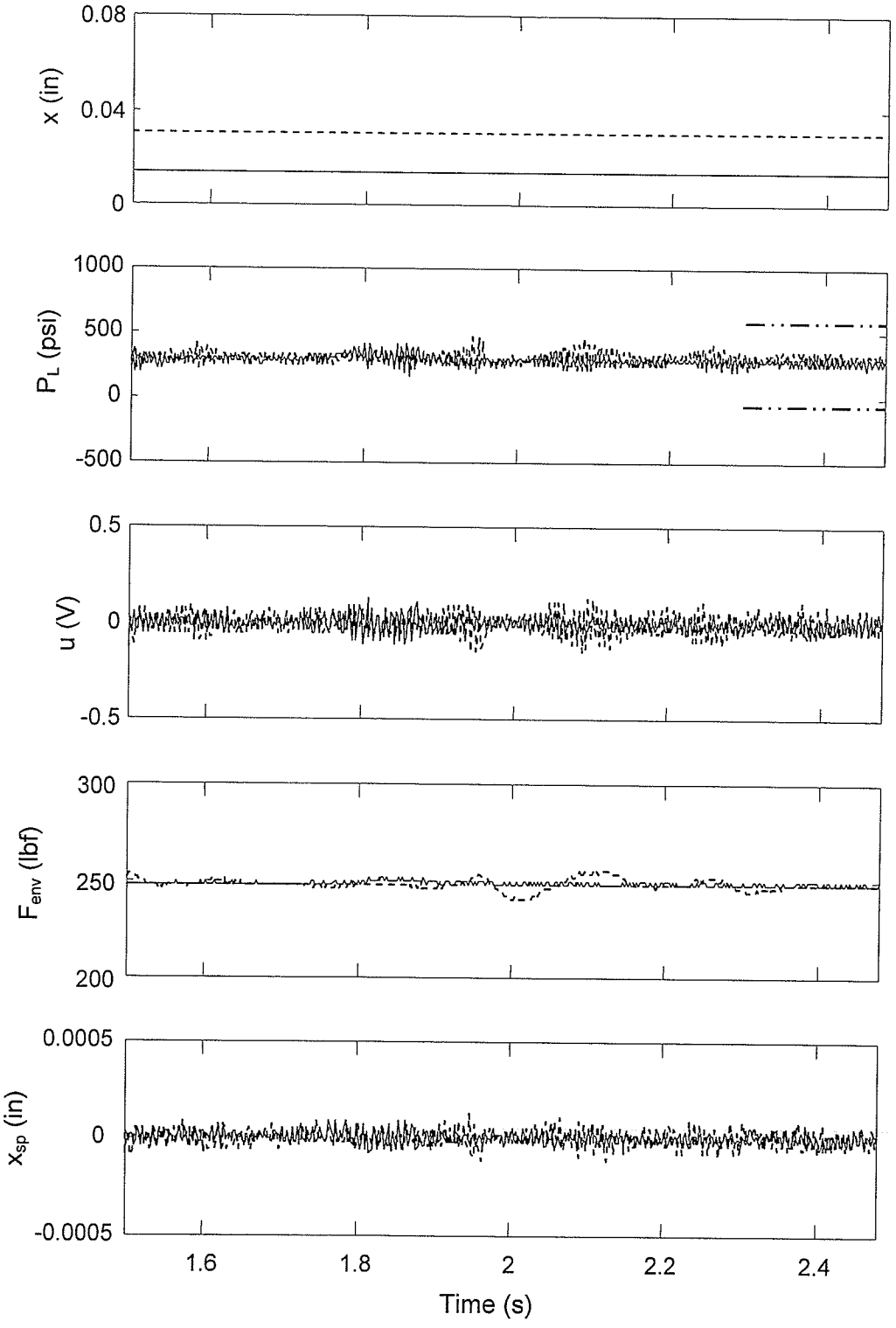

Fig. 6.3 Close-up of responses in Fig. 6.2.

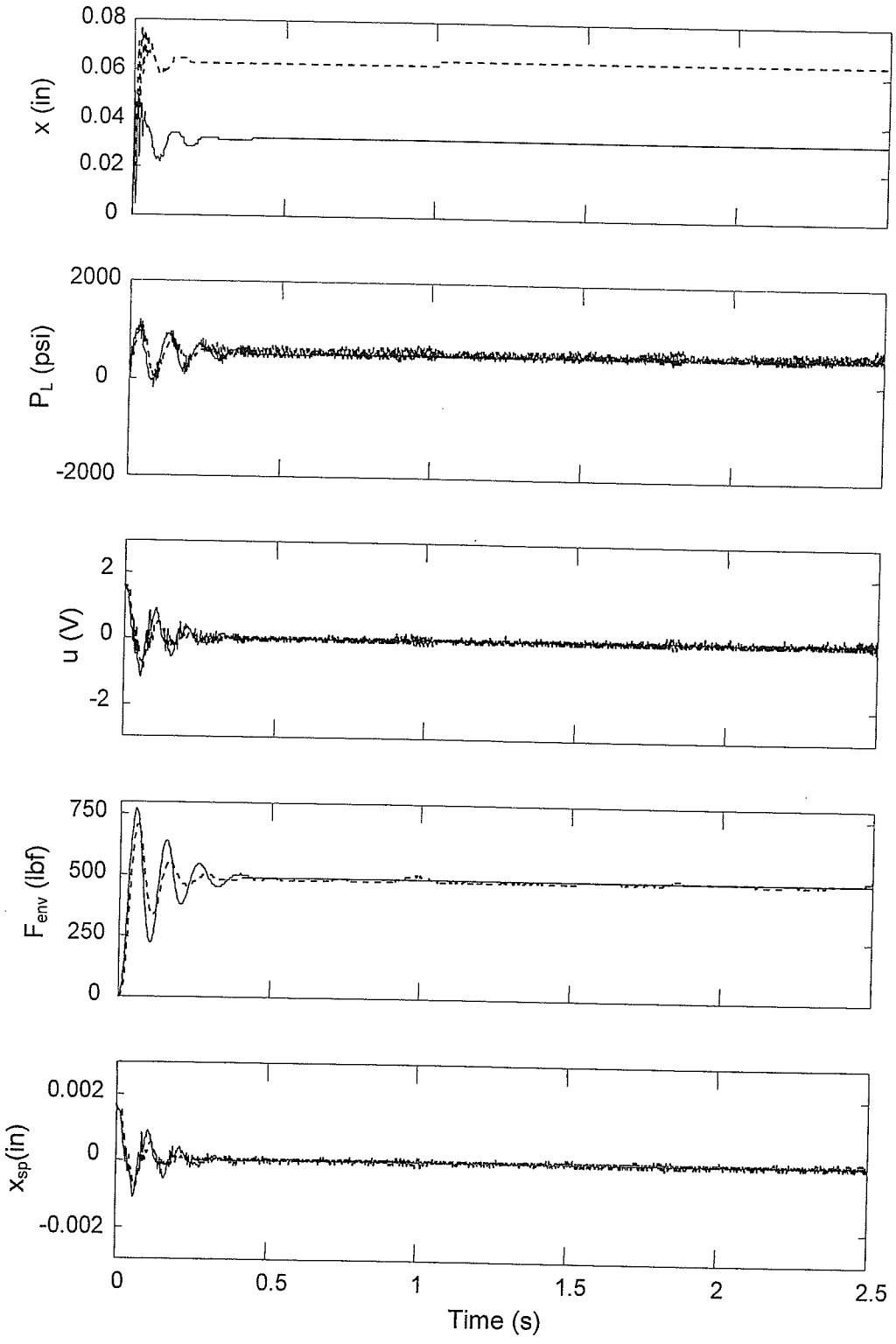

Fig. 6.4 Force control system response for F_{des}=500 *lbf*, —— Metal, ---- Wood.

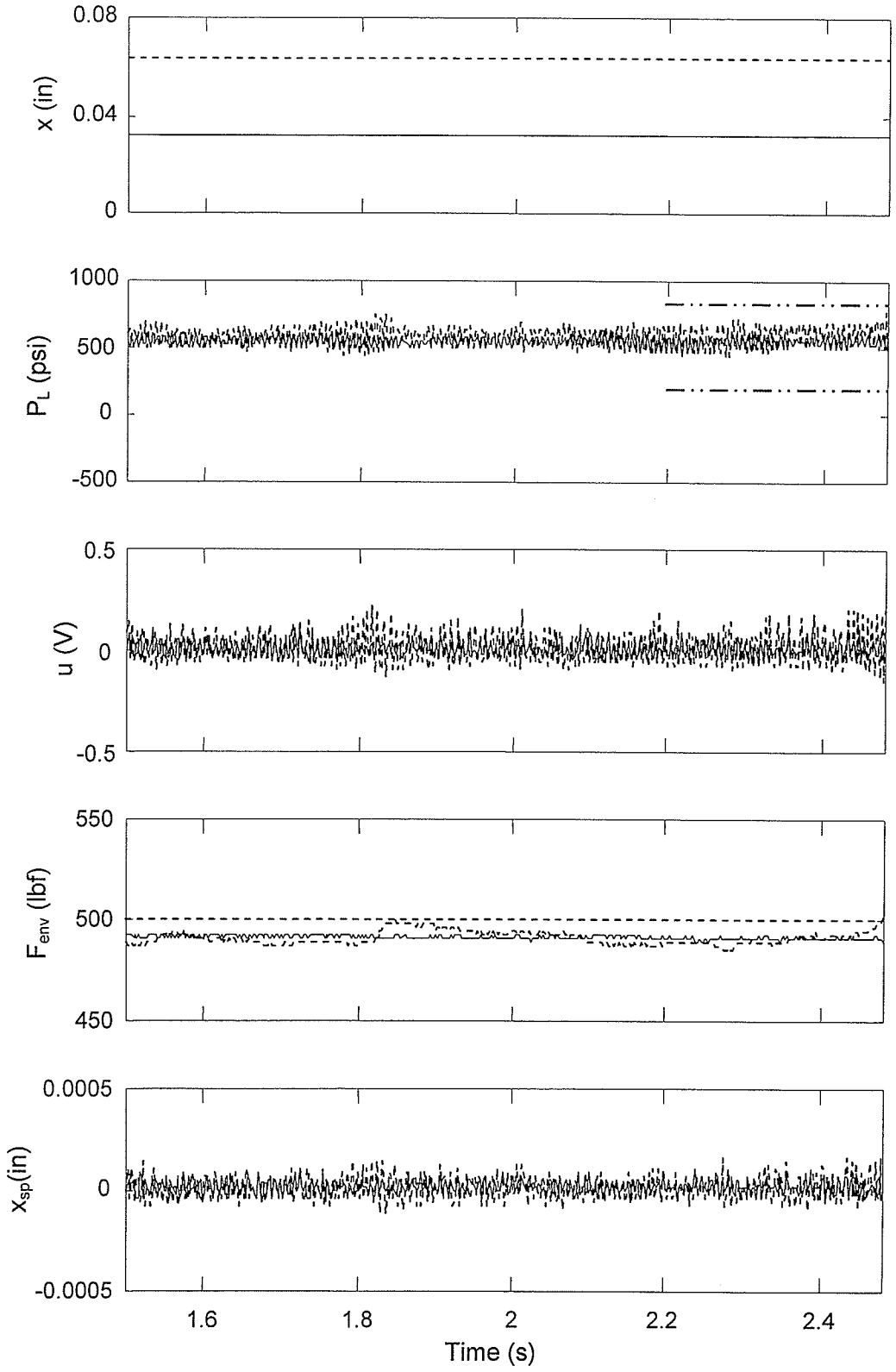

Fig. 6.5 Close-up of responses in Fig. 6.4.

Chapter 7

Stability Analysis of Switching Control Systems Using the Concept of Lyapunov Exponents

7.1 Introduction

Existence of at least two switchings between controllers (free-space to impact mode and impact mode to sustained-contact mode) in the overall contact task control results in an overall nonsmooth system. Employing the extension of Lyapunov stability theory to nonsmooth systems and finding the appropriate composite Lyapunov function for the general task is extremely difficult, if not impossible. Therefore, many studies have resorted to some restrictive assumptions such as those discussed in Section 1.2.3. To achieve a more generalized stability analysis of switching control systems with fewer restrictive assumptions, the concept of Lyapunov exponents is now adopted for the complete analysis of the qualitative behavior of the system.

Implementing the concept of Lyapunov exponents on dynamical systems with discontinuities entails several fundamental issues that should be thoroughly addressed. The first intrinsic issue is

the solution analysis of both the original nonlinear and the linearized systems that are used in the calculation process. Since the fundamental assumptions of conventional solution theories (Lipschitz continuity) are violated as a result of the system discontinuity, the solution concept is questionable. The second issue is to determine whether Lyapunov exponents exist when $t \to \infty$, and, if they do exist, how a suitable finite time limit can be found to terminate the calculation process. Linearization of nonlinear equations on the discontinuity surface is the third problem associated with systems with discontinuities. Since the purpose of calculating Lyapunov exponents is to investigate the stability of the system based on the signs of the exponents (see Section 2.4), suppression of numerical instabilities that may arise in numerical computations is of significant importance. Therefore, the fourth issue is the numerical stability and the convergence of the numerical results toward the exact Lyapunov exponents. In addition, Lyapunov exponents should be calculated over a sufficiently long period of time until the system reaches a steady state. Hence, the efficiency of the calculations in terms of computation time is to be considered.

Using previously developed theorems and techniques, the systematic framework established in this thesis addresses the above issues within the context of switching contact task control applications. First, the solution analyses of both nonlinear and linearized system of equations are conducted using Filippov's solution theories and the theory of Caratheodory differential equations (Filippov, 1988). Next, appropriate theorems (Kunze, 2000) are invoked to study the existence of Lyapunov exponents for such non-smooth control systems. The problem of linearizing the nonlinear equations on discontinuity surface is addressed by resorting to the works of Kunze (2000) and Muller (1995) in which the conventional calculation procedure by Wolf et al. (1985) has been extended to systems with discontinuities. To address the issue of numerical instabilities, a nonstandard finite difference discretization scheme ($\mathrm{NSF}\Delta$) based on the framework of Mickens (2002) is constructed for both noncontact and contact regions of motion. The scheme admits large step-sizes in comparison to other commonly used standard techniques such as the explicit Euler and Runge-Kutta methods (Mickens and Gumel, 2002) and, thus, enhances the reliability of numerical computations. It was shown that this calculation procedure is particularly appropriate for the calculation of Lyapunov exponents in discontinuous control systems (Sekhavat et al. 2003). The event-driven simulation algorithm is chosen for

numerical simulations and the contact or separation time instants are determined by implementing the so-called step back procedure (Brogliato et al., 2002).

In this Chapter, the above systematic procedure is exemplified with a typical contact task control system. The example is taken from the work by Wu and Payandeh (1999) where a simple implement is aimed to reach a desired position and later switches to follow a desired contact force. Using the extended Lyapunov's direct method, this problem has been proven to be stable under the bounce-less contact assumption with an environment modeled as a simple linear spring. Employing the more realistic Hertz-type model of contact allows multiple impacts as a result of bouncing on initial contact and rules out the previous stability analysis. Therefore, the example is chosen to demonstrate the applicability of the proposed systematic procedure in determining the system stability using the concept of Lyapunov exponents.

7.2 Description of a Typical Switching Control System

The system is a single degree of freedom implement aimed to reach a desired position, x_{des}, while there exists an immovable environment on its way (Fig. 7.1). Upon collision with the environment, the goal is to regulate the contact force towards the desired contact force. The equation of motion is described by the following differential equation:

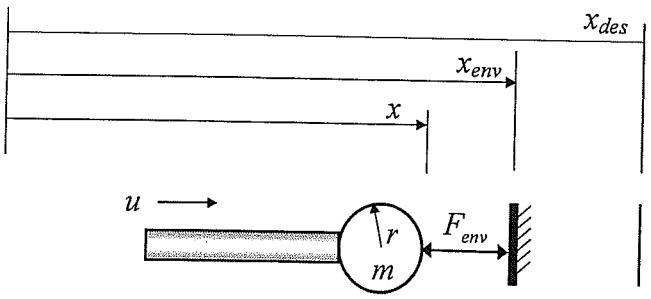

Fig. 7.1 Implement-environment configuration.

$$u - F_{env} = m\ddot{x} \tag{7.1a}$$

where x is the position of the implement's end-point, m is the mass of the implement, u is the control signal that acts as a force on the implement, and F_{env} is the contact force as described by (3.23):

$$F_{env} = \begin{cases} (1+p\dot{x})H(x-x_{env})^n & ; \quad (x-x_{env}>0)\ \&\ (1+p\dot{x}>0) \\ 0 & ; \quad otherwise \end{cases} \tag{7.1b}$$

The discontinuous control algorithm (Wu and Payandeh, 1999) consists of two control laws for free-space and constrained modes of motion. The free-space control law is to bring the implement to the desired position, x_{des}. Upon contact with the environment, the second control law is activated to regulate the contact force and to follow the desired force, F_{des}:

$$u = \begin{cases} -K_p(x-x_{des}) - K_{v_1}\dot{x} & ; \quad F_{env}=0 \quad (noncontact) \\ F_{des} - K_{v_2}\dot{x} - K_f(F_{env}-F_{des}) & ; \quad F_{env}\neq 0 \quad (contact) \end{cases} \tag{7.2}$$

In (7.2), K_p, K_{v_1}, K_f and K_{v_2} are the positive gains.

Defining $\boldsymbol{x}=\{x,\dot{x}\}^T=\{x_1,x_2\}^T$ as the state vectors, equations (7.1) and (7.2) yield the following state-space model of the system:

$$\dot{\boldsymbol{x}} = \boldsymbol{f}_1(\boldsymbol{x}) = \begin{cases} x_2 \\ -\dfrac{K_p}{m}(x_1-x_{des}) - \dfrac{K_{v_1}}{m}x_2 \end{cases} \quad \text{(noncontact)}$$

$$\dot{\boldsymbol{x}} = \boldsymbol{f}_2(\boldsymbol{x}) = \begin{cases} x_2 \\ -\dfrac{K_{v_2}}{m}x_2 - \dfrac{(K_f+1)}{m}\left((1+px_2)H(x_1-x_{env})^n - F_{des}\right) \end{cases} \quad (contact) \tag{7.3}$$

The equilibrium point ($\boldsymbol{x}_{eq}$) of (7.3) is a point in the contact region where $x_2=0$ and $x_1 = x_{env} + \left(\dfrac{F_{des}}{H}\right)^{1/n}$ (or $F_{env}=F_{des}$).

The switching control system described by (7.3) is non-smooth. A main preliminary before proceeding with the system stability analysis using the concept of Lyapunov exponents, is to prove that the switching system has a unique continuous solution (Kunze, 2000).

7.3 Solution Analysis

Existence and continuation of Filippov's solution

Consider region $\Omega = R^2 \times R$ and let D be an arbitrary compact set in Ω. The right-hand sides of

(7.3) are defined everywhere in Ω, and are bounded by, say, L. Let $A(t) = L$ which is integrable on D. Furthermore, each term of the right-hand sides of (7.3) is measurable. Therefore, equations (7.3) satisfy basic conditions of Filippov's solution theory and according to Theorems 8 and 9 [Section 7 of (Filippov, 1988)], we have the local existence of a solution which is continuous on $[t_0, t_f]$.

Uniqueness of Filippov's solution

Discontinuities of the system occur at instants of contact and separation. Contact happens when both conditions $x_1 - x_{env} > 0$ and $x_2 > -1/p$ are in effect [see equation (2.23)], and separation occurs when any of them is violated. Thus, we have the following three discontinuity surfaces:

$$\begin{aligned}
&\textit{Surface 1} \quad S_1^1 := \{(x_1, x_2) : x_1 - x_{env} = 0 \;\; \& \;\; x_2 + 1/p > 0\} \\
&\textit{Surface 2} \quad S_2^1 := \{(x_1, x_2) : x_2 + 1/p = 0 \;\; \& \;\; x_1 - x_{env} > 0\} \\
&\textit{Surface 3} \quad S_3^0 := \{(x_1, x_2) : x_2 + 1/p = 0 \;\; \& \;\; x_1 - x_{env} = 0\}
\end{aligned} \tag{7.4}$$

where the superscripts and subscripts denote the dimension and the number of the discontinuity surface, respectively. The right-hand sides of equations (7.3) are continuous in both regions of motion and all discontinuity surfaces (7.4) are smooth and independent of time. We start with proving the uniqueness of the solution with respect to the discontinuity surface S_1^1.

The discontinuity surface S_1^1 divides the solution domain Ω into two regions:

$$\begin{aligned}
\Omega^- &:= \{(x_1, x_2) : x_2 + 1/p > 0 \;\; \& \;\; x_1 - x_{env} < 0\} \\
\Omega^+ &:= \{(x_1, x_2) : x_2 + 1/p > 0 \;\; \& \;\; x_1 - x_{env} > 0\}
\end{aligned} \tag{7.5}$$

The vector functions $\mathbf{f}_1^+$ and $\mathbf{f}_1^-$ are defined as the limiting values of the right-hand sides of the state-space equations (7.3) in regions Ω^+ and Ω^- as the solution trajectory approaches the discontinuity surface S_1^1. Considering the fact that on S_1^1, $(x_1 - x_{env}) = 0$, the normal to this surface, denoted by $\mathbf{N}_1$, is:

$$\mathbf{N}_1 = \begin{Bmatrix} \dfrac{\partial S_1^1(x_1, x_2)}{\partial x_1} \\ \dfrac{\partial S_1^1(x_1, x_2)}{\partial x_2} \end{Bmatrix} = \begin{Bmatrix} 1 \\ 0 \end{Bmatrix} \tag{7.6}$$

Thus, the projections of $\mathbf{f}_1^+$ and $\mathbf{f}_1^-$ along the normal to the discontinuity surface, S_1^1, are:

$$\mathbf{f}_{\mathbf{N}_1}^{+} = \mathbf{f}_1^{+} \cdot \mathbf{N}_1 = x_2$$
$$\mathbf{f}_{\mathbf{N}_1}^{-} = \mathbf{f}_1^{-} \cdot \mathbf{N}_1 = x_2 \tag{7.7}$$

As is seen, $\mathbf{f}_{\mathbf{N}_1}^{+}$ and $\mathbf{f}_{\mathbf{N}_1}^{-}$ always have the same signs. Thus, the solution is unique and passes through an isolated point on the discontinuity surface (Lemma 9 of Filippov (1960)).

Similarly, on the second discontinuity surface, S_2^1, we have $x_2 + 1/p = 0$. Thus, the normal to this surface, $\mathbf{N}_2$, is:

$$\mathbf{N}_2 = \begin{Bmatrix} \dfrac{\partial S_2^1(x_1, x_2)}{\partial x_1} \\ \dfrac{\partial S_2^1(x_1, x_2)}{\partial x_2} \end{Bmatrix} = \begin{Bmatrix} 0 \\ 1 \end{Bmatrix} \tag{7.8}$$

and the projections of $\mathbf{f}_2^{+}$ and $\mathbf{f}_2^{-}$ along $\mathbf{N}_2$ are:

$$\mathbf{f}_{\mathbf{N}_2}^{+} = \mathbf{f}_2^{+} \cdot \mathbf{N}_2 = -\frac{K_{v_2}}{m} x_2 + \frac{(K_f + 1)}{m} F_{des}$$
$$\mathbf{f}_{\mathbf{N}_2}^{-} = \mathbf{f}_2^{-} \cdot \mathbf{N}_2 = -\frac{K_p}{m}(x_1 - x_{des}) - \frac{K_{v_1}}{m} x_2 \tag{7.9}$$

Considering the fact that on S_2^1, we have $x_2 = -1/p$ and $(x_1 - x_{des}) < 0$, the right hand sides of (7.9) are always positive and we have $\mathbf{f}_{\mathbf{N}_2}^{+} > 0$ and $\mathbf{f}_{\mathbf{N}_2}^{-} > 0$. Thus, according to Lemma 9 of (Filippov, 1960), the uniqueness of the solution on S_2^1 is also guaranteed. Uniqueness analysis for the third discontinuity surface, S_3^0, which is actually a unique point at the intersection of the two surfaces S_1^1 and S_2^1 is trivial.

7.4 Stability Analysis

Calculation of Lyapunov exponents is used for stability analysis of the above switching control system. For the second-order system (7.3), the largest Lyapunov exponent of the system being negative proves that the system has an asymptotically stable equilibrium point. First, the calculation procedure explained in Section 2.4.2 is used for the smooth parts of motion. Next, the extended calculation method stated in Section 2.4.4 is adopted to generalize the method to the switching systems.

7.4.1 Variational Equations for Smooth Parts of Motion

According to Section 2.4.2, in order to calculate the system's Lyapunov exponents, the variational equation $\dot{\psi}_t = \boldsymbol{F}(t)\psi_t$ of the linearized system $\delta \boldsymbol{x}(t) = \psi_t\, \delta \boldsymbol{x}_0$ is simultaneously integrated with the original nonlinear equations. For the system shown in (7.3), $\boldsymbol{F}(t)$ is determined as [see (2.26)]:

$$\boldsymbol{F}(t) = \boldsymbol{F}_1(t) = \begin{bmatrix} 0 & 1 \\ -\dfrac{K_p}{m} & -\dfrac{K_{v_1}}{m} \end{bmatrix} \qquad (noncontact)$$

$$\boldsymbol{F}(t) = \boldsymbol{F}_2(t) = \begin{bmatrix} 0 & 1 \\ -\dfrac{3(K_f+1)}{2m}\left(1+px_2\right)H\left(x_1 - x_{env}\right)^{n-1} & -\dfrac{K_{v_2}}{m} - \dfrac{(K_f+1)}{m}pH\left(x_1 - x_{env}\right)^n \end{bmatrix} \qquad (contact)$$

(7.10)

Thus, the variational equations of motion in smooth regions before and after discontinuity instants are:

$$\dot{\psi}_{11} = \psi_{21}$$

$$\dot{\psi}_{12} = \psi_{22}$$

$$\dot{\psi}_{21} = \begin{cases} -\dfrac{K_p}{m}\psi_{11} - \dfrac{K_{v_1}}{m}\psi_{21} & (noncontact) \\ -\dfrac{3(K_f+1)}{2m}\left(1+px_2\right)H\left(x_1 - x_{env}\right)^{n-1}\psi_{11} + \left(-\dfrac{K_{v_2}}{m} - \dfrac{(K_f+1)}{m}pH\left(x_1 - x_{env}\right)^n\right)\psi_{21} & (contact) \end{cases}$$

$$\dot{\psi}_{22} = \begin{cases} -\dfrac{K_p}{m}\psi_{12} - \dfrac{K_{v_1}}{m}\psi_{22} & (noncontact) \\ -\dfrac{3(K_f+1)}{2m}\left(1+px_2\right)H\left(x_1 - x_{env}\right)^{n-1}\psi_{12} + \left(-\dfrac{K_{v_2}}{m} - \dfrac{(K_f+1)}{m}pH\left(x_1 - x_{env}\right)^n\right)\psi_{22} & (contact) \end{cases}$$

(7.11)

7.4.2 Extension to Switching Control Systems

Application of the calculation procedure explained in Section 2.4.2 to the switching control systems entails several issues such as the solution concept of the linearized system, linearization of the nonlinear equations on the discontinuity surface, existence of the exponents as the limit stated in equation (2.6), and the numerical stability and convergence of the results to the exact Lyapunov exponents. In the following subsections, the theorems and methods of addressing these issues are discussed in systematic detail. They include the theory of Caratheodory

differential equations (Section 2.2), the extension of Oseledet's Multiplicative Ergodic to nonsmooth systems (Section 2.4.1), the method of calculating Lyapunov exponents at nonsmooth instants of motion (Section 2.4.4), and application of the nonstandard finite difference discretization scheme (Section 2.5) to enhance the validity and efficiency of computations.

Solution Analysis of the Variational Equation

The right-hand sides of the system shown in (7.11) are piecewise continuous in t. Definition of a solution for such systems can be obtained using the concept of the Lebesgue integral which is the basis of the theory of the Caratheodory differential equations (Section 2.2) and the existence and uniqueness of such a solution can be outlined accordingly. Since all the elements of the matrix $\boldsymbol{F}(t)$ in (7.10) are summable on each segment contained in the interval $[t_0, t_f]$, according to the Theorem outlined in Section 2.2 (Filippov, 1988), the solution of (7.11) with arbitrary initial condition $\psi_t(t_0) = \psi_{t_0}\ (t \in [t_0, t_f])$ exists on the whole interval $[t_0, t_f]$ and is unique.

Note that every solution in the sense of Caratheodory is a solution in the sense of Filippov and vise versa (Filippov, 1988) and the solution analysis of the linearized system is compatible with the solution analysis in Section 7.3 for the original nonlinear system using Filippov theories.

Existence of Lyapunov Exponents

In order to actually relate the λ_i (i=1,..,n) to the long-term behavior (or stability) of the system, the $\lim_{t\to\infty}$ in (2.6) should exist. A general powerful tool to prove the existence of the $\lim_{t\to\infty}$ in (2.6) is given by Oseledet's Multiplicative Ergodic Theorem (MET) (Oseledec, 1968) explained in Section 2.4.1. Since in switching control system (7.3) the semi-flow $\varphi : [0,\infty[\times\Re^2 \to \Re^2$ is no longer smooth with respect to $\boldsymbol{x}$, the cocycle (the linear part at $\boldsymbol{x}$ of the nonlinear maps) for such a non-smooth system should be first defined. Kunze (2000) has proven that under certain conditions, one could obtain a complete description of the cocycle corresponding to non-smooth semi-flows [Theorem 4.1.1 in (Kunze, 2000)] and the integrability conditions in MET are satisfied (Corollary 4.1.8). He has also introduced the additional conditions required for the existence of a "good" set G of initial values $\boldsymbol{x}_0$ where such a cocycle can be defined, i.e., for the trajectories starting in $\boldsymbol{x}_0$, the cocycle can be constructed meaningfully (Corollary 4.1.3 and Theorem 4.1.2). Such theorems provide the theoretical foundation for applying the MET to prove

the existence of Lyapunov exponents in non-smooth systems. Validity of their required conditions has been rigorously verified for the second-order pendulum with dry friction (Kunze, 2000) and can be intuitively verified for the system under study. The details of the mathematical proof on the validity of the conditions are beyond the scope of this study. Interested readers are referred to Section 4.2.2 in (Kunze, 2000). Theorem 4.1.1 of (Kunze, 2000) implies that a canonical cocycle lives on a set $G \subset \mathbf{R}^2$ of "good" initial values and according to the Oseledet's Multiplicative Ergodic Theorem, the existence of the Lyapunov exponents is guaranteed.

Calculation of Lyapunov Exponents at Discontinuous Instants of Motion

With respect to (7.3), the nonlinear equations of motion are not linearizable at switching instants from free-space to constrained-motion and vice-versa. Therefore, the original method of numerical calculations (Section 2.4.2) is no longer adequate for calculation of Lyapunov exponents of the system under study. The extension of the calculation procedure to nonsmooth systems was first explained in (Muller, 1995) and then re-confirmed in (Kunze, 2000). The method explained in Section 2.4.4 is based on supplementing the linearization of dynamic equations by transition conditions at the instant of discontinuity. The supplementary conditions require the knowledge of appropriate transition and indicator functions defined based on the physical behavior of the system (see Section 2.4.4).

The contact task control system described by (7.3) undergoes discontinuities at discrete time instants t_i (i is the number of discontinuity instants) by switching from one region to another region of motion and behaves smoothly otherwise. Since the Hertz-type contact model (3.23) is continuous, we have:

$$\boldsymbol{x}(t_1^+) = \boldsymbol{g}_1(\boldsymbol{x}(t_1^-)) = \boldsymbol{x}(t_1^-) \tag{7.12}$$

$$\boldsymbol{x}(t_2^+) = \boldsymbol{g}_2(\boldsymbol{x}(t_2^-)) = \boldsymbol{x}(t_2^-) \tag{7.13}$$

where "+" and "-" signs denote the time just after and before contact and separation instants t_1 and t_2, respectively. Since being in contact or separating is judged based on the contact force, with respect to (7.1b), the indicator functions $h_1(\boldsymbol{x})$ and $h_2(\boldsymbol{x})$ are defined as:

$$h_1(\boldsymbol{x}) = h_2(\boldsymbol{x}) = \begin{cases} x_1 - x_{env} = 0 & ; \quad (x_2 + 1/p \geq 0) \\ x_2 + 1/p = 0 & ; \quad (x_1 - x_{env} > 0) \end{cases} \tag{7.14}$$

where both x_1 and x_2 are evaluated at each discontinuity instant, t_i. Subsequently, Jacobians of $\boldsymbol{g}_1$, $\boldsymbol{g}_2$, h_1 and h_2 are (see Section 2.4.4):

$$\boldsymbol{H}_1(\boldsymbol{x}^-) = \boldsymbol{H}_2(\boldsymbol{x}^-) = \begin{cases} [1 \quad 0] & ; \quad (x_2 + 1/p \geq 0) \\ [0 \quad 1] & ; \quad (x_1 - x_{env} > 0) \end{cases} \tag{7.15}$$

$$\boldsymbol{G}_1(\boldsymbol{x}^-) = \boldsymbol{G}_2(\boldsymbol{x}^-) = \begin{bmatrix} 1 & 0 \\ 0 & 1 \end{bmatrix} \tag{7.16}$$

Substituting (7.3), (7.15) and (7.16) into (2.27) and (2.28) yields the transition conditions of the linearized equations at instants of discontinuities.

7.4.3 Numerical Integration

Except for a few special cases, Lyapunov exponents cannot be calculated exactly and in most cases one should resort to numerical computations (Medio and Lines, 2001). To construct a suitable finite difference scheme for (7.3) and (7.11), we resort to the nonstandard finite-difference discretization framework (Mickens, 2002). The goal is to reduce the possibility of numerical instabilities and to enhance the computational reliability of the procedure for calculating Lyapunov exponents over large periods of time. It is shown that in comparison to the standard fourth-order Runge-Kutta method, calculating Lyapunov exponents of switching control systems using the nonstandard finite difference discretization scheme provides numerically stable results with a larger critical integration step-size and less computation time (Sekhavat et al., 2003). Thus, the method is meritorious for stability analysis of switching control systems using Lyapunov exponents.

The first step in constructing the scheme is to approximate the derivatives by their respective forward-difference approximations and manipulate the right-hand sides as follows:

$$\frac{x_1^{(k+1)} - x_1^{(k)}}{h} = x_2^{(k)}$$

$$\frac{x_2^{(k+1)} - x_2^{(k)}}{h} = \begin{cases} -\dfrac{K_p}{m}\left(x_1^{(k)} - x_{des}\right) - \dfrac{K_{v_1}}{m} x_2^{(k+1)} & (noncontact) \\ -\dfrac{K_{v_2}}{m} x_2^{(k+1)} - \dfrac{(K_f + 1)}{m}\left((1 + p x_2^{(k+1)}) H(x_1^{(k)} - x_{env})^n - F_{des}\right) & (contact) \end{cases} \tag{7.17a}$$

$$\frac{\psi_{11}^{(k+1)}-\psi_{11}^{(k)}}{h}=\psi_{21}^{(k)}$$

$$\frac{\psi_{12}^{(k+1)}-\psi_{12}^{(k)}}{h}=\psi_{22}^{(k)}$$

$$\frac{\psi_{21}^{(k+1)}-\psi_{21}^{(k)}}{h}=\begin{cases}-\dfrac{K_p}{m}\psi_{11}^{(k)}-\dfrac{K_{v_1}}{m}\psi_{21}^{(k+1)} & (noncontact)\\ -\dfrac{3(K_f+1)}{2m}\left(1+p\,x_2^{(k)}\right)H\left(x_1^{(k)}-x_{env}\right)^{n-1}\psi_{11}^{(k)}+\left(-\dfrac{K_{v_2}}{m}-\dfrac{(K_f+1)}{m}\,pH\left(x_1^{(k)}-x_{env}\right)^{n}\right)\psi_{21}^{(k+1)} & (contact)\end{cases}$$

$$\frac{\psi_{22}^{(k+1)}-\psi_{22}^{(k)}}{h}=\begin{cases}-\dfrac{K_p}{m}\psi_{12}^{(k)}-\dfrac{K_{v1}}{m}\psi_{22}^{(k+1)} & (noncontact)\\ -\dfrac{3(K_f+1)}{2m}\left(1+p\,x_2^{(k)}\right)H\left(x_1^{(k)}-x_{env}\right)^{n-1}\psi_{12}^{(k)}+\left(-\dfrac{K_{v_2}}{m}-\dfrac{(K_f+1)}{m}\,pH\left(x_1^{(k)}-x_{env}\right)^{n}\right)\psi_{22}^{(k+1)} & (contact)\end{cases}$$

(7.17b)

where $x_i^{(k)}=x_i(t_k)$, $x_i^{(k+1)}=x_i(t_k+h)$, $\psi_{ij}^{(k)}=\psi_{ij}(t_k)$ and $\psi_{ij}^{(k+1)}=\psi_{ij}(t_k+h)$ $(i,j=1,2)$. The above equations can further be rearranged as

Noncontact mode

$$x_1^{(k+1)}=x_1^{(k)}+h\,x_2^{(k)}$$

$$x_2^{(k+1)}=\frac{x_2^{(k)}-\dfrac{K_p\,h}{m}\left(x_1^{(k)}-x_{des}\right)}{1+\dfrac{K_{v_1}h}{m}}$$

$$\psi_{11}^{(k+1)}=\psi_{11}^{(k)}+h\psi_{21}^{(k)}$$

$$\psi_{12}^{(k+1)}=\psi_{12}^{(k)}+h\psi_{22}^{(k)}$$

$$\psi_{21}^{(k+1)}=\frac{\psi_{21}^{(k)}-\dfrac{K_p\,h}{m}\psi_{11}^{(k)}}{1+\dfrac{K_{v_1}h}{m}}$$

$$\psi_{22}^{(k+1)}=\frac{\psi_{22}^{(k)}-\dfrac{K_p\,h}{m}\psi_{12}^{(k)}}{1+\dfrac{K_{v_1}h}{m}}$$

Contact mode

$$x_1^{(k+1)}=x_1^{(k)}+h\,x_2^{(k)}$$

$$x_2^{(k+1)}=\frac{x_2^{(k)}+\dfrac{(K_f+1)h}{m}F_{des}-\dfrac{(K_f+1)h}{m}H(x_1^{(k)}-x_{env})^{n}}{1+\dfrac{K_{v_2}h}{m}+\dfrac{(K_f+1)h}{m}pH(x_1^{(k)}-x_{env})^{n}}$$

$$\psi_{11}^{(k+1)}=\psi_{11}^{(k)}+h\psi_{21}^{(k)}$$

$$\psi_{12}^{(k+1)}=\psi_{12}^{(k)}+h\psi_{22}^{(k)}$$

$$\psi_{21}^{(k+1)}=\frac{\psi_{21}^{(k)}-\dfrac{3(K_f+1)h}{2m}\left(1+p\,x_2^{(k)}\right)H\left(x_1^{(k)}-x_{env}\right)^{n-1}\psi_{11}^{(k)}}{1+\dfrac{K_{v_2}h}{m}+\dfrac{(K_f+1)h}{m}pH\left(x_1^{(k)}-x_{env}\right)^{n}}$$

$$\psi_{22}^{(k+1)}=\frac{\psi_{22}^{(k)}-\dfrac{3(K_f+1)h}{2m}\left(1+p\,x_2^{(k)}\right)H\left(x_1^{(k)}-x_{env}\right)^{n-1}\psi_{12}^{(k)}}{1+\dfrac{K_{v_2}h}{m}+\dfrac{(K_f+1)h}{m}pH\left(x_1^{(k)}-x_{env}\right)^{n}}$$

(7.18)

Note that although the NSFΔ method is implicit by construction, the difference equations (7.18) enable the solution to be computed explicitly. Also, difference equations (7.18) have the same order as the differential equations (7.3) and (7.11) and the fixed point of (7.18) is the critical

point of the original dynamical system (7.3). These features reduce the possibility of introducing spurious or other numerical instabilities associated with unequal orders of differential and difference equations or dissimilar characteristics of differential and difference schemes (Mickens, 2002).

Another key issue in numerical integration of switching control systems is to determine the time that contact or separation occurs. For the motion that starts in free-space at time t_k $\left(x(t_k)-x_{env}\le 0 \text{ or } 1+p\dot{x}(t_k)\le 0\right)$, the contact made within (t_k,t_{k+1}) could be observed when $\left(x(t_{k+1})-x_{env}>0 \text{ and } 1+p\dot{x}(t_{k+1})>0\right)$. This can be numerically detected only if the time-step is small enough (Brogliato et al., 2002). Therefore, we adopt the so-called step back procedure (Brogliato et al., 2002; Taylor and Kebede, 1997) into our switching control system as follows:

Step1: Equations in contact or noncontact region are integrated. Each integrated point is considered as a "trial" point until the switching condition (7.1b) is checked. If no switching occurs, the point is "accepted".

Step 2: When switching from contact to noncontact or vice versa is detected, the trial point is discarded and an iterative procedure is initiated with half of the previous integration step-size ($h/2$) until either switching does not occur or the trajectory is on the discontinuity surface (with the machine accuracy of 10^{-15} *s*). The model does not switch during this step.

Step 3: On the discontinuity surface, nonlinear and linearized equations of motion are switched to the equations of the second region. The transition condition of the linearized equations is calculated from (2.27) or (2.28) after substituting (7.3), (7.15) and (7.16) in them.

Step 4: Normal integration with the preset integration step-size, *h*, proceeds.

7.4.4 Stability

The numerical results of Lyapunov exponent calculations are used to discuss the stability of the switching contact task control system described in (7.3).

System Parameters

The spectrum of the Lyapunov exponents is calculated for a 0.252 *Kg* implement with steel tip

colliding with a steel environment. The implement moves from the initial position, x_1^i=1 *m*, in free-space toward the desired position, x_{des}=1.15 *m*. Upon collision with the environment located at x_{env}=1.03 *m*, the controller brings the implement into a stable contact with the environment with the desired contact force of F_{des} =1 *N*. For steel on steel collision, $H_{steel} = 2.08\text{x}10^{10}\left(\frac{N}{m^{3/2}}\right)$ and the coefficient of restitution is assumed to be *e*=0.6. Thus, from (3.24):

$$p = \frac{0.975}{\dot{x}_0} \tag{7.19}$$

The noncontact control gains are selected as K_p =5000 *N/m* and K_{v_1} =100 *Ns/m* which provides an approach velocity of ≈4.66 *m/s* at the time of the first collision with the environment. The integration step-size is chosen as h=10^{-8} *s*.

Truncating the Calculation Time to a Finite Interval

Although theoretically Lyapunov exponents are calculated as $t \to \infty$, in practice, we need to determine the exponents on a finite time interval. Truncation of time to a finite interval is an important issue. Recently, Grune (2000) proved that, for linear flows, the finite time exponential growth rates for some fixed time, *T*, uniformly converge to the uniform exponential spectrum. Since the uniform exponential spectrum can be interpreted as an extension of Lyapunov exponents (Grune, 2000), this proposition provides the theoretical background to terminate the exponent calculations after a finite time *T*. For choosing the appropriate *T*, the strategy used in other studies with apparent success is to compute the exponents on progressively longer time intervals, while monitoring the variation in the results obtained. Convergence is declared if these variations are sufficiently low (Dieci and Van Vleck, 2002). In the present work, we adopt the same criteria in calculations of Lyapunov exponents. The range of force control gains are chosen as $10 \le K_{v_2} \le 100$ *Ns/m* and $600 \le K_f \le 1000$. The results showed that the largest Lyapunov exponent changes between 0.8 and 1 second is less than 0.25 %. The results for typical gains (K_f, K_{v_2}) = (600,10), (600,100), (1000,10) and (1000,100) are depicted in Fig. 7.2. Thus, in all simulations the spectrum of Lyapunov exponents is calculated for 1 *s*.

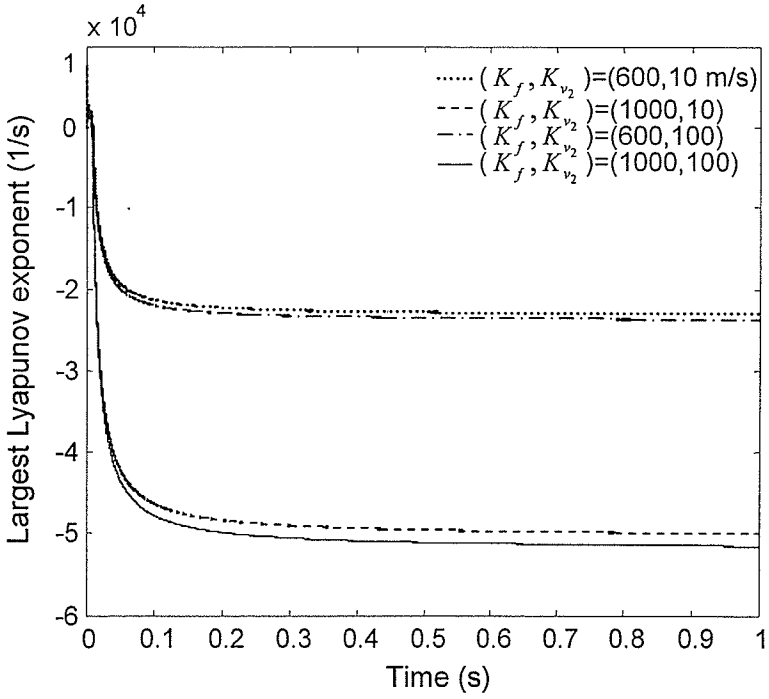

Fig. 7.2 Variation of the largest Lyapunov exponent over time.

Convergence to the Exact Solution and Stability

A crucial issue of the numerical solution to discontinuous differential equations is to prove that the numerical results converge to the true solution of the system. The matter becomes even more important when it comes to deciding on the stability of the systems based on numerically calculated Lyapunov exponents. Filippov has recently proven (Section 2.6) that if Filippov's solution of a discontinuous system exists and is unique, the approximate solution obtained using a Runge-Kutta method with sufficiently small integration step-size (h) exists, and as $h \to 0$, converges uniformly to the exact solution. Therefore, in order to illustrate the uniform convergence of the results obtained from the nonstandard finite difference (NSFΔ) scheme to the exact solution, numerical results are compared with the results of the fourth-order Runge-Kutta (RK4) method with sufficiently low step-size. Figures 7.3 and 7.4 show the largest Lyapunov exponent for the system with gains $K_{v_1} = 100\ Ns/m$, $K_{v_2} = 50\ Ns/m$, K_f = 800 and K_p=5700 N/m using NSFΔ and RK4 schemes with two step-sizes, 10^{-8} s and 10^{-9} s. These figures show that, as h decreases, the largest Lyapunov exponent computed by the NSFΔ method

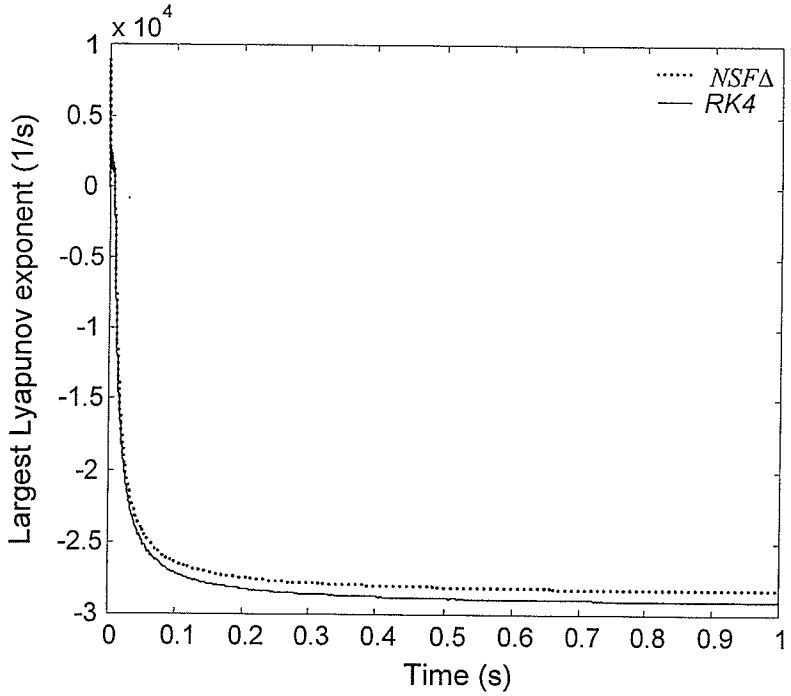

Fig. 7.3 Largest Lyapunov exponent (integration step-size h=10^{-8} s).

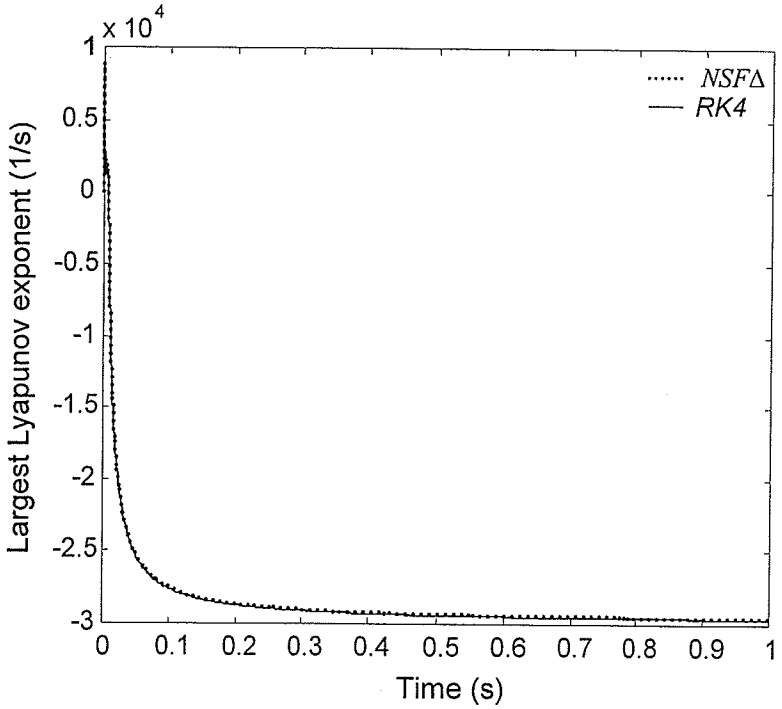

Fig. 7.4 Largest Lyapunov exponent (integration step-size h=10^{-9} s)

approaches to the one calculated using RK4 which itself is proven to converge to the exact solution (Filippov, 2001). Being assured from the convergence of the numerical results to the exact solution and based on the result that the largest Lyapunov exponent is negative (see Figs. 7.3 and 7.4), it can be concluded that the attractor of the system is a stable equilibrium point. In other words, the above chosen control gains would result in a stable switching contact task control system.

To further demonstrate that the system trajectories converge to $\boldsymbol{x}_{eq}$ where the implement is in stationary contact $(\dot{x} = 0)$ with the environment following the contact force of 1 N $(F_{des} = 1N)$, the nonlinear responses of the system are shown in Figs. 7.5 and 7.6. These figures not only demonstrate the convergence of the trajectories to the equilibrium point, but also illustrate that when contact with the environment is lost due to bouncing, contact is re-established until the desired contact force is achieved.

7.4.5 Basin of Attraction

As stated in Section 2.4.5, although Lyapunov exponents are calculated along a single solution trajectory, they have the same values for all trajectories in the same basin of attraction. To study the basin of attraction of the above system, the algorithm in (Nusse and York, 1998) is employed (see Section 2.4.5). The region $\Gamma := \{x, \dot{x};\ 0.5 \le x \le 1\, m\ \ \&\ \ 0.0 < \dot{x} \le 0.9\, m/s\}$ is divided into grid boxes neighboring the center box with sizes of 0.05 m and 0.1 m/s for x and $\dot{x}$, respectively. Extensive simulations revealed that the state trajectories from all the neighboring grid boxes enter the center box and stay thereafter. Thus, we conclude that the region, Γ, is a part of the basin of attraction and our previous discussions and observations on stability are valid for this region. Note that this region is not necessarily the entire basin of attraction. Finding a larger stability region is important, but is beyond the scope of this research.

7.4.6 Lyapunov Exponents and the Overall Convergence/Divergence Rate

Since the absolute values of Lyapunov exponents measure the rate of exponential convergence/divergence of two initially close trajectories, they have been used to compare the convergence rate of different smooth control systems to the equilibrium point (Wu et al., 2001). The more negative the largest exponent is, the faster the solution converges to the equilibrium

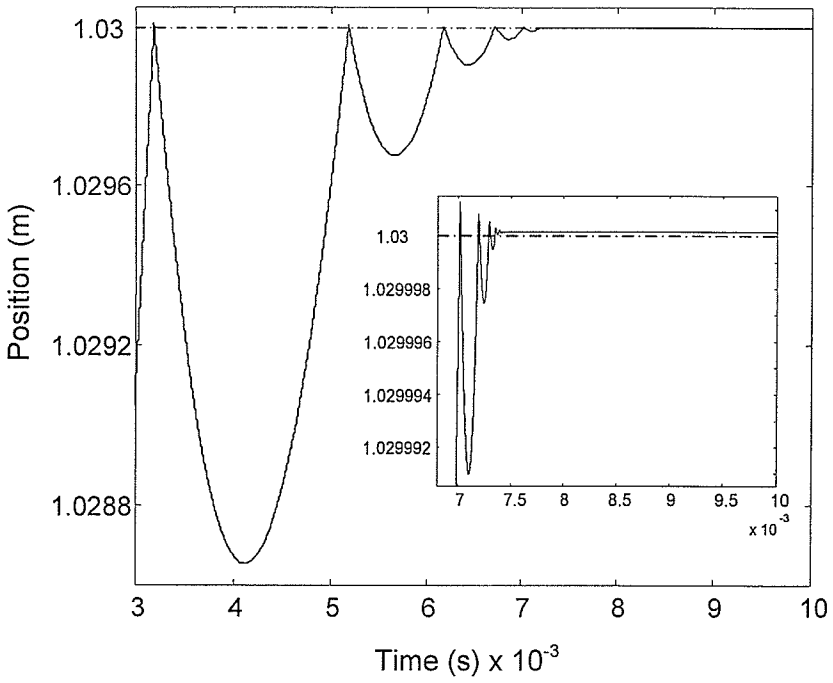

Fig. 7.5 Implement position response (K_p =5700 *N/m*, K_{v1}=100 *Ns/m*, K_f=800, K_{v2}=50 *Ns/m*).

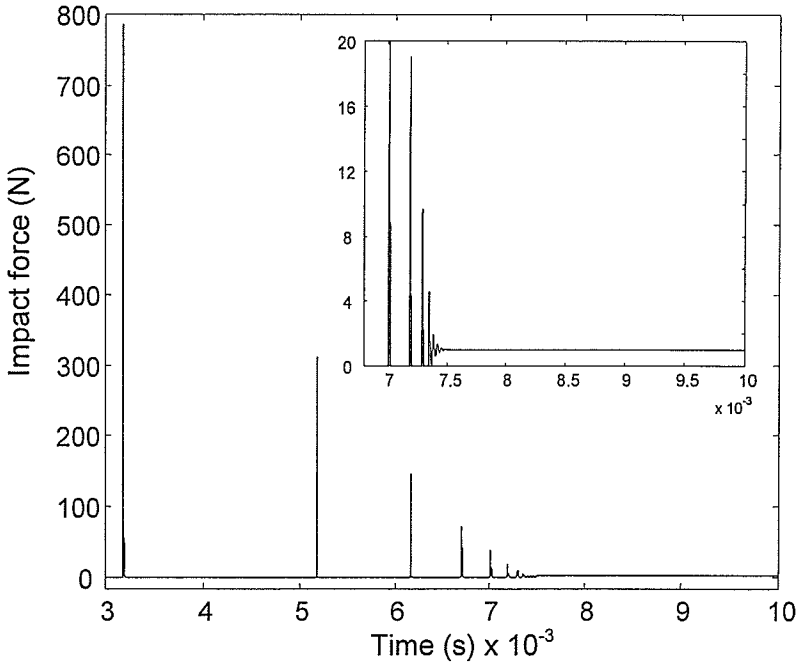

Fig. 7.6 Impact force response pertaining to Fig. 7.5.

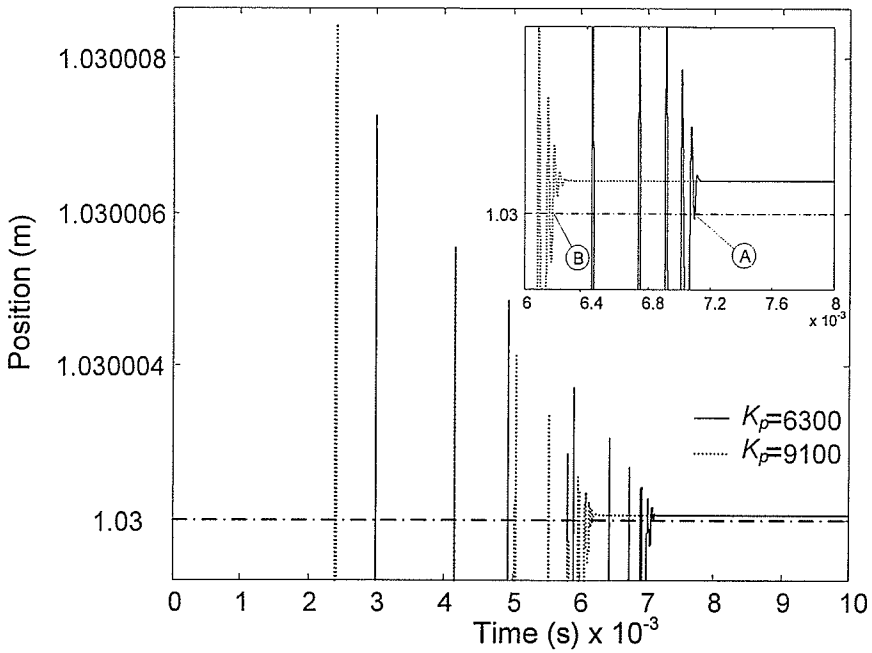

Fig. 7.7 Implement position response for various values of K_p.

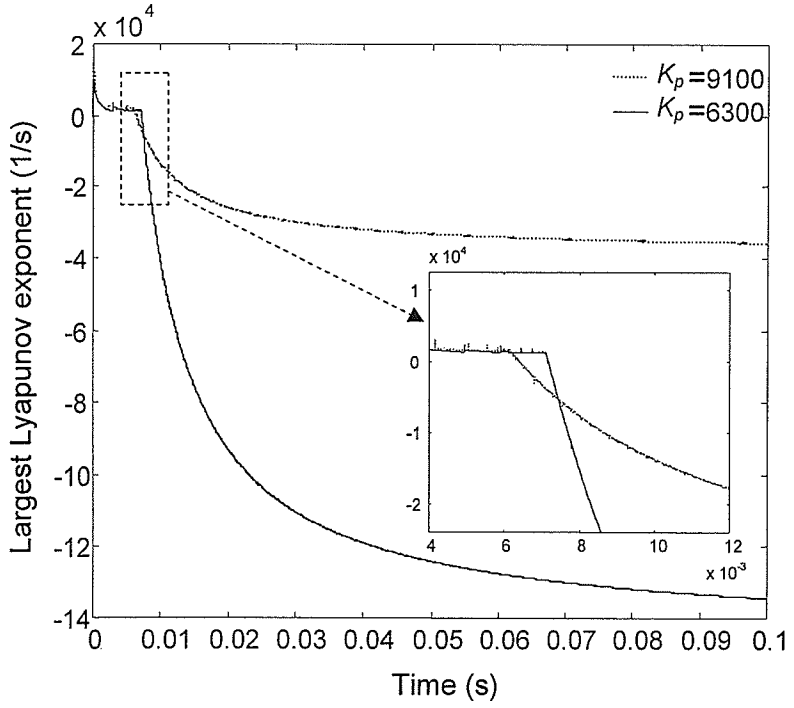

Fig. 7.8 Largest Lyapunov exponents pertaining to Fig.7.7.

point. However, Figs 7.7 and 7.8 reveal that this is not always the case for switching systems. Comparing the responses of systems with K_p =6300 *N/m* and K_p =9100 *N/m* (Fig. 7.7) shows that the system with the higher K_p converges to the equilibrium point faster. On the other hand, the corresponding largest Lyapunov exponents are -143740 1/*s* for K_p =6300 *N/m* and -35950 1/*s* for K_p =9100 *N/m*, respectively. Thus, the system with less negative largest Lyapunov exponent has a higher convergence rate to the stable equilibrium point. To explain the controversy, the close-up of the largest Lyapunov exponents is shown in Fig. 7.8. This figure shows that when the system is experiencing impacts, it is still in the transient period of motion. After the impact phase is completed, the convergence rate of the system with more negative largest Lyapunov exponent (K_p=6300) exceeds the convergence rate of the system with less negative largest Lyapunov exponent (K_p=9100). A closer look at the inset of Fig. 7.7 confirms that after completion of the impact period (starting at points A and B), the system with more negative largest Lyapunov exponent (K_p =6300) converges faster and with less number of oscillations to the equilibrium point. This observation brings us to the important conclusion that the value of the largest Lyapunov exponent is not a measure of overall convergence rate as for smooth systems, but it can be a measure of the convergence rate only during the remaining continuous period of response after the discontinuous period is completed.

7.4.7 Sensitivity Analysis Using Lyapunov Exponents

Lyapunov exponents can also assist in studying the effect of different control gains and system parameters on the stability of the switching control systems. To study the stability and robustness of the system with respect to different force control gains, the largest Lyapunov exponents of the system having the same position control gains are calculated with K_{v_2} increased from 10 *Ns/m* to 100 *Ns/m* with increments of 10 *Ns/m* and K_f increased from 600 to 1000 with increments of 50 (see Fig. 7.9). The fact that the largest Lyapunov exponent is always negative indicates that the system stability is not sensitive to the changes in these control gains.

In addition to the control gains and system parameters, the effect of the approach velocity on the system stability may also be of great interest. Therefore, as another example of using Lyapunov exponents for sensitivity analysis, we study the effect of various approach velocities before the first impact on the system stability. This is accomplished by fixing the force control gains K_{v_2} =50 *Ns/m* and K_f=800 as well as the velocity gain K_{v_1} =100 *Ns/m* and changing the position

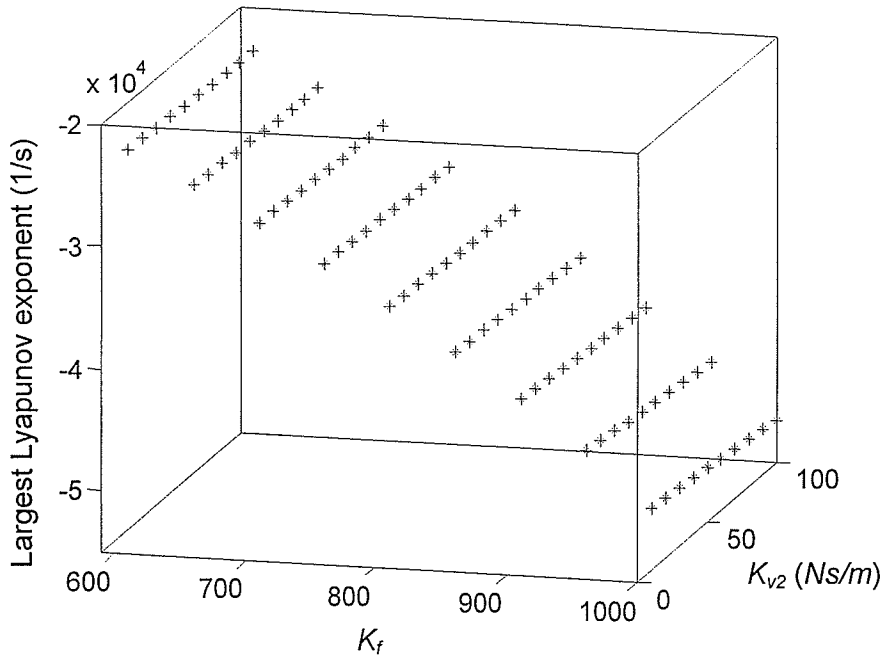

Fig. 7.9 Bifurcation diagram of the largest Lyapunov exponent.

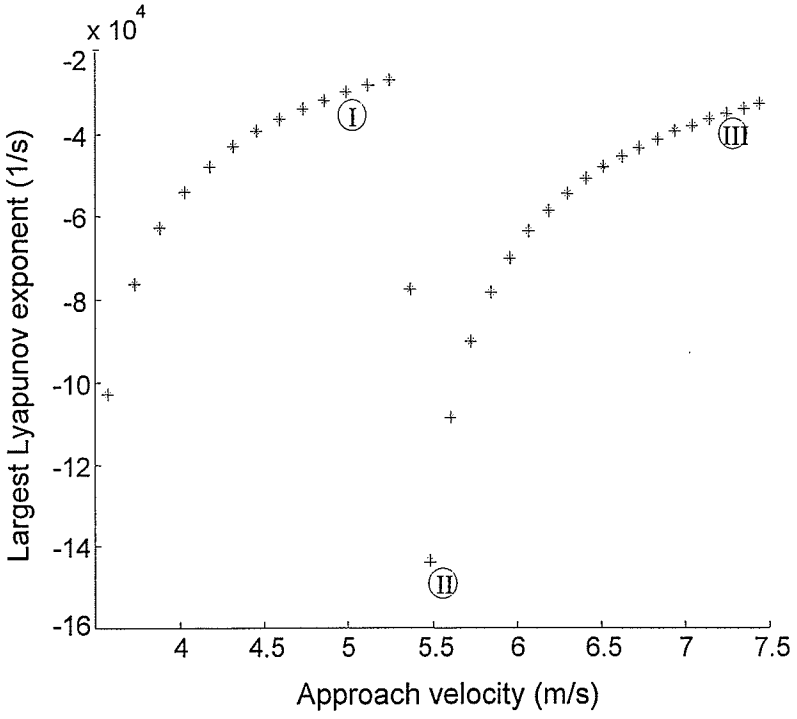

Fig. 7. 10 Largest Lyapunov exponent for various approach velocities.

controller gain K_p in each simulation. Fig. 7.10 shows the largest negative Lyapunov exponents obtained by changing K_p from 3500 *N/m* to 9900 *N/m* incrementally, which corresponds to approach velocities between 3.5 *m/s* and 7.5 *m/s*. According to this figure, the equilibrium point of the system is always asymptotically stable for the above approach velocities. Such an observation is useful in practical applications for setting the appropriate range of implement speed that would guarantee the stability of the system in case of unexpected collisions.

As it was explained in Section 7.4.6, the largest Lyapunov exponent in Fig. 7.10 is not a measure for comparing the overall convergence rates of the system with various approach velocities. Specifically, the jump in the value of the largest Lyapunov exponent around the approach velocity of 5.49 *m/s* (point II) is due to the fact that after the impact period, the system converges to the equilibrium point faster than the system with any other approach velocity within the above range. To further verify this phenomenon, the implement position responses pertaining to the cases (I), (II) and (III) (see Fig. 7.10) are illustrated in Fig. 7.11. Comparing the convergence rates of the system from points A, B, C to the equilibrium point in this figure demonstrates that the fastest convergence is from point B to the equilibrium point which belongs to the system II that has the largest negative Lyapunov exponent.

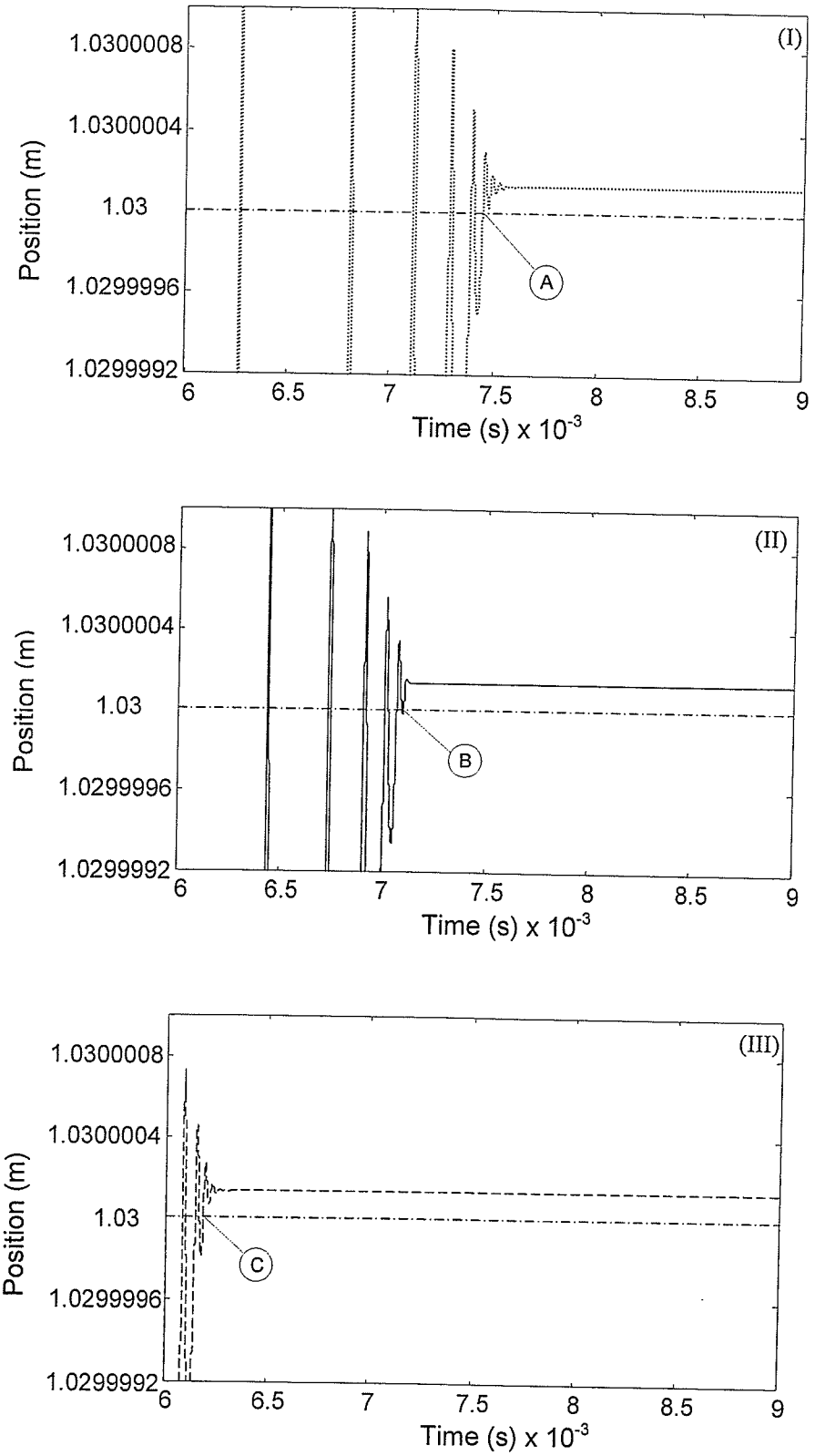

Fig. 7.11 Implement position responses pertaining to systems (I), (II) and (III) in Fig. 7.10.

Chapter 8

Overall Stability Analysis of Hydraulic Actuator's Switching Contact Controller

8.1 Introduction

The individually designed control laws in Chapters 4, 5, and 6 for different operation phases of contact task control are now combined into an overall switching contact task control scheme for hydraulic actuators. The overall scheme is capable of: (1) asymptotic desired position regulation in free space, (2) impact suppression and stable transition from free to constrained motion and, (3) asymptotic desired force regulation in sustained-contact motion of hydraulic actuators with friction. The impact control scheme is used for the first time to fill the gap of damping the undesirable impacts and dissipating the impact energy that could drive the whole system unstable. The position and force control schemes are capable of asymptotic set-point regulation in the presence of actuator friction without having the complexity of sliding mode or adaptive control techniques.

Existence of at least two switchings in the control scheme (free-space to impact mode, and impact to sustained-contact mode) results in an overall nonsmooth system. Although stability of the actuator motion under each individual controller has been addressed in previous chapters, stability of the overall system that experiences switchings between the controllers is an open

issue. Finding an overall Lyapunov function for the overall task is extremely difficult, if not impossible. In this chapter, the Lyapunov-exponent-based framework outlined in Chapter 7 is employed for rigorous stability analysis of the overall contact task control scheme of the hydraulic actuator. If numerical artifacts are under control, calculation of Lyapunov exponents provides a solid insight of the overall stability of the system without imposing the restrictive assumptions commonly required in order to construct a Lyapunov function for direct Lyapunov stability analysis.

Employing the concept of Lyapunov exponents for stability analysis not only allows the system to have numerous switches between different phases of motion, but also facilitates the following modifications on the dynamic model and control laws to enhance and/or generalize the performance and applicability of the control system:

1) In order to make the Lyapunov stability analysis manageable, the three distinct control laws introduced in Chapters 4, 5, and 6 were designed using the simplified hydraulic model based on assumptions of (*i*) the piston is initially centered in the cylinder, and, (*ii*) the whole motion occurs within the mid-point vicinity of the cylinder. These assumptions that are necessary for Lyapunov-based control design, can be released when the system stability is being studied using the concept of Lyapunov exponents.

2) Implementation of the discontinuous terms in the controllers developed in Chapters 4 to 6 in each phase of motion [see (4.16), (5.45), and (6.6)] may cause undesirable chattering in the control signal. The chatterings are removed by replacing the discontinuous *sign* functions in the control laws with smooth hypertangent functions with the price of weakening the previously conducted stability analysis. Stability analysis using the concept of Lyapunov exponents provides solid stability results for the modified system.

8.2 Combined Contact Task Control System

The dynamic model used for the overall contact task control employs the general hydraulic pressure-flow equations as follows:

$$\begin{cases} \dot{x} = v \\ \dot{v} = \dfrac{A(P_i - P_o)}{m} - \dfrac{F_f}{m} - \dfrac{F_{env}}{m} \\ \dot{P}_i = \dfrac{\beta}{\overline{V}_i + A(x - x_0)}\left(-Av + \sqrt{\dfrac{2}{\rho}} c_d w x_{sp} \sqrt{\dfrac{P_S - P_e}{2} + sign(x_{sp})\left(\dfrac{P_S + P_e}{2} - P_i\right)} \right) \\ \dot{P}_o = \dfrac{\beta}{\overline{V}_o - A(x - x_0)}\left(Av - \sqrt{\dfrac{2}{\rho}} c_d w x_{sp} \sqrt{\dfrac{P_S - P_e}{2} + sign(x_{sp})\left(P_o - \dfrac{P_S + P_e}{2}\right)} \right) \\ \dot{x}_{sp} = -\dfrac{1}{\tau} x_{sp} + \dfrac{k_{sp}}{\tau} u \end{cases} \tag{8.1}$$

In studying the contact task stability of hydraulic systems, in general, and their stability analysis using Lyapunov exponents, in particular, a good friction model for the actuator friction and a realistic impact/contact model that represents the real behavior of the system during impact transition and sustained-contact periods of motion are among the most important factors contributing to the true judgment of the system stability. Hertz-type contact model (equation 3.23) and the original Hertz model (equation 3.21) used in individual development of control schemes will also be used in the overall task's stability analysis using the concept of Lyapunov exponents:

$$F_{env} = \begin{cases} (1 + p\dot{x})H(x - x_{env})^n & ; \quad (x - x_{env} > 0) \,\&\, (1 + p\dot{x} > 0) \,\&\, (\dot{x}_0 \neq 0) \\ H(x - x_{env})^n & ; \quad (x - x_{env} > 0) \,\&\, (\dot{x}_0 = 0) \\ 0 & ; \quad otherwise \end{cases} \tag{8.2}$$

and $\dot{x}_0$ is the implement approach velocity or the velocity at the instant when the contact force increases from a constantly zero value to a non-zero value.

Employing the approach of Lyapunov exponents allows for replacing the previously employed discontinuous Tustin friction model with the continuous LuGre model [equations (3.19) and (3.20)] whose continuity complies with the continuous behavior of friction and the calculation procedure of Lyapunov exponents.

$$F_f = \sigma_0 z + \sigma_1 \dot{z} + d\dot{x} \tag{8.3}$$

$$\dot{z} = \dot{x} - \frac{\sigma_0 |\dot{x}|}{F_C + (F_S - F_C)e^{-(\dot{x}/v_s)^2}} z \tag{8.4}$$

Note that introduction of the bristle deflections as a new immeasurable state variable in this model adds to the order of the entire system dynamics. This was not desirable for control design

in Chapters 4 to 6 using Lyapunov stability analysis but can be accomodated when using the concept of Lyapunov exponents.

The overall contact task control algorithm is intended to be capable of: (*i*) asymptotic position regulation in the free-space, (*ii*) asymptotic impact control upon collision with an unknown environment by resting the hydraulic actuator on the surface of the environment recorded upon the onset of impact and, (*iii*) asymptotic desired force regulation when the impact oscillations are dissipated. Therefore, the control scheme is constructed by combining the three Lyapunov-based control laws previously designed in Chapters 4 to 6 and switching from one to the other based on the control task:

a) Free-space position control:

$$u_P = -\left(K_{p_P}|P_i - P_o|sign(x_{sp}) + K_{x_P}(x - x_{des})\right)\sqrt{P_s - sign(x_{sp})(P_i - P_o)}$$

b) Impact control:

$$u_I = -\left(K_{p_I}|P_i - P_o|sign(x_{sp}) + K_{x_I}(x - x_{env})\right)\sqrt{P_s - sign(x_{sp})(P_i - P_o)}$$

c) Constrained motion force control:

$$u_F = -\left(K_{p_C}\left|P_i - P_o - \frac{F_{des}}{A}\right|sign(x_{sp}) + K_f(F_{env} - F_{des})\right)\sqrt{P_s - sign(x_{sp})\,(P_i - P_o)} \qquad (8.5)$$

where K_{p_P}, K_{x_P}, K_{p_I}, K_{x_I}, K_{p_C}, and K_f are positive constant control gains.

Implementation of the above discontinuous control scheme may cause undesirable chattering in the control signal. Therefore, when a discontinuous controller is implemented, the discontinuous terms are replaced with continuous functions (Southward et al., 1991; Slotine and Li, 1991; Corless, 1993). Replacing the discontinuous *sign* functions with hypertangent functions leads to the following form of control algorithm:

a) Free-space position control:

$$u_P = -\left(K_{p_P}|P_i - P_o|\tanh(ax_{sp}) + K_{x_P}(x - x_{des})\right)\sqrt{P_s - \tanh(ax_{sp})(P_i - P_o)}$$

b) Impact control:

$$u_I = -\left(K_{p_I}|P_i - P_o|\tanh(ax_{sp}) + K_{x_I}(x - x_{env})\right)\sqrt{P_s - \tanh(ax_{sp})(P_i - P_o)}$$

c) Constrained motion force control:

$$u_F = -\left(K_{Pc} \left| P_i - P_o - \frac{F_{des}}{A} \right| \tanh(ax_{sp}) + K_f (F_{env} - F_{des}) \right) \sqrt{P_s - \tanh(ax_{sp})\,(P_i - P_o)} \qquad (8.6)$$

where a is a finite positive large constant.

The switching from position control to impact control happens when the implement's force sensor senses the first nonzero force. The switching from impact to sustained-contact mode of motion occurs when the implement is stopped on the surface of the environment ($x = x_{env}$ & $\dot{x} = 0$ & $\ddot{x} = 0$). If during the sustained-contact period of motion, the contact with the environment is inadvertently lost ($x - x_{env} < 0$), the control scheme switches back to the impact control law and rests the implement on the environment surface and then switches back to the force control law to follow the desired contact force. This leads to the following flowchart as the control algorithm:

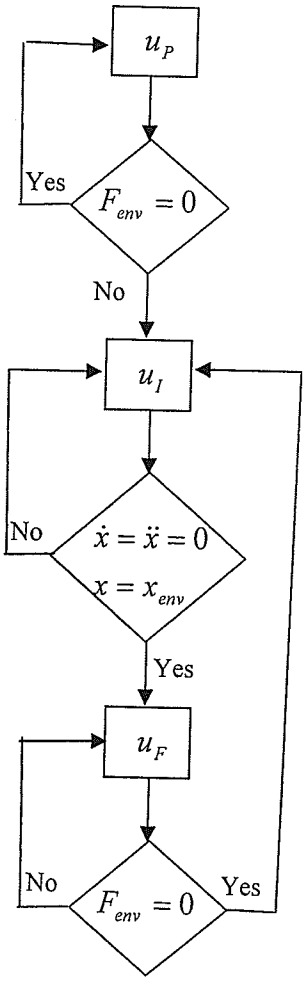

Fig. 8.1 The control switching's logic.

Combining equation (8.1) to (8.4) and (8.6), and defining the system states as $\boldsymbol{x} = (x_1, x_2, x_3, x_4, x_5, x_6)^T$ where $x_1 = x$, $x_2 = \dot{x}$, $x_3 = P_i$, $x_4 = P_o$, $x_5 = x_{sp}$, and $x_6 = z$, the state-space equations of motion are now constituted as follows:

$$\dot{\boldsymbol{x}} = \boldsymbol{f}(\boldsymbol{x}) = \begin{cases} \dot{x}_1 = e_2 \\ \dot{x}_2 = \dfrac{A(x_3 - x_4)}{m} - \dfrac{\sigma_0 x_6 + \sigma_1\left(x_2 - \dfrac{\sigma_0|x_2|}{F_C + (F_S - F_C)e^{-(x_2/v_s)^2}}x_6\right) + \sigma_2 x_2}{m} - \dfrac{F_{env}}{m} \\ \dot{x}_3 = \dfrac{\beta}{\overline{V}_i + A(x_1 - x_0)}\left(-Ax_2 + \sqrt{\dfrac{2}{\rho}}c_d w x_5 \sqrt{\dfrac{P_S - P_e}{2} + sign(x_5)\left(\dfrac{P_S + P_e}{2} - x_3\right)}\right) \\ \dot{x}_4 = \dfrac{\beta}{\overline{V}_o - A(x_1 - x_0)}\left(Ax_2 - \sqrt{\dfrac{2}{\rho}}c_d w x_5 \sqrt{\dfrac{P_S - P_e}{2} + sign(x_5)\left(x_4 - \dfrac{P_S + P_e}{2}\right)}\right) \\ \dot{x}_5 = -\dfrac{1}{\tau}x_5 + \dfrac{k_{sp}}{\tau}u \\ \dot{x}_6 = x_2 - \dfrac{\sigma_0|x_2|}{F_C + (F_S - F_C)e^{-(x_2/v_s)^2}}x_6 \end{cases} \tag{8.7a}$$

where

$$F_{env} = \begin{cases} (1 + px_2)H(x_1 - x_{env})^n & ; \quad (x_1 - x_{env} \geq 0)\ \&\ (1 + px_2 \geq 0)\ \&\ (x_2^i \neq 0) \\ H(x_1 - x_{env})^n & ; \quad (x_1 - x_{env} \geq 0)\ \&\ (x_2^i = 0) \\ 0 & ; \quad otherwise \end{cases} \tag{8.7b}$$

$$u = \begin{cases} u_P = -\left(K_{p_P}|x_3 - x_4|\tanh(\alpha x_5) + K_{x_P}(x_1 - x_{des})\right)\sqrt{P_s - \tanh(\alpha x_5)(x_3 - x_4)} \\ u_I = -\left(K_{p_I}|x_3 - x_4|\tanh(\alpha x_5) + K_{x_I}(x_1 - x_{env})\right)\sqrt{P_s - \tanh(\alpha x_5)(x_3 - x_4)} \\ u_F = -\left(K_{p_C}\left|x_3 - x_4 - \dfrac{F_{des}}{A}\right|\tanh(\alpha x_5) + K_f(H(x_1 - x_{env})^n - F_{des})\right)\sqrt{P_s - \tanh(\alpha x_5)(x_3 - x_4)} \end{cases} \tag{8.7c}$$

and x_2^i is the implement velocity at the last time instant when the implement position was on the surface of the environment, $x = x_{env}$.

In the presence of the environment, the equilibria ($\boldsymbol{x}_{eq}$) of the above nonsmooth system are those points in the contact region that satisfy the following conditions:

$$\begin{cases} x_2^{ss} = 0 \\ A(x_3^{ss} - x_4^{ss}) - \sigma_0 x_6^{ss} - F_{des} = 0 \\ x_5^{ss} = 0 \\ x_1^{ss} = \left(\dfrac{F_{des}}{H}\right)^{1/n} + x_{env} \end{cases} \tag{8.8}$$

In the absence of the environment, however, the system will never switch to impact or force control laws and the equilibrium of the system would be the same range of points obtained in Chapter 4.

The preliminary step before proceeding with the system stability analysis using the concept of Lyapunov exponents is to prove that the switching system has a unique continuous solution.

8.3 Solution Analysis

Existence and continuation of Filippov's solution

Let region $\Omega = R^6 \times R$ and let D be an arbitrary compact set in Ω. The right-hand sides of equations (8.7) are defined everywhere in Ω, and are bounded by $B(t)$. Let $B(t) = L$, which is obviously integrable on D. Furthermore, each term of the right-hand sides of (8.7) is measurable. Thus, the right-hand sides of equations (8.7) satisfy condition B of Filippov's solution theory (Filippov, 1960) and according to Theorems 4 and 5 developed by Filippov (1960), we have the local existence of a solution which is continuous on $[t_1, t_2]$ as $t_2 \to \infty$.

Uniqueness of Filippov's solution

Discontinuities of the system occur at instants of free-space to impact mode switching and also switchings between impact and contact modes of motion. Since at the time of the system's only switch from free-space to impact mode of motion, $x_2 + 1/p > 0$, the first discontinuity surface is defined as:

Surface 1 $$S_1^5 := \{(x_1, x_2, x_3, x_4, x_5, x_6) \ : \ x_1 - x_{env} = 0, x_2 > 0\} \tag{8.9}$$

Note that in this case the controller switches from u_P to u_I.

The second discontinuity surface is where the system switches from impact to contact phase of motion after the implement has rested on the surface of the environment:

Surface 2 $$S_2^4 := \{(x_1, x_2, x_3, x_4, x_5, x_6) : x_1 - x_{env} = 0 \ \& \ x_2 = 0 \ \& \ \dot{x}_2 = 0\} \quad (8.10)$$

If the system re-enters the free-space when the contact control law is in effect, the control would switch back to impact control law and, therefore, experiences discontinuity. This can be detected by monitoring the contact force (8.7b) and if F_{env} changes from a positive number to zero, command the control to switch back to impact mode. Therefore, the discontinuity surface of this case (u_F to u_I) is

Surface 3 $$S_3^5 := \{(x_1, x_2, x_3, x_4, x_5, x_6) \ : \ x_1 - x_{env} = 0, x_2 < 0\} \quad (8.11)$$

Note that the superscripts and subscripts in (8.9), (8.10) and (8.11) denote the dimension and the number of the discontinuity surface, respectively. Clearly, the vector-valued function of the right-hand sides of equations (8.8) is continuous up to the discontinuity surfaces and the discontinuity surfaces are smooth and independent of time. Therefore, conditions A, B and C of Filippov's solution theory (Filippov, 1979) are satisfied. Next, the analysis of the uniqueness of Filippov's solution must be carried out for each discontinuity surface. Here, we only show the detailed analysis for S_1^5.

The solution region is divided by the surface S_1^5 into two parts: $\Omega^+ := \{x : x_1 - x_{env} > 0\}$ and $\Omega^- := \{x : x_1 - x_{env} < 0\}$. The normal to this surface, denoted by $\mathbf{N}_1$, is:

$$\mathbf{N}_1 = \left(\frac{\partial S_1^5}{\partial x_1} \ \frac{\partial S_1^5}{\partial x_2} \ \frac{\partial S_1^5}{\partial x_3} \ \frac{\partial S_1^5}{\partial x_4} \ \frac{\partial S_1^5}{\partial x_5} \ \frac{\partial S_1^5}{\partial x_6} \right)^T = (1 \ 0 \ 0 \ 0 \ 0 \ 0)^T \quad (8.12)$$

The vector functions $\mathbf{f}_1^+$ and $\mathbf{f}_1^-$ are defined as the limiting values of the right-hand sides of state space equations in Ω^+ and Ω^-:

$$\mathbf{f}_1^- = \begin{cases} \dot{x}_1 = x_2 \\ \dot{x}_2 = \dfrac{A(x_3 - x_4)}{m} - \dfrac{\sigma_0 x_6 + \sigma_1\left(x_2 - \dfrac{\sigma_0|x_2|}{F_C + (F_S - F_C)e^{-(x_2/v_s)^2}} x_6\right) + \sigma_2 x_2}{m} \\ \dot{x}_3 = \dfrac{\beta}{\overline{V}_i + A(x_1 - x_0)}\left(-Ax_2 + \sqrt{\dfrac{2}{\rho}} c_d w x_5 \sqrt{\dfrac{P_S - P_e}{2} + sign(x_5)\left(\dfrac{P_S + P_e}{2} - x_3\right)}\right) \\ \dot{x}_4 = \dfrac{\beta}{\overline{V}_o - A(x_1 - x_0)}\left(Ax_2 - \sqrt{\dfrac{2}{\rho}} c_d w x_5 \sqrt{\dfrac{P_S - P_e}{2} + sign(x_5)\left(x_4 - \dfrac{P_S + P_e}{2}\right)}\right) \\ \dot{x}_5 = -\dfrac{1}{\tau}x_5 - \dfrac{k_{sp}}{\tau}\left(K_{p_P}|x_3 - x_4|\tanh(a x_5) + K_{x_P}(x_1 - x_{des})\right)\sqrt{P_s - \tanh(a x_5)(x_3 - x_4)} \\ \dot{x}_6 = x_2 - \dfrac{\sigma_0|x_2|}{F_C + (F_S - F_C)e^{-(x_2/v_s)^2}} x_6 \end{cases}$$

$$\mathbf{f}_1^+ = \begin{cases} \dot{x}_1 = x_2 \\ \dot{x}_2 = \dfrac{A(x_3 - x_4)}{m} - \dfrac{\sigma_0 x_6 + \sigma_1\left(x_2 - \dfrac{\sigma_0|x_2|}{F_C + (F_S - F_C)e^{-(x_2/v_s)^2}} x_6\right) + \sigma_2 x_2}{m} - \dfrac{(1 + p x_2) H(x_1 - x_{env})^n}{m} \\ \dot{x}_3 = \dfrac{\beta}{\overline{V}_i + A(x_1 - x_0)}\left(-Ax_2 + \sqrt{\dfrac{2}{\rho}} c_d w x_5 \sqrt{\dfrac{P_S - P_e}{2} + sign(x_5)\left(\dfrac{P_S + P_e}{2} - x_3\right)}\right) \\ \dot{x}_4 = \dfrac{\beta}{\overline{V}_o - A(x_1 - x_0)}\left(Ax_2 - \sqrt{\dfrac{2}{\rho}} c_d w x_5 \sqrt{\dfrac{P_S - P_e}{2} + sign(x_5)\left(x_4 - \dfrac{P_S + P_e}{2}\right)}\right) \\ \dot{x}_5 = -\dfrac{1}{\tau}x_5 - \dfrac{k_{sp}}{\tau}\left(K_{p_I}|x_3 - x_4|\tanh(a x_5) + K_{x_I}(x_1 - x_{env})\right)\sqrt{P_s - \tanh(a x_5)(x_3 - x_4)} \\ \dot{x}_6 = x_2 - \dfrac{\sigma_0|x_2|}{F_C + (F_S - F_C)e^{-(x_2/v_s)^2}} x_6 \end{cases} \tag{8.13}$$

The projections of $\mathbf{f}_1^+$ and $\mathbf{f}_1^-$ along the normal to the discontinuity surface, $\mathbf{N}_1$, are:

$$\mathbf{f}_{N_1}^+ = \mathbf{f}_1^+ \cdot \mathbf{N}_1 = x_2$$

$$\mathbf{f}_{N_1}^- = \mathbf{f}_1^- \cdot \mathbf{N}_1 = x_2 \tag{8.14}$$

It can be seen that $\mathbf{f}_1^+ > 0 \,\&\, \mathbf{f}_1^- > 0$ when $x_2 > 0$ and $\mathbf{f}_1^+ < 0 \,\&\, \mathbf{f}_1^- < 0$ when $x_2 < 0$. Therefore, according to Lemma 9 of Filippov (1960), the solution goes through the discontinuity surface with an isolated point and we have uniqueness and continuous dependence of solution on the initial conditions. When the discontinuity surface (8.11) is met at the time of switching from contact back to impact phase of motion, the 2nd and 5th equations of (8.7a) will be changed

according to (8.7b) and (8.7c) and it can be similarly proven that the system has a unique solution.

8.4 Stability Analysis

In this section, the methodology introduced in Chapter 7 is invoked for stability analysis of the switching control system (8.7) using the concept of Lyapunov exponents. First, variational equations of smooth parts of the motion are obtained. Next, methods of addressing the nonsmoothness problems are applied and the issues of solution analysis, existence of exponents, linearization at nonsmooth instants, and computational stability and efficiency are addressed in detail.

8.4.1 Variational Equations for Smooth Parts of Motion

With respect to the method explained in Section 2.4.2, the variational equation

$$\dot{\psi}_t = \boldsymbol{F}(t)\psi_t \tag{8.15}$$

should be integrated simultaneous with the original nonlinear equation (8.7). The Jacobian matrix $\boldsymbol{F}(t)$ in (8.15) can only be derived for the smooth parts of motion, i.e., parts with no switching between control laws and no sharp edge introduced to the system because of the absolute value function. In such smooth parts of motion, the Jacobian $\boldsymbol{F}(t)$ is obtained by substituting (8.7) in (2.14) as follows:

$\boldsymbol{F}(t)=$

$$\begin{bmatrix} 0 & 1 & 0 & 0 & 0 & 0 \\ g_{10} & \dfrac{\sigma_1 g_2+\sigma_2+Hpg_1}{m} & \dfrac{A}{m} & \dfrac{A}{m} & 0 & \dfrac{-\sigma_0+\dfrac{\sigma_0\sigma_1|x_2|}{g_1}}{m} \\ \dfrac{\beta A(Ax_2-C_1x_5g_3)}{V_i^2} & \dfrac{\beta A}{V_i} & \dfrac{C_1\beta|x_5|}{2V_i g_3} & 0 & \dfrac{C_1\beta g_3}{V_i} & 0 \\ \dfrac{\beta A(Ax_2-C_1x_5g_4)}{V_0^2} & \dfrac{\beta A}{V_o} & 0 & \dfrac{C_1\beta|x_5|}{2V_0 g_4} & \dfrac{C_1\beta g_4}{-V_o} & 0 \\ \dfrac{k_{sp}}{\tau}g_{12}g_6 & 0 & \dfrac{k_{sp}}{\tau}\left(g_7-\dfrac{g_5\tanh(x_5)}{2g_6}\right) & \dfrac{k_{sp}}{\tau}\left(g_7+\dfrac{g_5\tanh(x_5)}{2g_6}\right) & \dfrac{k_{sp}}{\tau}g_9 & 0 \\ 0 & g_2 & 0 & 0 & 0 & \dfrac{\sigma_0|x_2|}{g_1} \end{bmatrix}$$

where

$$V_i(x_1) = \overline{V_i} + A(x_1 - x_0)$$

$$V_0(x_1) = \overline{V_o} - A(x_1 - x_0)$$

$$C_1 = \sqrt{\frac{2}{\rho}} c_d w$$

$$g_1(x_2) = F_C + (F_S - F_C)e^{-(x_2/v_s)^2}$$

$$g_2(x_2, x_6) = 1 - \frac{\sigma_0 x_6 sign(x_2)}{g_1} - \frac{2\sigma_0 x_6 |x_2| x_2 (F_S - F_C)e^{-(x_2/v_s)^2}}{(v_s g_1)^2}$$

$$g_3(x_3, x_5) = \sqrt{\frac{P_S - P_e}{2} + sign(x_5)\left(\frac{P_S + P_e}{2} - x_3\right)}$$

$$g_4(x_4, x_5) = \sqrt{\frac{P_S - P_e}{2} + sign(x_5)\left(x_4 - \frac{P_S + P_e}{2}\right)}$$

$$g_5(x_1, x_3, x_4, x_5) = \begin{cases} -\left(K_{p_P}|x_3 - x_4|\tanh(a x_5) + K_{x_P}(x_1 - x_{des})\right) & ; \quad u = u_P \\ -\left(K_{p_I}|x_3 - x_4|\tanh(a x_5) + K_{x_I}(x_1 - x_{env})\right) & ; \quad u = u_I \\ -\left(K_{p_C}\left|x_3 - x_4 - \frac{F_{des}}{A}\right|\tanh(a x_5) + K_f(H(x_1 - x_{env})^n - F_{des})\right) & ; \quad u = u_F \end{cases}$$

$$g_6(x_3, x_4, x_5) = \sqrt{P_s - \tanh(a x_5)(x_3 - x_4)}$$

$$g_7(x_3, x_4, x_5) = \begin{cases} K_{p_P} sign(x_3 - x_4)\tanh(a x_5) g_6 & ; \quad u = u_P \\ K_{p_I} sign(x_3 - x_4)\tanh(a x_5) g_6 & ; \quad u = u_I \\ K_{p_C} sign(x_3 - x_4 - F_{des}/A)\tanh(a x_5) g_6 & ; \quad u = u_F \end{cases}$$

$$g_8(x_3, x_4, x_5) = \begin{cases} aK_{p_P}|x_3 - x_4|\left(1 - \tanh^2(a x_5)\right) & ; \quad u = u_P \\ aK_{p_I}|x_3 - x_4|\left(1 - \tanh^2(a x_5)\right) & ; \quad u = u_I \\ aK_{p_C}|x_3 - x_4 - F_{des}/A|\left(1 - \tanh^2(a x_5)\right) & ; \quad u = u_F \end{cases}$$

$$g_9(x_1, x_3, x_4, x_5) = g_8 g_6 + \frac{a(x_3 - x_4)\left(1 - \tanh^2(a x_5)\right) g_5}{2 g_6} + \frac{1}{k_{sp}}$$

$$g_{10}(x_1,x_2)=\begin{cases}-\dfrac{nH(1+px_2)(x_1-x_{env})^{n-1}}{m} & ;\ (x_1-x_{env}\geq 0)\ \&\ (1+px_2\geq 0)\ \&\ (x_2^i\neq 0)\\ -\dfrac{nH(x_1-x_{env})^{n-1}}{m} & ;\ (x_1-x_{env}\geq 0)\ \&\ (x_2^i=0)\\ 0 & ;\ otherwise\end{cases}$$

$$g_{11}(x_1)=\begin{cases}(x_1-x_{env})^n & ;\ (x_1-x_{env}\geq 0)\ \&\ (1+px_2\geq 0)\ \&\ (x_2^i\neq 0)\\ 0 & ;\ otherwise\end{cases}$$

$$g_{12}(x_1)=\begin{cases}K_{x_P} & ;\ u=u_P\\ K_{x_I} & ;\ u=u_I\\ nK_fH(x_1-x_{env})^{n-1} & ;\ u=u_F\end{cases}$$

(8.16)

Substituting (8.16) into (8.15) constitutes the system's variational equations in the smooth parts of motion.

8.4.2 Analysis of the Overall Nonsmooth Motion

Following a similar procedure as in Section 7.4.2, in order to calculate the Lyapunov exponents of the overall switching contact task control system, issues including the solution concept of the linearized system, linearization of the nonlinear equations on the discontinuity surface, existence of the exponents as the limit stated in (2.6), and the numerical stability and convergence of the results to the exact Lyapunov exponents should be addressed. In the following subsections, the theorems and methods introduced in Chapter 7 are used to address these issues in detail.

Solution Analysis of the Variational Equation

With respect to (8.15) and (8.16), the right-hand sides of the linearized equations of motion are piecewise continuous in t. Following the theory of the Caratheodory differential equations (Section 2.2), the existence and uniqueness of the solution can be outlined accordingly. Since all the elements of the matrix $\boldsymbol{F}(t)$ in (8.16) are summable on each segment contained in the interval $[t_0,t_f]$, the solution of (8.15) with arbitrary initial condition $\psi_t(t_0)=\psi_{t_0}\ (t\in[t_0,t_f])$ exists on the whole interval $[t_0,t_f]$ and is unique (see the Theorem in Section 2.2).

Existence of Lyapunov Exponents

Similar to the discussion in Section 7.4.2, the Kunze's extension theorems on existence of the $\lim_{t\to\infty}$ in (2.6) are the theoretical foundation for applying the Oseledet's Multiplicative Ergodic Theorem (MET) for the existence proof of Lyapunov exponents in non-smooth systems. Conditions (A1)-(A8) of Theorem 4.1.1 (Kunze, 2000) can be verified for the system under study and the details of the mathematical proof are beyond the scope of this study. Condition (A9) requires that there exist functions h_k where h_k=0 indicate the next switching to a different manifold of motion and the trajectory does not arrive at h_k=0 tangentially. Introducing such indicator functions for different switching cases of the system shown in (8.7) is the topic of the next section. The theorem 4.1.1 and Corollary 4.1.8 of (Kunze, 2000) provide the required basis on which a measurable cocycle can be defined and the existence of the Lyapunov exponents established.

Calculation of Lyapunov Exponents at Nonsmooth Instants of Motion

With respect to (8.7), the nonlinear equations of motion are not linearizable at the following instants:

i) switching the control law from free-space to impact mode of motion,

ii) switching the control law between impact mode and constrained mode of motion,

iii) $x_2 = 0$,

iv) $x_5 = 0$,

v) $x_3 - x_4 = 0$ (within constrained region this condition will be $x_3 - x_4 - F_{des}/A = 0$)

Therefore, it is imperative to resort to the extension method of the calculating the variational equation as explained in Section 2.4.4. For the system under our study with continuous contact model and friction models, the states evolve continuously in time and the Jacobian of the transition condition, $\boldsymbol{G}$, is always the identity matrix, $\mathbf{I}_{6x6}$. Thus, equation (2.27) simplifies to:

$$\delta x^+ = \delta x^- + \left[f_1(x^-) - f_2(x^+)\right]\frac{H(x^-)\,\delta x^-}{H(x^-)f_1(x^-)} \tag{8.17}$$

where f_1 and f_2 are the nonlinear equations of motion before and after the nonsmooth instant t_1, and the plus and minus signs characterize the right and left-sided limits, respectively. The

matrices $\boldsymbol{H}(\boldsymbol{x}^-)$ and $\boldsymbol{G}(\boldsymbol{x}^-)$ are the Jacobians of the indicator function, $h(\boldsymbol{x})$, and the transition condition $\boldsymbol{g}(\boldsymbol{x})$ as defined in Section 2.4.4. Careful examination of the dynamic model (8.7) manifests that the right-hand sides of the nonlinear equations of motion do not experience discontinuity when there is no control switching. In other words, in the last three of the above cases of nonsmoothness, (*iii*)-(*v*), $\boldsymbol{f}_1 = \boldsymbol{f}_2 = \boldsymbol{f}$ and equation (8.17) yields:

$$\delta \boldsymbol{x}^+ = \delta \boldsymbol{x}^- \tag{8.18}$$

Consequently, we only need to define indicator functions for cases (*i*) and (*ii*) where we have nonsmoothness due to switching between the control laws during transits between various modes of motion.

The definition of the indicator functions $h(\boldsymbol{x})$ for the first two cases (switchings between the control laws) is based on the physical motion. The control scheme switches from free-space to impact mode of motion upon detecting the first nonzero impact force (3.23). The second condition in (3.23), i.e., $(1+p\dot{x}>0)$, is always satisfied as p is always positive and, before the first impact, the implement approaches the environment with a positive velocity. Hence, the indicator function for the switching between free-space to impact mode of motion is the only condition that determines the first impact:

$$h_1(\boldsymbol{x}) := x_1 - x_{env} = 0 \tag{8.19}$$

The Jacobian $\boldsymbol{H}_1(\boldsymbol{x}^-)$ for this transitional case is:

$$\boldsymbol{H}_1(\boldsymbol{x}^-) = \left.\frac{\partial h_1(\boldsymbol{x})}{\partial \boldsymbol{x}^T}\right|_{x=x(t_1^-)} = (1,0,0,0,0,0)^T \tag{8.20}$$

When the impact mode is completed, the implement rests on the surface of the environment with zero velocity $(x_2 = 0)$ and acceleration $(\dot{x}_2 = 0)$. Therefore, the indicator function and its Jacobian for switching from impact to contact mode of motion are constituted as follows:

$$h_2(\boldsymbol{x}) := \frac{1}{2}\left(x_2^2 + (m\dot{x}_2)^2\right) =$$

$$\frac{1}{2}\left(x_2^2 + \left(A(x_3 - x_4) - \sigma_0 x_6 - \sigma_1\left(x_2 - \frac{\sigma_0|x_2|}{F_C + (F_S - F_C)e^{-(x_2/v_s)^2}}x_6\right) - \sigma_2 x_2 - (1+p\,x_2)H(x_1 - x_{env})^n\right)^2\right) = 0 \tag{8.21}$$

$$\boldsymbol{H}_2(x^-)=\left.\frac{\partial h_2(x)}{\partial x^T}\right|_{x=x(t_I^-)}=$$

$$\left(-nHm(1+px_2^-)(x_1^- - x_{env})^{n-1}\dot{x}_2^- \;,\; x_2^- - m\dot{x}_2^-\left(\sigma_1 g_2^- + \sigma_2 + Hpg_1^-\right) \;,\; m\dot{x}_2^- A \;,\; -m\dot{x}_2^- A \;,\; 0 \;,\; -m\dot{x}_2^-\left(\sigma_0 - \frac{\sigma_0\sigma_1|x_2^-|}{g_1^-}\right)\right)^T \tag{8.22}$$

Note that $\dot{x}_2$, F_f, g_1 and g_{11} are previously defined in (8.7) and (8.16).

If the system loses the contact while the sustained-contact controller is in effect, the control algorithm switches back to the impact control law and, therefore, introduces discontinuity to the system equations. This case of nonsmoothness is also detected using the same h_1 and $\boldsymbol{H}_I$ indicated in (8.19) and (8.20).

8.4.3 Numerical Discretization Scheme

Since the purpose of calculating Lyapunov exponents is to investigate the stability of the system based on the signs of the exponents, suppression of numerical instabilities induced through numerical discretization of the original differential equation is of significant importance. As explained in Section 7.4.3, the nonstandard finite-difference (NSFΔ) discretization scheme (Section 2.5) has shown to be capable of enhancing the efficiency of computations and particularly effective for the calculation of Lyapunov exponents in discontinuous control systems (Sekhavat et al., 2003). Therefore, in this section, the nonstandard finite difference scheme is constructed for both nonlinear and linear equations of motion. The scheme for nonlinear equations is obtained by substituting the forward-difference approximations, $\dot{x}=\frac{x(t_{k+1}+\varphi)-x(t_k)}{\varphi}$, for the derivatives:

$$
\begin{cases}
x_1^{(k+1)} = x_1^{(k)} + \varphi\, x_2^{(k)} \\
x_2^{(k+1)} = \dfrac{x_2^{(k)} + \dfrac{\varphi}{m}\left(A(x_3^{(k)} - x_4^{(k)}) - \sigma_0 x_6^{(k)} + \dfrac{\sigma_0 \left| x_2^{(k)} \right| x_6^{(k)}}{F_C + (F_S - F_C) e^{-\left(x_2^{(k)}/v_s\right)^2}} - H g_{13}(x_1^{(k)}) \right)}{1 + \dfrac{\varphi(\sigma_1 + \sigma_2)}{m} + \dfrac{\varphi H p}{m} g_{11}(x_1^{(k)})} \\
x_3^{(k+1)} = x_3^{(k)} + \dfrac{\beta\varphi}{\overline{V}_i + A(x_1^{(k)} - x_0)} \left(-A x_2^{(k)} + \sqrt{\dfrac{2}{\rho}} c_d w x_5^{(k)} \sqrt{\dfrac{P_S - P_e}{2} + sign(x_5^{(k)}) \left(\dfrac{P_S + P_e}{2} - x_3^{(k)} \right)} \right) \\
x_4^{(k+1)} = x_4^{(k)} + \dfrac{\beta\varphi}{\overline{V}_o - A(x_1^{(k)} - x_0)} \left(A x_2^{(k)} - \sqrt{\dfrac{2}{\rho}} c_d w x_5^{(k)} \sqrt{\dfrac{P_S - P_e}{2} + sign(x_5^{(k)}) \left(x_4^{(k)} - \dfrac{P_S + P_e}{2} \right)} \right) \\
x_5^{(k+1)} = \dfrac{x_5^{(k)} + \dfrac{\varphi k_{sp}}{\tau} u^{(k)}}{1 + \dfrac{\varphi}{\tau}} \\
x_6^{(k+1)} = \dfrac{x_6^{(k)} + \varphi\, x_2^{(k)}}{1 + \dfrac{\varphi \sigma_0 \left| x_2^{(k)} \right|}{F_C + (F_S - F_C) e^{-\left(x_2^{(k)}/v_s\right)^2}}}
\end{cases}
$$

where $x_i^{(k)} = x_i(t_k)$, $x_i^{(k+1)} = x_i(t_k + \varphi)$ (i=1..6), and

$$
u = \begin{cases}
-\left(K_{p_P} \left| x_3^{(k)} - x_4^{(k)} \right| \tanh(a x_5^{(k)}) + K_{x_P} (x_1^{(k)} - x_{des}) \right) \sqrt{P_s - \tanh(a x_5^{(k)})(x_3^{(k)} - x_4^{(k)})} & ;\ u = u_P \\
-\left(K_{p_I} \left| x_3^{(k)} - x_4^{(k)} \right| \tanh(a x_5^{(k)}) + K_{x_I} (x_1^{(k)} - x_{env}) \right) \sqrt{P_s - \tanh(a x_5^{(k)})(x_3^{(k)} - x_4^{(k)})} & ;\ u = u_I \\
-\left(K_{p_C} \left| x_3^{(k)} - x_4^{(k)} - \dfrac{F_{des}}{A} \right| \tanh(a x_5^{(k)}) + K_f (H(x_1^{(k)} - x_{env})^n - F_{des}) \right) \sqrt{P_s - \tanh(a x_5^{(k)})(x_3^{(k)} - x_4^{(k)})} & ;\ u = u_F
\end{cases}
$$

$$
g_{13}(x_1^{(k)}) = \begin{cases} (x_1^{(k)} - x_{env})^n & ;\quad x_1^{(k)} - x_{env} > 0 \\ 0 & ;\quad otherwise \end{cases}
$$

(8.23)

The derivatives of the linearized variational equations are similarly replaced with their forward-difference approximations and rearranged according to the nonstandard discretization rules (Section 2.5):

$$
\begin{aligned}
\psi_{1i}^{(k+1)} &= \psi_{1i}^{(k)} + \varphi\, \psi_{2i}^{(k)} \\
\psi_{2i}^{(k+1)} &= \frac{\psi_{2i}^{(k)} + \dfrac{\varphi}{m}\left(g_{10}^{(k)}\psi_{1i}^{(k)} + A\psi_{3i}^{(k)} - A\psi_{4i}^{(k)} - \sigma_0\left(1 - \dfrac{\sigma_1 \left|x_2^{(k)}\right|}{g_1^{(k)}}\right)\psi_{6i}^{(k)}\right)}{1 + \dfrac{\varphi}{m}\left(\sigma_1 g_2^{(k)} + \sigma_2 + Hpg_{11}^{(k)}\right)} \\
\psi_{3i}^{(k+1)} &= \frac{\psi_{3i}^{(k)} + \varphi\left(-\dfrac{\beta A\left(-Ax_2^{(k)} + \sqrt{\dfrac{2}{\rho}}\, c_d w x_5^{(k)}\, g_3^{(k)}\right)}{\left(V_i^{(k)}\right)^2}\psi_{1i}^{(k)} - \dfrac{\beta A}{V_i^{(k)}}\psi_{2i}^{(k)} + \sqrt{\dfrac{2}{\rho}}\,\dfrac{c_d w \beta g_3^{(k)}}{V_i^{(k)}}\psi_{5i}^{(k)}\right)}{1 + \dfrac{\varphi\ \beta\ c_d\ w\left|x_5^{(k)}\right|}{\sqrt{2\rho}\ V_i^{(k)}\ g_3^{(k)}}} \\
\psi_{4i}^{(k+1)} &= \frac{\psi_{4i}^{(k)} + \varphi\left(\dfrac{\beta A\left(Ax_2^{(k)} - \sqrt{\dfrac{2}{\rho}}\, c_d w x_5^{(k)}\, g_4^{(k)}\right)}{\left(V_o^{(k)}\right)^2}\psi_{1i}^{(k)} + \dfrac{\beta A}{V_o^{(k)}}\psi_{2i}^{(k)} - \sqrt{\dfrac{2}{\rho}}\,\dfrac{c_d w \beta g_4^{(k)}}{V_o^{(k)}}\psi_{5i}^{(k)}\right)}{1 + \dfrac{\varphi\ \beta\ c_d\ w\left|x_5^{(k)}\right|}{\sqrt{2\rho}\ V_o^{(k)}\ g_4^{(k)}}} \\
\psi_{5i}^{(k+1)} &= \frac{\psi_{5i}^{(k)} + \dfrac{k_{sp}\varphi}{\tau}\left(-g_{12}^{(k)}\, g_6^{(k)}\psi_{1i}^{(k)} - \left(g_7^{(k)} - \dfrac{g_5^{(k)}}{2g_6^{(k)}}\tanh(ax_5^{(k)})\right)\psi_{3i}^{(k)} + \left(g_7^{(k)} + \dfrac{g_5^{(k)}}{2g_6^{(k)}}\tanh(ax_5^{(k)})\right)\psi_{4i}^{(k)}\right)}{1 + \dfrac{k_{sp}\varphi}{\tau}\, g_9^{(k)}} \\
\psi_{6i}^{(k+1)} &= \frac{\psi_{6i}^{(k)} + \varphi\, g_2^{(k)}}{1 + \dfrac{\varphi\ \sigma_0\left|x_2^{(k)}\right|}{g_1^{(k)}}}
\end{aligned}
\tag{8.24}
$$

where i=1..6. The above NSFΔ scheme is implicit by construction, but explicit by implementation. Also, difference equations (8.23) and (8.24) have the same order as the differential equations (8.7) and (8.16). These features reduce the possibility of introducing spurious solutions or other numerical instabilities associated with inconsistent orders of differential and difference equations or dissimilar characteristics of differential and difference schemes (Mickens, 2002).

8.4.4 Stability

In this section the numerical results of Lyapunov exponent calculations are presented and used to

discuss the stability of the switching control system (8.7). The motion of the hydraulic actuator starts from the initial position $x_0 = 0$ *in* under controller u_P [see (8.6)] and proceeds toward the desired position, x_{des}=19 *in* until colliding with the environment. Upon unexpected collision with the environment, the control action switches to the impact control law u_I [see (8.6)] to suppress the impacts and rest the hydraulic actuator on the surface of the environment, recorded to be x_{env}=15 *in* on the onset impact. When the impact oscillations are dissipated, the control scheme switches to the force control law u_F [see (8.6)] to exert the desired force of F_{des} = 500 *lb* on the environment. During this period of motion, if the contact with the environment is inadvertently lost, the control scheme switches back to the impact control law u_I until the implement rests on the environment surface and then switches to the force control law u_F to follow the desired contact force.

System parameters

In order to resemble a true practical case, the system parameters used in calculation program are chosen as the parameters of the real hydraulic test rig listed in Table 3.1. The supply pressure is 2000 *psi* as before and value of *a* in tanh(*ax*) is chosen as 10000. Other control parameters used in numerical calculations are tabulated in Table 8.1 and are almost the same as the values in individual experimental analyses except for the position control gains. The position control gains are adjusted as the desired position is changed from 8 *in* in Chapter 4 to 19 *in* and the new position control values result in a period of free-space motion that is comparable to the periods of impact and sustained-contact modes of motion.

Table 8.1 Controller parameters.

$K_f (V/lb\sqrt{psi})$	4×10^{-5}	$K_{x_I} (V/in\sqrt{psi})$	0.4
$K_{pc} (V/\sqrt{psi^3})$	2×10^{-5}	$K_{pp} (V/\sqrt{psi^3})$	8×10^{-5}
$K_{pI} (V/\sqrt{psi^3})$	3×10^{-5}	$K_{x_P} (V/in\sqrt{psi})$	0.02

Since the convergence proof of the control laws in each phase of motion (Chapters 4, 5, and 6) were proven to be contingent upon satisfaction of inequalities (4.31), (5.56), and (6.19), the control gains are selected so that they satisfy such relations.

Stability Results

To determine the stability of the dynamic system (8.7) with parameters shown in Tables 3.1 and 8.1, the spectrum of Lyapunov exponents are calculated through simultaneous integration of nonlinear and linearized equations (8.23) and (8.24) and inserting their results into (2.6). At instants of discontinuity, equation (8.17) substitutes the linearized equations (8.24) and the required functions f_1, f_2, and H are chosen from (8.7) and (8.20)/(8.22) depending on the regions of motion before and after the discontinuity. Numerical results for wooden and metal environments are presented in Table 8.2 and clearly show that the system does not show chaotic behavior. Therefore, discontinuous switchings between various control schemes, employing the general pressure-flow equations (8.1) instead of restrictive load pressure equation (3.16), and replacing nonsmooth *sign* functions in control laws with smooth hypertangent functions, all have no effect in driving the overall switching contact task control scheme unstable.

Table 8.2 Spectrum of Lyapunov Exponents

	λ_1	λ_2	λ_3	λ_4	λ_5	λ_6
wood	0.00	0.00	-61.58	-61.60	-131.55	-427.32
metal	0.00	0.00	-33.28	-33.31	-201.85	-351.20

In order to interpret the physical meaning of the results, equations (8.7) are revisited. According to these equations, the system will eventually have fixed values for x_1^{ss}, x_2^{ss}, x_5^{ss}, but the values of x_3^{ss}, x_4^{ss}, or x_6^{ss} are not fixed. In other words, the system has a set of equilibrium points (equilibria) where three of the six variables of the system can have various values, two of which, say x_3^{ss} and x_4^{ss}, can arbitrary change and the third one, x_6^{ss}, derives from $A(x_3^{ss} - x_4^{ss}) - \sigma_0 x_6^{ss} - F_{des} = 0$. Therefore, any two trajectories of the nonlinear system with infinitesimal difference in their initial conditions may eventually converge to two distinct equilibrium points both belonging to the system's equilibria (8.8). Consequently, the steady-state lengths of $\|\delta \boldsymbol{x}_i(t)\|$ in two directions as $t \to \infty$ [see (2.6)] stays at a constant non-zero value leading to zero Lyapunov exponents. This conclusion is in line with numerical calculation of Lyapunov exponents shown in Table 8.2.

Truncating the Calculation Time to a Finite Interval

Although Lyapunov exponents are theoretically determined as $t \to \infty$, in numerical calculations of Lyapunov exponents, we need to determine the exponents on a finite time interval. Section 7.4.4 explained the strategy used in other studies to choose the truncation time. This strategy is particularly effective for systems with negative or positive largest Lyapunov exponent (systems with stable equilibrium points, or chaotic systems). In those cases, small fluctuations of the largest Lyapunov exponent after the truncation time do not change the negative or positive sign of the largest exponent and consequently the judgment on system's long-term behavior. When the largest Lyapunov exponent of the system is zero, however, calculations should be continued long enough to ensure the system's largest exponent does not change afterwards.

Extensive calculations for the system with parameters shown in Tables 3.1 and 8.1 has shown that after 5000 seconds of calculations with step-size of 0.0001 seconds, the spectrum of Lyapunov exponents reach their steady-state values with three points of decimal accuracy. This is shown in Figs. 8.2 where the spectrum of Lyapunov exponents for contact on the wooden environment is illustrated. Similar results were obtained for contact with metal environment.

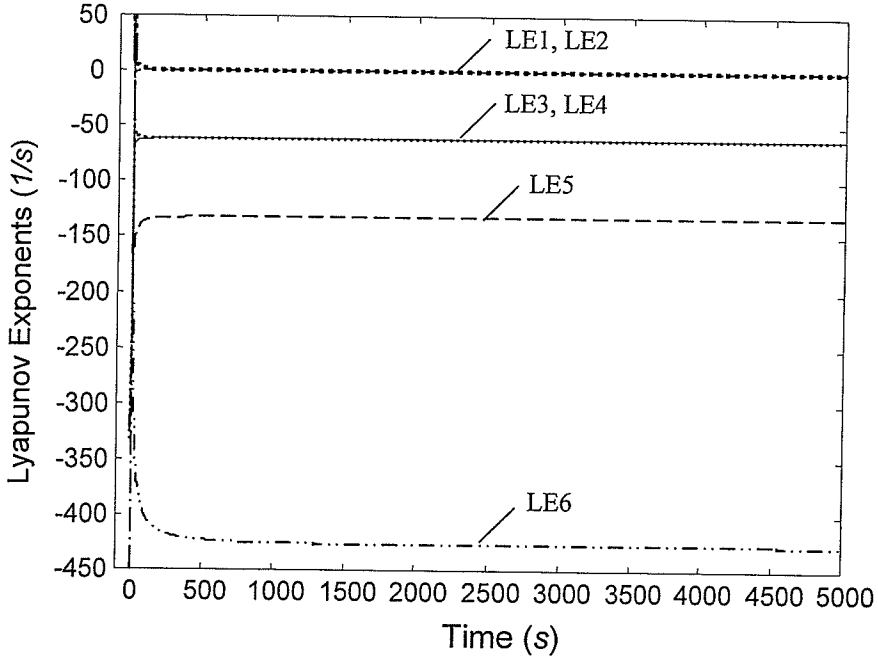

Fig. 8.2 Spectrum of Lyapunov exponents.

Convergence to the exact solution

An important issue in numerical approximation of discontinuous differential equations is to ensure that the numerical results are free of numerical artifacts and truly approximate the dynamic behavior of the system. Two different measures are considered to ensure the validity of the results and authenticity of the conclusions of the stability analysis of the system. Firstly, the spectrum of Lyapunov exponents for the wooden environment is calculated using smaller step-sizes of 0.000001 seconds. Results are given in Table 8.3 and are in good agreement with previous values given in Table 8.2.

The next important measure of computational stability is to compare the results obtained using NSFΔ with a typical result obtained using another numerical integrator. Here we calculate the spectrum of Lyapunov exponents using the fixed step fourth-order Runge-Kutta method. This choice is based on the recently proven theorem stating that if Filippov's solution of a discontinuous system exist and is unique, the approximate solution obtained using Runge-Kutta method exists, for a sufficiently small step-size (h), and as $h \to 0$, converges uniformly to the exact solution (see Section 2.6).

Table 8.3 Spectrum of Lyapunov Exponents for h=0.000001 s and T=5000 s.

	λ_1	λ_2	λ_3	λ_4	λ_5	λ_6
wood	0.00	0.00	-75.12	-75.14	-125.45	-458.24

Table 8.4 illustrates the values of Lyapunov exponents calculated using the Runge-Kutta integration scheme with similar h=0.0001 s. They are also in good agreement with the results of NSFΔ (Table 8.2) considering the fact that the Runge-Kutta has four times more accuracy in calculations.

Table 8.4 Spectrum of Lyapunov Exponents using RK4 with h=0.0001 s and T=5000 s.

	λ_1	λ_2	λ_3	λ_4	λ_5	λ_6
wood	0.00	0.00	-80.12	-80.16	-85.22	-488.66

Theoretical results are also complemented with test experiments to complete the solid foundation for implementing the proposed contact task control scheme on hydraulic actuators with friction.

8.5 Experimental Verification

Experiments were conducted on the electrohydraulic test rig described in Section (3.1) to observe the performance of the overall contact task control in practice. The task was to have the hydraulic actuator start from rest under controller u_P (8.6a), and proceed toward the desired position, x_{des}=19 *in* while there exists an environment on its way to the desired position. Upon collision with the environment ($F_{env} > F_{\min} = 5\ lbf$) and recording the location of the environment as x_{env}=15 *in*, the impact control law u_I (8.6b) is activated until the impact oscillations are dissipated and the implement has rested on the environment surface for a minimum specified time $t_{\min} = 2.5\ s$ [i.e., ($|x_2| < \varepsilon$ & $|\dot{x}_2| < \varepsilon$ & $|x_1 - x_{env}| < \varepsilon$) and ($t - t_{imp} > t_{\min}$)]. Then control scheme switches to the force control law u_F (8.6c) to exert the desired force of F_{des} = 500 *lb* on the environment. In case of losing contact during the sustained-contact period of motion ($x < x_{env}$), the control scheme switches back to the impact control law u_I until the implement rests on the environment surface and then switches back to u_F to follow the desired contact force. Schematic of the control switching plan is illustrated in Fig. 8.3.

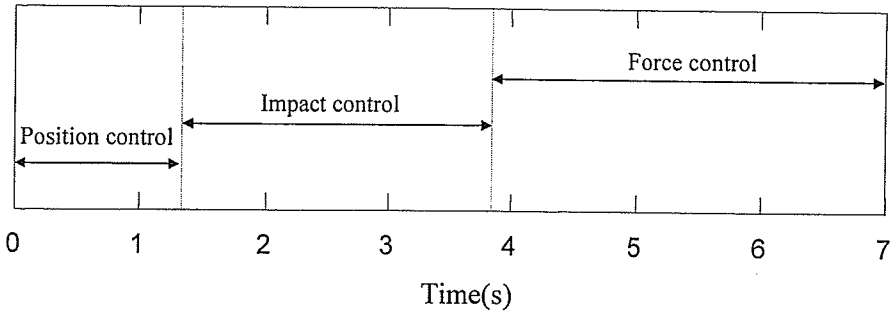

Fig. 8.3 Control scheme switching plan.

Metal sheet and wooden plate bolted to an I-beam were used to represent different environmental stiffness. The control gains were selected according to Table 8.1 and comply with equations (4.31), (5.56), and (6.19) obtained through theoretical analysis to guarantee the convergence of the system trajectories to the equilibria. The supply pressure of P_s=2000 *psi* was used in each experiment and the sampling time of the system was ≈2*ms*.

Figures 8.4 to 8.7 illustrate the responses for the above two types of environments. They confirm the previous theoretical stability analysis of the switching system and certify that the proposed control scheme in this thesis is capable of suppressing impact oscillations and asymptotic force regulation (without steady-state error) within the constrained phase of motion.

To further demonstrate that the system trajectories converge to $\boldsymbol{x}_{eq}$ when the Lyapunov exponents are numerically calculated a typical simulation response of is shown in Fig. 8.8. The figure demonstrates the convergence of the system trajectories to an equilibrium point belonging to the system's equilibria.

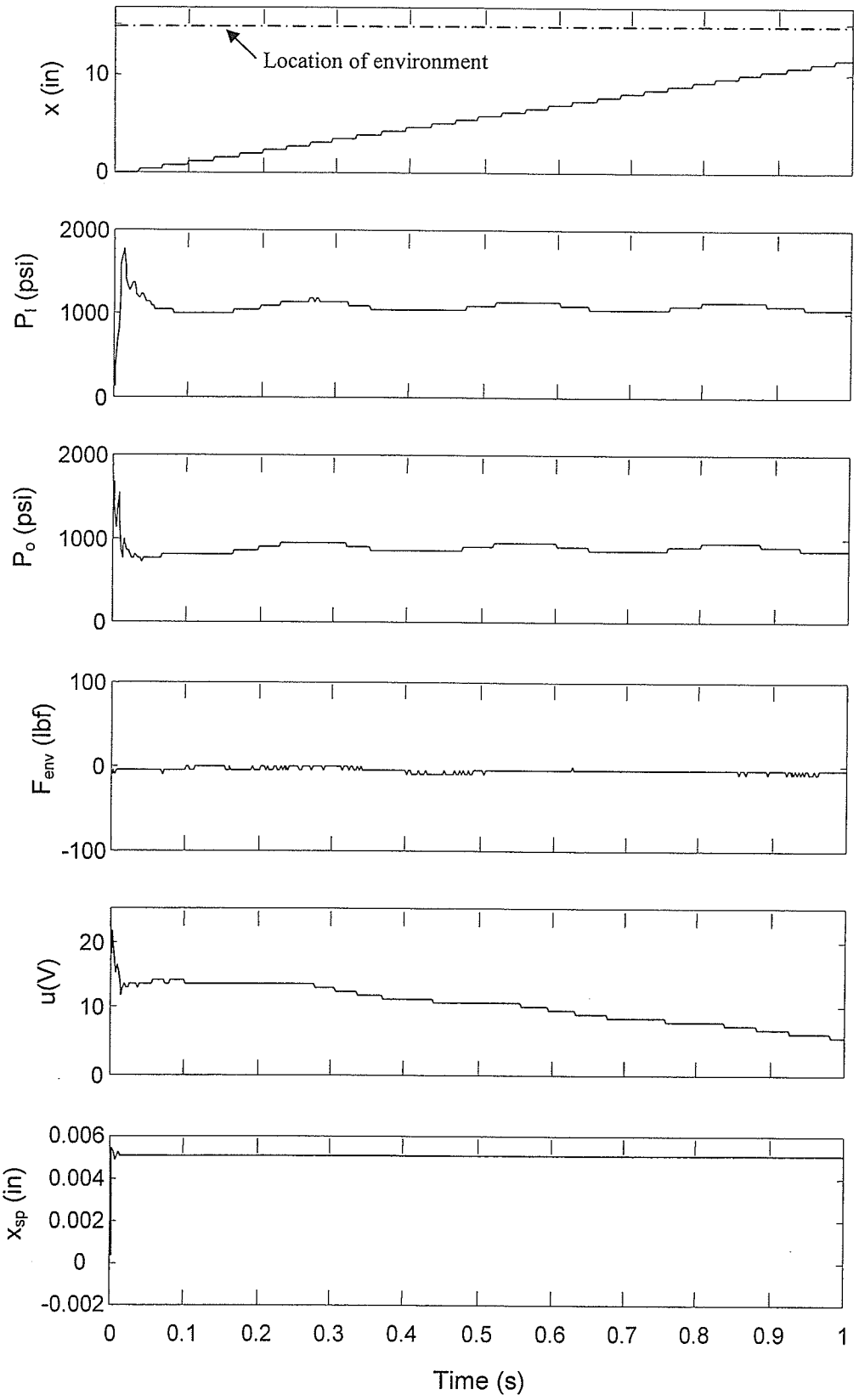

Fig. 8.4 Experimental system response for metal environment and F_{des}=500 *lbf* (before impact).

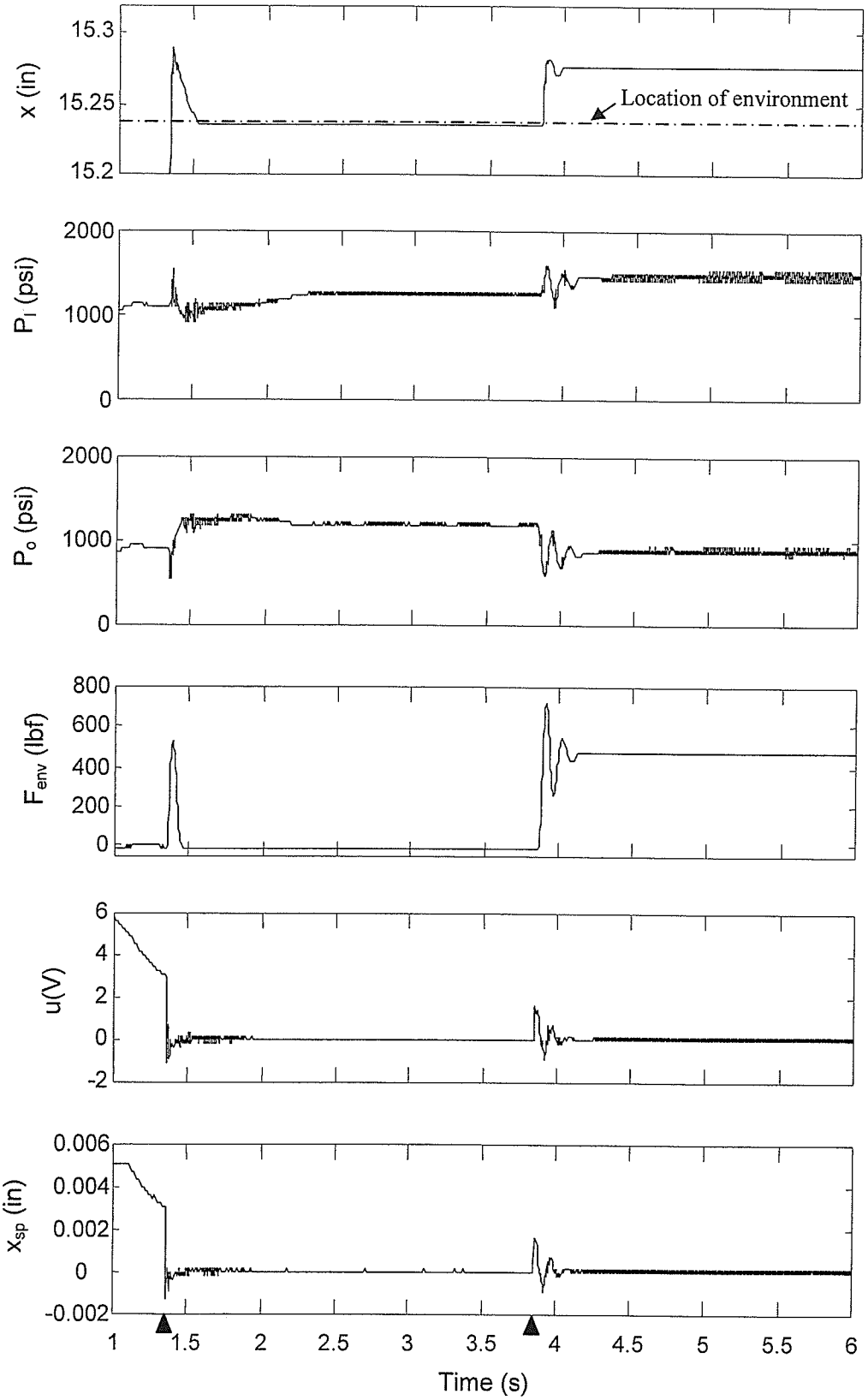

Fig. 8.5 Experimental system response for metal environment and F_{des}=500 *lbf* (after impact).

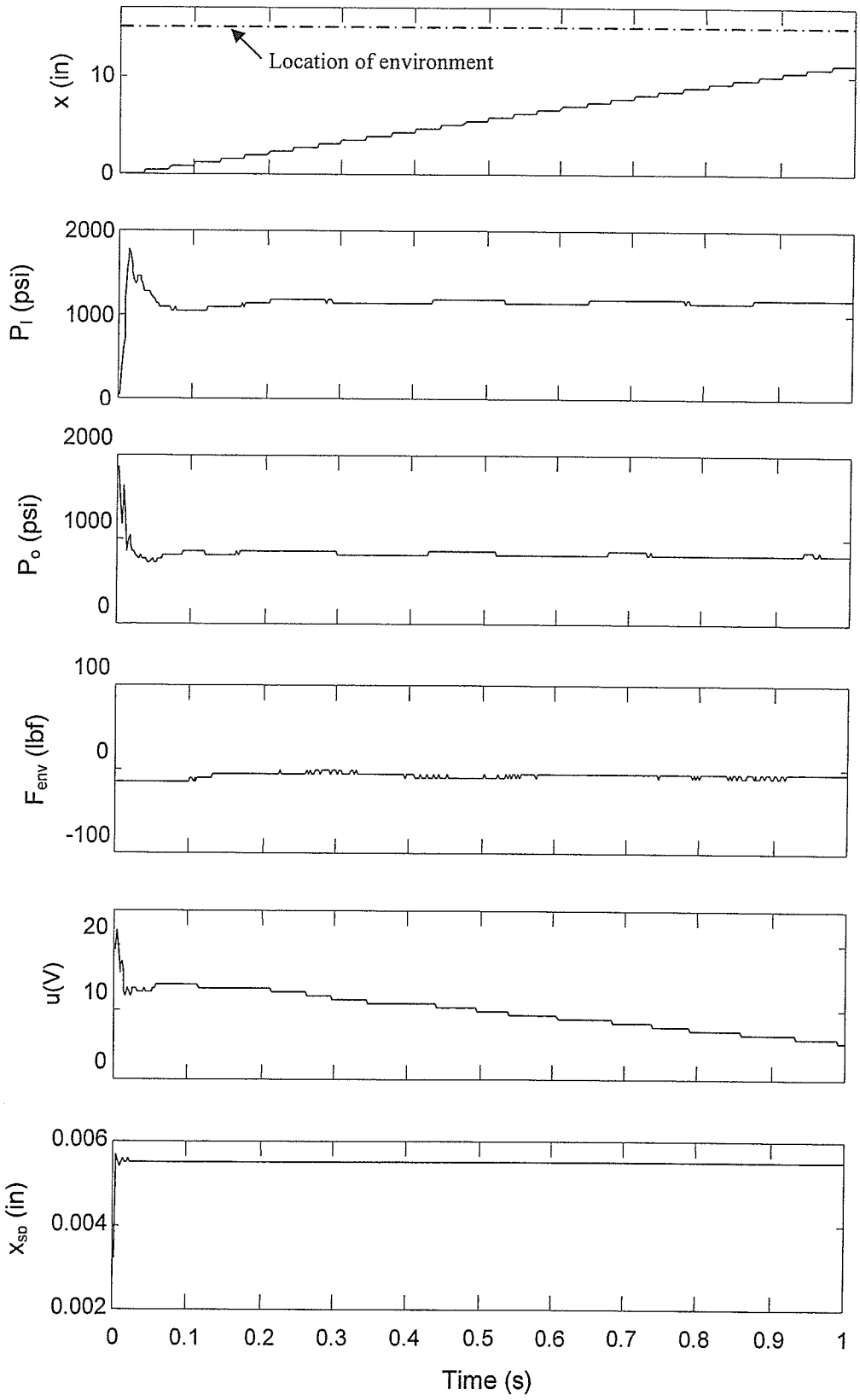

Fig. 8.6 Experimental system response for wooden environment and F_{des}=500 *lbf* (before impact).

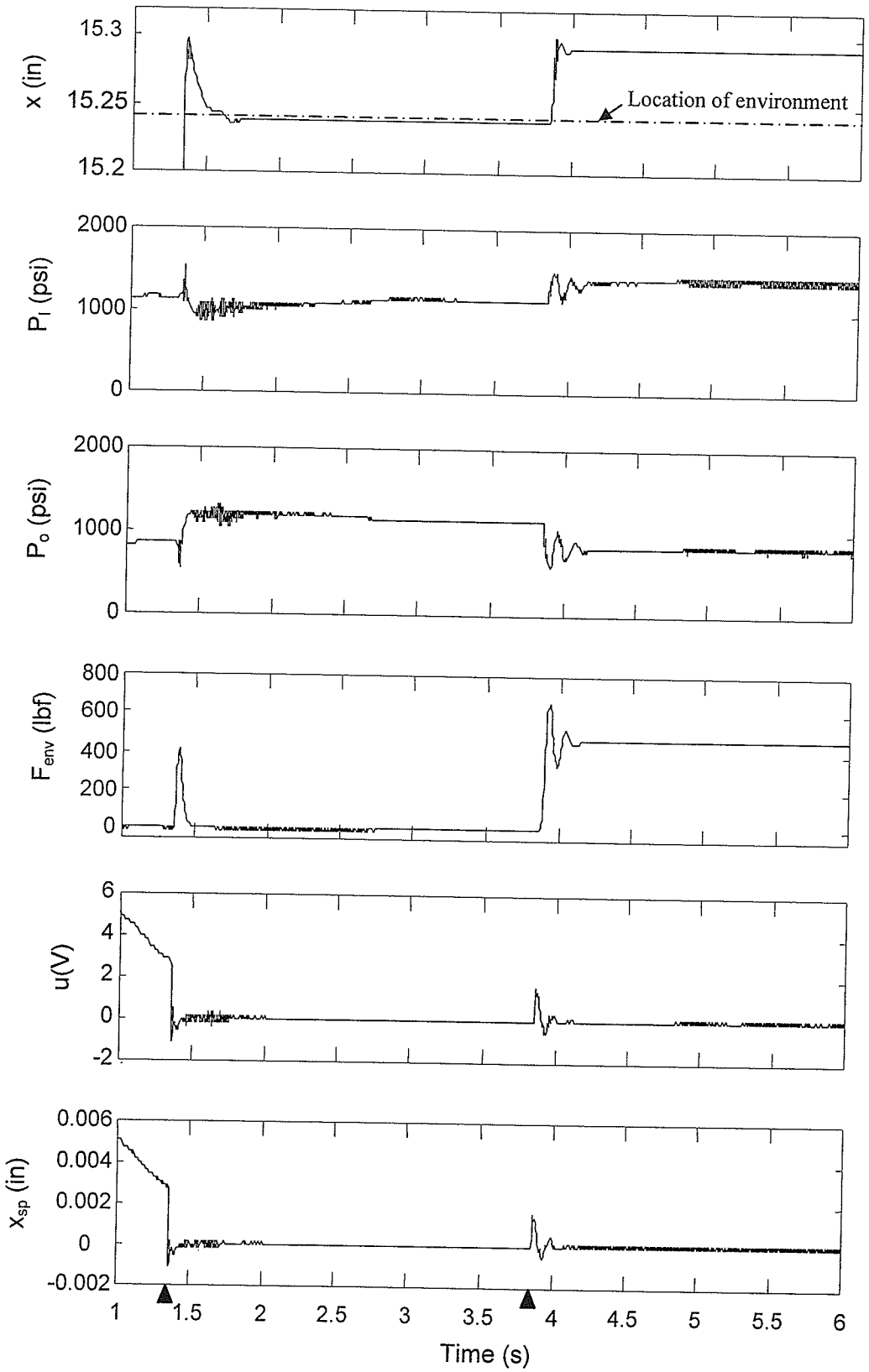

Fig. 8.7 Experimental system response for wooden environment and F_{des}=500 *lbf* (after impact).

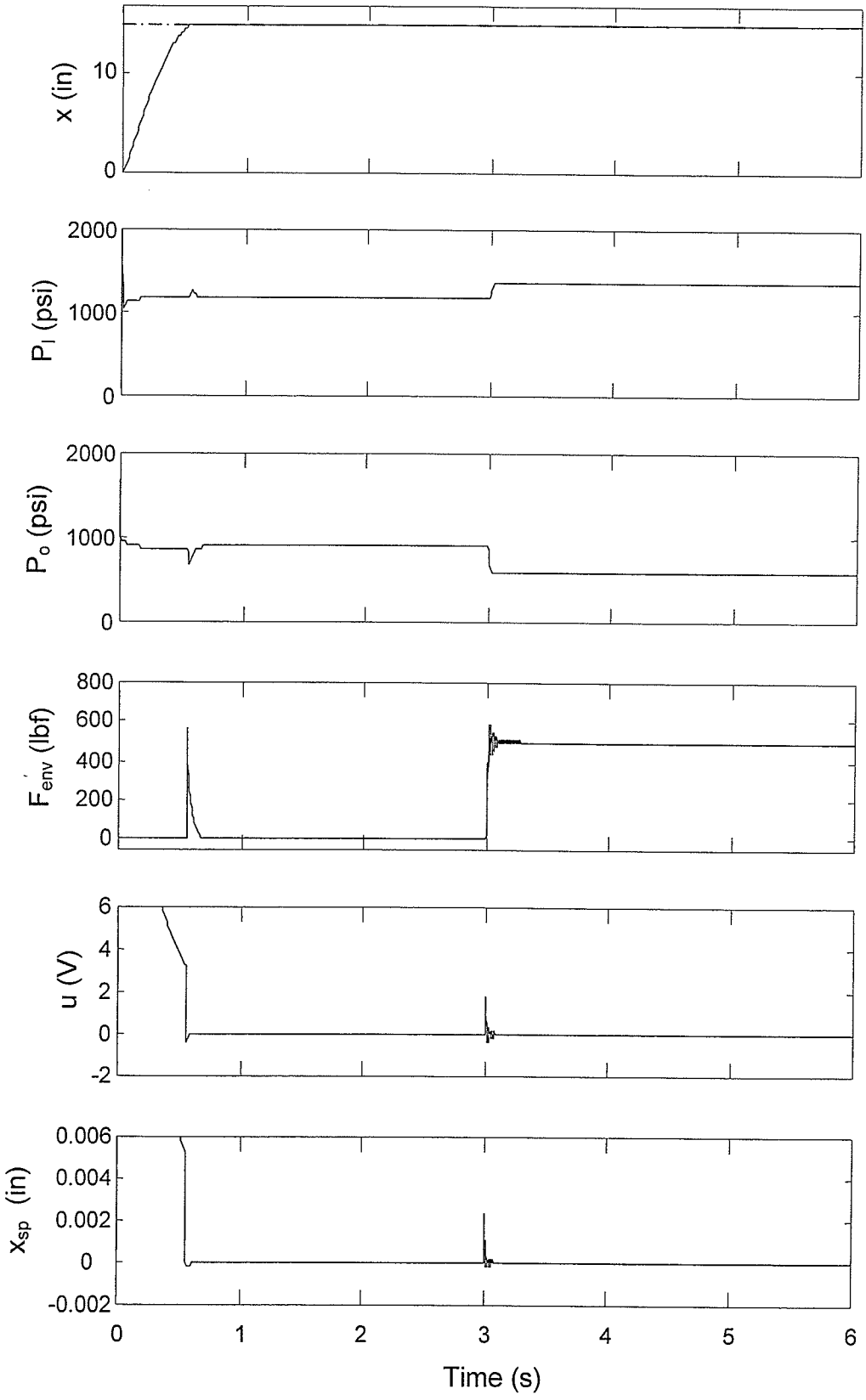

Fig. 8.8 Simulation response for metal environment and F_{des}=500 *lbf*.

Chapter 9

Concluding Remarks

The contributions of this thesis are in two main areas: control design and stability analysis.

1) Control Design

The extension of Lyapunov stability theory to nonsmooth systems based on Filippov's solution theory was used to derive a switching contact task control scheme for hydraulic actuators with friction. The control scheme essentially consists of three distinct control laws for asymptotic regulation of the desired position in free space motion, impact suppression and stable transition from free to constrained motion, and asymptotic regulation of the desired force in the sustained-contact period of motion, all in the presence of actuator's dry friction.

None of the controllers require any exact knowledge of the actuator friction, servovalve dynamics, environment stiffness, or hydraulic parameter for control action as in most practical cases such knowledge is not available. Compared with the previous relevant studies, the Lyapunov-based position and force regulation controllers have the advantage of being asymptotically convergent to the desired set-point, despite the hexistence of dry friction effects and without having the complexity of other control methods or the need for friction observers. The controller developed for the impact phase, is the first work in its kind for effectively

regulating impacts of a hydraulic actuator during the transition phase from free to constrained motion. It does not require continuous force or velocity feedback as they are difficult to be determined during the short transition phase.

Individual theoretical stability of all three controllers were thoroughly investigated considering nonlinear hydraulic functions, servovalve dynamics, complete model of actuator friction, and realistic impact/contact dynamics (if applicable) in the analysis. Employing the nonlinear Hertz-type contact model in the impact control system's stability analysis recognizes the realistic bounces, local elastic deformations and energy dissipations in the analysis. The model, used for both impact and sustained contact dynamics, is continuous and complies with the inherently continuous behavior of manipulators during collisions. All three controllers were individually tested experimentally on a hydraulic test rig to verify their practicality and effectiveness in real applications.

2) Stability Analysis

Although during the control design procedure each individual control law was shown to be convergent, existence of at least two switchings (free-to-impact and impact-to-contact control) in the overall combined switching contact control scheme results in an overall nonsmooth system for which stability analysis is not trivial. Finding a Lyapunov function for such a nonsmooth system is extremely difficult, if not impossible. In this thesis, a systematic procedure was developed for stability analysis of such a switching control system using the concept of Lyapunov exponents. Employing the concept of Lyapunov exponents for stability analysis not only allows the system to have switchings between different phases of motion, but also facilitates utilizing a more general dynamic model and modifying the control laws to remove undesirable chatterings in the control signal.

Application of the concept of Lyapunov exponents to dynamical systems with discontinuities entails several fundamental issues that were thoroughly investigated in this thesis. These issues included solution analysis of nonlinear and linearized systems, linearization of nonlinear equations at the instants of discontinuity, existence of Lyapunov exponents for nonsmooth systems, and stability of numerical computations. For complicated systems with practical relevance, it is in general almost impossible to determine the Lyapunov exponents analytically and they often have to be calculated numerically. Therefore, suppression of numerical

instabilities and convergence of the numerical results toward the exact Lyapunov exponents is of significant importance in judging the stability of the system based on the signs of the exponents.

Using previously developed theorems and techniques, the present work introduced a systematic framework to thoroughly address the above issues within the context of switching contact task control of hydraulic actuators. The solution analyses of both nonlinear and linearized system of equations were conducted using Filippov's solution theories and the theory of Caratheodory differential equations. Appropriate theorems were then employed to study the existence of Lyapunov exponents for such non-smooth control systems. The problem of linearizing the nonlinear equations on discontinuity surface was addressed by resorting to the works of Kunze (2000) and Muller (1995) in which the conventional calculation procedure by Wolf et al. (1985) is extended to systems with discontinuities. To address the issue of numerical instabilities, a nonstandard finite difference discretization scheme was constructed for both noncontact and contact regions of motion. The scheme enhances the efficiency of computations by providing results with step-sizes larger than those of other commonly used techniques. Thus, it is particularly appropriate for the calculation of Lyapunov exponents in discontinuous control systems.

The new methodology of studying the stability of switching control systems was first illustrated on a typical switching contact task control system without including hydraulic actuation. It was shown that under the conditions of existence and uniqueness of Filippov's solution, the method of Lyapunov exponents provides a rigorous stability proof for the switching contact task control system if numerical artifacts are under control. Finally the constructed framework was implemented for the overall stability analysis of the contact control of hydraulic actuator under the switching control scheme designed earlier. It was shown that the system would not exhibit chaotic behavior regardless of the environment stiffness. Theoretical results were complemented with test experiments to complete the solid foundation for implementation of the proposed contact task control scheme for hydraulic actuators with friction.

This work could be extended on the following subjects. Firstly, the model of the environment, currently assumed to be nonmoving, can be extended to a moving environment with a separate dynamics that is being excited upon the first impact. Secondly, it would be instructive to design Lyapunov-based control schemes using the original hydraulic equations without imposing

assumptions on the piston initial position and range of movements. Thirdly, a more rigorous mathematical study can be placed on proving the existence of Lyapunov exponents for the switching control system.

References

Alleyne, A., 1996. Nonlinear force control of an electrohydraulic actuator, *Japan/USA Symposium on Flexible Automation*, Boston, MA, pp 193-200.

Alleyne, A., and Hedrick, K., 1995. Nonlinear adaptive control of active suspensions, *IEEE Transactions on Control Systems Technology*, 3(1): 94-101.

Alleyne, A., and Liu, R., 2000. A simplified approach to force control for electrohydraulic systems, *Control Engineering Practice*, 8: 1347-1356.

Amin, J., Friedland, B., and Harnoy, A., 1997. Implementation of a friction estimation and compensation technique, *IEEE Control Systems Magazine*, 17(4): 71-76.

Armstrong-Helouvry, B., Dupont, P., and Canudas de Wit, C., 1994. A survey of models, analysis tools and compensation methods for the control of machines with friction, *Automatica*, 30(7): 1083-1138.

Benettin, G., Galgani, L., Giorgilli, A., and Strelcyn, J. M., 1980a. Lyapunov characteristic exponents for smooth dynamical systems and for Hamiltonian systems; A method for computing all of them. Part 1: Theory., *Meccanica*, 15(1): 9-20.

Benettin, G., Galgani, L., Giorgilli, A., and Strelcyn, J. M., 1980b. Lyapunov characteristic exponents for smooth dynamical systems and for Hamiltonian systems; A method for computing all of them. Part 2: Numerical application., *Meccanica*, 15(1): 21-30.

Bilodeau, G., and Papadopoulos, E., 1998. A model-based impedance control scheme for high-performance hydraulic joints. *Proc. IEEE/RSJ Int. Conf. Intelligent Robots and Systems,* pp. 1308-1313.

Bockman, S. F., 1991. Lyapunov exponents for systems described by differential equations with discontinuous right-hand sides, *Proc. American Control Conference,* pp. 1673-1678.

Bonchis, A., Corke, P. I ., and Rye, D. C., 2002. Experimental evaluation of position control methods for hydraulic systems, *IEEE Transactions on Control Systems Technology*, 10(6): 876-882.

Brogliato, B., 1999. Nonsmooth Mechanics. *Springer-Verlag.*

Brogliato, B., Niculescu, S. I., and Orhant, P., 1997. On the control of finite-dimensional mechanical systems with unilateral constraints. *IEEE Transactions on Automatic Control*, 42(2): 200-215.

Brogliato, B., and Orhant, P., 1998. Contact stability analysis of a one degree-of-freedom robot. *Dynamics and Control*, 8(1): 37-53.

Brogliato, B., ten Dam, A. A., Paoli, L., Genot, F., and Abadie, M., 2002. Numerical simulation of finite dimensional multibody nonsmooth mechanical systems, *Appl. Mech. Rev.*, 55 (2): 107-150.

Canudas de Wit, C., and Lischinsky, P., 1997. Adaptive friction compensation with partially known dynamic friction model, *International Journal of Adaptive Control and Signal Processing*, 11(1): 65-80.

Canudas de Wit, C., Noel, P., Aubin, A., and Brogliato, B., 1991. Adaptive friction compensation in robot manipulators. Low velocities, *International Journal of Robotics Research*, 10(3): 189-199.

Canudas de Wit, C., Olsson, H., Astrom, K. J., and Lischinsky, P., 1995. A new model for control of systems with friction, *IEEE Transactions on Automatic Control*, 40(3): 419-425.

Chiu, D., and Lee, S., 1996. Design and experimentation of jump impact controller. *Proc. IEEE Int. Conf. Robotics and Automation*, pp. 1903-1908.

Coreless, M., 1993. Control of uncertain nonlinear systems. *ASME J. Dynamic Systems, Measurement, and Control*, 115: 362-372.

Demir, B., and Kocak, S., 2001. A note on positive Lyapunov exponent and sensitive dependence on initial conditions. *Chaos, Solitans, and Fractals*, 12: 2119-2121.

Dieci, L., and Van Vleck, E. S., 2002. Lyapunov and other spectra: a survey. *SIAM book on "Preservation of stability under discretization"*.

Dunnigan, M. W., Lane, D. M., Clegg, A. C., and Edwards, I., 1996. Hybrid position/force control of a hydraulic underwater manipulator. *IEE Proc. Control Theory Appl.*, 143(2): 145-151.

Eckmann, J. P., and Ruelle, D., 1985. Ergodic theory of chaos and strange attractors. *Reviews of Modern Physics*, 57: 617-656.

Eppinger, S. D., and Seering, W. P., 1987. Understanding bandwidth limitations in robot force control. *Proc. IEEE Int. Conf. Robotics and Automation*, pp. 904-909.

Filippov, A. F., 1960. Differential equations with discontinuous right-hand side. *Math. Sbornik,* 51:99 [English Translation: (1964) *American Mathematical Society Translations,* 42: 199-231].

Filippov, A. F., 1979. Differential equations with second members discontinuous on intersecting surfaces. *Differentsial'nye Uravneniya,*15: 1814 [English Translation: (1980) *Differential Equations* 15: 1292-1299].

Filippov, A. F., 1988. Differential equations with discontinuous right-hand sides. *Kluwer Academic Publishers*.

Filippov, A. F., 2001. On the approximate computation of solutions of ordinary differential equations with discontinuous right-hand sides. *Moscow University Computational Mathematics and Cybernetics,* 2: 19-21.

Friedland, B., and Park, Y., 1992. On adaptive friction compensation, *IEEE Transactions on Automatic Control*, 37(10): 1609-1612.

Fujita, T., and Hattori, S., 1980. Periodic vibration and impact characteristics of a nonlinear system with collision. *Bulletin of the JSME*, 23(177): 409-418.

Gilardi, G., and Sharf, I., 2002. Literature survey of contact dynamics modeling. *Mechanism and Machine Theory,* 37: 1213-1239.

Grune, L., 1998. Asymptotic controllability and exponential stabilization of nonlinear control systems at singular points, *SIAM Journal on Control and Optimization*, 36(5): 1485-1503.

Grune, L., 2000. A uniform exponential spectrum for linear flows on vector bundles, *J. Dynam. Differential Equations*, 12(2): 435-448.

Ha, Q. P., Nguyen, Q. H., Rye, D. C., Durrant-Whyte, H. F., 2000. Impedance control of a hydraulically actuated robotic excavator. *Automation in Construction*, 9: 421-435.

Heinrichs, B., Sepehri, N., and Thornton-Trump, A. B., 1997. Position-based impedance control of an industrial hydraulic manipulator. *IEEE Control Systems*, 17(1): 46-52.

Hilborn, R. C., 2000. Chaos and nonlinear dynamics, *Oxford University Press*.

Honegger, M., and Corke, P., 2001. Model-based control of hydraulically actuated manipulators, *Proc. IEEE Int. Conf. Robotics and Automation*, pp. 2553-2559.

Hunt, K. H., and Crossley, F. R. E., 1975. Coefficient of restitution interpreted as damping in vibroimpact, *Journal of Applied Mechanics*: 440-445.

Hwang, C. L., and Lan, C. H., 1994. The position control of electrohydraulic servomechanism via a novel variable structure control, *Mechatronics*, 4(4): 369-391.

Hyde, J. M., and Cutkosky, M. R., 1993. Contact transition control: an experimental study, *Proc. IEEE Int. Conf. Robotics and Automation*, pp. 363-368.

Kapitaniak, T., 2000. Chaos for Engineers: Theory, Applications, and Cotrol. *Springer-Verlag*.

Kazerooni, H., Waibel, B. J., and Kim, S., 1990. On the stability of robot compliant motion control: theory and experiments, *ASME J. Dyn. Sys. Meas. Control*, 112: 417-426.

Kunze, M., 2000. Non-smooth dynamical systems. *Springer-Verlag*.

Laval, L., M'Sidiri, N. K., and Cadiou, J. C., 1996. H_∞-Force control of a hydraulic servo-actuator with environmental uncertainties, *Proc. IEEE Int. Conf. Robotics and Automation,* pp 1566-1571.

Lin, Z. C., Patel, R. V. and Balafoutis, C. A., 1995. Impact reduction for redundant manipulators using augmented impedance control, *Int. J. Robotics Research*, 12(5): 301-313.

Lischinsky, P., Canudas de Wit, C., and Morel, G., 1999. Friction compensation for an industrial hydraulic robot, *IEEE Control Systems Magazine*, 19(1): 25-32.

Liu, R., and Alleyne, A., 2000. Nonlinear Force/Pressure Tracking of an Electro-Hydraulic Actuator, *ASME J. Dynamic Systems, Measurement, and Control*, 122: 232-237.

Marhefka, D. W., and Orin, D. E., 1996. Simulation of contact using a nonlinear damping model, *Proc. IEEE Int. Conf. Robotics and Automation*, pp. 1662-1668.

Marhefka, D. W., and Orin, D. E., 1999. A compliant contact model with nonlinear damping for simulation of robotic systems, *IEEE Transactions on Systems, Man, and Cybernetics- Part A: Systems and Humans*, 29(6): 566-572.

Marth, G. T., Tarn, T. J., and Bejczy, A. K., 1993. Stable phase transition control for robot arm motion, *Proc. IEEE Int. Conf. Robotics and Automation*, pp. 355-362.

Marth, G. T., Tarn, T. J., and Bejczy, A. K., 1994. An event based approach to impact control: theory and experiments, *Proceedings of IEEE International Conference on Robotics and Automation*, pp. 918-923.

Medio, A., and Lines, M., 2001. Nonlinear dynamics: a primer. *Cambridge University Press.*

Merritt, H. E., 1967. Hydraulic Control Systems, *John Wiley.*

Mickens, R. E., 2002. Non-standard finite-difference schemes for differential equations. *Journal of Difference Equations and Applications,* 8(9): 823-847.

Mickens, R. E., and Gumel, A. B., 2002. Numerical study of a non-standard finite-difference scheme for the Van Der Pol equation. *Journal of Sound and Vibration*, 250(5): 955-963.

Mills, J. K., 1990. Manipulator transition to and from contact tasks: A discontinuous control approach, *Proc. IEEE Int. Conf. Robotics and Automation*, pp. 440-446.

Mills, J. K., and Lokhorst, D. M., 1993a. Control of robotic manipulators during general task execution: a discontinuous control approach, *Int. J. Robotics Research*, 12(2): 146-163.

Mills, J. K., and Lokhorst, D. M., 1993b. Stability and control of robotic manipulators during contact/noncontact task transition, *IEEE Trans. Rob. Auto.*, 9(3): 335-345.

Mills, J. K., and Nguyen, C. V., 1992. Robotic manipulator collisions: modeling and simulation. *ASME J. Dynamic Systems, Measurement, and Control*, 114: 650-659.

Muller, P. C., 1995. Calculation of Lyapunov exponents for dynamic systems with discontinuities. *Chaos, Solitans and Fractals*, 5(9): 1671-1681.

Nguyen, Q. H., Ha, Q. P., Rye, D. C., and Durrant-Whyte, H. F., 2000. Force/position tracking for electrohydraulic systems of a robotic excavator, *Proc. IEEE Conf. Decision and Control*, pp 5224-5229.

Niksefat, N., and Sepehri, N., 2000. Design and experimental evaluation of a robust force controller for an electrohydraulic actuator via quantitative feedback theory, *Control Engineering Practice*, 8:1335-1345.

Niksefat, N., Wu, C. Q., and Sepehri, N., 2001. Design of a Lyapunov controller for an electro-hydraulic actuator during contact tasks. *ASME J. Dynamic Systems, Measurement, and Control*, 123: 299-307.

Nusse, H. E., and Yorke, J. A., 1998. Dynamics: numerical explorations. *Springer-Verlag.*

Oseledec, V. I., 1968. A multiplicative ergodic theorem. Lyapunov characteristic numbers for dynamical systems. *Trudy Mosk. Mat. Obsch* 19: 179-210 (English Translation: (1968) *Trans. Mosc. Math. Soc.* 19: 197).

Owen, W. S., and Croft, E. A., 2003. The reduction of stick-slip friction in hydraulic actuators, *IEEE/ASME Transactions on Mechatronics*, 8(3): 362-371.

Paden, B. E., and Sastry, S. S., 1987. A calculus for computing Filippov's differential inclusion with application to the variable structure control of robot manipulators, *IEEE Transactions on Circuits and Systems*, 34: 73-82.

Pagilla, P. R., and Yu, B., 2001. A stable transition controller for constrained robots. *IEEE/ASME Transactions on Mechatronics*, 6(1): 65-74.

Parker, T. S., and Chua, L. O., 1989. Practical numerical algorithms for chaotic systems. *Springer-Verlag.*

Payandeh, S., 1995. On the effect of compliance in robotic contact tasks problem. *Proc. American Control Conference*, pp. 387-391.

Payandeh, S., 1996. A method for controlling robotic contact tasks. *Robotica*, 14: 281-288.

Peleties, P., and DeCarlo, R., 1993. Asymptotic stability of 2-switched systems based on Lyapunov functions, *Proceedings of American Control Conference*, pp 3089-3093.

Ravishankar, A. S., and Ghosal, A. S., 1999. Nonlinear dynamics and chaotic motions in feedback-controlled two- and three-degree-of-freedom robots. *Int. J. Rob. Res.*, 18(1): 93-108.

Sekhavat, P., and Sepehri, N., 2001. Cascade control of hydraulic actuators during contact tasks, *IEEE International Symposium on Computational Intelligence in Robotics and Automation*, pp. 172-177.

Sekhavat, P., Sepehri, N., and Wu, Q., 2002. Contact task stability analysis via Lyapunov exponents. *IEEE International Symposium on Intelligent Control (ISIC'02)*, pp. 148-152.

Sekhavat, P., Sepehri, N., and Wu, C. Q., 2003. Calculation of Lyapunov exponents using nonstandard finite difference discretization scheme: a case study, *Journal of Difference Equations and Applications*, 10(4): 369-378.

Sekhavat, P., Wu, C.Q., and Sepehri, N., 2004a. On stability analysis of switching contact control systems using the concept of Lyapunov exponents: A case study, submitted to *International Journal of Non-linear Mechanics*.

Sekhavat, P., Wu, C.Q., and Sepehri, N., 2004b. Lyapunov-based friction compensation in positioning a hydraulic actuator, *American Control Conference*, pp. 418-423

Sekhavat, P., Wu, C.Q., and Sepehri, N., 2004c. Impact control in hydraulic actuators with friction: theory and experiments, *American Control Conference*, pp. 4432-4437.

Sekhavat, P., Sepehri, N., and Wu, C. Q., 2004d. Asymptotic force control of hydraulic actuators with friction: theory and experiments, Acceptanced in *International Symposium on Advances in Robot Dynamics and Control.*

Sekhavat, P., Sepehri, N., and Wu, C. Q., 2004e. Asymptotic impact control of hydraulic actuators with friction, Acceptanced in *International Symposium on Advances in Robot Dynamics and Control.*

Sepehri, N., Wan, F. L. K., Lawrence, P. D., and Dumont, G. A. M., 1994. Hydraulic compliance identification using parallel genetic algorithm, *International Journal of Mechatronics*, 4(6): 617-633.

Seraji, H., Lim, D., and Steele, R., 1996. Experiments in contact control. *Journal of Robotic Systems*, 13(2): 53-73.

Shevitz, D., and Paden, B., 1994. Lyapunov stability theory of nonsmooth systems, *IEEE Transactions on automatic control*, 39(9):1910-1914.

Shoji, Y., Inaba, M., and Fukuda, T., 1991. Impact control of grasping. *IEEE Transactions on Industrial Electronics*, 38(3): 187-194.

Sirouspour, M. R., and Salcudean, S. E., 2001. Nonlinear control of hydraulic robots, *IEEE Transactions on Robotics and Automation*, 17(2): 173-182.

Slotine, J. I., and Li, W., 1991. Applied Nonlinear Control, *Prentice-Hall.*

Sohl, G. A., and Bobrow, J. E., 1999. Experiments and simulations on the nonlinear control of a hydraulic servosystem, *IEEE Transactions on Control Systems Technology*, 7(2): 238-247.

Song, G., Cai, L., Wang, Y., and Longman, R. W., 1998. A sliding-mode based smooth adaptive robust controller for friction compensation, *International Journal of Robust and Nonlinear Control*, 8(8): 725-739.

Southward, S. C., Radcliffe, C. J., and MacCluer, C. R., 1991. Robust nonlinear stick-slip friction compensation, *ASME J. Dynamic Systems, Measurement, and Control*, 113: 639-645.

Stuart, A. M., Humphries, A. R., 1998. Dynamical Systems and Numerical Analysis. *Cambridge University Press.*

Tafazoli, S., de Silva, C. W., and Lawrence, P. D., 1998. Tracking control of an electrohydraulic manipulator in the presence of friction, *IEEE Transactions on Control Systems Technology*, 6(3): 401-411.

Tarn, T. J., Wu, Y., Xi, N., and Isidori, A., 1996. Force regulation and contact transition control. *IEEE Contr. Syst. Mag.*, 16(1): 32-40.

Taylor, J. H., and Kebede, D., 1997. Rigorous hybrid systems simulation of an electro-mechanical pointing system with discrete-time control. *Proc. Amer. Cont. Conf.*, pp. 2786-2789.

Thompson, J. M. T., and Stewart, H. B., 2002. Nonlinear dynamics and chaos. *John Wiley & Sons.*

Timoshenko, S. P., and Goodier, J. N., 1970. Theory of elasticity. *McGraw-Hill.*

Tornambe, A., 1996. Global regulation of a planar robot arm striking a surface, *IEEE Transactions on Automatic Control*, 41(10): 1517-1521.

Tornambe, A., 1999. Modeling and control of impact in mechanical systems: theory and experimental results. *IEEE Transactions on Automatic Control*, 44(2): 294-309.

Van Vliet, J., Sharf, I., and Ma.O., 2000. Experimental validation of contact dynamics simulation of constrained robotic tasks. *Int. J. Robotics Research*, 19(12): 1203-1217.

Vedagarbha, P., Dawson, D. M., and Feemster, M., 1999. Tracking control of mechanical systems in the presence of nonlinear dynamic friction effects. *IEEE Transactions on Control Systems technology*, 7(4): 446-456.

Volpe, R., and Khosla, P., 1993a. A theoretical and experimental investigation of impact control for manipulators. *Int. J. Robotics Research*, 12(4): 351-365.

Volpe, R., and Khosla, P., 1993b. A theoretical and experimental investigation of explicit force control strategies for manipulators. *IEEE Transactions on Automatic Control*, 38(11): 1634-1650.

Vossoughi, G., and Donath, M., 1995. Dynamic feedback linearization for electrohydraulically actuated control systems, *ASME J. Dynamic Systems, Measurement, and Control*, 117: 468-477.

Vukobratovic, M., 1997. How to control robots interacting with dynamic environment. *Journal of Intelligent and Robotic Systems: Theory & Applications*, 19(2): 119-152.

Vukobratovic, M. , Potkonjak, V., and Matijevic, V., 2001. Contribution to the study of dynamics and dynamic control of robots interacting with dynamic environment. *Robotica*, 19: 149-161.

Wolf, A., Swift, J. B., Swinney, H. L., and Vastano, J. A., 1985. Determining Lyapunov exponents from a time series. *Physica*, 16D: 285-317.

Wu, Q., Onyshko, S., Sepehri, N., and Thornton-trump, A. B., 1998a. On construction of smooth Lyapunov functions for non-smooth systems. *Int. Journal of Control*, 69(3): 443-457.

Wu, Q., and Payandeh, S., 1999. Toward smooth analysis of robotic contact tasks problem. *Proc. American Control Conference*, pp. 1960-1964.

Wu, Q., Sekhavat, P., Peles, S., Sepehri, N., and Abo-shanab, R.F., 2001. An improved design procedure of Lyapunov feedback control. *IEEE International Symposium on Computational Intelligence in Robotics and Automation*, pp.486-491.

Wu, Q., and Sepehri, N., 2000. On Lyapunov's stability analysis of non-smooth systems with applications to control engineering. *Int. Journal of Nonlinear Mechanics*, 36(7): 1153-1161.

Wu, G., Sepehri, N., and Ziaei, K., 1998b. Design of a hydraulic force control system using a generalized predictive control algorithm. *IEE Proc. Control Theory Appl.*, 145(5): 428-436.

Xu, W. L., Han, J. D., and Tso, S. K., 2000. Experimental study of contact transition control incorporating joint acceleration feedback. *IEEE/ASME Trans. on Mechatronics*, 5(3): 292-301.

Yao, B., Bu, F., and Chiu, G. T. C., 2001. Non-linear adaptive robust control of electro-hydraulic systems driven by double-rod actuators, *International Journal of Control*, 74(8): 761-775.

Yao, B., Bu, F., Reedy, J., and Chiu, G., 2000. Adaptive robust motion control of single-rod hydraulic actuators: Theory and experiments, *IEEE/ASME Transactions on Mechatronics*, 5(1): 79-91.

Yousef-Toumi, K., and Gutz, D. A., 1994. Impact and force control: modeling and experiments. *ASME J. Dyn. Sys. Meas. Control*, 116: 89-98.

Zheng, Y. F., and Hemami, H., 1985. Mathematical modeling of a robot collision with its environment. *Journal of Robotic Systems*, 2(3): 289-307.

Zyada, Z., Hasegawa, Y., and Fukuda, T., 2002. Force control with fuzzy compensation of gravity and actuators' friction forces of a hydraulic parallel link manipulator, *Proc. IEEE Int. Conf. Systems, Man and Cybernetics*, v 2.